CYTOCHROMES P450 AS THERAPEUTIC TARGETS AND COUNTER-TARGETS FOR THE PREVENTION OF LUNG CANCER AND TREATMENT OF STEROIDOGENIC DISEASES

By

Linda Cherise Blake

Submitted to the graduate degree program in Medicinal Chemistry and the Graduate faculty of the University of Kansas in partial fulfillment of the requirements for the degree of Doctor of Philosophy

---

Chairperson: Emily Scott

Jane Aldrich

John Karanicolas

Audrey Lamb

Thomas Prisinzano

Date Defended: April 3, 2012

The Dissertation Committee for Linda C. Blake certifies that this is the approved version of the following dissertation:

CYTOCHROMES P450 AS THERAPEUTIC TARGETS AND COUNTER-TARGETS FOR THE PREVENTION OF LUNG CANCER AND TREATMENT OF STEROIDOGENIC DISEASES

Chairperson: Emily Scott

Date approved: April 13, 2012

Abstract

Cytochrome P450 (CYP) is a superfamily of heme-containing monooxygenase enzymes that metabolize a variety of endogenous and exogenous substrates. These transformations can be advantageous in the role of homeostasis or clearance of foreign compounds. However, aberrant CYP activity or biotransformations of procarcinogens can be detrimental to human health. Thus cytochrome P450 enzymes can be both therapeutic targets and counter-targets. In the process of drug discovery, *in vitro* evaluation of both the efficacy and selectivity of drug candidates is necessary before *in vivo* studies can be pursued. In the case of the xenobiotic-metabolizing cytochrome P450 2A13 (CYP2A13), *in vitro* analysis was used to identify and evaluate selective inhibitors for reducing the risk of lung cancer in tobacco users. Additionally, *in vitro* biochemical analysis of the steroidogenic cytochromes P450 21A2 (CYP21A2) and 11B1 (CYP11B1) is being pursued for counter-target evaluation in the development of selective CYP17A1 inhibitors for the treatment of prostate cancer and the rational design of selective CYP11B1 inhibitors for the treatment of cortisol-dependent diseases.

Lung cancer is the leading cause of all cancer related deaths and results in 6 million annual deaths worldwide. Since >80% of all lung cancer incidence is attributed to tobacco use but tobacco cessation methods are unsuccessful in 95% of users, an increased emphasis has been placed on lung cancer chemoprevention. 4-(Methylnitrosamino)-1-(3-pyridyl)-1-butanone (NNK) is one of the most prevalent procarcinogens compounds in tobacco and is selectively activated by CYP2A13 metabolism in the respiratory tract. The resulting diazonium ions are able to form DNA adducts and initiate lung cancer. Therefore, the selective inhibition of CYP2A13 offers a novel therapeutic strategy in the chemoprevention of lung cancer. High throughput screening identified the benzylmorpholine scaffold, and a small library was evaluated

for both binding (K_d) and inhibition (K_i) of CYP2A13 versus the 94% identical hepatic cytochrome P450 CYP2A6 (CYP2A6), which does not efficiently metabolize NNK. These investigations identified the structural features of benzylmorpholine analogs responsible for selective binding and inhibition of CYP2A13 versus CYP2A6, leading to the determination of structure-activity relationships for the benzylmorpholine scaffold. Docking and X-ray crystallography studies were further employed to identify the atomic-level interactions between benzylmorpholine analogs and CYP2A13 but were hampered by apparent binding in multiple orientations. Nevertheless, these results could be used to design additional selective and potent CYP2A13 inhibitors for reducing the risk of lung cancer in tobacco users who are unable, unwilling, or in the process of ceasing tobacco use.

In a similar pursuit to identify inhibitors of CYP17A1 for the treatment of prostate cancer, it became important to evaluate the selectivity of potential drug candidates against obvious counter-targets. CYP21A2 is involved in the biosynthesis of glucocorticoids and mineralocorticoids and has overlapping substrates with CYP17A1. CYP11B1 follows CYP21A2 in the steroid biosynthetic pathway and is also a counter-target for the development of CYP17A1 inhibitors. Additionally, CYP11B1's crucial role in cortisol production also presents this enzyme as an independent therapeutic target for the treatment of Cushing's disease resulting from cortisol overproduction. However, biochemical studies for both human CYP21A2 and CYP11B1 have been limited by protein availability. Human CYP21A2 was successfully cloned, expressed, purified, and crystallized for the first time, which allows for structural and functional studies of the human enzyme. CYP11B1 was also successfully cloned and expressed, but more optimization is necessary for consistent large-scale expression and purification. This work provides the necessary groundwork for a biochemical and biophysical understanding of both

CYP21A2 and CYP11B1 for the evaluation of these enzymes as counter-targets. In addition these studies could lead to the rational design of CYP11B1 inhibitors for the treatment of cortisol dependent diseases.

Acknowledgements

I am extremely grateful to everyone that has helped me throughout my graduate career. First, I would like to thank Dr. Kelin Li, Patrick Porubsky, Dr. Benjamin Neunswander, and John Kim for their contributions to my research, which are noted in the respective chapters. Next, I would like to thank all of the past and present Scott lab members: Melanie Blevins, Patrick Porubsky, Dr. Andi Skinner, Dr. Kathy Meneely, Dr. Fernando Estrada, Dr. Agnes Walsh, Dr. Natasha DeVore, Eva Stephens, Elyse Petrunak, Michelle Jackson, Lindsay Astleford, and Aaron Bart. Thank you for your encouragement, insights, and daily conversations that made working in the Scott lab such an enjoyable place. In particular, I am grateful to Dr. Natasha DeVore for her patience in reading numerous abstracts and editing parts of this dissertation.

I am also grateful to Dr. Jane Aldrich, Dr. John Karanicolas, Dr. Audrey Lamb, Dr. Thomas Prisinzano for serving on my committee. Thanks are also due to Dr. Jeff Aube and Dr. Frank Schoenen for their guidance in the design of the benzylmorpholine library. I am especially thankful to Dr. Emily Scott for her encouragement and guidance. She has truly been a wonderful mentor during my graduate career.

My research and time in graduate school would not have been possible without multiple funding sources. This work was funded by the Kansas Masonic Cancer Research Institute, University of Kansas General Research Fund, NIH grant NIGMS GM076343, and the Institute for Advancing Medical Innovation. I am also thankful for the NCAA post graduate scholarship, Gretta Jean & Gerry D Goetsch Scholarship, American Foundation for Pharmaceutical Education pre-doctoral fellowship, and the Institute for Advancing Medical Innovation graduate fellowship that have also funded my time at The University of Kansas.

Finally, I am extremely grateful to my friends and family both near and far for all of their love and support during my graduate career. Thank you for sticking by my side through all of the ups and downs.

Table of Contents

List of Figures

List of Tables

List of Schemes

Chapter 1

Introduction

Introduction to Cytochromes P450

Cytochromes P450 (CYP or P450) are heme-containing monooxygenase enzymes that catalyze a variety of reactions including hydroxylations and epoxidations. There are 57 human P450 enzymes and 58 pseudogenes that are divided amongst 18 families and 43 subfamilies. These enzymes metabolize a range of substrates including steroids, xenobiotics, fatty acids, eicosanoids, vitamins, and unknown compounds (Table 1.1).[1] Families 1-3 are primarily responsible for the conversion of exogenous compounds, while families 4 or greater are typically involved in the metabolism of endogenous substrates.[2] Oxidations performed by P450 enzymes are vital for maintaining homeostasis and for clearing toxic or foreign compounds from the body.

Table 1.1. Classification of human cytochromes P450 according to their primary substrates.

Steroids		Xenobiotics		Fatty Acids	Eicosanoids	Vitamins	Orphan	
1B1	17A1	1A1	2C19	2J2	4F2	2R1	2A7	4F22
7A1	19A1	1A2	2D6	4A11	4F3	24A1	2S1	4V2
7B1	21A2	2A6	2E1	4B1	4F8	26A1	2U1	4X1
8B1	27A1	2A13	2F1	4F12	5A1	26B1	2W1	4Z1
11A1	39A1	2B6	3A4		8A1	26C1	3A43	20A1
11B1	46A1	2C8	3A5			27B1	4A22	27C1
11B2	51A1	2C9	3A7				4F11	
		2C18						

P450 enzymes were independently identified by Garfinkel and Klingenberg who observed a pigment that had an absorption maxima at 450 nm when bound to carbon monoxide in a reduced environment (Figure 1.1).[1,3] This was unusual for heme proteins and was later found to be a result of heme ligation via cysteine versus histidine or tyrosine in other heme proteins.

Hence, the name P450 was born, and this unique spectral characteristic is still used to determine the concentrations of P450 enzymes. P450 enzymes are divided into their respective families based upon sequence similarity. A minimum of 40% amino acid sequence identity must be achieved for cytochrome P450 enzymes to belong to the same family (CYP2). Furthermore, sequences with ≥ 55% amino acid sequence identity are considered to belong to the same subfamily (CYP2A).[4] The final number in the name indicates the individual enzyme (CYP2A13).

Figure 1.1. Reduced carbon monoxide difference spectra for a CYP2A enzyme with an absorbance maxima at ~450 nm.

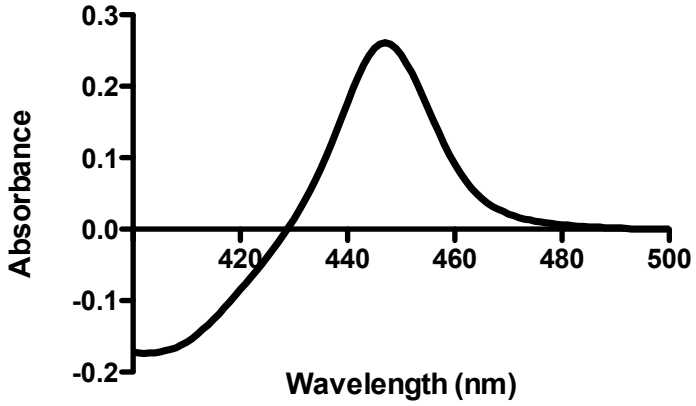

Cytochrome P450 Catalytic Cycle[1]

In order to perform their monooxygenase activity, cytochrome P450 enzymes require the presence of a redox partner. There are two classes of redox systems. Class I redox systems provide electrons via an electron transfer chain consisting of adrenodoxin (Adx) with a single Fe_2S_2 cluster and a NADPH-dependent adrenodoxin reductase (AdR) containing FAD.[1] The

surface of Adx and AdR have complementary charge distributions that facilitate binding to each other through electrostatic interactions.[1] The class I redox system is relevant to mitochondrial enzymes such as the CYP11 and CYP27 families. Class II consists of the NADPH-dependent cytochrome P450 oxidoreductase (POR) that delivers electrons to P450 enzymes anchored in the endoplasmic reticulum.[1] For both class I and class II electron delivery systems, NADPH is the initial source of electrons, delivering a hydride ion to the reductase enzymes for the sequential single electron transfer to cytochromes P450. POR is comprised of an NADPH and FAD binding domain and a FMN domain connected by a linker.[5] POR facilitates the transfer of electrons from NADPH to FAD to FMN and finally to cytochromes P450 for completion of the catalytic cycle. The negatively charged POR redox partner is thought to bind to the proximal side of a cytochrome P450 enzyme, positioning the FMN domain near the heme for electron transfer.[6]

The catalytic cycle involving the activation of molecular oxygen and subsequent incorporation of oxygen to form metabolites involves several steps (Figure 1.2).[1] Cytochromes P450 have an iron protoporphyrin IX coordinated to a cysteine thiolate. In the resting state, the ferric heme iron is bound to a water molecule (State 1). The binding of substrates or inhibitors facilitates two paths, both of which involve the displacement of the water molecule from the sixth coordinate position. Nitrogen-containing inhibitors have the ability to replace water and directly coordinate to the heme iron via the lone pair (State 2). Alternatively, substrates often bind within the active site in such a way as to displace the water molecule (State 3) but do not directly bind iron. This alters the spin state and prepares the enzyme for electron acceptance by altering the electron potential from -300 mV to -170 mV. A NADPH-derived electron is delivered to the heme via POR or Adr, reducing the iron to the ferrous species (State 4).

Molecular oxygen can then bind, forming ferric Fe resulting in a P450-peroxo species (State 5). The P450-peroxo species is further reduced by the delivery of a second electron resulting in the peroxoanion intermediate (State 6), which is then protonated to form the hydroperoxy complex (State 7). Addition of a second proton followed by heterolytic cleavage results in the formation of a water molecule and the reactive iron(IV)-oxo complex (State 8). Hydrogen abstraction from the substrate by the iron-oxo intermediate followed by oxygen rebound results in the transfer of a hydroxyl group to the substrate (State 9) forming a more hydrophilic metabolite that dissociates, enabling a water molecule to bind and complete the catalytic cycle.

There are three points at which the catalytic cycle can be uncoupled. The first point, called the autoxidation shunt, the superoxide anion bound to the ferric enzyme (State 5) is released, returning the protein to State 3. The second process is called the peroxide shunt and occurs at the stage in which the hydroperoxo compound is coordinated to the heme Fe (State 7). Dissociation and protonation of the hydroperoxo compound forms hydrogen peroxide (State 7 to State 3). Finally, the oxidase shunt introduces two electrons and two protons to reduce the ferryl iron-oxo intermediate to water (State 8 to State 3) rather than hydrogen abstraction and substrate oxygenation.[1] These shunts consume reducing equivalents and can generate damaging oxygen species but do not result in productive catalysis of the substrate.

Figure 1.2. Catalytic cycle for cytochromes P450.[1,7]

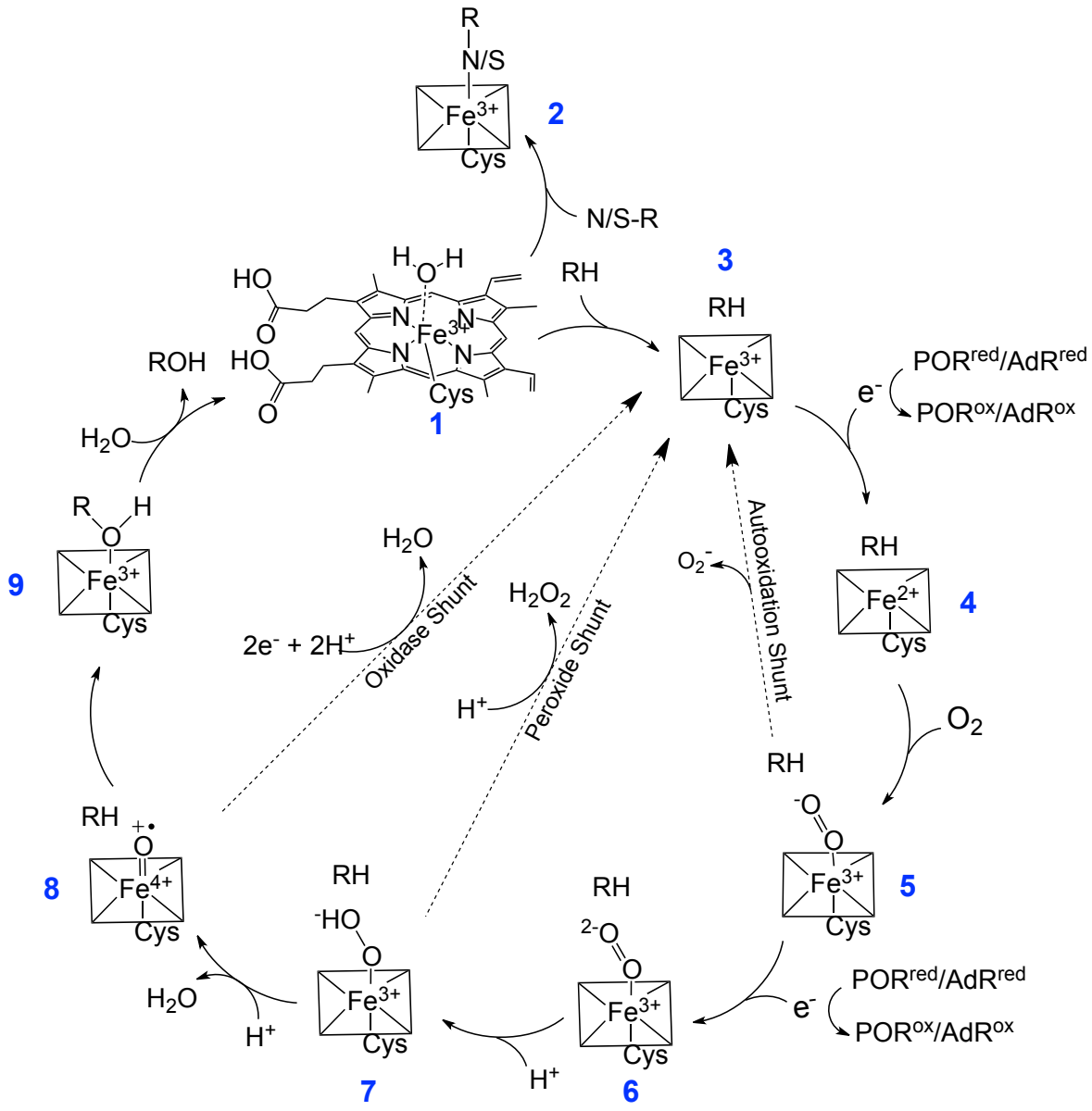

Structural Features of Cytochromes P450

Mammalian cytochromes P450 are membrane bound enzymes located either in the endoplasmic reticulum or mitochondrial membrane. Even with a significant variation in sequence identity, all P450 enzymes maintain a conserved structural fold characterized by 12 major α helices (A-L), 3-4 β sheets, and smaller variable helices designated with a prime symbol (Figure 1.3).[8] One of the more notable helices is the I helix (Figure 1.3, yellow central helix) which spans the length of the protein and serves as one wall of the active site. The heme serves as the floor of the active and interacts with the L helix (red).[1] Active site volumes and topologies vary greatly among P450 enzymes and are dependent upon the placement and mobility of active site amino acid side chains and their surrounding helices. Known structures reveal that the active sites of xenobiotic-metabolizing enzymes can vary from 250 $Å^3$ (CYP2A6 with coumarin, PDB 1Z10)[9] to 1438 $Å^3$ (CYP2C8 with palmitic acid, PDB 1PQ2)[10] and appear to be more flexible as they accommodate a variety of substrates and inhibitors.[8] Although there are fewer structures available of P450 enzymes that metabolize endogenous compounds, it appears that these enzymes may be more rigid than those that metabolize xenobiotic compounds as they have stricter selectivity and have to distinguish between substrates that may differ, for example, by a single hydroxyl group.[8]

To aid in expression and purification, mammalian P450 enzymes are often modified. These modifications have enabled numerous structure/function studies and crystal structures.[11] Native P450 enzymes are anchored to the endoplasmic reticulum or mitochondrial membrane through an N-terminal transmembrane helix composed of ~20 amino acids followed by a proline-rich sequence.[1] Truncation of the N-terminal transmembrane helix in mammalian P450 enzymes prior to this proline rich region is commonly used to generate larger quantities of more

soluble protein for biochemical studies and also often increases expression in *E. coli*.[12] This N-terminal transmembrane helix truncation does not affect intrinsic enzyme activity or the stereo- or regioselectivity of metabolites produced and has been one of the most pivotal modifications in advancing the structural knowledge of human cytochromes P450.[12] However, the truncated enzyme remains associated with the membrane, and detergent is required for membrane extraction. The F′ and G′ helices have the most hydrophobic surface and are thought to compose this second site of membrane association.[1] Additionally, a C-terminal histidine tag is often added to allow for the use of affinity chromatography during purification. The cytochromes P450 discussed in this dissertation have all been engineered with various N-terminal deletions and a C-terminal histidine tag, expressed in *E. coli*, and extracted from the membrane with detergent.

Figure 1.3. Structure of CYP2A13 with an N-terminal truncation. Helices are colored from blue to red starting with the N-terminus. The heme is indicated by the black sticks.

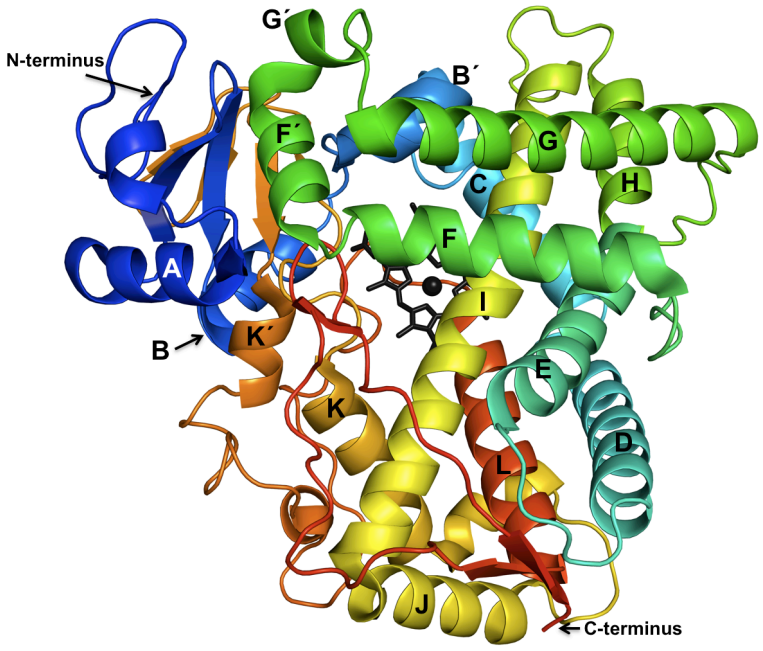

Cytochrome P450 Enzymes and Lung Cancer Chemoprevention Characterization

The first of two project described in this dissertation pertains to the human xenobiotic-metabolizing enzymes cytochrome P450 2A13 (CYP2A13) and cytochrome P450 2A6 (CYP2A6). Cytochromes P450 have always been of pharmacological interest as they are known to metabolize ~75% of drugs currently on the market with the remaining 25% percent being metabolized by flavin-containing monooxygenase, N-acetyltransferase, monoamine oxidase, esterases, and glucuronosyltransferase.[13] Historically, pharmaceutical companies have avoided inhibiting xenobiotic metabolizing P450 enzymes for therapeutic intervention due to the risk of drug-drug interactions.[14] However, there are 15 xenobiotic-metabolizing enzymes with >95% of P450 mediated drug metabolism attributed to only eight enzymes: CYP1A1/2, CYP3A4/5, CYP2C9, CYP2C19, and CYP2D6 (Figure 1.4).[13-15] The selective inhibition of P450 enzymes not involved in drug metabolism is gaining attention as therapeutic targets in multiple areas, and inhibition of the xenobiotic-metabolizing P450 CYP2A13 could pave the way for a new generation of chemopreventative therapeutics.

Figure 1.4 Drug metabolism occurring via cytochrome P450 enzymes is dominated by contributions from eight major enzymes.[16]

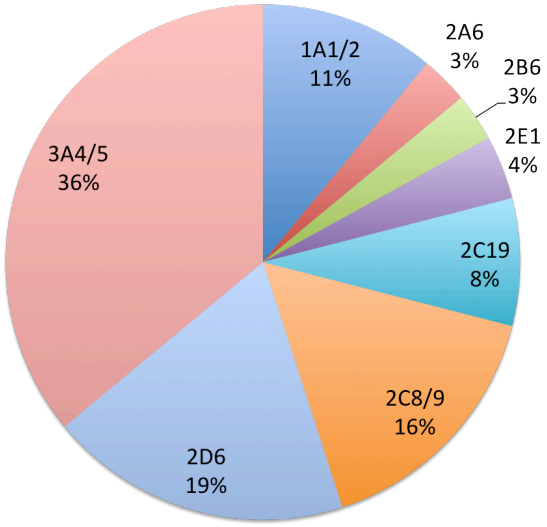

Despite the 1964 surgeon general's warning linking tobacco use to lung cancer,[17] 20% of the U.S. population continues to use tobacco products,[17] and it is estimated that 7 million of the current tobacco users will develop lung cancer.[17] In addition, current chemotherapeutic and surgical lung cancer treatments are not only expensive with patient liability costs of $19,000 - $24,000 per year,[18] but have a low 5-year survival rate of 15%,[19] emphasizing the need for alternative methods such as preventing lung cancer formation. Since 80% of all lung cancer incidence is the result of tobacco use,[20] an obvious solution to reducing the risk of lung cancer would be to cease tobacco use. However, nicotine is highly addictive and current tobacco cessation methods such as nicotine replacement therapy with products such as Nicorette, Nicoderm CQ, and Nicotrol, and pharmaceutical products such as Chantix and bupropion, are successful in only 5% of users.[19] Another solution is to reduce the *in vivo* formation of tobacco

carcinogens. With over 55 reported carcinogens in tobacco products, this task may seem daunting, but targeting downstream effects and individual carcinogens in tobacco products such as benzo[a]pyrene (BAP) and 4-(methylnitrosamino)-1-(3-pyridyl)-1-butanone (NNK) has demonstrated success in reducing the risk of tobacco-initiated lung cancer in animal models.[19,21]

There are two methods by which to approach the chemoprevention of lung cancer. The first method is with a suppressing agent such as myo-inositol, which blocks downstream effects following carcinogen exposure. Myo-inositol is a naturally occurring glucose derivative under clinical development.[22] In early studies, myo-inositol was shown to reduce the development of BAP- and NNK-induced lung tumors or lung tumor multiplicity in mice[23,24] by moderating the serine, threonine Akt kinase pathway involved in cell survival.[25] This compound recently completed phase I clinical trials and is currently in phase II trials.[22]

The second chemopreventative approach consists of a blocking agent, which directly inhibits the formation of carcinogens. Since BAP and NNK are the most prevalent procarcinogens in tobacco products they are prime targets for reducing metabolite formation. However, BAP is metabolized by CYP1A1,[26] which participates in minor drug metabolism and would not be an optimal therapeutic target for inhibition. NNK, on the other hand, is selectively metabolized by CYP2A13, to form DNA alkylating agents that can result in lung cancer. CYP2A13 does not appear to be involved in drug metabolism, and tobacco users with natural occurring polymorphisms resulting in reduced CYP2A13 activity exhibit normal physiological characteristics but have a decreased risk for lung adenocarcinoma.[27,28] Thus, a selective inhibitor of CYP2A13 could reduce the risk of lung cancer in tobacco users.

Animal studies have validated this hypothesis. Mouse studies identified the CYP2A13 ortholog, CYP2A5, as being responsible for NNK bioactivation,[29] and lung-POR-null mice had

decreased NNK-induced tumors, illustrating the role of the respiratory tract in NNK bioactivation.[30] In addition, NNK-induced tumors were reduced in rats from 70% to 5% with the known CYP2A inhibitor, phenethyl isothiocyanate (PEITC),[31] and CYP2A13 inhibition has been correlated to a decrease in NNK metabolite formation and an increase in NNK glucuronidation and excretion.[32] Thus once CYP2A13 is inhibited, an increased amount of NNK is cleared via nontoxic, non-carcinogenic metabolites. However, while PEITC demonstrated promising results in *in vitro* and *in vivo* animal studies, it is not a viable drug candidate due to undesired reactivity in promoting cancer in the urinary tract.[33] Therefore, there is still an unmet need for a selective CYP2A13 inhibitor to reduce the risk of lung cancer in tobacco users who are unable or unwilling to cease tobacco use. In addition, the combination of a suppressing and blocking agent proved twice as efficacious as each agent individually and offers a unique approach to chemoprevention in the future.[19]

One of the major advantages of a selective CYP2A13 inhibitor is that this approach to chemoprevention does not necessarily require tobacco users to alter their habits to reduce their risk of lung cancer. Although this has led to initial opposition, the social and economic benefits should be considered. It is estimated that 70% of tobacco users desire to cease tobacco use but most have been unsuccessful with current cessation aids.[34] In addition to the annual death toll of 6 million individuals worldwide[20] and the expensive treatment cost associated with each new occurrence of lung cancer (patient liability of $19,000-$24,000 per year),[18] it is estimated that all tobacco-related diseases result in an annual loss of over $97 billion due to lost productivity and an additional $96 billion for direct health care costs.[35] Therefore, a blocking and/or suppressing agent could also alleviate some of the significant societal financial burden associated with lung cancer.

The emphasis of this project was the identification and evaluation of small molecule inhibitors of CYP2A13 as chemopreventative agents for lung cancer in tobacco users. High throughput screening was initially used to identify the benzylmorpholine scaffold. Subsequently, a small library composed of both purchased and synthesized benzylmorpholine analogs (Figure 1.5) was evaluated for both binding and inhibition of CYP2A13 versus the 94% identical counter-target, CYP2A6. X-ray crystallography was used to analyze the atomic-level interactions between CYP2A mutant enzymes and select benzylmorpholine analogs.

Figure 1.5. The benzylmorpholine library that was evaluated for the selective inhibition of cytochrome P450 2A13 consisted of 24 individual compounds.

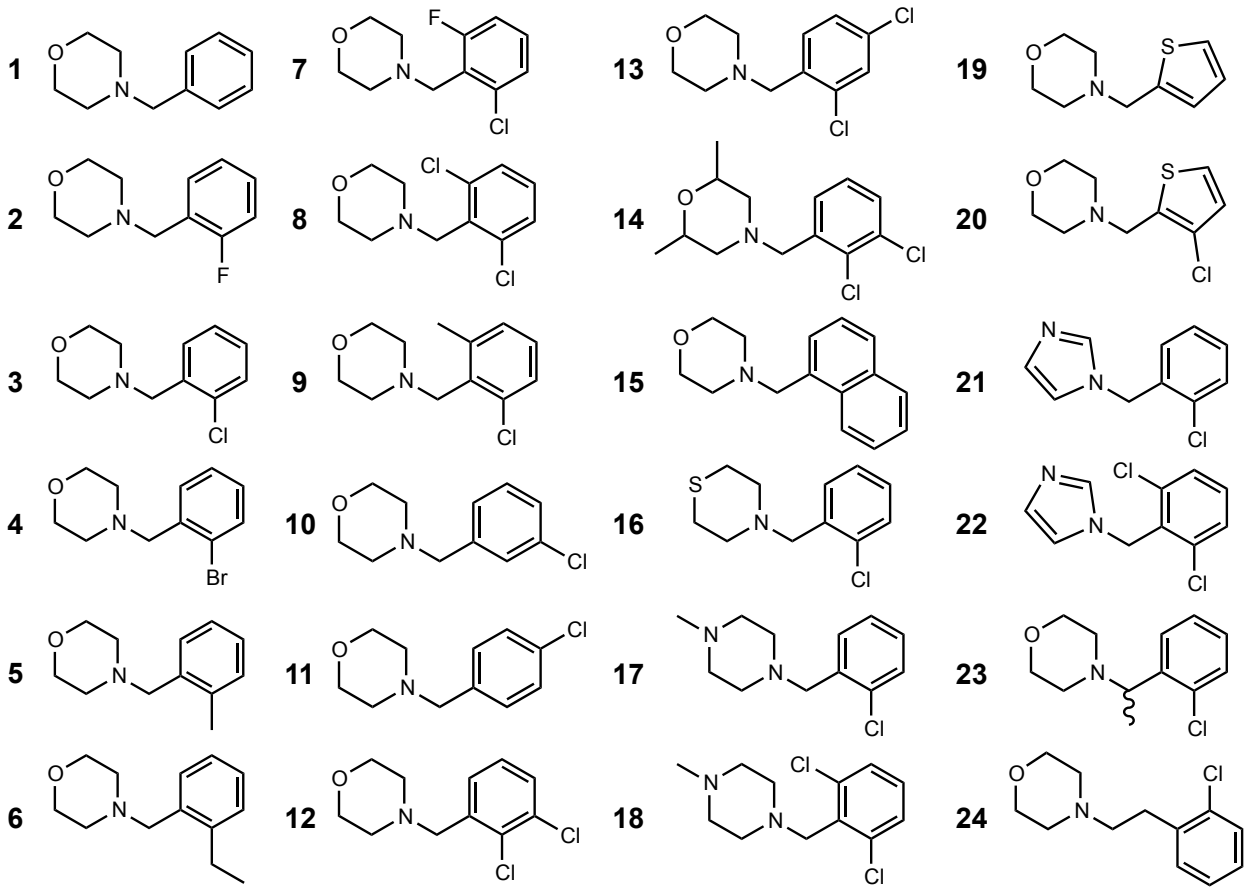

Advancing Knowledge of the Steroid Biosynthetic Pathway for Therapeutic Intervention

The second project in this dissertation transitions from xenobiotic metabolizing P450 enzymes to those involved in the steroid biosynthetic pathway. Specifically, cytochromes P450 11B1 (CYP11B1) and 21A2 (CYP21A2) are involved in the biosynthesis of glucocorticoid and mineralocorticoid steroids. Unlike the P450 enzymes involved in xenobiotic metabolism where deficiencies may go unnoticed until exposure to a particular xenobiotic, aberrant P450 activity in both deficiencies and excessive hormone production in the steroid biosynthetic pathway can have severe physiological repercussions.[14]

There are six cytochrome P450 enzymes involved in the conversion of cholesterol to progestagens, mineralocorticoids, glucocorticoids, androgens, and estrogens (Figure 1.6).[1] Deficiencies in any of these enzymes can have significant downstream effects. Deficiencies in CYP11A1, which is the first step in the pathway and performs a side chain cleavage on cholesterol for the formation of pregnenolone, can lead to the formation of lipoid adrenal hyperplasia.[1,36] CYP17A1 catalyzes multiple reactions required for the formation of glucocorticoids, androgens, and estrogens,[1] and CYP17A1 deficiencies result in excess mineralocorticoid production leading to hypertension and/or insufficient levels of glucocorticoids and sex hormones.[36] CYP19A1 is necessary for the formation of estrone and estradiol.[1] Absence of CYP19A1 can lead to virilization of external genitalia in females and hypervirilization in males.[36] CYP21A2 is necessary for the formation of 11-deoxycorticosterone and 11-deoxycortisol in mineralocorticoid and glucocorticoid biosynthesis, respectively.[1] CYP21A2 deficiencies are responsible for 90-95% of all cases of congenital adrenal hyperplasia (CAH) and result in excess androgen production.[37] CYP11B1 and CYP11B2 also participate in

glucocorticoid and mineralocorticoid production, and deficiencies result in CAH and excess androgen production.[1,36,38]

Figure 1.6. Human steroid biosynthetic pathway. Image courtesy of Dr. Emily Scott and modified from Mikael Häggström's biosynthetic pathway.

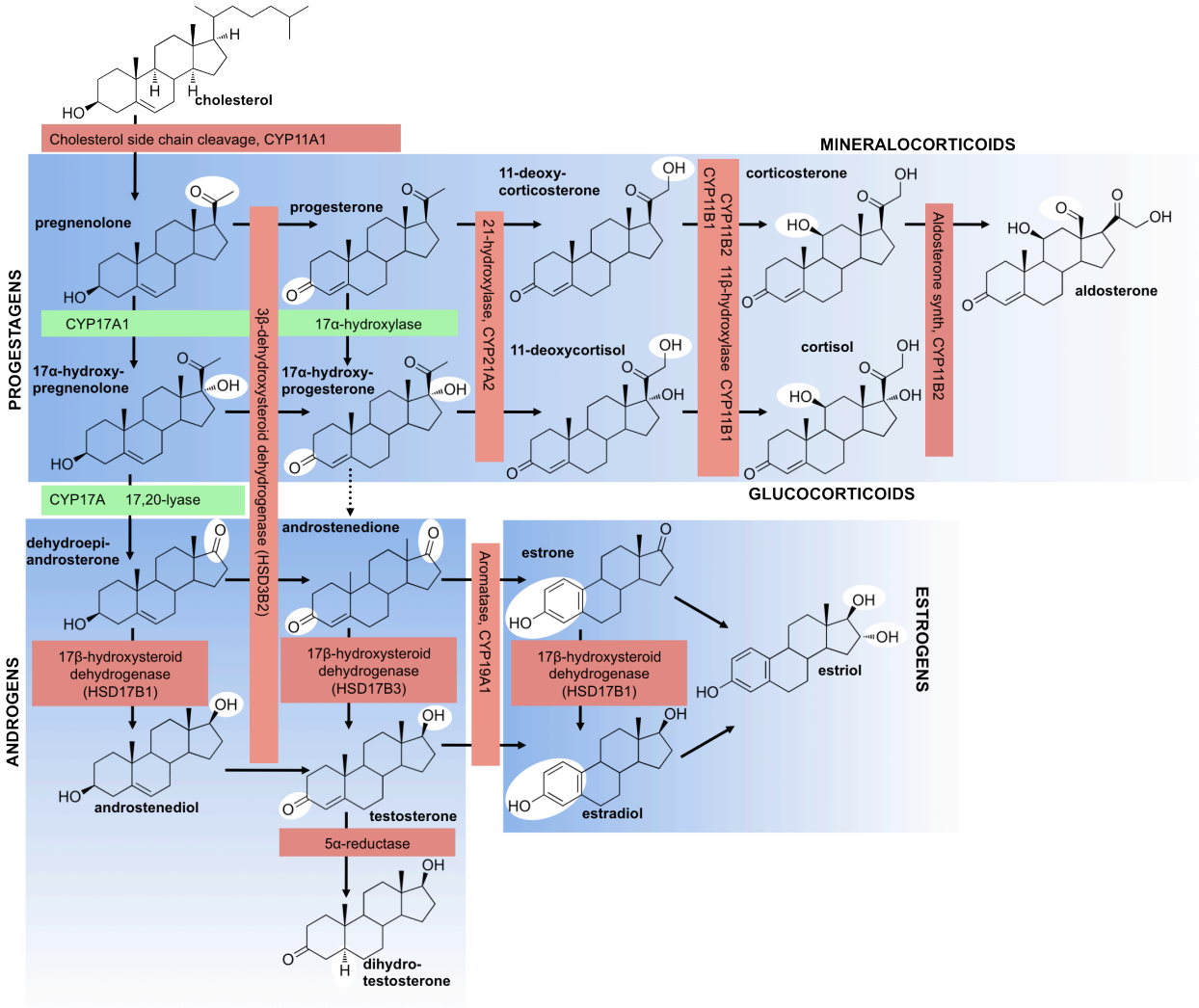

Just as deficiencies in steroidogenic enzyme activity can negatively impact human health, excessive or unwanted signaling resulting in hormone production can also be detrimental. In prostate and breast cancer patients, the roles of CYP17A1 and CYP19A1 in the formation of

androgens and estrogens can enhance cancer growth.[1] In addition, elevated levels of aldosterone mediated by CYP11B2 can contribute to hypertension and congestive heart failure,[39] and overproduction of cortisol by CYP11B1 due to excessive regulator signaling can result in Cushing's disease.[1,38] However, unlike deficiencies, these disease states can often be moderated through inhibitors (Figure 1.7). Abiraterone and TOK-001 have demonstrated success in extending survival times in prostate cancer patients through CYP17A1 inhibition and are becoming preferred over the classical treatment with the non-selective P450 inhibitor, ketoconazole.[40] Tamoxifen has been the gold standard of breast cancer treatment through inhibition of the estrogen receptor, but new entities such as anastrozole, letrozole, and exemestane, which inhibit aromatase (CYP19A1), are becoming more widely used.[41] Ketoconazole and metyrapone have been used to diagnose and treat Cushing's disease resulting from an overproduction of cortisol by CYP11B1,[42-44] and a CYP11B2 inhibitor (LC-1699) is in phase II clinical trials for the treatment of hypertension.[45]

Figure 1.7. Drugs used clinically or in development to inhibit cytochromes P450 involved in the steroid biosynthetic pathway.[40-42] The structure of LC-1699 is not available.

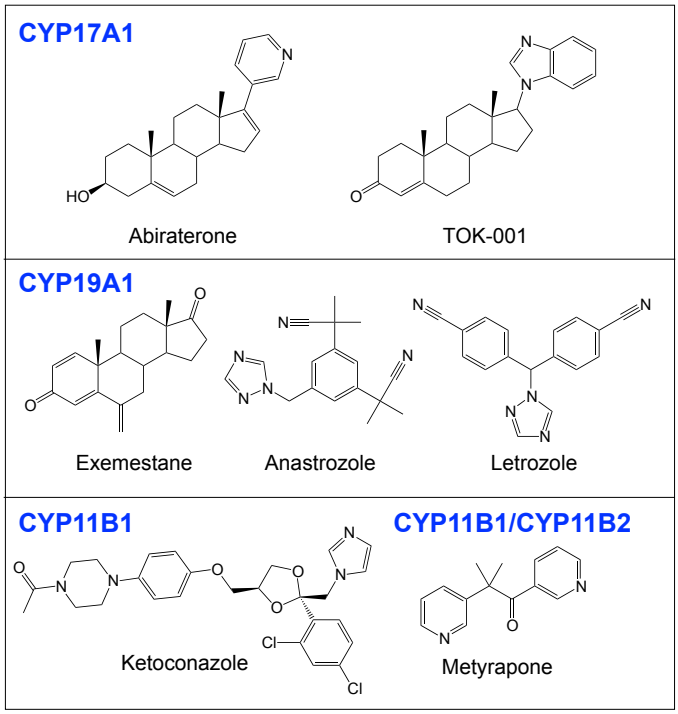

The rational design of selective inhibitors for therapeutic intervention is aided by biochemical studies and structural knowledge of the targets. Recent work in the Scott lab produced the first crystal structure of CYP17A1,[46] and the combination of this structural knowledge with biochemical studies is facilitating the design of novel selective CYP17A1 inhibitors for the treatment of prostate cancer. However, selectivity of potential drug candidates cannot be determined without evaluation against counter-targets in the steroid biosynthetic pathway such as CYP21A2 and CYP11B1. CYP21A2 is of special importance as it has substrate overlap with CYP17A1.[1] Additionally, CYP11B1 is both a counter-target for CYP17A1 inhibitors and a therapeutic target itself for the treatment of Cushing's disease.[44] However, there is a significant deficiency in the biochemical analysis of both human CYP21A2 and CYP11B1

due to the lack of protein availability resulting from enzyme instability or poor protein yields from *E. coli* expression and purification protocols.[47,48]

The goal of my projects with CYP21A2 and CYP11B1 was to further the biochemical and biophysical knowledge for evaluation of these enzymes as counter-targets, and in the case of CYP11B1, as a therapeutic target for the rational design of inhibitors relating to cortisol-dependent diseases. The work described herein lays the necessary groundwork for the biochemical studies and encompasses the cloning, expression, and purification for both CYP11B1 and CYP21A2 in addition to assay development and crystal formation for CYP21A2.

Conclusions

Cytochromes P450 play crucial roles in maintaining homeostasis and clearance of foreign chemicals in the body. While xenobiotic biotransformations performed by these enzymes are typically advantageous in promoting the health of individuals, this is not always the case, as demonstrated by the metabolism of the tobacco procarcinogen NNK to reactive metabolites. The work described in chapters 3 and 4 of this dissertation sheds light on the benzylmorpholine scaffold and its ability to selectively inhibit CYP2A13, and therefore has the potential to reduce the risk of lung cancer in tobacco users.

However, inhibition or reduction of endogenous metabolism in the steroid biosynthetic pathway can have detrimental effects on otherwise healthy individuals, but can be extremely useful in the treatment of cancer. The design of selective inhibitors is aided by the evaluation of the potential drug candidates against counter-targets. Such targeting of enzymes in the steroid biosynthetic pathway has been limited. Unfortunately, biochemical studies on some of these enzymes have been hampered by protein availability. The work in chapters 5 and 6 describes the cloning, expression, purification, and initial metabolic characterization of the human CYP21A2

and CYP11B1 enzymes, which are involved in the production of mineralocorticoids and glucocorticoids and are important counter-targets for CYP17A1. The study of both endogenous and exogenous metabolizing cytochrome P450 enzymes contributes to the knowledge of a structurally similar yet metabolically diverse class of enzymes and has the potential to facilitate the rational design of drug candidates for advanced therapy in the treatment of metabolic disorders.

References

1. *Cytochrome P450: Structure, Mechanism, and Biochemistry*, (Kluwer Academic/ Plenum Publishers, New York, 2005).
2. Stark, K. & Guengerich, F.P. Characterization of orphan human cytochromes P450. *Drug Metab Rev* **39**, 627-37 (2007).
3. Estabrook, R.W. A passion for P450s (rememberances of the early history of research on cytochrome P450). *Drug Metab Dispos* **31**, 1461-73 (2003).
4. Nelson, D.R. Cytochrome P450 nomenclature, 2004. *Methods Mol Biol* **320**, 1-10 (2006).
5. Aigrain, L., Pompon, D., Morera, S. & Truan, G. Structure of the open conformation of a functional chimeric NADPH cytochrome P450 reductase. *EMBO Rep* **10**, 742-7 (2009).
6. Porubsky, P.R., Meneely, K.M. & Scott, E.E. Structures of human cytochrome P-450 2E1. Insights into the binding of inhibitors and both small molecular weight and fatty acid substrates. *J Biol Chem* **283**, 33698-707 (2008).
7. Guengerich, F.P. & Johnson, W.W. Kinetics of ferric cytochrome P450 reduction by NADPH-cytochrome P450 reductase: rapid reduction in the absence of substrate and variations among cytochrome P450 systems. *Biochemistry* **36**, 14741-50 (1997).
8. Johnson, E.F. & Stout, C.D. Structural diversity of human xenobiotic-metabolizing cytochrome P450 monooxygenases. *Biochem Biophys Res Commun* **338**, 331-6 (2005).
9. Yano, J.K., Hsu, M.H., Griffin, K.J., Stout, C.D. & Johnson, E.F. Structures of human microsomal cytochrome P450 2A6 complexed with coumarin and methoxsalen. *Nat Struct Mol Biol* **12**, 822-3 (2005).
10. Schoch, G.A. et al. Structure of human microsomal cytochrome P450 2C8. Evidence for a peripheral fatty acid binding site. *J Biol Chem* **279**, 9497-503 (2004).
11. Barnes, H.J. Maximizing expression of eukaryotic cytochrome P450s in Escherichia coli. *Methods Enzymol* **272**, 3-14 (1996).
12. Williams, P.A. et al. Crystal structure of human cytochrome P450 2C9 with bound warfarin. *Nature* **424**, 464-8 (2003).
13. Guengerich, F.P. Cytochrome p450 and chemical toxicology. *Chem Res Toxicol* **21**, 70-83 (2008).
14. Guengerich, F.P. Cytochromes P450, drugs, and diseases. *Mol Interv* **3**, 194-204 (2003).
15. Wagner, R.L., White, P.F., Kan, P.B., Rosenthal, M.H. & Feldman, D. Inhibition of adrenal steroidogenesis by the anesthetic etomidate. *N Engl J Med* **310**, 1415-21 (1984).
16. Rogers, J.F., Nafziger, A.N. & Bertino, J.S., Jr. Pharmacogenetics affects dosing, efficacy, and toxicity of cytochrome P450-metabolized drugs. *Am J Med* **113**, 746-50 (2002).
17. CDC. Smoking and Tobacco Use. (2012). http://www.cdc.gov/tobacco/
18. Cipriano, L.E. et al. Lung cancer treatment costs, including patient responsibility, by disease stage and treatment modality, 1992 to 2003. *Value Health* **14**, 41-52.
19. Hecht, S.S., Kassie, F. & Hatsukami, D.K. Chemoprevention of lung carcinogenesis in addicted smokers and ex-smokers. *Nat Rev Cancer* **9**, 476-88 (2009).
20. American Chemical Society. Cancer Facts and Figures 2012. (2012). http://www.cancer.org/Research/CancerFactsFigures/CancerFactsFigures/cancer-facts-figures-2012.

21. Hecht, S.S. Tobacco smoke carcinogens and lung cancer. *J Natl Cancer Inst* **91**, 1194-210 (1999).
22. Lam, S. et al. A phase I study of myo-inositol for lung cancer chemoprevention. *Cancer Epidemiol Biomarkers Prev* **15**, 1526-31 (2006).
23. Kassie, F. et al. Inhibition of lung carcinogenesis and critical cancer-related signaling pathways by N-acetyl-S-(N-2-phenethylthiocarbamoyl)-l-cysteine, indole-3-carbinol and myo-inositol, alone and in combination. *Carcinogenesis* **31**, 1634-41 (2010).
24. Witschi, H., Espiritu, I., Ly, M. & Uyeminami, D. The effects of dietary myoinositol on lung tumor development in tobacco smoke-exposed mice. *Inhal Toxicol* **16**, 195-201 (2004).
25. Brognard, J., Clark, A.S., Ni, Y. & Dennis, P.A. Akt/protein kinase B is constitutively active in non-small cell lung cancer cells and promotes cellular survival and resistance to chemotherapy and radiation. *Cancer Res* **61**, 3986-97 (2001).
26. Androutsopoulos, V.P., Tsatsakis, A.M. & Spandidos, D.A. Cytochrome P450 CYP1A1: wider roles in cancer progression and prevention. *BMC Cancer* **9**, 187 (2009).
27. Wang, H. et al. Substantial reduction in risk of lung adenocarcinoma associated with genetic polymorphism in CYP2A13, the most active cytochrome P450 for the metabolic activation of tobacco-specific carcinogen NNK. *Cancer Res* **63**, 8057-61 (2003).
28. Zhang, X. et al. Genetic polymorphisms of the human CYP2A13 gene: identification of single-nucleotide polymorphisms and functional characterization of an Arg257Cys variant. *J Pharmacol Exp Ther* **302**, 416-23 (2002).
29. Zhou, X., D'Agostino, J., Xie, F. & Ding, X. Role of CYP2A5 in the Bioactivation of the Lung Carcinogen 4-(Methylnitrosamino)-1-(3-Pyridyl)-1-Butanone in Mice. *J Pharmacol Exp Ther* **341**, 233-41 (2012).
30. Weng, Y. et al. Determination of the role of target tissue metabolism in lung carcinogenesis using conditional cytochrome P450 reductase-null mice. *Cancer Res* **67**, 7825-32 (2007).
31. Hecht, S.S. et al. Complete inhibition of 4-(methylnitrosamino)-1-(3-pyridyl)-1-butanone-induced rat lung tumorigenesis and favorable modification of biomarkers by phenethyl isothiocyanate. *Cancer Epidemiol Biomarkers Prev* **5**, 645-52 (1996).
32. Morse, M.A., Eklind, K.I., Toussaint, M., Amin, S.G. & Chung, F.L. Characterization of a glucuronide metabolite of 4-(methyl-nitrosamino)-1-(3-pyridyl)-1-butanone (NNK) and its dose-dependent excretion in the urine of mice and rats. *Carcinogenesis* **11**, 1819-23 (1990).
33. Hirose, M. et al. Strong promoting activity of phenylethyl isothiocyanate and benzyl isothiocyanate on urinary bladder carcinogenesis in F344 male rats. *Int J Cancer* **77**, 773-7 (1998).
34. Gilpin, E.A. & Pierce, J.P. Demographic differences in patterns in the incidence of smoking cessation: United States 1950-1990. *Ann Epidemiol* **12**, 141-50 (2002).
35. A clinical practice guideline for treating tobacco use and dependence: 2008 update. A U.S. Public Health Service report. *Am J Prev Med* **35**, 158-76 (2008).
36. Nebert, D.W. & Russell, D.W. Clinical importance of the cytochromes P450. *Lancet* **360**, 1155-62 (2002).
37. White, P.C. & Speiser, P.W. Congenital adrenal hyperplasia due to 21-hydroxylase deficiency. *Endocr Rev* **21**, 245-291 (2000).
38. White, P.C. Genetic diseases of steroid metabolism. *Vitam Horm* **49**, 131-95 (1994).

39. Williams, J.S. & Williams, G.H. 50th anniversary of aldosterone. *J Clin Endocrinol Metab* **88**, 2364-72 (2003).
40. Vasaitis, T.S., Bruno, R.D. & Njar, V.C. CYP17 inhibitors for prostate cancer therapy. *J Steroid Biochem Mol Biol* **125**, 23-31 (2011).
41. Tomao, F. et al. Current role and safety profile of aromatase inhibitors in early breast cancer. *Expert Rev Anticancer Ther* **11**, 1253-63 (2011).
42. Roumen, L. et al. Construction of 3D models of the CYP11B family as a tool to predict ligand binding characteristics. *J Comput Aided Mol Des* **21**, 455-71 (2007).
43. Schoneshofer, M., Schefzig, B. & Oelkers, W. Evidence of adrenal 18-hydroxylase inhibition by metyrapone in man. *Horm Metab Res* **11**, 306-8 (1979).
44. Tritos, N.A. & Biller, B.M. Advances in medical therapies for Cushing's syndrome. *Discov Med* **13**, 171-9 (2012).
45. Calhoun, D.A. et al. Effects of a novel aldosterone synthase inhibitor for treatment of primary hypertension: results of a randomized, double-blind, placebo- and active-controlled phase 2 trial. *Circulation* **124**, 1945-55 (2011).
46. DeVore, N.M. & Scott, E.E. Structures of cytochrome P450 17A1 with prostate cancer drugs abiraterone and TOK-001. *Nature* **482**, 116-9 (2012).
47. Zollner, A. et al. Purification and functional characterization of human 11beta hydroxylase expressed in Escherichia coli. *FEBS J* **275**, 799-810 (2008).
48. Guzov, V.M. et al. [Expression of functionally active hyman cytochrome P-450c21 (CYPXXIA2) in Escherichia coli and single-stage purification of it using metal-affinity chromatography]. *Biokhimiia* **61**, 1758-71 (1996).

Chapter 2

Methods for CYP2A Enzymes

Introduction

The methods used in this dissertation for the production and characterization of cytochrome P450 2A (CYP2A) enzymes and their activities are generally well-established techniques. These techniques were essentially only optimized for current instrumentation. As a result, the methods for these enzymes are aggregated in this chapter. The methods involved in the production and characterization of the steroid cytochrome P450 enzymes 21A2 and 11B1, encompassed original work. This work included method development and optimization in the cloning, expression, and purification protocols and thus can be found in the respective chapters for these individual enzymes.

All assays of cytochrome P450 catalysis required rat cytochrome P450 oxidoreductase (POR). Production of this oxidoreductase was joint between our lab and the COBRE Protein Production Group. Expression of POR was conducted in our lab, by myself and other group members, as were the initial purifications. I later helped transfer the purification procedures to the COBRE Protein Production Group. However, even in this case, the final dialysis, characterization, and standardization of the purified oxidoreductase were performed in our lab by me and occasionally by other group members.

Cytochrome P450 2A Expression and Purification[1,2]

Transformation: A modified, ampicillin resistant pKK233-2 plasmid containing the gene for CYP2A6 or CYP2A13 that had an N-terminal truncation and C-terminal 4X histidine tag was transformed and expressed in tetracycline-resistant Topp3 *Escherichia coli* cells.[1,2] One microliter of pKKCYP2AdH plasmid was incubated with 50 µl of thawed Topp3 *E. coli* cells

(Stratagene, La Jolla, CA) for 30 minutes. Following incubation, the cells were heat shocked for 35 seconds at 42 ˚C to induce DNA uptake, and the competent cells were plated on Luria Bertani (LB) media containing 50 µg/mL ampicillin. Plates were incubated for ~16 hours at 37 ˚C.

Expression: A single colony was inoculated into 5 mL LB broth with 50 µg/mL ampicillin and 25 µg/mL tetracycline and incubated at 37 ˚C for 7-8 hours with shaking at 250 rpm. Following incubation, 50 µl of the culture was transferred to 200 mL LB media with 50 µg/mL ampicillin and 25 µg/mL of tetracycline and incubated overnight at 37 ˚C at 250 rpm. Alternatively, a 200 mL culture can be started from a stab of a glycerol stock containing 800 µl of a previous 200 mL LB growth and 200 µl of sterile 80% glycerol. A glycerol stock enables a bypass of the transformation procedure and was the primary source for starting many cultures in 200 mL of LB media. Fifteen milliliters of the overnight culture was added to sterile 1 L flasks containing 225 mL of terrific broth media (TB media), 25 mL of TB salts, and 50 µg/mL ampicillin. The cultures were incubated at 37 ˚C with shaking at 250 rpm until an OD_{600} of 1.0-1.5 was reached after ~2 hours. After reaching the desired optical density, CYP2A expression was induced with the addition of 240 µg/mL isopropyl β-D-1-thiogalactopyranoside (IPTG). At this time 80 µg/mL of delta aminolevulinic acid (ALA) was also added to promote bacterial heme production. The temperature and shaking were reduced to 30 ˚C and 190 rpm, and the cultures were allowed to grow for ~72 hours before harvesting by centrifugation at 6,500 x g and 4 ˚C for 10 minutes. Cell pellets from the 4.5 L expression were divided between two containers and stored at -80 ˚C.

CYP2A Purification:[1] Purified CYP2A protein was necessary for both assays and crystallography and was achieved by cell lysis with lysozyme, flash freeze, and sonication followed by a three column purification. Harvested cells were thawed and resuspended with

resuspension buffer #1 (20 mM potassium phosphate, pH 7.4, 20% glycerol). Lysozyme was added to the suspension to a final concentration of 0.3 mg/mL and stirred at 4 ˚C for 30 minutes to hydrolyze the 1,4-β-linkages between acetyl-D-glucosamine and acetylmuramic acid in the bacterial peptidoglycan cell wall. The weakened cell wall was subjected to osmotic stress and lysis by the addition of 200 mL of 4 ˚C distilled water with stirring for 10 minutes at 4 ˚C. The solution was centrifuged at 8,700 x g for 15 minutes, and the supernatant was discarded. The pellet was flash frozen in a dry ice - ethanol slurry to further promote lysis. Following flash freezing, a homogenous solution was achieved by resuspending and homogenizing the pellet with a tissue grinder on ice with ~100 mL resuspension buffer #2 (500 mM potassium phosphate, pH 7.4, 20% glycerol, 300 mM NaCl). The resuspension was divided into three 50 mL aliquots and sonicated on ice for 3 x 30 seconds with 1 minute intervals between each round of sonication. Centrifugation at 8,700 x g for 15 minutes separated the P450-containing supernatant from cellular debris. Solubilization of the cytochrome P450 enzyme from membrane lipid was accomplished by adding Cymal-5 detergent (Anatrace, Santa Clara, CA) at two times the critical micelle concentration (CMC) (4.8 mM) to the supernatant and stirring at 4 ˚C for a minimum of 30 minutes. Ultracentrifugation at 4 ˚C and an average speed of 70,400 x g for 1 hour pelleted membrane lipids while the detergent-solubilized CYP2A enzyme remained in the supernatant.

An ÄKTA purification system was utilized to perform the affinity, cation exchange, and size exclusion chromatography. Affinity chromatography with nickel nitrilotriacetic acid resin (Ni-NTA) was the first stage in the chromatography process. Purification was achieved through the interaction between the C-terminal 4X histidine tag and the Ni^{2+} bound to the nitrilotriacetic acid resin. Prior to sample injection, the Ni-NTA resin was equilibrated with two columns of Ni-NTA loading buffer (100 mM potassium phosphate, pH 7.4, 20% glycerol, 0.2 M NaCl, and 4.8

mM Cymal-5). Following sample loading, the Ni-NTA resin was washed with two column volumes of Ni-NTA loading buffer to remove unbound proteins. The bound protein was washed with three column volumes of Ni-NTA 8 mM histidine wash buffer (100 mM potassium phosphate, pH 7.4, 20% glycerol, 0.2 M NaCl, 4.8 mM Cymal-5, 8 mM histidine). This low histidine concentration wash removed weakly bound impurities, while the desired CYP2A protein was subsequently eluted with Ni-NTA 80 mM histidine elution buffer (100 mM potassium phosphate, pH 7.4, 20% glycerol, 0.2 M NaCl, 4.8 mM Cymal-5, 80 mM histidine, and 2 mM EDTA). The high histidine concentration displaced the interactions between the Ni^{2+} and the cytochrome P450 C-terminal histidine tag by competing with CYP2A protein for binding sites on the Ni-NTA resin.

Nickel affinity chromatography was followed by cation exchange with a 5 mL carboxymethyl (CM) cellulose resin. The protein sample was prepared for cation exchange chromatography by diluting the protein collected from affinity chromatography 5-fold with CM wash buffer (5 mM potassium phosphate, pH 7.4, 20% glycerol, and 1 mM EDTA) augmented with 4.8 mM Cymal-5 to reduce the ionic strength. Inclusion of the Cymal-5 in the buffer at this stage was critical as it helped stabilize the protein in the absence of a high salt concentration. After equilibrating the CM column with three column volumes of CM wash buffer, the protein sample was loaded onto the column. The bound protein was washed with 10 column volumes of the low salt CM wash buffer and then eluted with 4 column volumes of a high salt CM elution buffer (50 mM potassium phosphate, pH 7.4, 20% glycerol, 500 mM NaCl, and 1 mM EDTA).

Size exclusion chromatography was the final step in the purification of the CYP2A enzymes and required that the eluted fractions from the CM column were concentrated to approximately 1 mL. The concentration step was necessary as low volume sample injection

result in a tighter protein band as the protein traverses the 120 mL column, which is run with CM elution buffer. All chromatography steps were monitored by UV/Vis absorbance at 280 nm for general protein and at 393 nm and 417 nm for ligand-bound and water-bound P450 enzyme, respectively. The final protein concentration was evaluated by absolute absorption spectra and reduced carbon monoxide difference spectra as described later in this chapter.

Rat Cytochrome P450 Oxidoreductase (POR) Expression and Purification [3]

Purified cytochrome P450 oxidoreductase (POR) is necessary for electron delivery to all cytochrome P450 enzymes to support catalysis and product formation during metabolism assays. Expression and purification were accomplished following published procedures.[3]

Expression: The HMS174 (DE3) cell line (Novagen) and pETOR262 plasmid were used to express rat POR. LB media (100 mL) containing 50 µg/mL kanamycin was inoculated from a HMS174(DE3)/pETOR262 glycerol stock and incubated overnight at 37 ˚C with shaking at 250 rpm. A 0.5 mL aliquot of the overnight culture was transferred to each of eighteen 1 L flasks containing 225 mL of TB media, 25 mL TB salts, and 50 µg/mL kanamycin. These cultures were incubated at 37 ˚C with shaking at 250 rpm until an $OD_{550} > 0.8$ was reached after 4 hours. IPTG at a final concentration of 0.5 mM was used to induce POR expression, and both the incubation temperature and shaking were reduced to 30 ˚C and 190 rpm. Cultures were grown for ~48 hours before harvesting by centrifugation at 6,500 x g and 4 ˚C for 10 minutes. Cell pellets were stored at -80 ˚C.

Purification: Purification was completed at 4 ˚C with a BioRad ECONO system. Harvested cells were thawed and resuspended with 150 - 200 mL buffer A (75 mM Tris pH 8.0, 250 mM sucrose, and 0.25 mM EDTA). Lysozyme was added to a final concentration of 20 µg/mL and stirred at 4 ˚C for 30 minutes to facilitate cell lysis. The suspension was centrifuged at 4400 x g

for 30 minutes at 4 ˚C to pellet the resulting spheroplasts. Pellets were resuspended with 100 mL of affinity buffer (50 mM Tris, pH 7.7, 0.1 mM EDTA, pH 8.0, 0.05 mM DTT, 10% glycerol, and 0.1% Triton X-100) via a tissue grinder on ice. The solution was divided into three 50 mL aliquots on ice and sonicated 10 times for 10 seconds with 20 seconds intervals between each pulse. Combined aliquots were stirred for 3 hours at 4 ˚C to allow sufficient time for optimal reductase solubilization from the membranes by the triton X-100 detergent. The lysis solution was ultracentrifuged at 87,600 x g for 45 minutes at 4 ˚C to pellet membranes. The POR-containing supernatant was diluted to 7 mg/mL in affinity buffer and applied to a 100 mL bed volume of DE-52 resin at 1 mL/min for anion exchange chromatography. Prior to sample addition, the resin was prepared by soaking the DE-52 resin with 8-10 bed volumes of 100 mM Tris, pH 7.7, decanting the solution, and repeating four times. The resin was washed with 10 bed volumes of distilled water and checked to ensure the pH remained at 7.7. The water was decanted and the resin was resuspended in a 1:3 ratio of resin to water solution, which was used to pack the column. Column equilibration was achieved with 500 mL of affinity buffer. Following sample loading, the bound protein was washed with 500 mL of affinity buffer. A 600 mL gradient elution of 0 – 350 mM KCl in affinity buffer was used for elution. The yellow elution fractions were combined and flavin mononucleotide (FMN) was added to a final concentration of 1 μM.

The second and final column was a 2′,5′-ADP sepharose 4B affinity column. The resin was prepared by suspending 1 gram of resin in ~20 mL of water. Once the resin had settled, the water was discarded, and 10 mL of affinity buffer was used to resuspend the resin and pack the column. The column was equilibrated with 120 mL of affinity buffer at 0.5 mL/min, and the protein sample was loaded at 0.15 mL/min. POR-containing yellow fractions eluted with 2-4

mM 2′-adenosine monophosphate were pooled and dialyzed versus 1 L of dialysis buffer (30 mM potassium phosphate, pH 7.7, 20% glycerol, 0.1 mM EDTA, and 2.0 µM FMN) for every 3 L of expression culture. The two rounds of dialysis each had a minimum duration of 8 hours.

Activity of the purified POR was evaluated by monitoring cytochrome c reduction since one unit of POR reduces one micromole of cytochrome c per minute. Two microliters of a 1:50 – 1:100 diluted POR protein sample was added to 978 µL of 300 mM potassium phosphate, pH 7.7, 0.05 mM cytochrome c, and 0.1 mg/mL nicotinamide adenine dinucleotide phosphate (NADPH) in a cuvette. The reaction was monitored at the λ_{max} for reduced cytochrome c (550 nm) on a Shimadzu UV-2501PC UV/Vis Spectrophotometer. The following equation was used to determine the final protein concentration.

$$\frac{(Average\ absorption\ per\ mL)}{21 * 0.002\ mL\ sample} X\ dilution\ factor = \frac{units}{mL} \div 4\ \frac{units}{nmol} = \frac{nmol}{mL}$$

Absolute Absorption Spectra [4]

A UV-2501PC UV/Vis spectrophotometer (Shimadzu Scientific Instruments, Inc., Columbia, MD) was used to determine the concentration of cytochrome P450 present in protein samples. Eight hundred microliters of buffer were pipetted into a 1 cm path length cuvette and placed in the spectrophotometer. The absorbance was zeroed at 700 nm and a baseline scan from 700 - 250 nm was performed prior to the addition of 100 µL of the P450 protein sample. The protein sample was mixed by inversion and the cuvette was reinserted into the spectrophotometer. Absorbance was zeroed at 700 nm and scanned from 700 - 250 nm. A rearrangement of Beers Law to C = (ε x l) / A, where C is the concentration, ε is the absorptivity coefficient of 0.1 $\mu M^{-1}\ cm^{-1}$, l is the path length of 1 cm, and A is the absorbance, was used to determine the micromolar concentration of the P450 protein. The absorbance was based on the

Soret peak maximum between 393 nm – 424 nm, which depended on the liganded state of the protein.

Reduced Carbon Monoxide Difference Spectra [4]

Reduced carbon monoxide difference spectra were used to determine the concentration of cytochrome P450 protein with a λ_{max} = 450 nm, which is the active form, and λ_{max} = 420 nm, which is thought to be a catalytically inactive form. One hundred microliters of protein sample was diluted into 800 µL of buffer, followed by the addition of a few grains of sodium dithionite for enzyme reduction. The reaction mixture was mixed by inversion, and the absorbance was zeroed in a UV-2501PC UV/Vis Spectrophotometer (Shimadzu Scientific Instruments, Inc., Columbia, MD) at 500 nm and across a baseline from 500 - 400 nm. Carbon monoxide was then bubbled through the protein sample until 50 bubbles were observed. The reduced P450 carbon monoxide solution was scanned from 500 – 400 nm and monitored for peak formation at 420 (inactive protein) or 450 nm (active protein). As necessary, scans were repeated over time until the peak at 450 nm no longer increased.

Analysis: The protein concentration was determined using Beer's law in the same manner as the absolute absorption assay with the exception of an extinction coefficient of 0.091 μM^{-1} cm^{-1} was used for the analysis of the 450 nm peak.

Spectral Ligand Binding Assays [5-7]

The spectral properties of cytochromes P450 enable the use of this chromophore in a ligand binding assay. Thus determination of the spectral dissociation constant, K_d, for various cytochrome P450 ligands can be easily measured. Shifts in maximum absorption attributed to the properties of the iron d orbitals and alterations in spin determine the spectral properties that are observed with different ligands. The resting state of the ferric heme has a water molecule

bound at the sixth position and is in a low spin state with a λ_{max} of ~420 nm in the absolute spectrum. Ligands have the ability to displace this water molecule, resulting in spectral shifts indicative of their mode of binding. A type I ligand displaces the water molecule resulting in a high spin pentacoordinate state ($\lambda_{max} \approx$ 393 nm in absolute spectra).[7,8] Ligands with an available nitrogen or sulfur atom can coordinate to the heme iron, replacing the water, and stabilizing the low spin hexacoordinate state. Such ligands are called type II ligands ($\lambda_{max} \approx$ 424 nm).[7,8] Stabilization of this position leads to lower energy and results in the red shift in the spectral peak.[9] There is one additional mode of binding which is classified as a reverse type I. A reverse type I ligand stabilizes the low spin, water bound state and a λ_{max} is observed at 420 nm in difference mode.[10] Titrating a cytochrome P450 enzyme and monitoring the difference spectra can be used to determine the spectral dissociation constant. In the difference spectrum mode, a type I ligand will demonstrate increasing absorbance at approximately 385 nm and decreasing absorbance at 420 nm, while a reverse type I ligand will have opposing increasing and decreasing absorbance at the identical wavelengths. In this difference spectrum mode, type II ligands will have increasing absorbance at 424-435 nm and decreasing absorbance from 390 – 410 nm. In such titrations the concentration of the ligand solvent, often ethanol or dimethylsulfoxide, is maintained below 2% in order to minimize solvent effects on the P450 protein.

CYP2A protein was diluted to a final concentration of 1 μM in 100 mM potassium phosphate buffer. Eight hundred microliters of the protein solution were aliquotted into two cuvettes with a 1 cm path length and placed into the UV-2501PC UV/Vis spectrophotometer (Shimadzu Scientific Instruments, Inc., Columbia, MD) in the sample and reference positions. Absorbance was zeroed at 500 nm and across a baseline from 500 – 300 nm. An absorption scan

from 500 – 300 nm was used to determine the quality of the baseline. If necessary, the baseline procedure was repeated until the absorption at all wavelengths was zero. A titration of the CYP2A protein sample was accomplished by sequential ligand additions to the sample cuvette and a equivalent volume addition of solvent to the reference cuvette. Following each ligand addition, the solution was mixed and equilibrated for 8 minutes at 20 ˚C prior to collection of the spectrum across 500 – 300 nm. Iterative spectra were collected until changes in absorbance maxima and minima were no longer observed.

GraphPad Prism5 (Graphpad Software, San Diego, CA) was used to apply nonlinear least-squares regression fitting was used to determine the K_d with the equation shown below.

$$Y = \left(\frac{\Delta A \max}{2P}\right) * \left(P + L + K_d - \sqrt{(P + L + K_d)^2 - 4 * P * L)}\right)$$

where A_{max} is the maximum absorption, P is the path length, and L is the ligand concentration.

Imidazole-containing compounds were observed to bind very tightly and required modification of both the assay and the analysis. The protein concentration was reduced to 0.1 μM, and cells with a 5 cm path length were used to compensate for the decreased absorbance changes. As above, the absolute difference between the absorbance maxima and minima were calculated from a set of such titration spectra, plotted versus ligand concentration, and fit to determine the spectral equilibrium dissociation constant, K_d. In addition the tight binding equation was used to account for ligand depletion in determining the K_d for these compounds:

$$[ML] = \left(-b + \sqrt{b * b - 4ac}\right) / 2a$$
$$a = -1, \quad b = K_d + L_{total} + A_{max}, \quad c = -1 * L_{total} * A_{max}$$

where [ML] is total binding, K_d is the equilibrium dissociation constant, L_{total} is the total ligand concentration, and A_{max} is the maximum absorption.

Coumarin Metabolism Assay[11,12]

Evaluation of the inhibition constants for the benzylmorpholine library was achieved by monitoring a coumarin metabolism assay. Coumarin is a selective substrate for the CYP2A enzymes and is metabolized to 7-hydroxycoumarin (Figure 2.1).[5] Monitoring the formation of 7-hydroxycoumarin, which is fluorescent, enables an evaluation of the potency and selectivity of the potential benzylmorpholine inhibitors by determining the inhibition constant (K_i) with both recombinant purified CYP2A enzymes.

Figure 2.1. Coumarin metabolism by CYP2A enzymes results in the formation of 7-hydroxycoumarin.

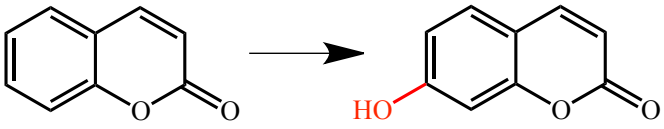

Since cytochromes P450 require the presence of POR for electron delivery during metabolic reactions, the CYP2A enzyme (50 pmol) was first incubated with POR (200 pmol) for 50 minutes on ice to maximize the association of these enzymes. This reconstituted protein system (RPS) was mixed with 0-90 µM coumarin and varying inhibitor concentrations in reaction buffer (50 mM Tris, HCl, pH 7.4 and 5 mM $MgCl_2$). Following a 3 minute incubation at 37 ˚C 1 mM NADPH, the electron source for POR, was added to initiate the catalytic reaction. The 250 µL reaction was allowed to proceed for 10 minutes before being stopped by precipitation of the protein with 75 µl of 10-20% trichloroacetic acid (TCA). Two hundred microliters of buffer and 100 µl of 1.6 M glycine (pH 10.4) were added to each tube to increase the pH of the solutions, followed by centrifugation at 4,400 x g for 6 minutes to pellet the

precipitated protein. Because 7-hydroxycoumarin production was so high from CYP2A6, these samples required an additional 5-fold dilution to avoid overwhelming the High Pressure Liquid Chromatography (HPLC) fluorescence detector.

Standard samples resembled the reaction samples. A concentration range of 7-hydroxycoumarin (0-3 μM for CYP2A13 reactions or 0-20 μM 7-hydroxycoumarin for CYP2A6 reactions) was combined with 10-20% TCA in reaction buffer. These standards were incubated at 37 ˚C for 3 minutes before NADPH addition to a final reaction volume of 250 μL. Following a 10 minute incubation at 37 ˚C, the standards were placed on ice and diluted with 200 μL buffer and 1.6 M glycine before centrifugation at 4400 x g for 6 minutes. Like the samples, standards for the CYP2A6 samples were additionally diluted 5-fold.

Reaction and standard samples were transferred to HPLC vials, and 10 μL of the CYP2A6 samples or 15 μL of the CYP2A13 samples were injected onto a C18 reverse phase 100 mm Luna Column (Phenomenex, Torrance, CA) using a mobile phase consisting of 60% solvent A (0.2% acetic acid) and 40% solvent B (100% methanol) at 0.8 mL/min. Following reverse phase chromatography, the separated reaction components were analyzed through fluorescence detection with an excitation wavelength of 355 nm and an emission wavelength of 460 nm on a Prominence HPLC system (Shimadzu Scientific Instruments, Inc., Columbia, MD), with 7-hydroxycoumarin eluting at 6.3 minutes.

GraphPad Prism5 (Graphpad Software, San Diego, CA) was used to analyze the results with the Michaelis-Menten formula: $Y = \frac{V_{max} * [S]}{K_m + [S]}$ where V_{max} is the maximal velocity, K_m is the Michaelis-Menten constant and [S] is the substrate concentration. The results were further

evaluated based upon their K_m, V_{max}, and mode of inhibition and analyzed with the appropriate formula shown below.

Competitive inhibition: $Y = \frac{V_{max} * [S]}{K_{mObs} + [S]}$ and $K_{mObs} = K_m\left(1 + \frac{[I]}{K_i}\right)$ where $K_{m\ Obs}$ is the observed K_m, [I] is the inhibitor concentration, and K_i is the inhibition constant.

Noncompetitive inhibition: $Y = \frac{V_{max\,app} * [S]}{K_m + [S]}$ and $V_{max\,app} = \frac{V_{max}}{\left(1 + \frac{[I]}{K_i}\right)}$ where $V_{max\ app}$ is the apparent maximal velocity.

Uncompetitive inhibition: $Y = \frac{V_{max\,app} * [S]}{K_{m\,app} + [S]}$, $K_{m\,app} = \frac{K_m}{\left(1 + \frac{[I]}{\alpha K_i}\right)}$, and $V_{max\,app} = \frac{V_{max}}{\left(1 + \frac{[I]}{\alpha K_i}\right)}$

Mixed model inhibition: $Y = \frac{V_{max\,app} * [S]}{K_{m\,app} + [S]}$, $K_{m\,app} = K_m * \frac{\left(1 + \frac{[I]}{K_i}\right)}{\left(1 + \frac{[I]}{\alpha K_i}\right)}$, and $V_{max\,app} = \frac{V_{max}}{\left(1 + \frac{[I]}{\alpha K_i}\right)}$

Unknown metabolite affecting K_i determination

The determination of inhibition constants in recent CYP2A13 data sets has been affected by the formation of a second, unknown product detected in only the lowest substrate sample (5 μM) when no inhibitor was present. This unknown product, which was not present in control samples, unfortunately altered the initial activity, decreasing the slope and subsequently increasing the K_m value. Since the K_m value is used to determine the inhibition constant, the K_i value was significantly impacted. In one example, when Prism5 was used with automatic outlier exclusion analysis, it detected the 5 μM coumarin sample as an outlier, and the K_i value was 19.7 ± 1.2 μM. However, when the 5 μM coumarin point was included, the K_i value was increased to 31.8 ± 3.1 μM. This same trend was observed for two additional data sets where the K_i values

increased from 219.2 ± 18.7 µM to 393.1 ± 49.0 µM and from 2.1 µM to 9.2 µM when the 5 µM coumarin point was included (Figure 2.2). The K_i values reported in this dissertation for compounds **9**, **15**, and **22** (Figure 1.5) excluded the outlier. However, while the 5 µM coumarin sample affects the K_i value, it did not alter overall whether the benzylmorpholine analogs were low or high micromolar inhibitors.

Figure 2.2. Comparison of the A) inclusion and B) exclusion of the 5 µM coumarin sample in the absence of inhibitor with CYP2A13 and **22**. The K_m and K_i values vary between the inclusion or exclusion of the 5 µM coumarin point.

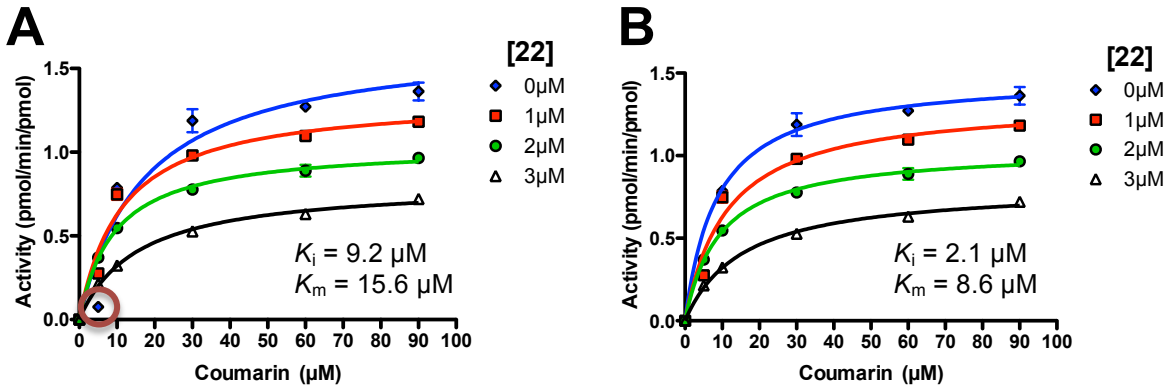

Inhibitors:

High throughput screening of a chemibridge library (36,000 compounds) first identified the benzylmorpholine scaffold as potentially selective CYP2A inhibitors. A small library of purchased and synthesized benzylmorpholine compounds was compiled for evaluation with spectral ligand binding assays and inhibition of coumarin 7-hydroxylation.

Purchased analogs: The benzylmorpholine analogs **4-(2-fluorobenzyl)morpholine (2), 4-(2-chlorobenzyl)morpholine (3), 4-(2-bromobenzyl)morpholine (4), 4-(2-methylbenzyl)morpholine (5), 4-(2-chloro-6-fluorobenzyl)morpholine (7), 4-(2,6-**

dichlorobenzyl)morpholine (8), 4-(2,3-dichlorobenzyl)morpholine (12), 4-(2,4-dichlorobenzyl)morpholine (13), 4-(2,3-dichlorobenzyl)-2,6-dimethylmorpholine (14), 4-(naphthalen-1-ylmethyl)morpholine (15), and **4-(2-chlorobenzyl)thiomorpholine (16)** were purchased from Chembridge Chemicals (San Diego, CA).

Synthesis Procedures: The parent 4-benzylmorpholine compound and remaining analogs were synthesized using one of the following procedures. The synthesis and analytical results for 4-benzylmorpholine (**1**)[13] and 4-(4-chlorobenzyl)morpholine (**11**)[14] were previously reported in the literature and correlated with the compounds that I synthesized. ^{1}H NMR spectra corresponding to the remaining synthesized compounds can be found in the appendix.

*Procedure A***:** Morpholine (1.0 mmol) or methyl piperazine (1.1 mmol) was reacted with 1.1 mmol of the appropriate substituted benzaldehyde reagent with 1.6 mmol triacetoxyborohydride in 5 mL dry tetrahydrofuran. The reactions were stirred under argon for 20 hours at room temperature in a miniblock apparatus (Mettler Toledo Bohdan, Vernon Hills, IL) before quenching with sodium hydroxide, extracting with ether, drying with magnesium sulfate, and solvent removal under vacuum.[15] Scheme 2.1 illustrates the procedure described above.

Scheme 2.1. Synthesis of benzylmorpholine analogs by reductive amination as described in *Procedure A.*

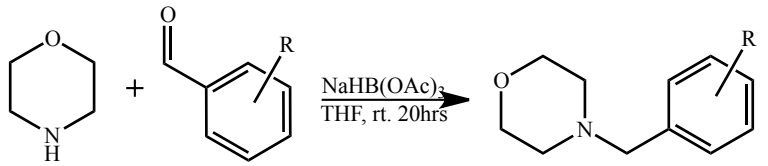

*Procedure B***:**[16] Five millimoles of imidazole was dissolved in 6 mL of dried dimethyl ether under inert gas and combined in a reaction vessel containing 6 mmol sodium hydride on ice. Six and one half millimoles of a substituted (bromomethyl)benzene was added once the temperature

of the reaction was at room temperature, and after 4 hours the product was extracted with ethyl acetate, washed with water, dried with magnesium sulfate, and the solvent removed under vacuum. Scheme 2.2 shows *Procedure B***.**

Scheme 2.2. Synthesis of benzylimidazole analogs through reductive amination as described in Procedure B.

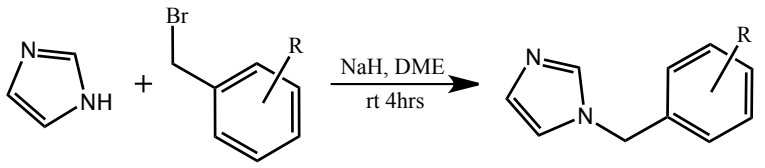

Procedure C: 2-Chlorophenethyl bromide (1.3 mmol), morpholine (1.0 mmol), and potassium carbonate (2.0 mmol) were combined in 4 mL of dry acetonitrile, which were stirred at 80 ˚C overnight. The product was extracted with ethyl acetate, washed with sodium bicarbonate, dried with magnesium sulfate, and the solvent removed under vacuum. Scheme 2.3 provides a summary of the reaction described above.

Scheme 2.3. Synthesis of benzylmorpholine analogs through S_N2 bimolecular nucleophilic substitution.

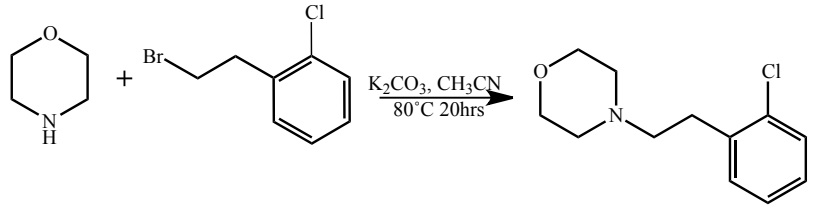

Analysis: All compounds were purified by silica gel chromatography and analyzed by ^{1}H and ^{13}C NMR on a Bruker 400 MHz instrument (Bruker, Billerica, MA) and LCMS on a Waters 2795

HPLC and Waters LCT Premier TOF mass spectrometer (Waters, Milford, MA). MestReNova was used to analyze the ^{1}H and ^{13}C NMR data. Purity was determined by HPLC analysis through monitoring the UV area percent at 214 nm. For the HPLC analysis, an Acquity BEH C-18 column was used with a mobile phase consisting of a 5-95% organic gradient with solvents A (99% water (pH 9.8 ammonium hydroxide), 1% acetonitrile) and B (99% acetonitrile, 1% water) and a flow rate of 0.6 mL/min.

Synthesized Analogs:

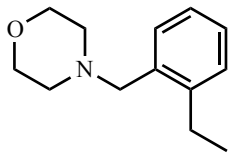

4-(2-Ethylbenzyl)morpholine (6). *Procedure A* with 2-ethylbenzaldehyde afforded the desired oily compound **6** with a yield of 77.9 mg (35%) and a purity of >99.9%. MS (m/z): [M+H] was calculated to be 206.15 and 206.15 was found. Compound **6** had an HPLC retention time of 2.11 minutes. ^{1}H NMR (400 MHz, chloroform-d) δ 7.35 - 7.12 (m, 4H), 3.79 - 3.67 (m, 4H), 3.52 (s, 2H), 2.78 (q, J = 7.5 Hz, 2H), 2.48 (dd, J = 5.8, 3.7 Hz, 4H), 1.27 (t, J = 7.5 Hz, 3H). ^{13}C NMR (101 MHz, $CDCl_3$) δ 143.62, 135.29, 130.18, 128.63, 127.40, 125.38, 67.17, 60.93, 53.73, 25.41, 15.37.

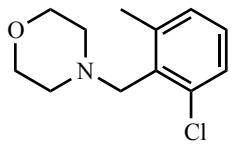

4-(2-Chloro-6-methylbenzyl)morpholine (9). 2-Chloro-6-methylbenzaldehyde and *Procedure A* yielded 55.6 mg (27%) of **9**, which was an oil with 98.0% purity. MS (m/z): [M+H] was calculated to be 226.09 and 226.10 was found, **9** had an HPLC retention time of 2.22 minutes. ^{1}H NMR (400 MHz, chloroform-d) δ 7.31 - 7.19 (m, 1H), 7.14 - 7.07 (m, 2H), 3.73 - 3.60 (m,

6H), 2.57 - 2.49 (m, 4H), 2.47 (s, 3H). ^{13}C NMR (101 MHz, $CDCl_3$) δ 141.02, 135.64, 133.77, 129.00, 128.11, 126.99, 67.22, 56.55, 53.66, 53.27, 19.92.

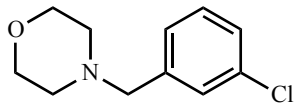

4-(3-Chlorobenzyl)morpholine (10). Compound **10** was synthesized using *Procedure A* and 3-chlorobenzaldehyde resulting in 25 mg (44.7%) of an oil and 97.7% purity. MS (m/z): [M+H] was calculated to be 212.08 and 212.09 was found. The HPLC retention time was 1.67 minutes. ^{1}H NMR (400 MHz, chloroform-d) δ 7.37 (d, *J* = 2.0 Hz, 1H), 7.33 - 7.05 (m, 3H), 3.81 - 3.62 (m, 4H), 3.49 (s, 2H), 2.46 (dd, *J* = 5.7, 3.7 Hz, 4H). ^{13}C NMR (101 MHz, $CDCl_3$) δ 140.06, 134.20, 129.51, 129.06, 127.33, 127.18, 66.97, 62.80, 53.58.

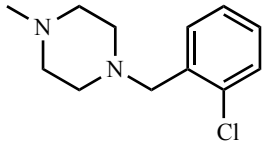

1-(2-Chlorobenzyl)-4-methylpiperazine (17). Compound **17** was synthesized through the use of *Procedure A* with 2-chlorobenzaldehyde to yield an oil with a yield of 168.8 mg (75%) and a purity of 95.6%. MS (m/z): [M+H] was calculated to be 225.11 and 225.12 was found. The HPLC retention time for compound **17** was 1.69 minutes. ^{1}H NMR (400 MHz, chloroform-d) δ 7.49 (dd, *J* = 7.5, 1.9 Hz, 1H), 7.36 (dd, *J* = 7.7, 1.5 Hz, 1H), 7.31 - 7.15 (m, 2H), 3.65 (s, 2H), 2.58 (s, 4H), 2.48 (s, 4H), 2.31 (s, 3H). ^{13}C NMR (101 MHz, $CDCl_3$) δ 135.95, 134.29, 130.65, 129.40, 128.03, 126.52, 59.19, 55.21, 53.13, 46.09.

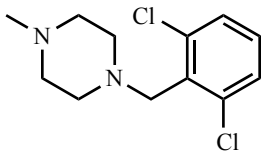

1-(2,6-Dichlorobenzyl)-4-methylpiperazine (18). *Procedure A* was used with 2,6-dichlorobenzaldehyde to synthesize **18**. The result was 184.1 mg (71.0%) of an isolated oil with a purity of ≥99.9%. MS (m/z): [M+H] was calculated to be 259.07 and 259.08 was found. Compound **18** had an HPLC retention time of 1.88 minutes. ^{1}H NMR (400 MHz, chloroform-d) δ 7.26 (d, *J* = 8.0 Hz, 2H), 7.09 (dd, *J* = 8.5, 7.5 Hz, 1H), 3.73 (s, 2H), 2.60 (s, 5H), 2.43 - 2.34 (m, 3H), 2.24 (s, 3H). ^{13}C NMR (101 MHz, $CDCl_3$) δ 136.94, 134.41, 128.69, 128.27, 56.34, 55.14, 52.93, 46.03.

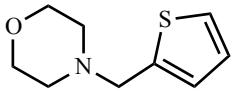

4-(Thiophen-2-ylmethyl)morpholine (19). Thiophene-2-carbaldehyde was used with *Procedure A* to synthesize **19**. The procedure resulted in 130 mg (71%) of an oil with 98.9% purity. MS (m/z): [M+H] was calculated to be 184.07 and 184.08 was found. A retention time of 1.39 minutes was observed with HPLC analysis. ^{1}H NMR (400 MHz, chloroform-d) δ 7.24 (dd, *J* = 5.0, 1.3 Hz, 1H), 6.94 (ddd, *J* = 7.4, 4.4, 2.2 Hz, 2H), 3.75 - 3.68 (m, 6H), 2.53 - 2.45 (m, 4H). ^{13}C NMR (101 MHz, $CDCl_3$) δ 141.12, 126.44, 126.19, 125.18, 66.95, 57.52, 53.32.

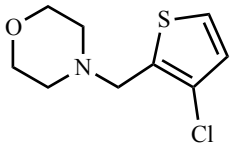

4-((3-Chlorothiophen-2-yl)methyl)morpholine (20). *Procedure A* was used with the reagent 3-chlorothiophene-2-carbaldehyde to afford **20**, which was an oil with a yield of 150 mg (70%) at a purity of ≥99.9%. MS (m/z): [M+H] was calculated to be 218.03 and 218.04 was found.

Compound **20** had an HPLC retention time of 1.72 minutes. ^{1}H NMR (400 MHz, Chloroform-d) δ 7.23 (d, *J* = 5.3 Hz, 1H), 6.87 (d, *J* = 5.3 Hz, 1H), 3.85 - 3.65 (m, 6H), 2.67 - 2.38 (m, 4H). ^{13}C NMR (101 MHz, chloroform-d) δ 133.84 , 127.39 , 124.48 , 123.60 , 66.92 , 54.66 , 53.27 .

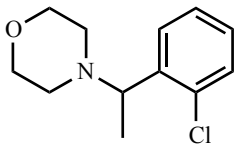

4-(1-(2-Chlorophenyl)ethyl)morpholine (23). *Procedure A* was modified for the synthesis of **23**. 2-Chloroacetophenone (1.1 mmol) was exchanged for a substituted benzaldehyde, and 1.5 mmol acetic acid was added to the reaction. The modified procedure resulted in a low yield of 48.1 mg (21%) of an oil with ≥99.9% purity. MS (m/z): [M+H] was calculated to be 226.09 and 226.10 was found, and this compound had an HPLC retention time of 1.88 minutes. ^{1}H NMR (400 MHz, chloroform-d) δ 7.60 (dd, *J* = 7.8, 1.8 Hz, 1H), 7.35 (dd, *J* = 7.9, 1.4 Hz, 1H), 7.31 - 7.23 (m, 1H), 7.18 (dd, *J* = 7.7, 1.8 Hz, 1H), 3.89 (q, *J* = 6.6 Hz, 1H), 3.72 (dt, *J* = 5.8, 3.6 Hz, 4H), 2.57 (dt, *J* = 9.8, 4.6 Hz, 2H), 2.41 (ddd, *J* = 11.3, 5.8, 3.3 Hz, 2H), 1.31 (d, *J* = 6.6 Hz, 3H). ^{13}C NMR (101 MHz, $CDCl_3$) δ 141.86, 133.61, 129.46, 128.43, 127.74, 126.98, 67.23, 60.46, 51.33, 19.38.

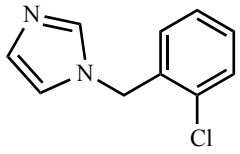

1-(2-Chlorobenzyl)-1*H*-imidazole (21). *Procedure B* was used with 1-(bromomethyl)-2-chlorobenzene to synthesize **21**. Compound **21** was an oil with a yield of 30.7 mg (17%) and ≥99.9% purity. MS (m/z): [M+H] was calculated to be 193.05 and 193.05 was found. Compound **21** had an HPLC retention time of 1.50 minutes. ^{1}H NMR (400 MHz, chloroform-d) δ 7.57 (s, 1H), 7.41 (dd, *J* = 7.7, 1.6 Hz, 1H), 7.33 - 7.18 (m, 2H), 7.10 (s, 1H), 6.99 - 6.88 (m,

2H), 5.23 (s, 2H). ^{13}C NMR (101 MHz, $CDCl_3$) δ 137.63, 134.03, 133.06, 129.81, 129.76, 129.67, 128.95, 119.37, 48.32.

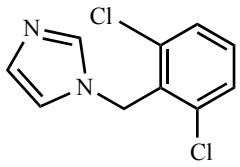

1-(2,6-Dichlorobenzyl)-1*H*-imidazole (22). Compound **22** was synthesized with 2-(bromomethyl)-1,3-dichlorobenzene and *Procedure B*. The resulting product was an oil with a yield of 171.3 mg (75%) and a purity of ≥99.9%. MS (m/z): [M+H] was calculated to be 227.01 and 227.01 was found. Also, a retention time of 1.50 minutes was observed during HPLC analysis. ^{1}H NMR (400 MHz, chloroform-d) δ 7.61 (s, 1H), 7.39 - 7.24 (m, 2H), 7.17 (dd, J = 8.8, 7.4 Hz, 1H), 6.98 (d, J = 14.9 Hz, 2H), 5.33 (s, 2H). ^{13}C NMR (101 MHz, $CDCl_3$) δ 137.57, 136.18, 131.58, 130.60, 129.11, 128.83, 119.10, 45.47.

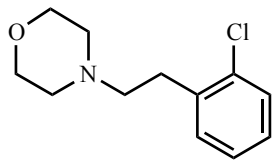

4-(2-Chlorophenethyl)morpholine (24). Compound **24** was synthesized through the use of *Procedure C.* This procedure afforded 129 mg (58%) of an oil with a purity of ≥99.9%. MS (m/z): [M+H] was calculated to be 226.09 and 226.10 was found. Compound **24** had a retention time of 1.77 minutes during HPLC analysis. ^{1}H NMR (400 MHz, Chloroform-d) δ 7.39 - 7.03 (m, 4H), 3.88 - 3.62 (m, 4H), 3.00 - 2.83 (m, 2H), 2.65 - 2.40 (m, 6H). ^{13}C NMR (101 MHz, $CDCl_3$) δ 137.74, 133.98, 130.75, 129.47, 127.61, 126.82, 66.97, 58.73, 53.60, 30.90.

Acknowledgements

I would like to thank Dr. Jeff Aube, Dr. Frank Shoenen, and Dr. Kelin Li at the University of Kansas Center for Chemical Methodologies and Library Design for their aid in designing and guiding the synthesis of the benzylmorpholine library. I am also grateful to Ben Neuenswander and Patrick Porubsky for completing the mass spectroscopy data analysis.

References

1. Smith, B.D. et al. Structure of the human lung cytochrome P450 2A13. *J Biol Chem* **282**, 17306-13 (2007).
2. DeVore, N.M., Smith, B.D., Urban, M.J. & Scott, E.E. Key residues controlling phenacetin metabolism by human cytochrome P450 2A enzymes. *Drug Metab Dispos* **36**, 2582-90 (2008).
3. Shen, A.L., Porter, T.D., Wilson, T.E. & Kasper, C.B. Structural analysis of the FMN binding domain of NADPH-cytochrome P-450 oxidoreductase by site-directed mutagenesis. *J Biol Chem* **264**, 7584-9 (1989).
4. Schenkman, J.B. & Jansson, I. Spectral analyses of cytochromes P450. *Methods Mol Biol* **320**, 11-8 (2006).
5. DeVore, N.M., Smith, B.D., Wang, J.L., Lushington, G.H. & Scott, E.E. Key residues controlling binding of diverse ligands to human cytochrome P 450 2A enzymes. *Drug Metab Dispos* **37**, 1319-1327 (2009).
6. Schlicht, K.E., Michno, N., Smith, B.D., Scott, E.E. & Murphy, S.E. Functional characterization of CYP2A13 polymorphisms. *Xenobiotica* **37**, 1439-49 (2007).
7. Jefcoate, C.R. Measurement of substrate and inhibitor binding to microsomal cytochrome P-450 by optical-difference spectroscopy. *Methods Enzymol* **52**, 258-79 (1978).
8. Schenkman, J.B., Remmer, H. & Estabrook, R.W. Spectral studies of drug interaction with hepatic microsomal cytochrome. *Mol Pharmacol* **3**, 113-23 (1967).
9. Harris, D. & Loew, G. Mechanistic origin of the correlation between spin state and spectra of model cytochrome P450 ferric heme proteins. *Journal of the American Chemical Society* **115**, 5799-5802 (1993).
10. Schenkman, J.B., Cinti, D.L., Orrenius, S., Moldeus, P. & Kraschnitz, R. The nature of the reverse type I (modified type II) spectral change in liver microsomes. *Biochemistry* **11**, 4243-51 (1972).
11. He, X.Y. et al. Identification of Val117 and Arg372 as critical amino acid residues for the activity difference between human CYP2A6 and CYP2A13 in coumarin 7-hydroxylation. *Arch Biochem Biophys* **427**, 143-53 (2004).
12. Rahnasto, M., Raunio, H., Poso, A. & Juvonen, R.O. More potent inhibition of human CYP2A6 than mouse CYP2A5 enzyme activities by derivatives of phenylethylamine and benzaldehyde. *Xenobiotica* **33**, 529-39 (2003).
13. Ohta, H., Yuyama, Y., Uozumi, Y. & Yamada, Y.M.A. In-water dehydrative alkylation of ammonia and amines with alcohols by a polymeric bimetallic catalyst. *Org Lett* **13**, 3892-3895 (2011).
14. Long, T.R., Maity, P.K., Samarakoon, T.B. & Hanson, P.R. ROMP-Derived Oligomeric Phosphates for Application in Facile Benzylation. *Org. Lett.* **12**, 2904-2907 (2010).
15. Abdel-Magid, A.F., Carson, K.G., Harris, B.D., Maryanoff, C.A. & Shah, R.D. Reductive amination of aldehydes and ketones with sodium triacetoxyborohydride. studies on direct and indirect reductive amination procedures. *J Org Chem* **61**, 3849-3862 (1996).
16. de Figueiredo, R.M., Thoret, S., Huet, C. & Dubois, J. Palladium-catalyzed intramolecular arylation of N-benzyl-2-iodoimidazoles: a facile and rapid access to 5H-imidazo[2,1-a]isoindoles. *Synthesis*, 529-540 (2007).

Chapter 3

Benzylmorpholine Structure-Activity Relationships with CYP2A Enzymes

Introduction

The process of drug development begins with the identification of a problem and an understanding of the gaps in current therapeutic strategies. Once these gaps have been identified, alternative methods can be devised for the design and development of novel therapeutic entities. *In vitro* evaluation of drug candidates with the target of interest can lead to the determination of structure-activity relationships (SAR). This process was used to address the problem of lung cancer with the identification and evaluation of small molecules for the selective inhibition of cytochrome P450 2A13.

Lung cancer is the leading cause of all cancer related deaths resulting in over 6 million annual deaths worldwide.[1] The low 5-year survival rate of 15% illustrates the need for alternative therapeutic strategies.[2] Since tobacco use is the cause of 80% of lung cancer incidence,[3] current methods of preventing lung cancer involve tobacco cessation techniques, but these methods are unsuccessful for 95% of users.[2] An alternative strategy that has previously not been commercially explored is to block the activation of tobacco procarcinogens. 4-(Methylnitrosamino)-1-(3-pyridyl)-1-butanone (NNK) is one of the most prevalent procarcinogens in tobacco products and is selectively activated to carcinogens by CYP2A13 in the respiratory tract. Therefore, the selective inhibition of CYP2A13 offers a novel therapeutic strategy in reducing the risk of lung cancer in tobacco users.

CYP2A13 is one of two functional human xenobiotic metabolizing CYP2A enzymes, and is 94% identical to the hepatic CYP2A6.[4] Both enzymes are located on chromosome 19, and while there is an additional CYP2A enzyme, cytochrome P450 2A7, no activity has been

reported for this enzyme.[4] The CYP2A enzymes share activity towards a number of substrates and inhibitors such as nicotine, cotinine, NNK, methoxypsoralen, phenethyl isothiocyanate (PEITC), 2′-methoxyacetophenone, coumarin, and aflatoxin B_1.[5-7] There are only 32 out of 494 amino acids that differ between the CYP2A enzymes, but these differences cause varying metabolic rates for the common substrates listed above.[6-8] Extensive studies have been performed on the differential metabolism of the tobacco procarcinogen NNK as it is selectively metabolized by CYP2A13 and has a significant role in the development of lung cancer.[8-11]

NNK is predominantly formed during the tobacco curing process,[12] but *in vivo* conversion of nicotine to the ring-opened metabolite NNK could also occur (Scheme 3.1).[13] Following exposure, NNK can undergo metabolism at one of two positions by CYP2A13 (Scheme 3.2). First, CYP2A13 performs an α-methyl hydroxylation to form the unstable α-hydroxymethyl-NNK (**26**) intermediate, which spontaneously decomposes to form formaldehyde and 4-(3-pyridyl)-4-oxobutane 1-diazohydroxide (**28**). Intermediate **28** further decomposes to form a 4-(3-pyridyl)-4-oxobutane 1-diazonium ion (**32**) and the stable keto alcohol (**31**) (keto alcohol k_{cat} = 0.646 $min^{-1}\mu M^{-1}$). Alternatively, CYP2A13 performs the α-methylene hydroxylation of NNK to result in an unstable α-methylenehydroxy-NNK (**27**) intermediate, which decomposes to methanediazohydroxide (**29**) and keto aldehyde (**30**) (keto aldehyde k_{cat} = 0.185 $min^{-1}\mu M^{-1}$).[8,9] Methanediazohydroxide further decomposes to a methanediazonium ion (**33**). The two diazonium ions (**32** and **33**) formed from the CYP2A13-mediated hydroxylation reactions of NNK in the respiratory tract are able to form O^6-(pyridyloxobutyl)deoxyguanosine (**34**), 7-(pyridyloxobutyl)deoxyguanosine (**35**), O^6-methyl-deoxyguanosine (**36**), and 7 methyl-deoxyguanosine (**37**) DNA adducts (Scheme 3.2) and result in lung cancer initiation.[9,14] Meanwhile CYP2A6 has a significantly reduced catalytic efficiency of 0.003 $min^{-1}\mu M^{-1}$ for the

α-methylene hydroxylation and no detectable α-methyl hydroxylation,[8] further illustrating the primary role of CYP2A13 in NNK metabolism. Thus inhibiting CYP2A13 in the respiratory tract could reasonably be expected to significantly decrease NNK derived DNA adduct levels in human smokers.

Scheme 3.1. *In vivo* metabolism of nicotine by CYP2A enzymes to form cotinine, nornicotine, or amino ketone, which could result in the formation of NNK.[13]

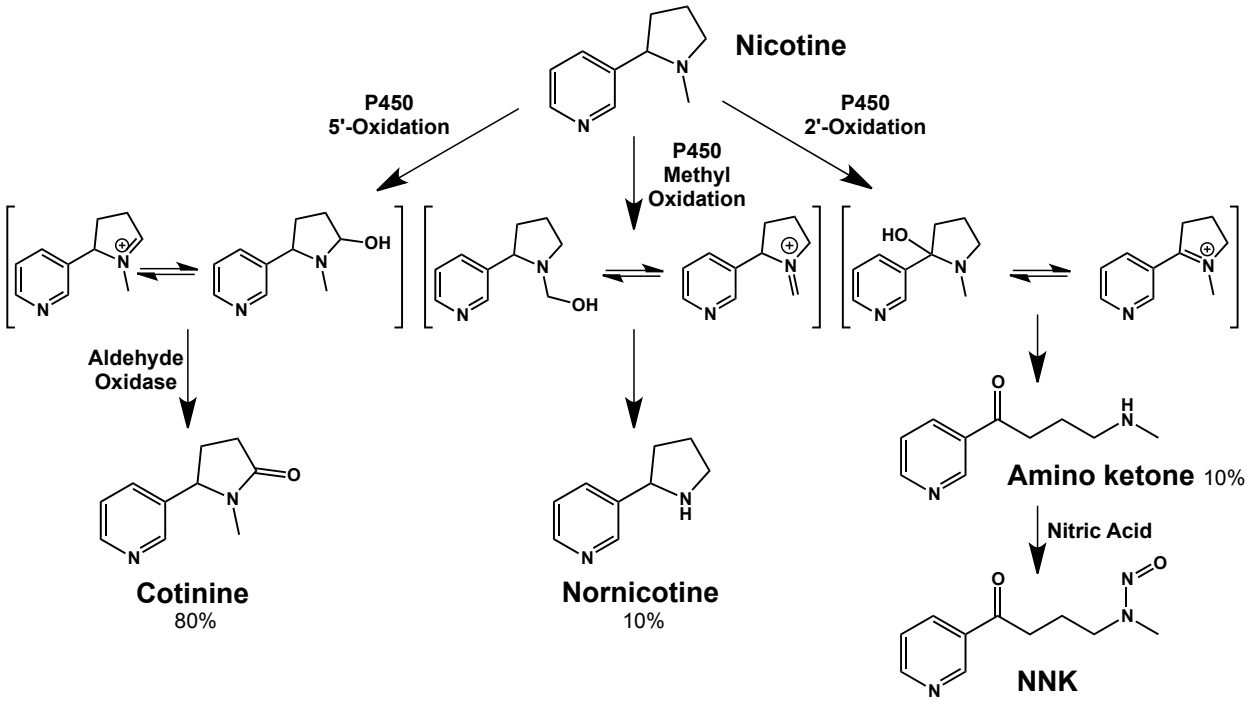

Scheme 3.2. Metabolism of NNK by CYP2A13 results in the formation pyridyloxobutyl (blue) and methyl (red) DNA adducts that can initiate lung cancer.[9]

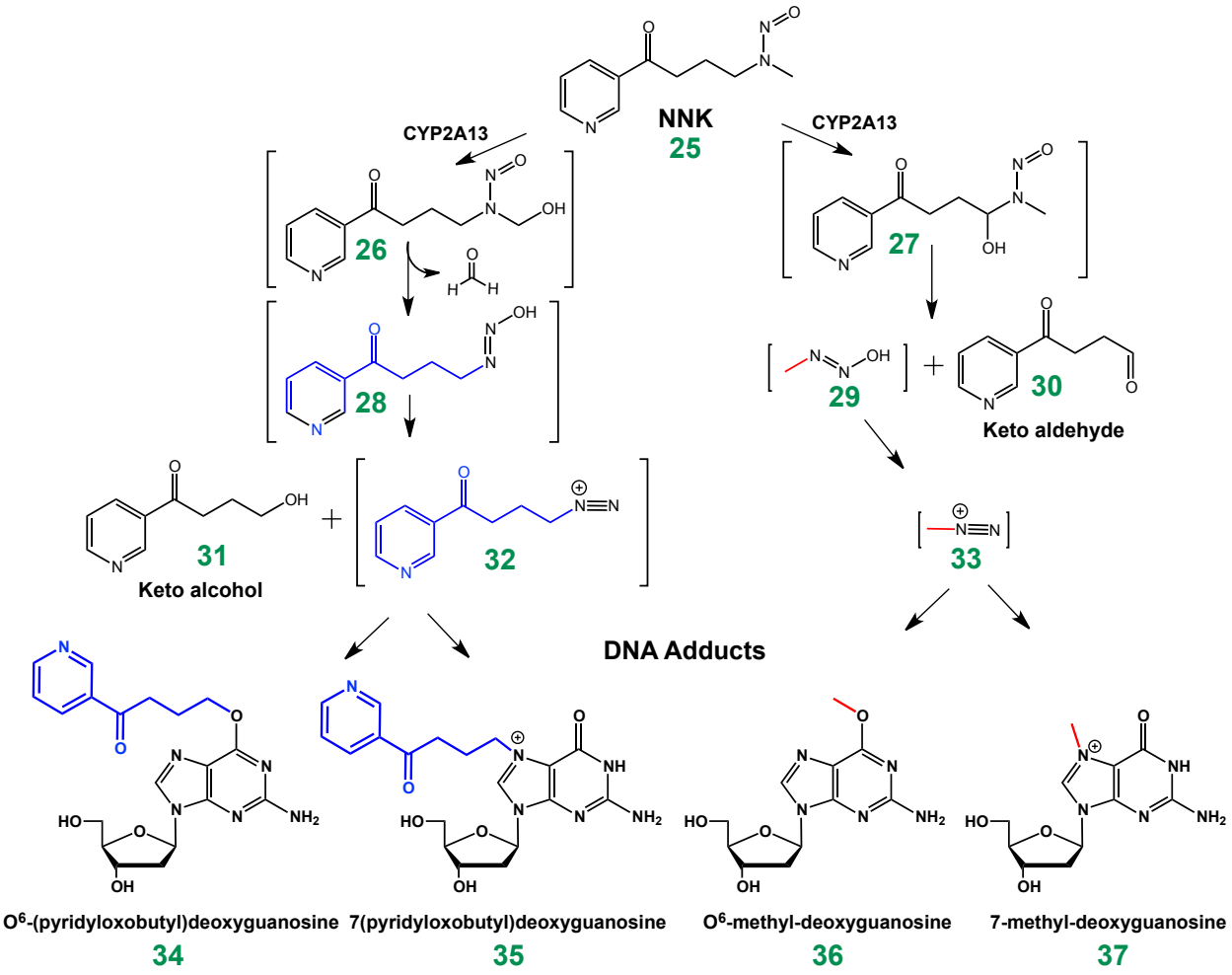

Identifying selective inhibitors is one of the major challenges in drug development, but this is even truer for xenobiotic metabolizing cytochrome P450 enzymes, which have substantial substrate overlap with other P450 enzymes. However, selectivity is vital among cytochromes P450 because non-selective inhibitors increase the risk of adverse drug-drug interactions. Identification of inhibitors and initial selectivity determination for CYP2A13 was achieved by analyzing compounds with both of the CYP2A enzymes, the lung CYP2A13 and the 94% identical hepatic enzyme cytochrome CYP2A6.[4] Although CYP2A6 does not efficiently

metabolize NNK, it does metabolize other xenobiotic compounds and thus its inhibition would be undesirable.[15] It was thought that differentiating between these two very similar enzymes would be the biggest challenge as the other human P450 enzymes are <55% identical and therefore less likely to have substrate overlap with our compounds.

The benzylmorpholine scaffold that is the basis of the compounds examined herein was originally identified by high throughput screening. Three compounds (Figure 1.5 compounds **3**, **5**, and **7**) with this scaffold structure were originally identified as selective inhibitors of CYP2A13 versus CYP2A6. The specific characteristics accounting for this selectivity were unknown. Beginning with the benzylmorpholine scaffold, analogs were purchased or synthesized to generate a small library of 24 compounds to explore the SAR (Figure 1.5). These compounds were evaluated to identify structural features relevant for potent and selective inhibitors of CYP2A13. Specifically, the benzylmorpholine library was evaluated to determine the spectral binding constants (K_d) and inhibition constants (K_i) for the CYP2A enzymes. These results enabled the assignment of structure-activity relationships (SAR) for the benzylmorpholine scaffold with CYP2A13 and thus aid in the rational design and optimization of potential chemopreventative drug candidates.

Materials and Methods

Chemicals and Reagents: Coumarin and 7-hydroxycoumarin were purchased from Sigma Aldrich (St. Louis, MO) and Acros (via Fisher Scientific, Pittsburgh, PA), respectively. Construction of the benzylmorpholine library compounds is described in chapter 2.

Protein Expression and Purification: Recombinant purified CYP2A protein and reductase were produced using the methods described in chapter 2.

Assays: Assays for spectral ligand binding and inhibition of coumarin 7-hydroxylation are also described in detail in chapter 2.

Results

Spectral Dissociation Constants for CYP2A13 and CYP2A6

Titration of CYP2A13 and CYP2A6 with the benzylmorpholine analogs (Figure 1.5 or Table 3.1) demonstrated either type I or type II spectral shifts. Type I spectral shifts occur when a ligand binds in the P450 active site and displaces a water molecule coordinated to the heme iron. The displacement is observed by a transition of the iron from the hexacoordinate low spin state with water bound (λ_{min} = 420 nm) to a pentacoordinate high spin state (λ_{max} = 385 nm) (Figure 3.1A). Compounds **1-20**, **23**, and **24** were type I ligands with CYP2A13 and compounds **2-9**, **12-15**, **17-20**, and **23-24** were type I ligands for CYP2A6. Alternatively, type II binding spectra was observed for **1**, **10**, **11**, and **16** with CYP2A6 and **21** and **22** with both CYP2A13 and CYP2A6. Type II spectral shifts are characterized by a λ_{max} at ~433 nm and a trough at 393 - 413 nm (Figure 3.1B). Type II ligands coordinate to the heme iron resulting in a transition from the hexacoordinate low spin water-bound state to the nitrogen- or sulfur-bound hexacoordinate low spin state.[16]

Figure 3.1 A) Titration of CYP2A13 enzyme with **8**, a classical type I ligand. B) Type II spectral shift observed with CYP2A13 and **21**.

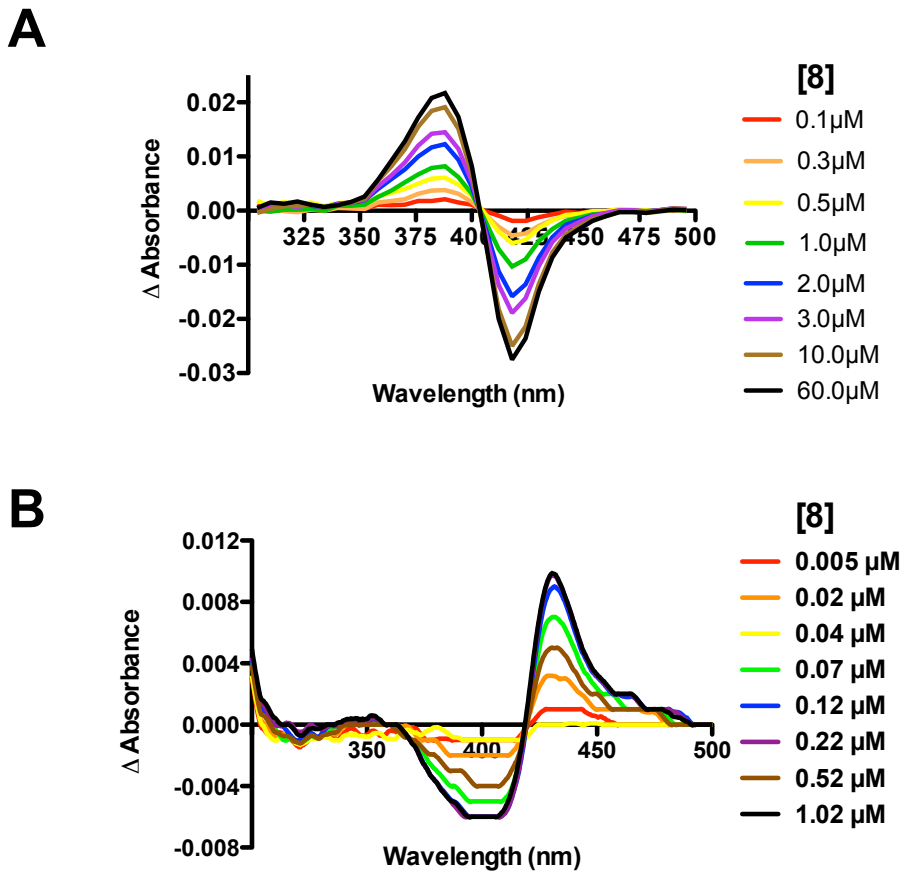

Analysis of the binding spectra of CYP2A6 and CYP2A13 with various benzylmorpholine compounds revealed not only the type of spectral shift, but also the ligand binding constants (K_d) and binding selectivity between the two CYP2A enzymes. Table 3.1 summarizes this information for all 24 compounds.

Table 3.1. Spectral equilibrium dissociation constants (K_d) and inhibition constants (K_i) for the benzylmorpholine library with the human CYP2A6 and CYP2A13 enzymes, along with selectivity ratios for each.[a]

	Compound	Structure	K_d (μM)[b,c]		Selectivity K_d (2A6)/ K_d (2A13)	K_i (μM)[d]		Selectivity K_i (2A6)/ K_i (2A13)
			2A6	2A13		2A6	2A13	
Parent	**1**	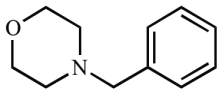	≥300 (I➔II)	116 (I)	≥2.6	329 (C)	477 (C)	0.7
Ortho Substitution	**2**	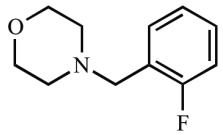	No** Spectral Shift	71.7 (I)	NA	≥1000	379 (C)	≥2.6
	3	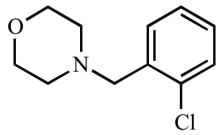	No** Spectral Shift	5.9 ± 3.4 (I)	NA	≥1000	39.7±4.3 (C)	≥25.2
	4	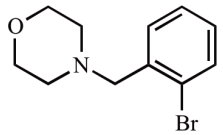	No** Spectral Shift	6.3 (I)	NA	≥1000	17.6±3.1 (C)	≥56.8
	5	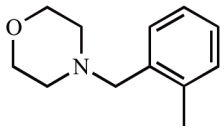	No** Spectral Shift	18.5+ (I)	NA	≥1000	66.9++ (C)	≥14.9
	6	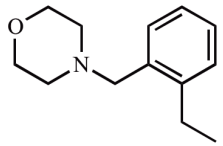	≥575 (I)	4.5+ (I)	128	818.3++ α=13.3 (M)	16.9 (C)	48.4

	Compound	Structure	K_d (μM)[b,c]		Selectivity	K_i (μM)[d]		Selectivity
			2A6	2A13	K_d (2A6)/ K_d (2A13)	2A6	2A13	K_i (2A6)/ K_i (2A13)
Ortho Disubstitution	**7**	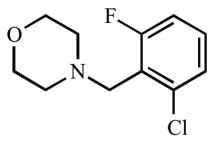	No[**] Spectral Shift	5.2[+] (I)	NA	287 (C)	38.1 (C)	7.5
	8	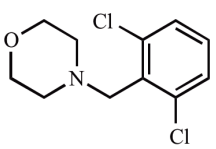	≥522 (I)	1.3[+] (I)	401	237[++] (C)	18.1 (C)	13.7
	9	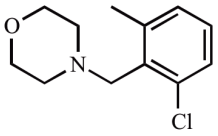	515.0 (I)	1.1[+] (I)	468	296 (C)	19.7±1.2* (C)	15.0
Meta, Para Substitutions	**10**	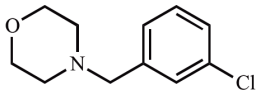	≥400 (I➔II)	69.1±30.2 (I)	≥5.8	352 (C)	260 (C)	1.4
	11	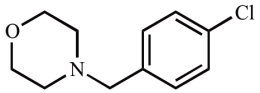	≥245.0 (I)	161.9[+] (I)	≥1.5	448 (C)	458 (C)	1.0
	12	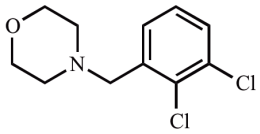	≥305 (I)	30.8 ± 8.1 (I)	9.9	836 (C)	88.9[++] (C)	9.4

	Compound	Structure	K_d (μM)[b,c]		Selectivity	K_i (μM)[d]		Selectivity
			2A6	2A13	K_d (2A6)/ K_d (2A13)	2A6	2A13	K_i (2A6)/ K_i (2A13)
	13	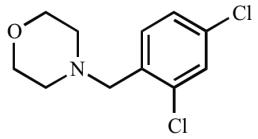	≥198 (I)	34.2 (I)	≥5.8	995.0 (C)	113±14 (C)	8.9
	14	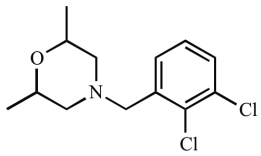	≥462 (I)	37.0 (I)	12.5	≥1000	646 α=19.6 (M)	≥2.6
Ring Analogs	**15**	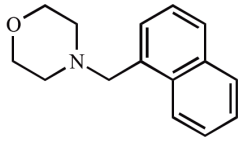	Weak Spectral Shift	41.8*[+] (I)	NA	500[++] α=3.1 (M)	219±18.7* (C)	2.3
	16	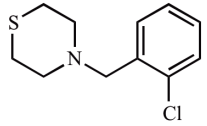	154 (II)	8.3 ± 4.1 (I)	18.6	483[++] α=3.1 (M)	59.0 (C)	8.2
	17	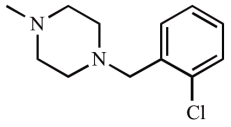	Weak Spectral Shift	306 (I)	NA	≥1000	≥1000	NA
	18	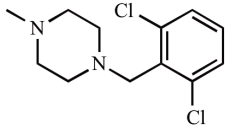	No Spectral Shift	≥362 (I)	NA	≥1000	≥1000	NA

	Compound	Structure	K_d (μM)[b,c]		Selectivity	K_i (μM)[d]		Selectivity
			2A6	2A13	K_d (2A6)/ K_d (2A13)	2A6	2A13	K_i (2A6)/ K_i (2A13)
	19	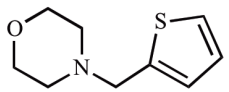	≥464 (I)	30.8^{+} (I)	15.1	270 (C)	131 (C)	2.1
	20	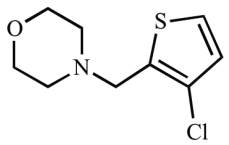	≥239 (I)	10.7^{+} (I)	22.3	433 (C)	54.7 (C)	7.9
	21	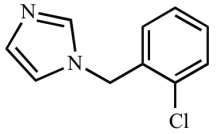	0.1^{+} (II)	<0.1 (II)	≥1.0	2.9 (C)	2.8^{++} α=3.9 (M)	1.0
	22	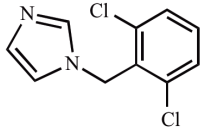	0.9 (II)	<0.1 (II)	≥9.0	0.9 (C)	2.1*,$^{++}$ α=2.0 (M)	0.4

	Compound	Structure	K_d (μM)[b,c]		Selectivity	K_i (μM)[d]		Selectivity
			2A6	2A13	K_d (2A6)/ K_d (2A13)	2A6	2A13	K_i (2A6)/ K_i (2A13)
Linkers	**23**	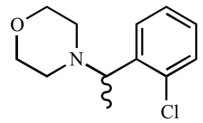	≥538 (I)	7.6 ± 2.8 (I)	≥70.8	98.5 (C)	15.9 (C)	6.2
	24	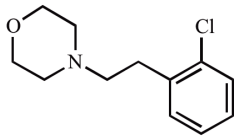	≥604 (I)	160 (I)	≥3.8	≥1000	604 (C)	≥1.7

[a] Standard error is reported for data with ≥ 3 trials, but most data presented as the average of duplicate assays and varied by ≤20%; + individual trials varied by >20% for K_d values; [++] standard error for K_i determination in duplicate was between 21-35%

[b] NA: Not applicable

[c] Spectral shift notes: (I), Type I spectral shift; (II), Type II spectral shift; (I➔II), Change from type I to type II spectral shift at inhibitor concentrations ≥300 μM; ≥ Minimal K_d value, except with **1** and **10** which had spectral shifts at ≥300 nm but no K_d value could be determined; *[+] K_d value from average of duplicate samples with <4% variation, but an additional assay reported a value of 120.6 μM; [**] Evaluated concentrations greater than or equal to the maximum CYP2A13 concentration tested

[d] Inhibition notes: (C), Competitive Inhibitor; (M), Mixed Inhibitor; *Outlier exclusion

The unsubstituted 4-benzylmorpholine parent compound (**1**) bound weakly and rather non-selectively to CYP2A13 and CYP2A6 with K_d values of 116 μM and ≥300 μM, respectively. A K_d value for CYP2A6 with **1** could not be definitively determined due to poor binding and background absorption, but a spectral shift was observed at a ligand concentration of ≥300 μM (Figure 3.2A). In addition, compound **1** was a type I ligand with CYP2A13, but appeared to be primarily a type II ligand of CYP2A6 when the ligand concentration was ≥300 μM. This shift was also observed with **10** (Figure 3.2B). However, in both cases there is little change in absorbance and high background absorbance.

Figure 3.2. Titration of CYP2A6 with A) 4-benzylmorpholine (**1**) and B) **10** indicating a type II spectral shift at concentrations ≥300 μM, but due to weak binding and interference of background absorption, the spectral binding constant could not be determined.

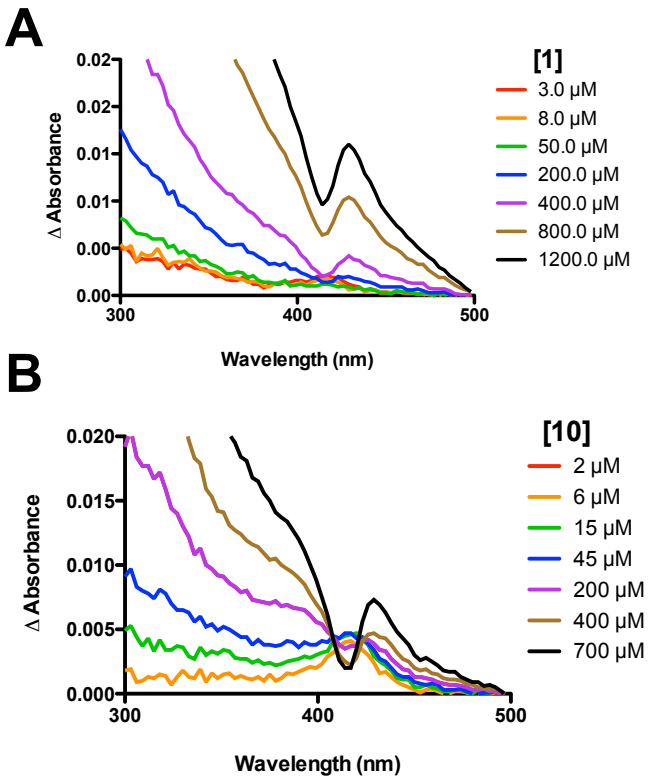

Comparison with the benzylmorpholine parent compound revealed that substitution at the ortho (two) position on the benzene ring was crucial for low micromolar and selective binding to CYP2A13 (Table 3.1, compounds **2-6**). Compounds **2-6** contain substitutions with varying electronegativity, size, and lipophilicity. While the electronegative fluorine atom in **2** increased the affinity for the benzylmorpholine analog with CYP2A13 by 1.6-fold over the parent compound (**1**), it had a decreased affinity for CYP2A13 in comparison to compounds **3-6**. Compounds **3-6** confer low micromolar binding to CYP2A13 ranging from 4.5-18.6 μM. A minimum K_d value of ≥575 μM (**6**) or no observable binding with CYP2A6, as indicated by the lack of a spectral shift (Figure 3.3), was observed at concentrations equivalent to or greater than the maximum concentration tested with CYP2A13. The individual trials for CYP2A13 with compounds **5** (13.8 μM, 23.3 μM) and **6** (3.9 μM, 5.1 μM) had >20% variation, but the values were all in the low micromolar range. A minimum K_d value was reported for **6** because of a poor curve fit when plotting the change in absorption versus ligand concentration. A λ_{max} was observed at 385 nm with a λ_{min} at 420 nm, but an exact K_d value could not be determined. Small changes in absorbance and poorer curve fit were frequently observed for K_d values with CYP2A6 due to poor binding. Thus with the exception of **1** and **10**, a '≥' symbol denotes a minimum dissociation constant for the remainder of the results.

Figure 3.3. Lack of spectral shift during titration of CYP2A6 with benzylmorpholine ligands is indicative that the compounds such as **2-5**, **7**, and **18** do not cause a spectral shift, suggesting that they do not bind in the active site.

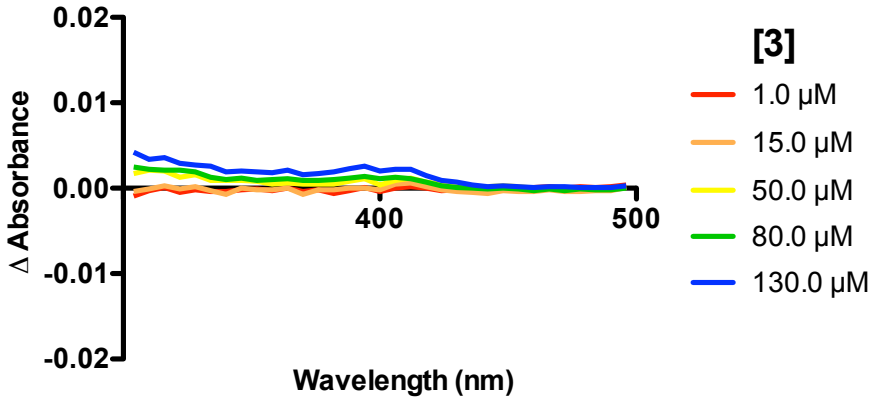

Disubstitution at both ortho positions on the benzene ring (Table 3.1, compounds **7-9**) also demonstrated high affinity for CYP2A13 with K_d values of 5.2 μM (**7**), 1.3 μM (**8**), and 1.1 μM (**9**). Due to the low K_d values, the individual trials for **7** (3.7 μM, 6.6 μM), **8** (1.1 μM, 1.5 μM), and **9** (≤1.0 μM, 1.5 μM) had a variation >20%, but only one value was >5 μM. Additionally, the slight increase in affinity for **8** and **9** over **7** was compensated for by the decreased selectivity for CYP2A13 due to the increased binding of CYP2A6. CYP2A6 had no observable spectral shift with **7** and a K_d value of ~500 μM with **8** and **9**, but these compounds were still >400-fold selective for CYP2A13.

Shifting the chlorine atom around the benzene ring revealed the importance of the ortho substitution in comparison to analogs with substitutions at the meta and para positions (Table 3.1, compounds **10-14**). Substitution at the meta position, **10,** and para position, **11,** both decreased affinity for CYP2A13 with binding constants of 69.1 ± 30.2 μM and 161.9 μM (101 μM and 122 μM for individual trials), respectively, in comparison to the ortho position, **3** (K_d =

5.9 ± 3.4 μM). In addition, increased binding to CYP2A6 was observed with dissociation constants of ≥ 300 μM for **10** and ≥ 245 μM for **11** indicating a decrease in selective binding between the CYP2A enzymes to ≥1.5 and ≥5.8-fold, respectively. The spectral shift for **10** with CYP2A6 mimicked **1** with a transition from a type I to a type II ligand at concentrations ≥300 μM (Figure 3.2B). This same shift was also observed once with **11**, but two out of the three trials for **11** demonstrated only type I binding allowing for the determination of the minimum K_d value of ≥245 μM.

Disubstitution resulting from the combination of an ortho substituent with either meta or para substitution (**12, 13**) increased the affinity and selectivity for CYP2A13 over either the meta or para substituents alone. The K_d values for CYP2A13 were 30.8 ± 8.1 μM for **12** and 34.2 μM for **13**. Titration of CYP2A6 led to dissociation constants of ≥305 μM for **12** and ≥198 μM for **13**, which were 9.9- and 5.8-fold higher, respectively, than the corresponding singly substituted meta (**10**) or para (**11**) compound. Thus these compounds were more selective for CYP2A13, but not as selective as the ortho monosubstituted compounds. Additionally, **13** had significant background absorption with CYP2A6, and the K_d value was determined by the differential absorbance between the λ_{min} at 420 nm and the baseline. The addition of methyl groups on the morpholine ring, **14**, did not decrease the dissociation constant, 37.0 μM for CYP2A13, in comparison to **12**. These results indicated that overall substitution at the meta and para positions oppose selective binding to CYP2A13 with increasing affinity for CYP2A6, while dimethylation on the morpholine ring had no effect.

A series of ring analogs were analyzed to identify additional opportunities to improve selectivity of ligands for CYP2A13 versus CYP2A6 (Table 3.1, compounds **15-22**). A naphthalene analog, **15**, was designed to take advantage of hydrophobic interactions within the

CYP2A13 active site. Compound **15** bound CYP2A13 with a K_d value of 41.8 μM when determined with duplicate samples with less than 4% variation. However, a third assay, which likely used an older inhibitor stock solution, reported a K_d value of 121 μM. Additionally, compound **15** had high background absorption during the titration of both CYP2A13 and CYP2A6 and bound too weakly to CYP2A6, as evidence by a weak spectral shift, to accurately determine a K_d value. The thiomorpholine analog, **16**, had a spectral binding constant of 8.3 ± 4.1 μM with CYP2A13 and was a type I ligand (Figure 3.4A). However, this ligand also bound to CYP2A6 with a K_d value of 154 μM. In contrast to CYP2A13, with CYP2A6 **16** caused a type II spectral shift indicating a direct coordination of the sulfur atom to the heme, which suggests a different binding mode between the two enzymes (Figure 3.4B). Additionally, **16** was the tightest binder to CYP2A6 with the exception of **21** and **22,** but was still 18-fold more selective for CYP2A13. Substitution of the morpholine ring for a methyl piperazine in **17** and **18** added steric bulk and an additional positive charge to the morpholine analog and decreased the affinity for CYP2A13 with K_d values of 306 μM and ≥362 μM, respectively. Compound **17** displayed a weak spectral shift with CYP2A6, but no spectral shift was observed with **18**.

Figure 3.4. Titration of CYP2A enzymes with the thiomorpholine analog, **16**. A) Titration with CYP2A13 resulted in a type I spectral shift, while **16** bound to B) CYP2A6 displays a type II spectral shift.

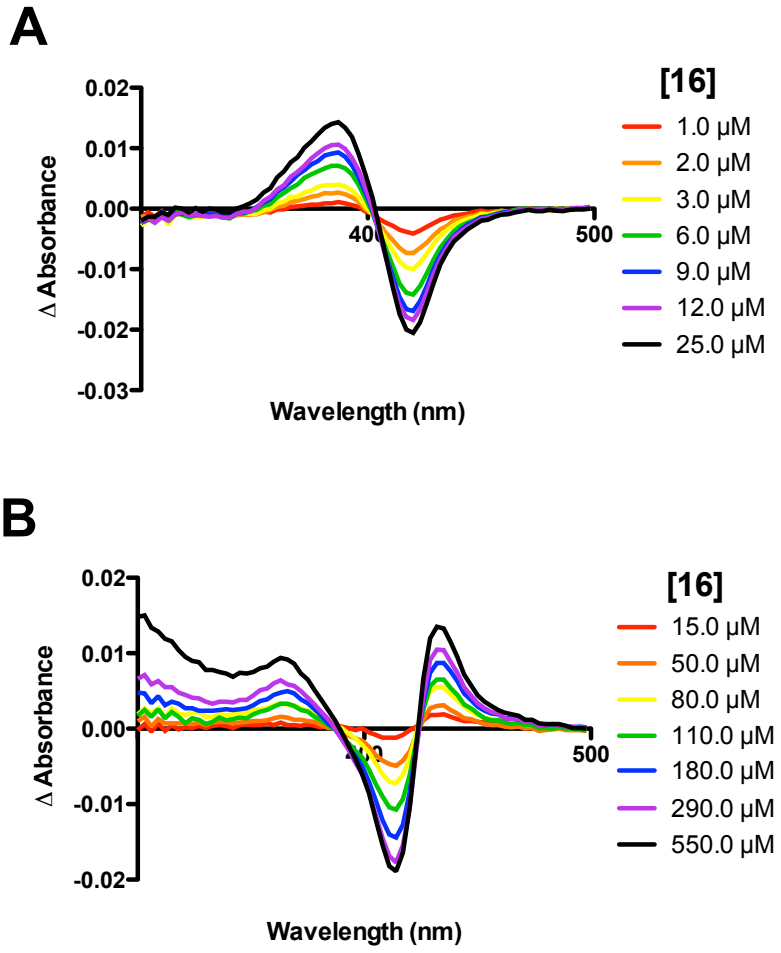

Bioisosteric replacement of the benzene ring with a thiophene ring, **19**, increased the affinity for CYP2A13 over the parent compound, **1**, with a K_d value of 30.8 μM (25.6 μM, 36.0 μM for the individual trials), but had similar affinity to **1** for CYP2A6, K_d = 505 μM. The ortho position of the sulfur may rationalize why **19** has a >3-fold affinity for CYP2A13 versus the parent compound (**1**) even though **19** had the same spatial arrangement. Addition of a chlorine substituent at the ortho position on the thiophene analog, **20**, decreased the spectral ligand binding constant to 10.7 μM (7.5 μM, 14.0 μM for the individual trials) for CYP2A13 but did

not significantly impact the binding to CYP2A6, K_d = ≥239 μM, which resulted in a 22.3-fold selectivity for CYP2A13. Additionally, due to the higher concentrations necessary for the titration of CYP2A6 versus CYP2A13, both **19** and **20** had high background absorbance, and the K_d value for CYP2A6 was determined using only the λ_{min} at 420 nm. The imidazole analogs, **21** and **22**, were chosen because nitrogen-containing inhibitors are known to bind tightly to P450 enzymes through a direct coordination to the heme iron. As expected, compounds **21** and **22** bound tightly to CYP2A13 and CYP2A6 and displayed type II spectral shifts. Equilibrium dissociation constants of ≤0.1 μM were observed with CYP2A13 for both **21** and **22**. However, the binding constants with CYP2A6 were also submicromolar at 0.1 μM (≤0.10 μM and 0.17 μm for the individual trials) and 0.9 μM for **21** and **22**, respectively. Thus, while the incorporation of imidazole for the morpholine ring significantly increases the affinity for CYP2A13 and CYP2A6, selective binding between these enzymes was eliminated.

In order to examine the spatial relationship between the rings and the tolerability of CYP2A13 to bulk on the carbon linker, the remaining analogs had alterations to the carbon linker between the morpholine and benzene rings (Table 3.1, compounds **23-24**). Addition of a methyl group in **23** did not have a significant impact on binding to CYP2A13 (K_d = 7.6 ± 2.8 μM) in comparison to **3**, and **23** bound weakly to CYP2A6 (K_d = ≥538 μM). Expanding the linker to two carbons, **24**, had a negative impact on CYP2A13 binding, increasing the binding constant to 160.4 μM, but this compound still had minimal binding with CYP2A6, K_d = ≥ 604 μM. These results indicate that lengthening the ligand was detrimental for CYP2A13 binding, but additional steric bulk between the rings is tolerated.

Inhibition Constants for CYP2A13 and CYP2A6

Inhibition of CYP2A13 and CYP2A6 was evaluated by monitoring decreases in the formation of 7-hydroxycoumarin resulting from coumarin metabolism. Evaluation of enzyme activity in the presence of a high inhibitor concentration (1 mM) in addition to the determination of preliminary IC_{50} values were used as an initial screen of the benzylmorpholine library and to guide subsequent inhibition studies. Based on the spectral ligand binding assays, it was anticipated that the benzylmorpholine ligands would inhibit CYP2A13, and the determination of IC_{50} values (Figure 3.5) aided in the selection of appropriate inhibitor concentrations for inhibition constant (K_i) determination. However, the generally weak binding of many of the benzylmorpholine compounds to CYP2A6 meant that this library was best evaluated at 1 mM inhibitor concentration with CYP2A6 to enable the prioritization of the library for K_i determination with this enzyme. Additionally, this method was used with CYP2A13 to prioritize compounds such as **1**, **10**, **11**, **15**, **17**, and **24** that bound weakly to CYP2A13 (Figure 3.6). The last three columns of Table 3.1 summarize the K_i values and degree of selectivity for the CYP2A enzymes.

Figure 3.5. For CYP2A13, preliminary IC_{50} values were determined to guide the selection of appropriate inhibitor concentrations for full steady-state inhibition studies with the benzylmorpholine compounds. Data shown below is for the inhibition of CYP2A13 by **4**.

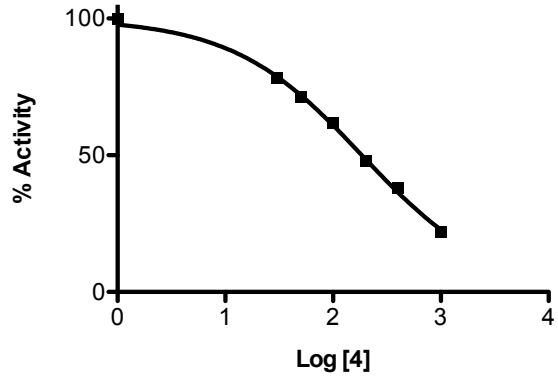

Figure 3.6. Since many benzylmorpholine compounds did not bind with very high affinity to CYP2A6 and occasionally to CYP2A13, compounds were first evaluated to determine inhibition at a single inhibitor concentration (1 mM) to prioritize potent inhibitors and guide further inhibition studies. In this example, inhibitor **15** displays the greatest degree of inhibition with CYP2A13 and would receive the highest priority for inhibition studies.

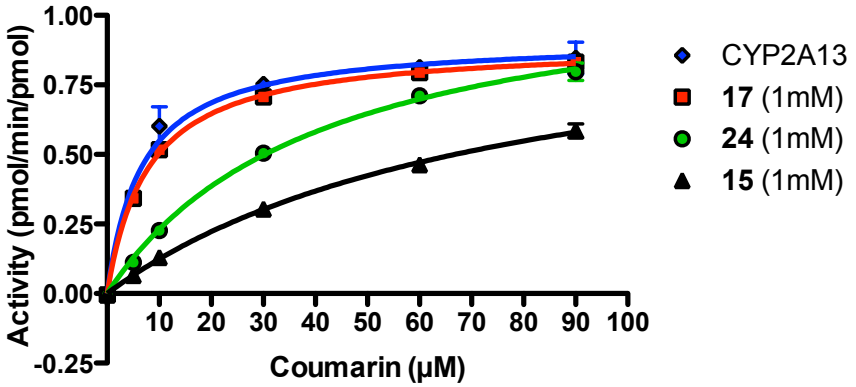

Overall, the trends observed with enzyme kinetics resemble those with the K_d values. The parent compound (**1**) was not selective between the CYP2A enzymes with K_i values of 477 μM for CYP2A13 and 329 μM for CYP2A6. As previously observed, the ortho substitution on the benzene ring was necessary for potent and selective inhibition of CYP2A13. Among compounds **2-6**, compound **2** had the highest dissociation constant and also had the highest micromolar inhibition constant with CYP2A13 (K_i = 379 μM) and minimal inhibition of CYP2A6 (K_i = ≥1000 μM), resulting in a selectivity of ≥2.6-fold for CYP2A13. Compounds **3-6** had inhibition constants ranging from 16.9 μM to 66.9 μM resulting in ~>15-50-fold selectivity for CYP2A13 over CYP2A6 with the most selective compounds sporting a bromine or ethyl substituent at the two position. Disubstitution at both ortho positions maintained low micromolar inhibition with K_i values of 38.1 μM, 18.1 μM, and 19.7 ± 1.2 μM with CYP2A13 for **7-9**, respectively. However, unlike the singly substituted compounds, the disubstitution analogs also better inhibited CYP2A6 with K_i values ranging from 248 μM to 296 μM, thus reducing the selectivity to 7.5 – 15-fold.

Analogs with a substitution on the benzene ring at the meta or para position (**10, 11**) were poor inhibitors of CYP2A13 and CYP2A6 and were not selective for either enzyme. Compound **10** inhibited CYP2A13 with a K_i = 260 μM and CYP2A6 with K_i = 352 μM. Compound **11** had inhibition constants of 458 μM with CYP2A13 and 448 μM with CYP2A6. Disubstitution with a chlorine atom at the ortho position (**12, 13**) somewhat rescued the inhibition activity and selectivity for CYP2A13 with K_i values of 88.9 μM (**12**) and 113 ± 14.0 μM (**13**) for CYP2A13 and 836 μM (**12**) and 995 μM (**13**) for CYP2A6. In this context, the ortho substitutions increased selectivity for CYP2A13 from ~1- to ~9-fold.

The various ring analogs, **15-22**, provided additional information about the benzylmorpholine scaffold. The naphthalene analog, **15**, was a relatively poor inhibitor of both CYP2A13 and CYP2A6 with respective K_i values of 219 μM and 500 μM. Compared to **3**, replacement of the morpholine ring with a thiomorpholine ring (**16)** resulted in decreased inhibition with CYP2A13 (K_i = 59.0 μM) and increased inhibition of CYP2A6 (K_i = 483 μM). As anticipated from the binding studies, the methylpiperizine analogs (**17, 18**) did not inhibit CYP2A13 or CYP2A6 with K_i values ≥1000 μM for both CYP2A enzymes. Inclusion of a chlorine atom at the ortho position on the thiophene analogs (**19**, **20**) increased selectivity for CYP2A13 from 2.1- to 7.9-fold by increasing the inhibition of CYP2A13 from 131.1 μM (**19**) to 54.7 μM (**20**) while simultaneously decreasing inhibition of CYP2A6 from 270 μM to 433 μM, for **19** and **20**, respectively. The imidazole ring substitutions (**21**, **22**) significantly increased the inhibition of CYP2A13 resulting in K_i values of 2.8 μM with **21** and 2.1 μM for **22**, but the selectivity was eliminated as the inhibition constants for CYP2A6 were 2.9 μM and 0.9 μM for **21** and **22**, respectively.

Evaluation of the linker analogs (**23** and **24**) continued with the trend of the inhibition results resembling those from the binding studies. Compound **23**, which had an additional methyl group on the one carbon linker between the morpholine and benzene rings, inhibited CYP2A13 with a K_i value of 15.9 μM which was lower than **3** due to an increase in hydrophobic interactions with CYP2A13. Compound **23** also had an inhibition constant of 98.5 μM with CYP2A6. These results indicated that this compound was a potent inhibitor of CYP2A13 but not as selective as other benzylmorpholine analogs with only a 16-fold preference for CYP2A13 versus ≥25-fold for **3**. Increasing the chain length by one carbon (**24**) decreased the inhibition of

CYP2A13 compared to **3** (K_i = 604 μM) and was also a poor inhibitor of CYP2A6, as indicated by a K_i value of ≥ 1000 μM.

Competitive and Mixed Inhibition

All but six benzylmorpholine analogs were competitive inhibitors of both CYP2A13 and CYP2A6. Compounds **14**, **21**, and **22** were mixed inhibitors of CYP2A13, and compounds **6**, **15**, and **16** displayed mixed inhibition of CYP2A6. Figure 3.7 provides example results of the observed competitive and mixed inhibition. Compounds **6** and **14** had the highest alpha values of 13.3 and 19.6, respectively, indicating these inhibitors bound significantly more tightly to the enzyme (E) state than the enzyme-substrate (ES) state. However, the remaining compounds had alpha values between 2.0-3.9 indicating that binding affinity was more similar for the E and ES states.

Figure 3.7. Representative inhibition of the CYP2A enzymes with benzylmorpholine inhibitors. A) Michaelis Menten kinetics of a competitive benzylmorpholine analog (**3**) with CYP2A13. B) Lineweaver Burk plot of the competitive inhibitor. C) Michaelis Menten kinetics and D) Lineweaver Burk plot results from the mixed benzylmorpholine inhibitor **15** with CYP2A6.

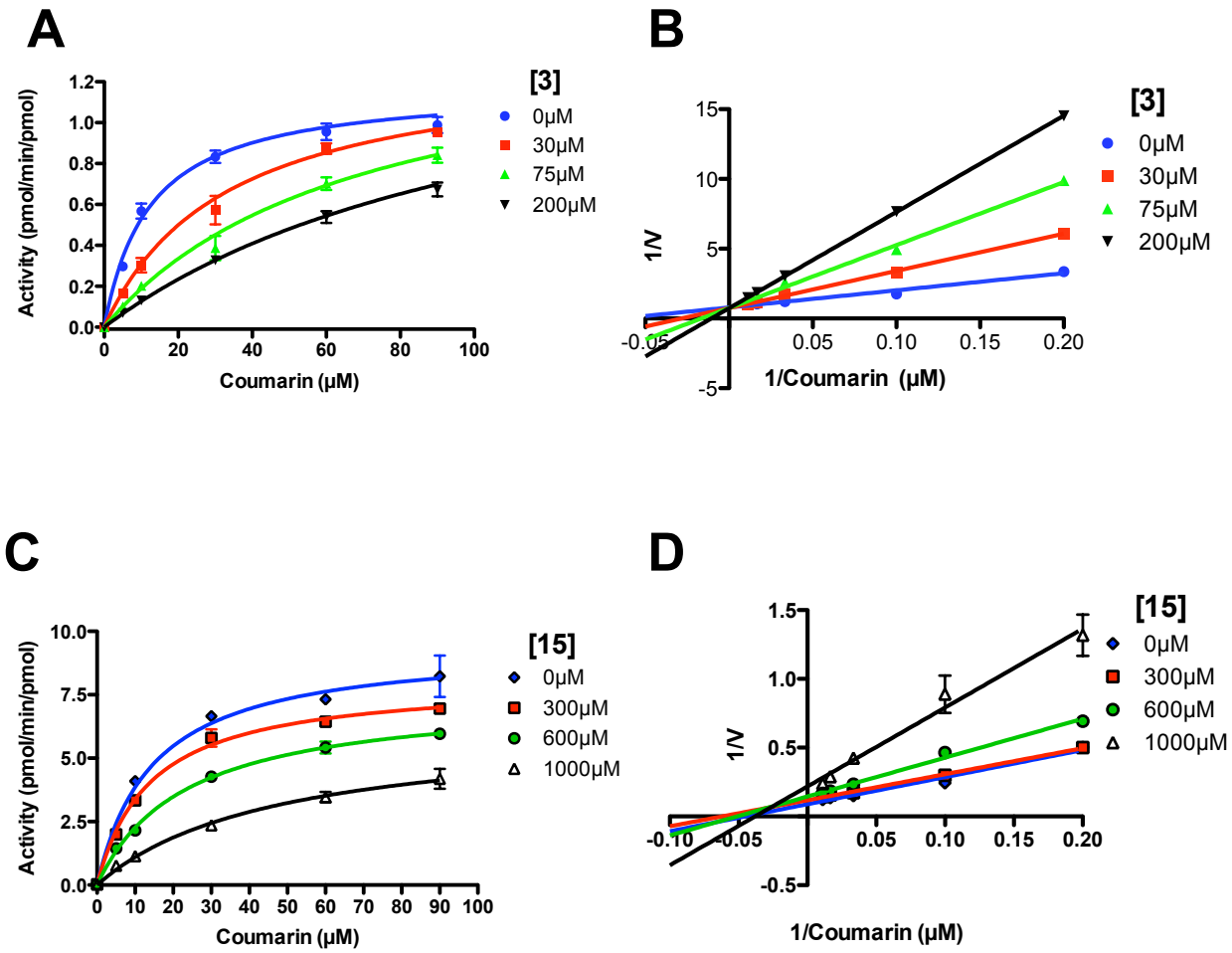

Discussion

Ortho (C2) substitution on the benzene ring

A substituent at the ortho position on the benzene ring proved to be the most vital feature in conferring selective binding and inhibition of CYP2A13 versus CYP2A6. Compounds **3-9,** and **16** illustrated this point with CYP2A13 with K_d values ranging from 1.1 μM – 18.5 μM, K_i values between 16.9 μM – 66.9 μM, and selective inhibition of ~5-≥57-fold for CYP2A13 over CYP2A6. Analysis of the various ortho substituents provides insight into the features contributing to the selectivity of the benzylmorpholine analogs.

In using **1** and **3** as reference compounds, it appears that the size and lipophilicity of the substituent play a major role in selective binding and inhibition of CYP2A13, while electronegativity and inductive effects have a minor role. When comparing compounds **2** and **3**, the fluorine atom in compound **2** is more electronegative, less lipophilic, and occupies a smaller portion of the active site than chlorine. These differences resulted in reduced affinity and inhibition for CYP2A13 with **2** versus **3**. Comparison of **2** versus the parent compound (**1**), which were of similar size, indicated that electronegativity, inductive effects, and overall increased lipophilicity may slightly enhance binding and inhibition as **2** displayed small increases in both affinity and inhibition of CYP2A13. However, with less than a 2-fold difference in the K_d and K_i values, this assumption may not be definitive. Further comparison of compounds **4** and **6** which had either electron withdrawing or electron donating substituents that were comparable in both size and lipophilicity, revealed similar binding and inhibition results to each other and to **3**. These comparisons support the conclusion that the size and lipophilicity of the substituent were more important for interactions within the hydrophobic active site, but electronic effects may also play a role.

Disubstituted compounds **7-9** demonstrated a slight increase in affinity for CYP2A13 but lost selectivity since binding and inhibition of CYP2A6 was increased. These results were interesting as CYP2A6 has an overall smaller active site volume than CYP2A13[17] and does not demonstrate a spectral shift with **7**, yet competitive inhibition was observed. This could be due to the lack of displacement of the water molecule during binding assays.

Meta and Para (C3 and C4) substitution on the benzene ring

Substitutions at the meta or para positions on the benzene ring opposed the objective of finding selective inhibitors for CYP2A13. Compounds **10** and **11** had reduced affinity and inhibition of CYP2A13 with increasing affinity and inhibition of CYP2A6 in comparison to compound **3**. These substitutions were not selective for either CYP2A enzyme. However, the addition of an ortho substituent (**12, 13**) was able to rescue some affinity and selectivity for CYP2A13, further illustrating the importance of the ortho substituent. Additional di-methyl substitution on the morpholine ring as shown in **14** had minimal effects on K_d values, but substitution had a greater effect in decreasing the inhibition of both CYP2A13 and CYP2A6.

Ring Substitutions

Multiple ring analogs demonstrated a wide range of binding and inhibition constants. Replacing the morpholine ring with imidazole (**21, 22**) resulted in extremely potent but non-selective analogs. Not surprisingly, the nitrogen of the imidazole ring coordinated to the heme as demonstrated by the type II spectral shift. This bond greatly enhanced the affinity of the compounds, but selectivity between the CYP2A enzymes was lost as a result. While the type II ligand characterization was anticipated for the imidazole compounds (**21** and **22)** due to the accessible nitrogen atom, it was unexpected to observe a type II spectral shift for **16** with CYP2A6 versus a type I spectral shift with CYP2A13. It was unknown as to what active site

features resulted in the different binding modes. Docking studies in chapter 4 were used to evaluate the differences between the CYP2A enzymes with **16**.

The sulfur atoms in the thiophene rings of compounds **19** and **20** differed from **16** in that only type I spectral shifts were observed for these compounds. The thiophene ring mimics a benzene ring, and it was expected that **19** and **20** would correlate with **1** and **3**, respectively. These results were observed with an increase in binding and inhibition of CYP2A13 with **19**.

The remaining analogs with substitution of the morpholine ring for a methylpiperazine ring (**17, 18**) resulted in poor affinity and inhibition of both CYP2A enzymes due to either the disruption of optimal interactions within the active site and/or charge addition. It was hypothesized that the methyl group would disrupt a hydrogen bond with N297, a hypothesis later tested by X-ray crystallography (see chapter 4). In addition, incorporation of the methylpiperazine ring would have introduced a second positive charge on the ligand at physiological pH. This charge may not have been well tolerated and therefore result in the poor binding and inhibition that was observed.

Linker Substitutions

Attachment of a methyl group to the one carbon linker (**23**) yielded a compound that maintained comparable affinity and inhibition of CYP2A13 as **3**, but decreased selectivity since **23** also inhibited CYP2A6. These trends were not observed with **24** when the linker was extended to an ethyl group between the morpholine and benzene ring. Instead, a decrease in both affinity and inhibition was observed. Decreased affinity for CYP2A13 could be due to the poor fit of the longer molecule within the active site, while the methyl group on the linker in **23** did not significantly clash within the active site but rather may have had additional van der Waals

interactions with hydrophobic residues of the active site. However, it remains unknown which enantiomer of **23** was more potent as assays were performed with a racemic mixture.

Compilation of the binding and inhibition studies has enabled the determination of structure-activity relationships (SAR) for the benzylmorpholine scaffold (Figure 3.8). The results led to the conclusion that the substitution at the ortho position of the benzene ring was the most vital feature of the benzylmorpholine scaffold promoting selective binding and inhibition of CYP2A13. Disubstitution at both ortho positions enhanced affinity. Meta and para substitutions on the benzene ring, linkage extension between the rings, and exchange of the morpholine ring for a methylpiperazine ring proved to be the most detrimental alterations in achieving selective binding and inhibition. By altering various parts of the benzylmorpholine small molecule scaffold, we were able to identify the key structural aspects of the benzylmorpholine scaffold that contribute to its CYP2A inhibition. This knowledge forms the basis for rationally optimizing drug candidates for selective inhibition of CYP2A13.

Figure 3.8. Structure-activity relationships for the benzylmorpholine scaffold as determined by spectral ligand binding assays and inhibition studies.

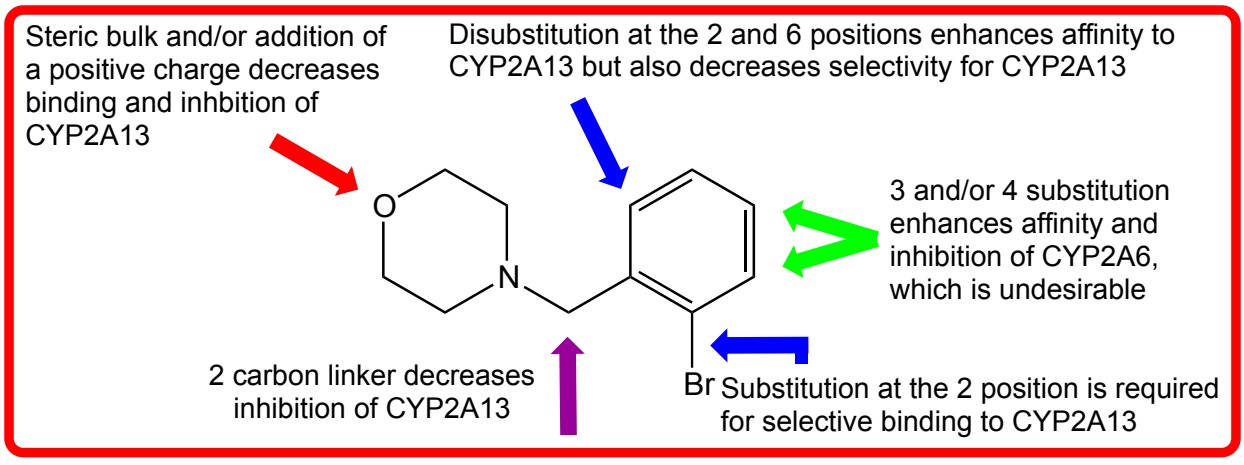

Conclusions

Assays evaluating ligand binding and the inhibition of coumarin metabolism were effective for evaluating a small library of 24 benzylmorpholine analogs and determining structure-activity relationships. Thus far, the benzylmorpholine analogs have proven successful as selective inhibitors of CYP2A13 and could be used as chemopreventative agents for tobacco users by inhibiting the bioactivation of the tobacco procarcinogen, NNK. The use of a chemopreventative agent would reduce the health care costs associated with lung cancer and the number of premature deaths. While this is not a replacement for tobacco cessation, tobacco users could use a CYP2A13 inhibitor while smoking or in concurrent use with most cessation aids and therefore reduce the risk of lung cancer in tobacco users who are unable, unwilling, or in the process of ceasing tobacco use.

Acknowledgements

I am grateful for the completion of five binding assays by John Kim, who was an undergraduate researcher under my guidance.

References

1. WHO. Cancer. (World Health Organization, 2011).
2. Hecht, S.S., Kassie, F. & Hatsukami, D.K. Chemoprevention of lung carcinogenesis in addicted smokers and ex-smokers. *Nat Rev Cancer* **9**, 476-88 (2009).
3. American Cancer Society. Cancer Facts and Figures 2012. http://www.cancer.org/Research/CancerFactsFigures/CancerFactsFigures/cancer-facts-figures-2012.
4. *Cytochrome P450: Structure, Mechanism, and Biochemistry*, (Kluwer Academic/ Plenum Publishers, New York, 2005).
5. DeVore, N.M., Smith, B.D., Wang, J.L., Lushington, G.H. & Scott, E.E. Key residues controlling binding of diverse ligands to human cytochrome P 450 2A enzymes. *Drug Metab Dispos* **37**, 1319-1327 (2009).
6. He, X.Y. et al. Identification of Val117 and Arg372 as critical amino acid residues for the activity difference between human CYP2A6 and CYP2A13 in coumarin 7-hydroxylation. *Arch Biochem Biophys* **427**, 143-53 (2004).
7. He, X.Y. et al. Efficient activation of aflatoxin B1 by cytochrome P450 2A13, an enzyme predominantly expressed in human respiratory tract. *Int J Cancer* **118**, 2665-71 (2006).
8. He, X.Y., Shen, J., Ding, X., Lu, A.Y. & Hong, J.Y. Identification of critical amino acid residues of human CYP2A13 for the metabolic activation of 4-(methylnitrosamino)-1-(3-pyridyl)-1-butanone, a tobacco-specific carcinogen. *Drug Metab Dispos* **32**, 1516-21 (2004).
9. Hecht, S.S. Biochemistry, biology, and carcinogenicity of tobacco-specific N-nitrosamines. *Chem Res Toxicol* **11**, 559-603 (1998).
10. Hecht, S.S. et al. Metabolism of the tobacco-specific nitrosamine 4-(methylnitrosamino)-1-(3-pyridyl)-1-butanone in the patas monkey: Pharmacokinetics and characterization of glucuronide metabolites. *Carcinogenesis* **14**, 229-36 (1993).
11. Hecht, S.S. et al. Complete inhibition of 4-(methylnitrosamino)-1-(3-pyridyl)-1-butanone-induced rat lung tumorigenesis and favorable modification of biomarkers by phenethyl isothiocyanate. *Cancer Epidemiol Biomarkers Prev* **5**, 645-52 (1996).
12. Andersen, R.A. & Kemp, T.R. Accumulation of 4-(N-methyl-N-nitrosamino)-1-(3-pyridyl)-1-butanone in alkaloid genotypes of burley tobacco during postharvest processing: comparisons with N'-nitrosonornicotine and probable nitrosamine precursors. *Cancer Res* **45**, 5287-93 (1985).
13. Murphy, S.E., Raulinaitis, V. & Brown, K.M. Nicotine 5'-oxidation and methyl oxidation by P450 2A enzymes. *Drug Metab. Dispos.* **33**, 1166-1173 (2005).
14. Hecht, S.S. Progress and Challenges in Selected Areas of Tobacco Carcinogenesis. *Chem. Res. Toxicol.* **21**, 160-171 (2008).
15. Bieche, I. et al. Reverse transcriptase-PCR quantification of mRNA levels from cytochrome (CYP)1, CYP2 and CYP3 families in 22 different human tissues. *Pharmacogenet Genomics* **17**, 731-42 (2007).
16. Schenkman, J.B., Remmer, H. & Estabrook, R.W. Spectral studies of drug interaction with hepatic microsomal cytochrome. *Mol Pharmacol* **3**, 113-23 (1967).
17. Smith, B.D. et al. Structure of the human lung cytochrome P450 2A13. *J Biol Chem* **282**, 17306-13 (2007).

Chapter 4

CYP2A Crystallography

Introduction

Protein crystallography is a useful technique for evaluating the atomic level interactions between proteins and their ligands. The resulting three-dimensional structures can provide insight into the amino acid residues controlling ligand selectivity. This information can be applied to the rational design of drug candidates. In addition, once a crystal structure has been determined, as in the case of the CYP2A enzymes, new drug candidates can often be evaluated using docking studies as a preliminary step in the evaluation of interactions within the active site in the overall process of drug optimization. Docking studies and co-crystal structures of CYP2A13 with a benzylmorpholine ligand could aid in the rational drug design of potent CYP2A13 inhibitors to reduce the risk of lung cancer in tobacco users.

Cytochrome P450 2A13 is 94% identical to the hepatic CYP2A6, yet these enzymes have some substrate selectivity and metabolize a variety of common substrates at different rates.[1-3] The known CYP2A structures have only minor global differences resulting in a root mean square deviation of all the Cα carbons of ~0.5 Å (CYP2A13, PDB 2P85; CYP2A6, PDB 1Z10), but differ by 32 amino acids with 10 of those residues within or surrounding the active site (Figure 4.1).[4] For these two structures with indole and coumarin, respectively, these differences result in an active site volume for CYP2A13 of ~300 $Å^3$, which is 15-20% greater than CYP2A6 (~250 $Å^3$).[4] Both CYP2A enzymes are extremely hydrophobic, with the roof of the CYP2A13 active site being lined with six phenylalanine residues (F107, F111, F118, F209, F300, and F480).[4]

Figure 4.1. Active site residues that differ between CYP2A13 and CYP2A6 are highlighted in blue in the CYP2A13 structure (PDB 2P85).

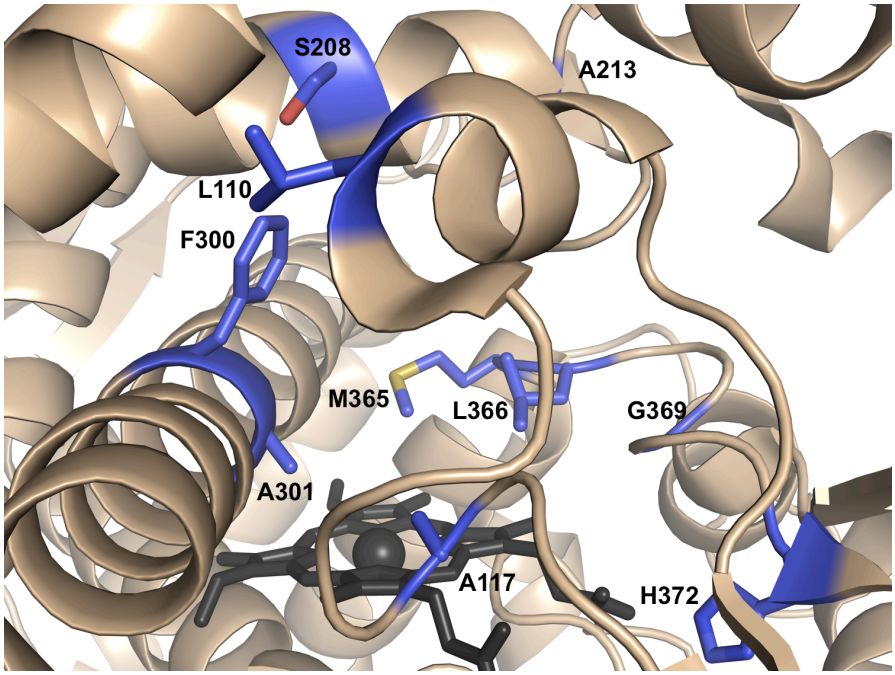

Site-directed mutagenesis and functional and structural studies have identified key residues that control the binding of diverse CYP2A ligands.[3,5] Exchange of the active site residues between the human CYP2A enzymes illustrates this point. For example, CYP2A6 metabolizes coumarin with a higher catalytic efficiency compared to CYP2A13, but replacement of the CYP2A13 residues alanine and histidine at positions 117 and 372 for the residues found at these sites in CYP2A6, valine and arginine (CYP2A13 A117V and H372R), increases the catalytic efficiency of CYP2A13 for coumarin.[6] Furthermore, these same substitutions in addition to the incorporation of the CYP2A6 residue into the CYP2A13 enzyme at position 208 (S208I) decreased metabolism of the CYP2A13 substrate NNK to be more like that of wild type CYP2A6 for NNK.[7] Phenacetin is a specific substrate for CYP2A13, and does not bind and is not metabolized by CYP2A6 at all. Individually, the CYP2A13 mutants containing CYP2A6

residues S208I, A213S, F300I, A301G, M365V, and G369S each decrease binding and metabolism of the CYP2A13 substrate phenacetin.[3,5] However, incorporation of several of these CYP2A13 residues in CYP2A6 imparts CYP2A6 with the ability to metabolize phenacetin. Specifically, the CYP2A6 quadruple mutant I208S/I300F/G301A/S369G was able to bind and metabolize phenacetin with similar K_d, K_m, and k_{cat} as CYP2A13. This so called "quad mutant" also binds substrates such as phenethyl isothiocyate and 2′-methoxyacetophenone more similarly to CYP2A13 than wild type CYP2A6.[3,5]

In addition, there are two conserved amino acids between the CYP2A enzymes that are important for the positioning of substrates within the respective active sites. First, N297 is the only polar residue within the active site and is important for the metabolism of NNK in CYP2A13[8] and the orientation and stabilization of coumarin in CYP2A6 through hydrogen bond interactions.[9] Second, the side chain of L370 is also known to rotate for positioning of substrates.[5,10] In compiling the knowledge of these residues from previous mutagenesis studies, it appears that substrate selectivity may be controlled by the steric bulk of the different amino acid residues and limited flexibility in movement in the side chains.[3-5,10] This contrasts with many other mammalian cytochrome P450 enzymes where active site cavities appear to be more flexible depending on the bound ligand.

The ultimate goal of this study was to understand how these residues interact with benzylmorpholine compounds to impart the observed selectivity between the human CYP2A enzymes. In order to accomplish this, we desired to determine a co-crystal structure of CYP2A13 with one of our selective benzylmorpholine inhibitors. Figure 4.2 displays the compounds used in the crystallography experiments described herein. We anticipated that a co-crystal structure would facilitate the rational design of benzylmorpholine inhibitors by

suggesting ways to maximize interactions within the CYP2A13 active site over the CYP2A6 active site, further enhancing selectivity for CYP2A13.

Figure 4.2. Structures of the benzylmorpholine analogs used for protein crystallography with the CYP2A enzymes. Numbering of the structures correlate with chapters 1-3.

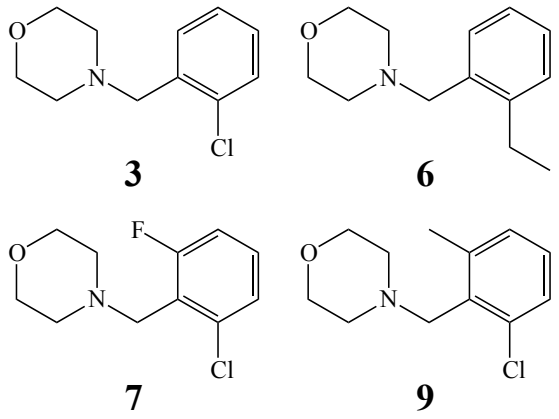

Materials and Methods

Docking studies: Surflex[11] was used to dock the benzylmorpholine compounds **2-5, 7-8, 12-13,** and **16** with both CYP2A13 (PDB 2P85) and CYP2A6 (PDB 1Z10). Structures for these compounds are shown in chapters 1-3. Ligand files used in the docking studies were prepared in Sybyl with energy minimization and assignment of Gasteiger and Marsili charges. Sybyl was also used to prepare the CYP2A files by extraction of the published ligand, assignment of Gasteiger and Marsili charges, addition of a 3^+ charge to the ferric heme iron, and deletion of an artificial hydrogen bond to the heme at the 6th coordinate position resulting from a program error. Next, molecular fragments such as CH_4, C=O, and N-H were placed into the active sites of the CYP2A enzymes where 1 $Å^3$ void volumes were identified.[11] Placement of each fragment was scored based upon hydrophobic and polar complementarity and entropic and solvation terms.[11,12] Fragments with scores above a threshold were used to generate a pseudo-molecule called a

protomol, which was then used for alignment of the ligands in the active site during docking. The resulting ligand poses were scored using the criteria described above and ranked from highest to lowest scores, with the highest test scores indicating the most favorable interactions. These scores also take into account inappropriate interactions and penetrations within the ligand and between the ligand and the CYP2A protein. Docking scores for the top ten results were recorded and the ligand poses were viewed with PyMOL.[13]

However, it is important to note that the docking results may not be optimal. During Sybyl ligand preparation, a positive charge was not assigned to the nitrogen of the ligand morpholine ring, as it should have been. At physiological pH and in the buffers that are described in this dissertation, the morpholine nitrogen, which has a pka of ~10, would be protonated. Therefore the docking results may not be entirely accurate without the proper charge assignment.

Site-Directed Mutagenesis: The QuikChange Site Directed Mutagenesis Kit (Agilent Technologies, Santa Clara, CA) was used with the forward primer 5′-GGCTATGGCGTGGCATTCAGCAACGGGGAGCG-3′, reverse primer 5′-CGCTCCCCGTTGCTGAATGCCACGCCATAGCC-3′, and the pKKCYP2A6 I208S/I300F/G301A/S369G "quad mutant" DNA template to create the CYP2A6 V117A/I208S/I300F/G301A/S369G "pent mutant", while also incorporating a silent mutation that removed a BbsI restriction site from the parent plasmid. The mutagenesis reaction was transformed into XL1-Blue supercompetent cells. The cells were plated on LB media containing 50 μg/mL ampicillin for selection of cells containing the mutated plasmid and incubated for 16 hours at 37˚ C. Individual colonies were grown overnight in 5 mL LB media containing 50 μg/mL ampicillin. The QIAprep Spin Miniprep Kit was used to purify the plasmid. The entire

CYP2A6 pent mutant gene was sequenced by Idaho State University Molecular Research Core Facility with pKK forward (5′-GCGCCGACATATAAACGGTTCTGGC-3′) and reverse (5′ GCAAATTCTGTTTTATCAGACCGC-3′) primers to verify the presence of intended mutations and absence of undesired mutations.

Protein Expression and Purification: The CYP2A13, CYP2A6 quad mutant, and CYP2A6 pent mutant proteins were expressed and purified with the protocols described in chapter 2 with minor changes, including purification with either 4.8 mM Cymal-5 (Anatrace, Santa Clara, CA) or 0.5% Anapoe-35 (Anatrace, Santa, Clara, CA).

Spectral Ligand Binding Assays: The spectral ligand binding constants of the CYP2A6 mutant enzymes with the benzylmorpholine compounds **3, 6, 7,** and **9** were determined in duplicate using the procedures described in chapter 2.

Kinetic Analysis: Inhibition of coumarin metabolism by the CYP2A mutant enzymes using compounds **3, 6, 7,** and **9** was evaluated following the protocol described in chapter 2.

Protein Crystallography:

First, a detergent (0.2 % Anapoe-X-405, 0.5% Anapoe-35, 4.8 mM Cymal-5, 3.4 M Cymal-1, or 3 mM n-dodecyl-N,N-dimethylglycine) was added to the purified CYP2A protein solution with 5 mM of **3**, 5 mM of **6**, 7 mM of **7**, or 5 mM of **9**, which were the highest inhibitor concentrations that could be achieved in the buffer solution. Next, twenty-four well plates and hanging drop vapor diffusion equilibration were used to grow P450 crystals. A 3:1 or 1:1 ratio of 11 mg/mL or 50 mg/mL CYP2A solution to well solution was equilibrated against 750 µl precipitant solution and incubated at room temperature.

High throughput crystal screening was performed with Wizard III and Wizard IV crystal screens (Emerald Bioscience, Bainbridge Island, WA), ninety-six well plates were used with

sitting drop vapor diffusion. In this case, the CYP2A protein solution included either 0.2 % Anapoe-X-405 or 4.8 mM Cymal-5 with either 5 mM of **3** or 7 mM of **7**. A 1:1 ratio of 50 mg/mL CYP2A to precipitant solution was equilibrated against 75 µL of precipitant solution and incubated at room temperature.

Precipitant conditions that produced crystals are described in the results section and summarized in table 4.1. Crystals that were of suitable size (minimum length of ~ 0.05 µm) and morphology were flash cooled with liquid nitrogen after soaking in a cryoprotectant solution consisting of 350 µl of precipitant solution, 350 µl of CM elution buffer (50 mM KPi, pH 7.4, 20% glycerol, 0.5 M NaCl, and 1 mM EDTA), and 300 µl of ethylene glycol. X-ray diffraction data sets were collected at the Stanford Synchrotron Radiation Lightsource (SSRL) on beam lines 9-2, 11-1, or 12-2.

CYP2A6 structures (PDB 1Z10 or PDB 2FDV) were used as search models to solve the CYP2A6 mutant structures with molecular replacement using the software Phaser,[14] and the resulting log-likelihood gains were >13,000 for all of the structures. COOT[15] and REFMAC5[16] in the CCP4 suite[17] were used to perform iterative rounds of model building and refinement on the CYP2A models. WHAT-IF[18] and PROCHECK[19] were used to validate the CYP2A6 quad mutant structure with **3** bound. The remaining structures will be fully validated if the ligand density is of publishable quality. Voidoo[20] was used to determine cavities using a probe radius of 1.4 Å.

Results

Docking

Docking studies were performed to gain insights into the orientations of benzylmorpholine analogs. Three examples with three different benzylmorpholine ligands

(Figure 4.3) are used to summarize the type of data that was observed. These three compounds were chosen as they represented a variety of experimental observations. Compound **4** represented a substitution at the ortho position on the benzene ring and was selective for CYP2A13 as it did not appear to bind to CYP2A6. Compound **7** is a disubstituted ligand that was still selective for CYP2A13 but less so (7.5-fold). The last compound, **16,** was chosen for its unique difference in binding modes between the CYP2A enzymes. In discussing each set of docking results, the roles of amino acid residues F209 and F300 (CYP2A13) or I300 (CYP2A6) are highlighted for later comparisons with the X-ray crystallography data.

Figure 4.3. Structures of the benzylmorpholine analogs that are discussed as examples for the docking results.

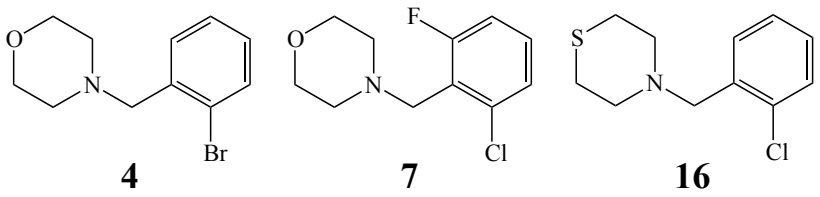

Compound **4** selectively binds and inhibits CYP2A13 (K_d = 6.3 μM, K_i = 17.6 ± 3.1 μM) versus CYP2A6 (K_d = no spectral shift, K_i = ≥1000 μM), with a ≥56-fold preference for the inhibition of CYP2A13. However the docking scores did not qualitatively reflect the *in vitro* experimental results as the higher docking scores pertained to CYP2A6 compared to CYP2A13 (Figure 4.4). Thus selectively was not apparent from comparison of the scores.

In the top 10 poses ranked by the highest docking scores, which were reflective of the best interactions within the active site, there were two proposed ligand-binding orientations of **4** with CYP2A13 and one orientation with CYP2A6. The most frequently observed CYP2A13

pose placed the oxygen of the morpholine ring 2.81 Å away from N297, where a potential hydrogen bond could be formed (Figure 4.5A). This orientation would be consistent with a type I ligand and experimental data from the spectral ligand binding assays. Additionally, the second pose resulted in two of the best docking scores with **4** and CYP2A13 and placed the oxygen of the morpholine ring 2.52 Å above the heme iron. The single orientation observed with CYP2A6 also placed the oxygen of the morpholine ring above the heme Fe with a slightly closer distance of 2.14 Å (Figure 4.5B). These latter poses may or may not cause a spectral shift, as bound water does not cause a shift with a λ_{max} at 418 nm, resulting in an inconsistency with either CYP2A13 or CYP2A6 experimental data as **4** binds CYP2A13 but does not appear to bind or inhibit CYP2A6. These results demonstrated the difficulty in generating reliable docking results even with a benzylmorpholine analog that was known to be selective for CYP2A13.

Figure 4.4. Comparison of docking scores for **4** with both CYP2A13 and CYP2A6 demonstrating preferential docking of **4** with CYP2A6.

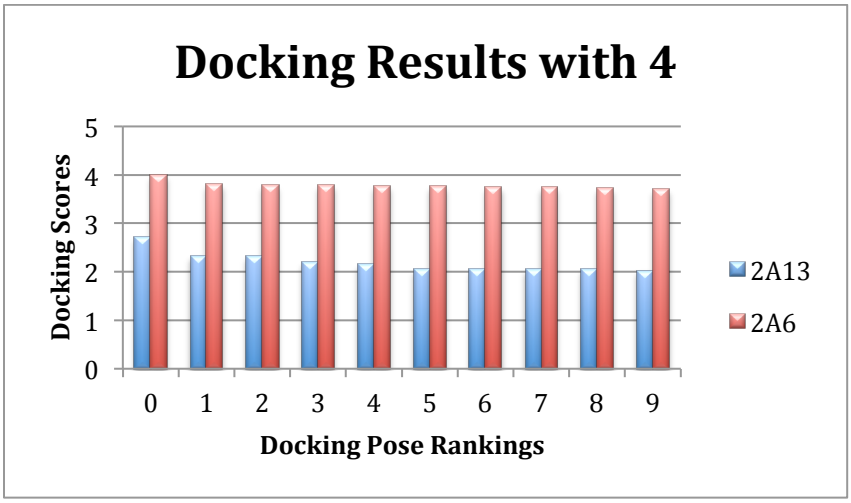

Figure 4.5. Primary ligand binding orientations for **4** (cyan) with A) CYP2A13 and B) CYP2A6 resulting from docking studies.

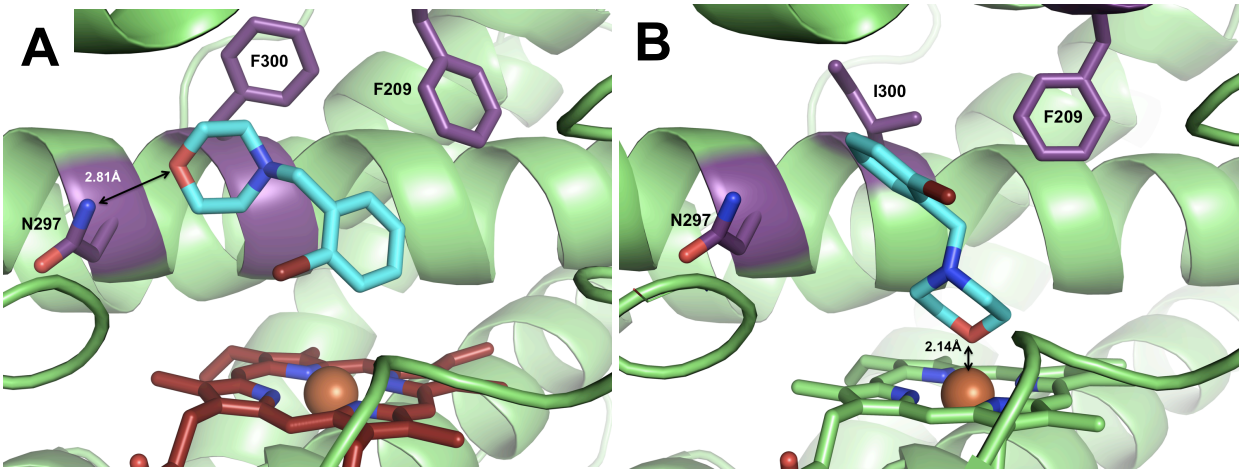

The second docking example is for the disubstituted compound **7** in both CYP2A13 and CYP2A6. Unlike **4**, **7** demonstrated *in vitro* binding to both CYP2A enzymes but is 7.5-fold more selective for CYP2A13 versus CYP2A6. However, comparison of the docking scores from the top 10 poses did not reflect the *in vitro* data (Figure 4.6). The scores were more similar between the two enzymes than observed for **4**, but still with a slight preference for CYP2A6. This demonstrates that the relative docking scores did not reflect the selectivity of **7** between the CYP2A enzymes.

In these docking studies, **7** displayed two orientations in CYP2A13 with almost equivalent scores (Figure 4.7A). Both orientations place the morpholine ring closer to the heme than the substituted benzene ring, but the molecules are rotated horizontally almost 180˚ from one another. In addition the placement of the chlorine and fluorine substituents vary. Both ligand orientations might be expected to result in the experimentally observed type I ligand shift, but neither takes advantage of N297 for hydrogen bonding.

Within the top 10 poses, **7** adopted three different orientations with CYP2A6. The first ligand orientation represented the six lowest docking scores and placed the morpholine ring towards N297, which could result in the type I spectral shift consistent with experimental data. The remaining two orientations represented by the top four docking scores placed the morpholine ring near the heme. In one case, the oxygen of the morpholine ring was placed directly above the heme Fe as seen with **4** and may or may not produce the expected type I spectral shift. The third and final orientation with CYP2A6 placed a carbon atom above the heme (Figure 4.7B), which could be consistent with the type I binding shift observed. Overall, the results with **7** did not instill confidence in the docking studies as they were unable to accurately portray the selectivity of **7** between the CYP2A enzymes.

Figure 4.6. Comparison of docking scores for **7** with both CYP2A13 and CYP2A6 demonstrating preferential docking with CYP2A6.

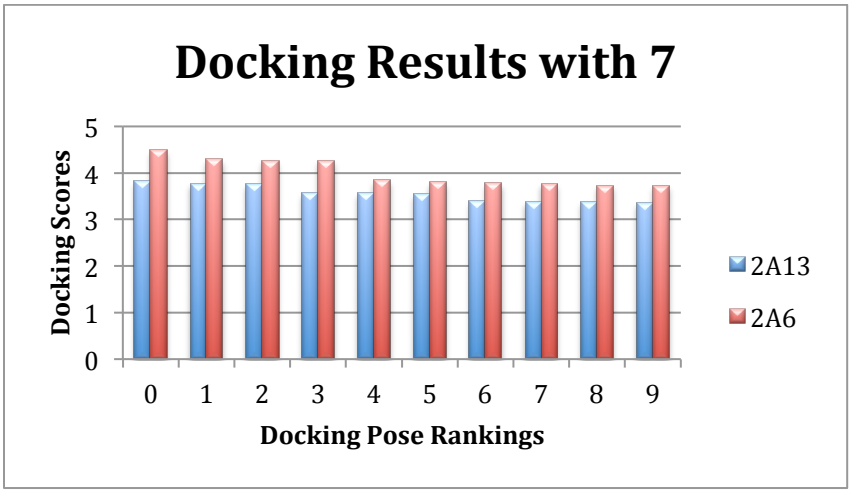

Figure 4.7. Ligand binding orientations for **7** (cyan) with A) CYP2A13 and B) CYP2A6 resulting from docking studies.

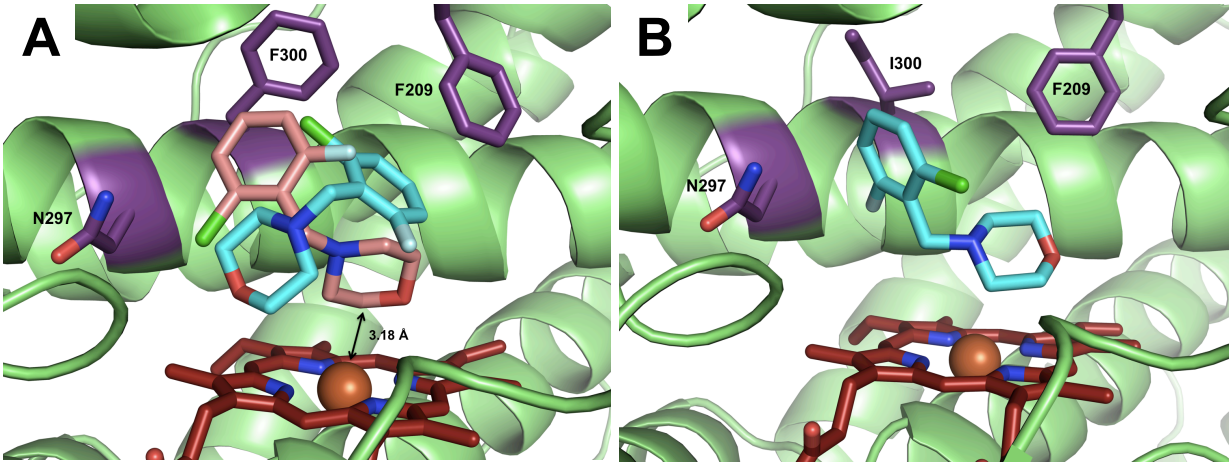

The third and final docking example was with compound **16**. This benzylmorpholine analog was chosen due to its unique differences in binding mode between the CYP2A enzymes. With CYP2A13, **16** was a type I ligand, but when CYP2A6 was titrated with **16**, spectral shifts for a type II ligand were observed. With the exception of the imidazole analogs (**21** and **22**), **16** was also the tightest binding compound with CYP2A6, but it remained 18-fold more selective for CYP2A13 (K_d = 8.3 ± 4.1 μM) than for CYP2A6 (K_d = 150 μM). However, this selectivity was not strongly reflected in the relative docking scores (Figure 4.8). While these scores did demonstrate a slight preference for CYP2A13, the selectivity did not compare very well with the 18-fold difference observed during *in vitro* experimentation.

Three orientations of **16** were observed with CYP2A13, two of which were consistent with the type I spectral shifts observed during *in vitro* binding studies. The orientations consistent with experimental results placed the benzylmorpholine ligands with the morpholine ring angled towards N297 (3.4 Å) (Figure 4.9A) or with the morpholine above but not coordinating to the heme iron (3.18 Å). Both of these orientations could be expected to produce a type I spectra. However, the third orientation may not correlate with the experimental data as it placed the oxygen of the morpholine ring 2.48 Å above the heme iron, which could result in a type II spectral shift as observed for CYP2A6. For CYP2A6, only one of the ten orientations predicted **16** in a position to coordinate to the heme iron with a distance of 2.6 Å between the heme iron and the thiol moiety (Figure 4.9B), which would result in the experimentally observed type II spectral shifts. The remaining 9 orientations placed the thiol near the roof of the active site between N297 and I300. Thus, only 10% of the predictions for **16** with CYP2A6 were consistent with experimental observations.

Figure 4.8. Comparison of docking scores for **16** with both CYP2A13 and CYP2A6.

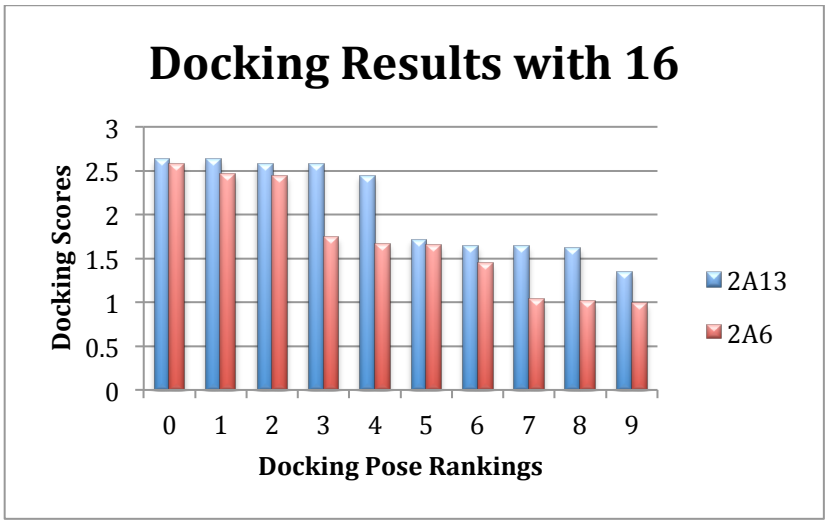

Figure 4.9. Ligand binding orientations for **16** with A) CYP2A13 and B) CYP2A6 from docking studies that could correlate with experimental results.

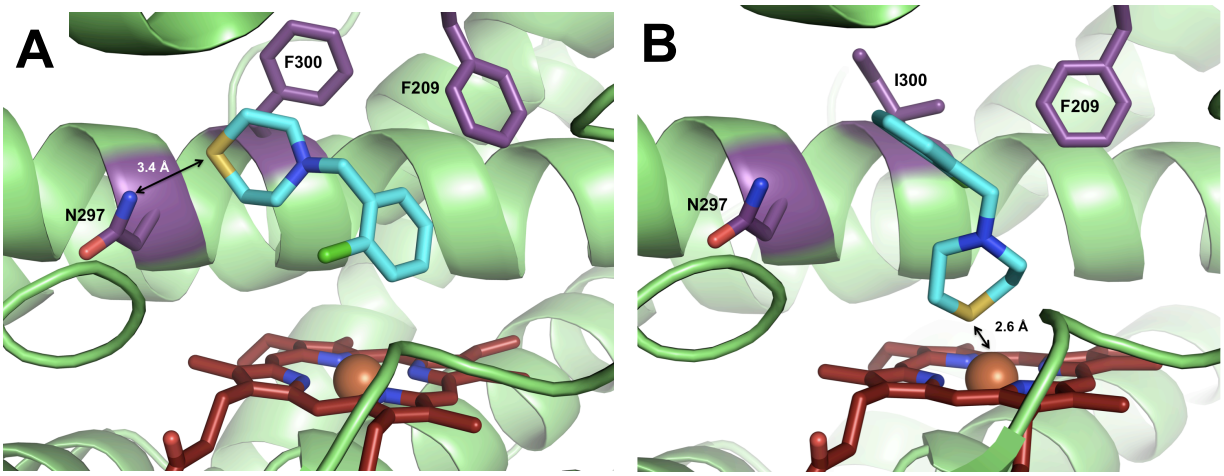

Overall, these three examples revealed that using docking studies to predict the ligand binding orientations of the benzylmorpholine library within the CYP2A active sites were often not consistent with observations from *in vitro* studies. The docking results were inconclusive as to enzyme selectivity in addition to poor correlation with experimental data. However, some of this poor correlation may be attributed to the lack of a positive charge on the ligand that should have been present during docking studies. Regardless, alternative methods are needed to understand the CYP2A active site features that are responsible for benzylmorpholine selectivity. X-ray crystallography offers an alternative technique in analyzing the atomic-level interactions between a CYP2A enzyme and a benzylmorpholine ligand.

Crystallography with CYP2A13

X-ray crystallography was used to elucidate the atomic interactions between CYP2A13 and benzylmorpholine analogs. Compounds **3** and **7** were chosen as they represented singly and disubstituted benzylmorpholine analogs that were selective for CYP2A13. As described in the methods, protein solutions with either compound were equilibrated versus a precipitant using hanging drop vapor diffusion. Many modifications of protein, detergents, buffer, and precipitant were made to generate benzylmorpholine bound structures, which are discussed below and summarized in Table 4.1.

Table 4.1. Summary of crystal formation and collected data for CYP2A13. Changes from previous attempts are underlined. (P) denotes the detergent used to purify CYP2A13 while (C) indicates the detergent added prior to hanging drop vapor diffusion.

	Enzyme	Detergent	Hanging Drop Information	Crystal Picture	Diffraction Information
A	CYP2A13	0.5% Anapoe-35 (P) 0.2% Anapoe-X-405 (C)	3:1 ratio of 11 mg/mL CYP2A13 to precipitant solution (30% PEG 3350, 0.175 M Tris pH 8.5, 0.2 M $((NH_4)_2SO_4)$ with **3** and **7**	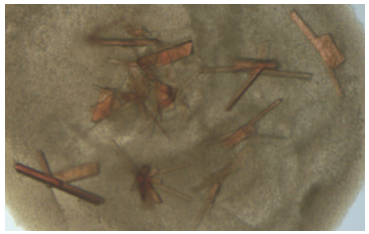	Collected 3.25 Å data set with **3** and a 3.35 Å data set with **7**, but no ligand density was observed following refinement
B	CYP2A13	0.5% Anapoe-35 (P) 0.2% Anapoe-X-405 (C)	3:1 ratio of 11 mg/mL CYP2A13 to precipitant solution (30% PEG 3350, 0.175 M Tris pH 8.5, 0.25 M $((NH_4)_2SO_4)$ with **3**	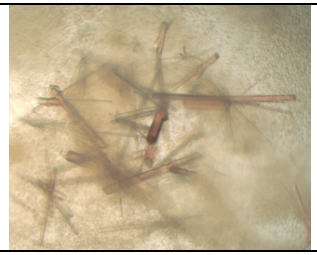	Collected 3.15 Å data set with **3**, but only minimal ligand density was observed after refinement
C	CYP2A13	0.5% Anapoe-35 (P) 0.2% Anapoe-X-405 (C)	Attempted microseeding with 3:1 ratio of 11 mg/mL CYP2A13 to precipitant solution (30% PEG 3350, 0.175 M Tris pH 8.5, 0.2 M $((NH_4)_2SO_4)$ with **3** and **7**	No improvement: Observed micro and small clustered rods	Not determined

	Enzyme	Detergent	Hanging Drop Information	Crystal Picture	Diffraction Information
D	CYP2A13	0.5% Anapoe-35 (P) 4.8 mM Cymal-5 (C)	1:1 ratio of 50 mg/mL CYP2A13 to precipitant solution (20% PEG 400, 0.1 M sodium HEPES pH 7.5, 0.2 M $MgCl_2$) with **7**	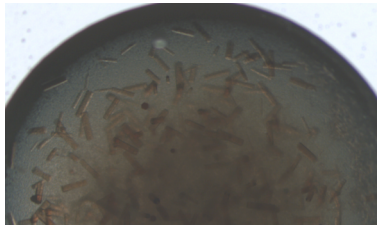	Weak diffraction during screening
E	CYP2A13	0.5% Anapoe-35 (P) 0.2% Anapoe-X-405 (C)	1:1 ratio of 50 mg/mL CYP2A13 withWizard III.27 (30% PEG 400, 0.1 M sodium HEPES pH 7.5, 0.2 M $MgCl_2$) with **3**	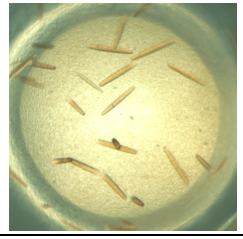	Diffracted to 7.91 Å during screening
F	CYP2A13	0.5% Anapoe-35 (P) 0.2% Anapoe-X-405 (C)	1:1 ratio of 50 mg/mL CYP2A13 with Wizard IV.14 optimized precipitant solution (40% PEG 400, 0.075 M Tris pH 8.5, 0.2 M $LiSO_4$) with **3**	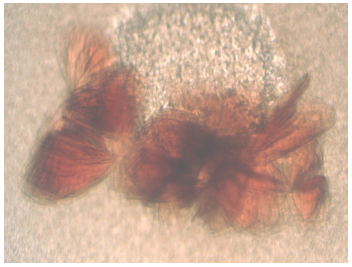	Not determined
G	CYP2A13	4.8 mM Cymal-5 (P) 0.006 mM n-hexadexyl-β-D-maltoside (C)	1:1 ratio of 50 mg/mL CYP2A13 with Wizard IV.14 optimized precipitant solution (40% PEG 400, 0.075 M Tris pH 8.5, 0.2 M $LiSO_4$) with **3**	Picture Not Available	Not determined

	Enzyme	Detergent	Hanging Drop Information	Crystal Picture	Diffraction Information
H	CYP2A13	4.8 mM Cymal-5 (P) 15 mM n-dodecyl-N,N-dimethylglycine (C)	Hampton research detergent screens1-3 with 1:1 ratio of 50 mg/mL CYP2A13 to precipitant solution (20% PEG 400, 0.1 M sodium HEPES pH 7.5, 0.2 M $MgCl_2$) with **3**		Diffracted to 3.4 Å during screening
I	CYP2A13	0.5% Anapoe-35 (P) 15 mM n-dodecyl-N,N-dimethylglycine (C)	Hampton research detergent screens1-3 with 1:1 ratio of 50 mg/mL CYP2A13 to precipitant solution (20% PEG 400, 0.1 M sodium HEPES pH 7.5, 0.2 M $MgCl_2$) with **3**	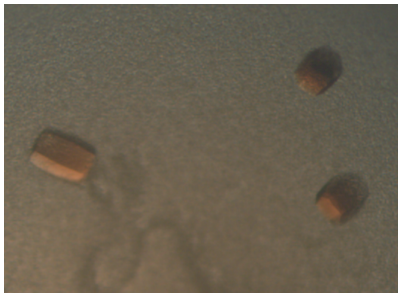	Diffracted to ≥ 3.31 Å during screening
J	CYP2A13	4.8 mM Cymal-5 (P) 10% w/v Anapoe-58 (C)	Hampton research detergent screens 1-3 with 3:1 ratio of 11 mg/mL CYP2A13 to precipitant solution (30% PEG 3350, 0.175 M Tris pH 8.5, 0.2 M $((NH_4)_2SO_4)$ with **7**	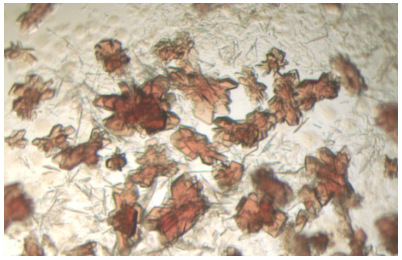	Not determined
K	CYP2A13	0.5% Anapoe-35 (P) 3.4 M Cymal-1 (C)	During the detergent screens 3:1 ratio of 11 mg/mL CYP2A13 to precipitant solution (30% PEG 3350, 0.175 M Tris pH 8.5, 0.2 M $((NH_4)_2SO_4)$ with **7**	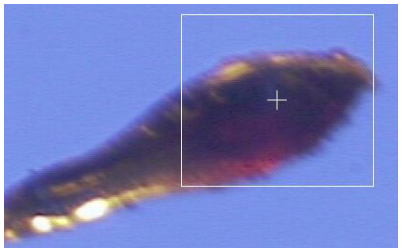	Collected 3.05 Å data set with **7**, but only minimal ligand density was observed after refinement

	Enzyme	Detergent	Hanging Drop Information	Crystal Picture	Diffraction Information
L	CYP2A13	4.8 mM Cymal-5 (P) 3.4 M Cymal-1 (C)	11 mg/mL CYP2A13 to precipitant solution (30% PEG 3350, 0.175 M Tris pH 8.5, 0.2 M $((NH_4)_2SO_4)$ with **7**	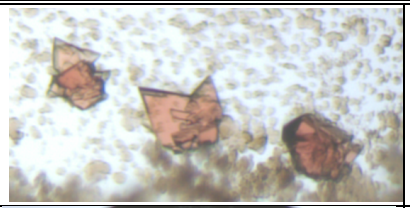	Weak diffraction to 3.64 Å during screening
M	CYP2A13	0.5% Anapoe-35 (P) 3 mM n-dodecyl-N,N-dimethylglycine (C)	2:1 ratio of 11 mg/mL CYP2A13 in sucrose buffer (0.5 M sucrose, 0.125 M potassium phosphate pH 7.4, and 1 mM EDTA) to precipitant solution (30% PEG 3350, 0.175 M Tris pH 8.5, 0.25 M $((NH_4)_2SO_4)$ with **7**		Diffracted to 6.38 A during screening
N	CYP2A13	0.5% Anapoe-35 (P) 0.2% Anapoe-X-405 (C)	Macroseeded into a 1:1 ratio of 50 mg/mL CYP2A13 or 3:1 ratio of 11 mg/mL CYP2A13 to precipitant solution (20% PEG 400, 0.1 M sodium HEPES pH 7.5, 0.2 M $MgCl_2$).	No effect: Observed microcrystals and precipitate	Not determined
O	CYP2A13	0.5% Anapoe-35 (P) 0.2% Anapoe-X-405 (C)	3:1 ratio of 11 mg/mL CYP2A13 to precipitant solution (30% PEG 3350, 0.175 M Tris pH 8.5, 0.2 M $((NH_4)_2SO_4)$ with **6**		Diffracted to 3.42 Å during screening

	Enzyme	Detergent	Hanging Drop Information	Crystal Picture	Diffraction Information
P	CYP2A13	0.5% Anapoe-35 (P) 0.2% Anapoe-X-405 (C)	3:1 ratio of 11 mg/mL CYP2A13 to precipitant solution (30% PEG 3350, 0.175 M Tris pH 8.5, 0.2 M $((NH_4)_2SO_4)$ with **9**	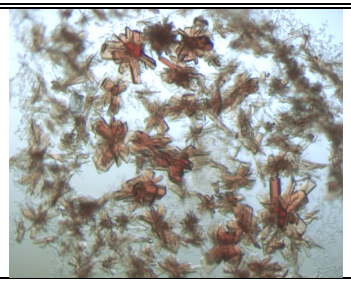	Diffracted to ≥3.0 Å during screening

Initial CYP2A13 crystallization began with a precipitant solution that had previously been used to crystallize CYP2A13, CYP2A6, and CYP2A6 mutant enzymes (30% polyethylene glycol 3350, 0.175 M Tris pH 8.5, and 0.2 M ammonium sulfate).[10] CYP2A13 was purified with 0.5% Anapoe-35, concentrated to 11 mg/mL, and Anapoe-X-405 added to a final concentration of 0.2% prior to hanging drop vapor diffusion, resulting in rod-shaped crystals (Table 4.1A) that diffracted to 3.25 Å with **3** and 3.35 Å with **7**. However, no ligand density was observed within the active site. Since we were interested in structures with density for benzylmorpholine ligands, further refinement was not pursued on these 3 Å structures.

Optimization of the precipitant solution was the next step in the crystallography process. Variations of precipitant components in twenty-four well plates confirmed that 30% PEG 3350 was the optimal PEG concentration, but crystals grew in a range of Tris pH 8.5 and ammonium sulfate concentrations that might yield an increase in resolution and ligand occupancy. The increase in ammonium sulfate concentrations from 0.2 M to 0.25 M yielded similar crystals that diffracted to 3.15 Å with **3,** but only minimal electron density was observed for the benzylmorpholine ligand in the active site following molecular replacement and refinement (Table 4.1B). In other words some electron density was present in the active site in a $2|F_o|-|F_c|$ map at 1 σ, but the size of the density was insufficient to place a ligand. Microseeding was also used in an attempt to obtain larger, thicker crystals but only small rod clusters or micro clusters resulted (Table 4.1C). The poor results with microseeding was perhaps not surprising as the thickness and size of the crystals rather than nucleation has been the primary issue in obtaining high resolution diffraction data.

Since the CYP2A13 rods proved unsuccessful in providing a co-crystal structure, additional precipitant solutions previously observed to yield CYP2A13 hexagonal crystals were

used (20% PEG 400, 0.1 M sodium HEPES, pH 7.5, and 0.2 M magnesium chloride). Under these conditions, hexagonal rod shaped crystals that were screened had a space group of P3 with unit cell dimensions of 95.15 Å, 95.15 Å, and 527.24 Å and angles of 90˚, 90˚, and 120˚. Although a smaller unit cell and increased symmetry are desirable, if a co-crystal structure resulted from this work, it would be worthwhile to pursue refinement of the data. The majority of the experimentation with hexagonal rod crystallization technique used a precipitant solution comprised of 20% PEG 400, 0.1 M sodium HEPES, pH 7.5, and 0.2 M magnesium chloride. Additional changes included an increase in protein concentration from 11 mg/mL to 50 mg/mL, a decrease in the drop ratio of CYP2A13 to precipitant solution from 3:1 to 1:1, and either 4.8 mM Cymal-5 or 0.2% Anapoe-X-405 was added to the protein solution prior to hanging drop vapor diffusion. Combination of the changes described above resulted in large hexagonal rods (Table 4.1D). However, these crystals only weakly diffracted during screening, and an estimated resolution could not be determined.

High throughput screening with commercially available Emerald Biosciences Wizard III and Wizard IV sparse matrix screens originally yielded hexagonal torpedo-like crystals with Wizard III #27 (30% PEG 400, 0.1 M sodium HEPES, pH 7.5, 0.2 M magnesium chloride) (Table 4.1E) and needle clusters with Wizard IV #14 (40% PEG 400, 0.1 M Tris, pH 8.5, and 0.2 M lithium sulfate). Optimization of the Wizard III #27 components did not result in better crystals from the original hit, which diffracted to only 7.91 Å. Wizard IV #14 (40% PEG 400, 0.075 M Tris, pH 8.5, and 0.2 M lithium sulfate) component optimization resulted in thin plates that were too fragile to harvest (Table 4.1F).

Cytochrome P450 stability and crystallization are sensitive to detergents used in both purification and crystallography, so detergent screens were performed next. Detergents from

Hampton research detergent screens 1-3 were added to either 0.5% Anapoe-35 or 4.8 mM Cymal-5 purified protein and equilibrated against the hexagonal rod solution (20% PEG 400, 0.1 M Tris, pH 8.5, and 0.2 M lithium sulfate) or clustered rod solution (30% PEG 3350, 0.175 M Tris, pH 8.5, and 0.2 M ammonium sulfate). All combinations contained either 5 mM **3** or 7 mM **7**. Three detergents yielded interesting results. Cymal-5 purified protein with the hexagonal rod solution yielded larger hexagonal rods than previously seen with 0.006 mM n-hexadexyl-β-D-maltoside (Table 4.1G) and hexagonal cones with 15 mM n-dodecyl-N,N-dimethylglycine (Table 4.1H). Meanwhile, 0.5% Anapoe-35 purified CYP2A13 with 15 mM n-dodecyl-N,N-dimethylglycine resulted in short hexagonal rods (Table 4.1I). Unfortunately crystals harvested from these conditions diffracted only to ≥3.31 Å with the best crystals. Since using the same detergent during purification and crystallography can sometimes yield higher quality crystals, purifications were attempted with n-dodecyl-N,N-dimethylglycine at 2-5 times the critical micelle concentration (3 – 8 mM), but the purification failed due to significant protein precipitation and only resulted in 1.2 nmol of P420 after cation exchange chromatography.

The detergent screens with the clustered rod solution yielded only one solution that resulted in diffraction-quality crystals. While most crystals with the clustered rod solution were short rods (Table 4.1J), CYP2A13 purified in 0.5% Anapoe-35 and crystallized with 3.4 M Cymal-1 resulted in a flat rod (Table 4.1K). A data set was collected to 3.05 Å, but unfortunately only minimal ligand density was observed following refinement. When CYP2A13 was purified with 4.8 mM Cymal-5 and combined with 3.4 M Cymal-1 prior to hanging drop vapor diffusion, the crystals were spiky clusters that only weakly diffracted to 3.64 Å (Table 4.1L). A purification was not performed with Cymal-1 due to the cost of the detergent.

Since the detergent screens were unable to produce a co-crystal structure, an alternative approach was the use of sucrose buffer (0.5 M sucrose, 0.125 M potassium phosphate, pH 7.4, and 1 mM EDTA) with or without additional detergent. This method proved successful in solving the X-ray crystal structure of cytochrome P450 2E1.[21,22] CYP2A13 purified with 0.5% Anapoe-35 was exchanged into sucrose buffer and crystal conditions were screened without detergent or with 0.2 % Anapoe-X-405, 4.8 mM Cymal-5, 3.4 M Cymal-1, or 3 mM n-dodecyl-N,N-dimethylglycine in the presence of 5 mM **3** or 7 mM **7** (Table 4.1M). Only 3 mM n-dodecyl-N,N-dimethylglycine with **7** resulted in crystals. However, these long rods were twinned and only diffracted to 6.38 Å.

An alternative approach to obtaining better diffraction data was the use of macroseeding in order to grow thicker crystals. Macroseeding experimentation used varying protein concentrations with **7** equilibrated against 20% PEG 400, 0.1 M Tris pH 8.5, and 0.2 M lithium sulfate but only yielded microcrystals (Table 4.1N).

Finally, crystal growth can be sensitive to different ligands. For this reason, benzylmorpholine ligands **6** and **9** were substituted for **3** and **7** in hanging drop vapor diffusion crystallization trials. An 11 mg/mL CYP2A13 protein solution was equilibrated against 30% PEG 3350, 0.175 M Tris, pH 8.5, and 0.25 M ammonium sulfate. Crystals with compound **6** bound to CYP2A13 diffracted to 3.42 Å (Table 4.1O), while **9** diffracted to ≥3.0 Å (Table 4.1P), but this resolution was too low to warrant data collection. The combined results from the CYP2A13 crystallography attempts illustrated the need for alternative methods to understand the structural basis for benzylmorpholine selectivity between CYP2A13 and CYP2A6.

CYP2A6 I208S/I300F/G301A/S369G (quad) mutant and CYP2A6 V117A/I208S/I300F/G301A/S369G (pent) mutant validations

Despite numerous attempts, crystal structures with CYP2A13 and a bound benzylmorpholine could not be obtained. However the CYP2A6 wild type enzyme has crystallized more readily in our hands. For this reason, the focus was shifted to the CYP2A13-like enzymes CYP2A6 I208S/I300F/G301A/S369G (quad) mutant and CYP2A6 V117A/I208S/I300F/G301A/S369G (pent) mutant with select benzylmorpholine analogs. The four mutations incorporated into the CYP2A6 quad mutant were previously demonstrated to impart CYP2A6 with CYP2A13 activity regarding phenacetin metabolism and have been used successfully for crystallography.[5] Additionally the V117A mutation impacts substrate binding and metabolism[6] and was incorporated into the CYP2A6 quad mutant to create an even more CYP2A13-like enzyme in terms of its function, while potentially retaining the advantageous crystallization likely facilitated by CYP2A6 surface residues.

To determine if the CYP2A6 quad and pent mutants could be realistic surrogates in structural analysis of benzylmorpholine binding, we first had to determine if the CYP2A6 quad and pent mutants interacted with select benzylmorpholine analogs more like the CYP2A13 or CYP2A6 wild type enzymes. Selective benzylmorpholine compounds already used for crystallography (**3**, **6**, **7**, and **9**) were evaluated with the CYP2A6 quad and pent mutant proteins for binding (Table 4.2) and inhibition (Table 4.3). The CYP2A6 quad mutant had a spectral equilibrium dissociation constant of 6.9 μM for compound **3**, which compared well to the CYP2A13 K_d value of 5.9 ± 3.4 μM, but not to CYP2A6 as no spectral shift was observed with this enzyme (Table 4.2). The K_i value of the CYP2A6 quad mutant with **3** was 78.7 μM, which was 2-fold higher than the CYP2A13 value of 39.7 ± 4.3 μM but much more comparable to

CYP2A13 than CYP2A6 (K_i = ≥1000 μM) (Table 4.3). In addition, **3** was a mixed inhibitor of the CYP2A6 quad mutant, rather than a competitive inhibitor as observed for **3** with CYP2A13. Similar trends were observed for compounds **6**, **7**, and **9**. All of the compounds were type I ligands and bound to the CYP2A6 quad mutant with K_d values more similar to those observed for CYP2A13 than those observed for CYP2A6. However, while **6** and **7** were competitive inhibitors and their K_i values more closely resembled CYP2A13, **9** was a mixed inhibitor with the CYP2A6 quad mutant and had a K_i value between that of CYP2A13 and CYP2A6.

Table 4.2 Equilibrium dissociation constants for wild type CYP2A13 and CYP2A6 proteins as well as the CYP2A6 quad and pent mutants designed to mimic the CYP2A13 active site interactions with select benzylmorpholine analogs.

Compound	**Structure**	**K_d (μM)[a,b,c]**			
		2A6	**2A13**	**2A6 Quad**	**2A6 Pent**
3	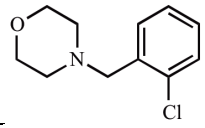	No Spectral Shift	5.9 ± 3.4 (I)	6.9[+] (I)	3.5[*] (I)
6	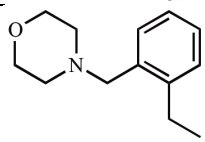	≥575.4 (I)	4.5 (I)	4.1[**] (I)	-
7	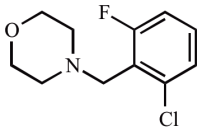	No Spectral Shift	5.2 (I)	12.3[*] (I)	1.9[**] (I)
9	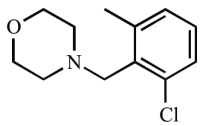	515 (I)	1.1 (I)	3.7[**] (I)	-

[a] CYP2A6 quad and pent mutant individual trials differed by * ≤1 μM, **≤2.1 μM, or + ≤3 μM
[b] (I): Type I Ligand
[c] - Assay was not performed

Table 4.3. Inhibition constants for wild type CYP2A13 and CYP2A6 proteins as well as the CYP2A6 quad and pent mutants designed to mimic the CYP2A13 active site interactions with select benzylmorpholine analogs.

Compound	Structure	K_i (μM)[a,b,c,d]			
		2A6	2A13	2A6 Quad	2A6 Pent
3	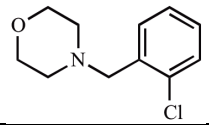	≥1000	39.7 ± 4.3 (C)	78.7[+] α=5.8 (M)	76.4 (C)
6	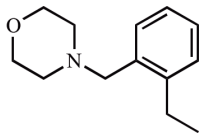	818.3 α=13.3 (M)	16.9 (C)	29.3 (C)	-
7	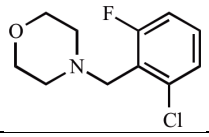	286.8 (C)	38.1 (C)	30.5 (C)	46.7 (C)
9	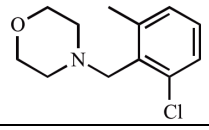	296.1 (C)	19.6* (C)	109.3 α=4.5 (M)	-

[a] + Standard error was 27% rather than ≤20%
[b] (C): Competitive Inhibition; (M), Mixed Inhibition
[c] - Assay was not performed
[d] *See chapter 3 for explanation

Insertion of the V117A mutation into the CYP2A6 quad mutant created the CYP2A6 V117A/I208S/I300F/G301A/S369G pent mutant. The binding and inhibition by select benzylmorpholine ligands (**3** and **7**) with the CYP2A6 pent mutant were largely comparable with the binding and inhibition of the CYP2A6 quad mutant and CYP2A13 wild type enzyme (Table 4.2 and Table 4.3). Specifically, the dissociation constants of 3.5 μM and 1.9 μM with **3** and **7**, respectively, compared well to the CYP2A13 values. Compound **3** inhibited the CYP2A6 pent mutant with a K_i of 76.4 μM, and a K_i value of 46.7 μM was determined for **7**. While there are some differences between CYP2A13 and the CYP2A6 quad and pent mutants, these results indicated that overall the benzylmorpholine inhibitors resemble binding and inhibition of

CYP2A13 more than CYP2A6, suggesting that a structure of the CYP2A6 quad and pent mutants with a benzylmorpholine inhibitor might facilitate understanding of the selectivity of these compounds for CYP2A13.

Comparisons of the catalytic efficiency of coumarin metabolism with the CYP2A6 quad and pent mutants may provide insight as to the slight differences in the inhibition data between the CYP2A6 mutant and CYP2A13 wild type enzymes. In comparing the k_{cat} values, the CYP2A6 pent mutant (1.29 ± 0.03 min^{-1}) resembled CYP2A13 (1.29 ± 0.03min^{-1}) while the CYP2A6 quad mutant (9.93 ± 1.03 min^{-1}) was more similar to CYP2A6 (8.61 ± 0.20 min^{-1}) (Table 4.4). However, the K_m values varied between the enzymes from ~6-14 μM with the CYP2A6 pent mutant having the lowest K_m value while the CYP2A6 quad mutant had the highest value. An overall comparison of the catalytic efficiency between the enzymes revealed that the CYP2A6 quad (0.47 $min^{-1}\mu M^{-1}$) and CYP2A6 pent mutants (0.26 $min^{-1}\mu M^{-1}$) had values between CYP2A13 (0.11 $min^{-1}\mu M^{-1}$) and CYP2A6 (0.66 $min^{-1}\mu M^{-1}$). The higher turnover rate by the mutant enzymes in comparison to wild type CYP2A13 may be the cause of the higher K_i values as a higher concentration of inhibitor is required to compete with the faster substrate turnover.

Table 4.4. Comparison of experimentally determined steady-state kinetic parameters for the metabolism of coumarin by CYP2A13 and CYP2A6 wild type enzymes and the CYP2A6 quad and pent mutants.

Enzyme	k_{cat} (min^{-1})	K_m (μM)	k_{cat}/K_m ($min^{-1}\mu M^{-1}$)
CYP2A13	1.29 ± 0.03	11.7 ± 1.05	0.11
CYP2A6	8.61 ± 0.20	13.98 ± 1.10	0.66
CYP2A6 quad mutant	9.93 ± 1.03	21.07 ± 6.5	0.47
CYP2A6 pent mutant	1.44 ± 0.05	6.32 ± 0.89	0.26

Crystallography for the CYP2A6 I208S/I300F/G301A/S369G (quad) mutant and CYP2A6 V117A/I208S/I300F/G301A/S369G (pent) mutant with select benzylmorpholine inhibitors

Crystallography experimentation with the CYP2A6 quad mutant began with **3** and the CYP2A13 precipitant solution that yielded the highest diffraction quality crystals (30% PEG 3350, 0.175 M Tris, pH 8.5, and 0.2 M magnesium chloride). The CYP2A6 quad enzyme was purified with either 0.5% Anapoe-35 or 4.8 mM Cymal-5 and resulted in rods with varying morphologies (Table 4.5 A and B), and data sets were collected to 2.1 Å and 2.15 Å.

Additional experimentation with the CYP2A6 mutant included a purification with 4.8 mM Cymal-5 and hanging drop vapor diffusion with compounds **6**, **7**, and **9**. Crystals grew well when purified with either 0.5% Anapoe-35 or 4.8 mM Cymal-5, but the addition of 0.2% Anapoe-X-405 prior to the formation of the hanging drop resulted in the best crystals. Data sets were collected with **6** to 2.25 Å (Table 4.5C), **7** to 1.9 Å and 2.0 Å (Table 4.5D), and **9** to 2.02 Å and 2.06 Å (Table 4.5E). The CYP2A6 pent mutant also co-crystalized well with **3** (Table

4.5F) and **7** (Table 4.5G) using the same conditions as the CYP2A6 quad mutant, and data was collected to 2.21 Å (**3**) and 2.06 Å (**7**). Like CYP2A6 (but unlike CYP2A13), all of the structures contained 4 molecules in the asymmetric unit with appreciable ligand density in at least two of the molecules. These resolution limits were determined by evaluating the multiplicity, Rpim, and mean (I/σ) with a minimum of ~90% completeness. The CYP2A6 quad structures were solved first, and as such, some of the data collection statistics were at the upper or lower limits of acceptable values. However, the data collection statistics for the CYP2A6 pent structures were more conservative and well within acceptable limits. Data collection and refinement statistics can be found in tables 4.6 and 4.7 for the CYP2A6 quad and pent mutants, respectively, and the structural details are described below.

Table 4.5. Summary of crystal formation and collected data for the CYP2A6 quad and pent mutants. Changes from previous attempts were underlined. (P) denotes the detergent used to purify CYP2A13 while (C) indicates the detergent added prior to hanging drop vapor diffusion.

	Enzyme	Detergent	Hanging Drop Information	Crystal Picture	Diffraction Information
A	CYP2A6 Quad Mutant	0.5% Anapoe-35 (P) 0.2% Anapoe-X-405 (C)	1:1 ratio of 11 mg/mL CYP2A6 quad mutant to mother liquor solution (30% PEG 3350, 0.1 M Tris, and 0.2 M $((NH_4)_2SO_4)$ with **3**		Collected 2.1 Å data set which displayed ligand density
B	CYP2A6 Quad Mutant	4.8 mM Cymal-5 (P) 0.2% Anapoe-X-405 (C)	1:1 ratio of 11 mg/mL CYP2A6 quad mutant to mother liquor solution (30% PEG 3350, 0.1 M Tris, and 0.2 M $((NH_4)_2SO_4)$ with **3**	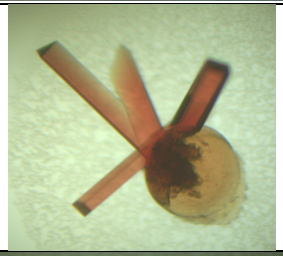	Collected 2.15 Å
C	CYP2A6 Quad Mutant	0.5% Anapoe-35 (P) 0.2% Anapoe-X-405 (C)	1:1 ratio of 11 mg/mL CYP2A6 quad mutant to mother liquor solution (30% PEG 3350, 0.1 M Tris, and 0.2 M $((NH_4)_2SO_4)$ with **6**	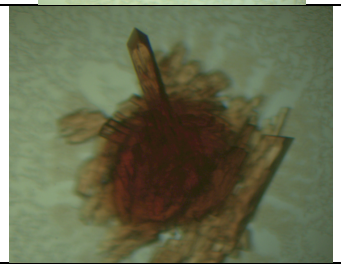	Collected 2.25 Å data set which displayed ligand density

	Enzyme	Detergent	Hanging Drop Information	Crystal Picture	Diffraction Information
D	CYP2A6 Quad Mutant	4.8 mM Cymal-5 (P) 0.2% Anapoe-X-405 (C)	1:1 ratio of 11 mg/mL CYP2A6 quad mutant to mother liquor solution (30% PEG 3350, 0.1 M Tris, and 0.2 M (NH4)2SO4) with 7	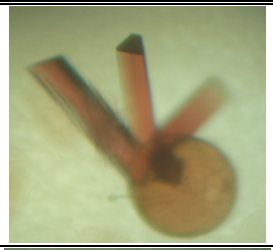	Collected data sets to 1.9 Å and 2.0 Å which displayed ligand density
E	CYP2A6 Quad Mutant	0.5% Anapoe-35 (P) 0.2% Anapoe-X-405 (C)	1:1 ratio of 11 mg/mL CYP2A6 quad mutant to mother liquor solution (30% PEG 3350, 0.1 M Tris, and 0.2 M (NH4)2SO4) with **9**	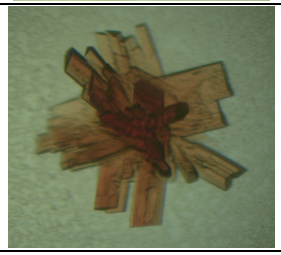	Collected data sets to 2.02 Å and 2.06 Å which displayed ligand density
F	CYP2A6 Pent Mutant	4.8 mM Cymal-5 (P) 0.2% Anapoe-X-405 (C)	1:1 ratio of 11 mg/mL CYP2A6 quad mutant to mother liquor solution (30% PEG 3350, 0.1 M Tris, and 0.25 M (NH4)2SO4) with **3**	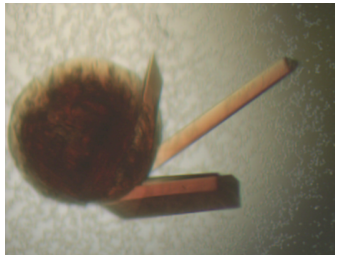	Collected 2.21 Å data set which displayed ligand density
G	CYP2A6 Pent Mutant	4.8 mM Cymal-5 (P) 0.2% Anapoe-X-405 (C)	1:1 ratio of 11 mg/mL CYP2A6 quad mutant to mother liquor solution (30% PEG 3350, 0.2 M Tris, and 0.275 M (NH4)2SO4) with **7**	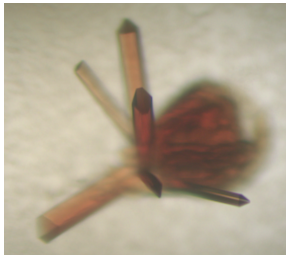	Collected data sets to 2.06 Å and 2.20 Å which displayed ligand density

Table 4.6. Current refinement statistics for the CYP2A6 quad mutant co-crystallized with **3**, **6**, **7**, and **9**.

	CYP2A6 I208S/I300F/G301A/S369G			
Ligand	**3**	**6**	**7**	**9**
Crystal data				
Space group	P 1 2_1 1	P 1 2_1 1	P 1 2_1 1	P 1 2_1 1
Unit Cell				
a, b, c (Å)	70.5, 159.2, 103.9	70.5, 159.2, 103.6	70.3, 158.8, 103.8	70.7, 160.3, 103.9
α, β, γ (˚)	90.0, 92.1, 90.0	90.0, 92.1, 90.0	90.0, 92.1, 90.0	90.0, 91.9, 90.0
Molecules per AU	4	4	4	4
Data Collection				
Resolution Limits (Å) *	42.6-2.1 (2.21-2.1)	43.6-2.25 (2.31-2.25)	46.4-1.9 (1.95-1.90)	31.13-2.02 (2.07-2.02)
Total observations*	914,929 (119,824)	408,463 (29,631)	673,430 (49,110)	1,129,928 (77,209)
Unique observations*	125,603 (17,312)	108,886 (8,019)	178,184 (13,165)	150,561 (11,140)
Completeness (%)*	94.6 (89.3)	100.0 (100.0)	99.9 (100.0)	99.8 (100.0)
Multiplicity*	7.3 (6.9)	3.8 (3.7)	3.8 (3.7)	7.5 (6.9)
R_{pim} *	0.04 (0.588)	0.05 (0.338)	0.061 (0.581)	0.058 (0.467)
Mean (I/σ) *	12.9 (1.7)	8.2 (1.8)	8.8 (1.8)	8.4 (2.1)
Refinement Statistics				
Resolution (Å)	29.66-2.1	43.60-2.25	41.01-1.9	31.13-2.02
No. of reflections	119,224	103,387	169,163	141,039
R/Rfree (%)	21.6/27.2	21.3/27.6	21.0/25.5	23.7/28.5
Rmsd bond lengths (Å)	0.023	0.022	0.024	0.023
Rmsd bond angles (˚)	1.933	1.934	1.890	1.962
Number of atoms/ Average B-factor	15,325/40.98	15,433/35.72	15,344/32.53	15,409/35.95
Protein	15,017/41.09	14,938/36.11	14,929/32.85	14,924/36.16
Heme	172/32.03	172/27.31	172/24.06	172/26.86
Ligand	42/48.10	45/69.68	45/42.64	30/51.44
Water	88/37.93	123/36.72	190/31.17	283/41.77

* Parentheses indicate highest-resolution shell

Table 4.7. Current refinement statistics for the CYP2A6 pent mutant co-crystallized with **3** and **7**.

	CYP2A6 V117A/I208S/I300F/G301A/S369G	
Ligand	**3**	**7**
Crystal data		
Space group	P 1 2_1 1	P 1 2_1 1
Unit Cell		
a, b, c (Å)	70.8, 160.5, 103.8	70.4, 159.0, 103.7
α, β, γ (˚)	90.0, 92.0, 90.0	90.0, 92.0, 90.0
Molecules per AU	4	4
Data Collection		
Resolution Limits (Å) *	42.57-2.21 (2.27-2.21)	47.49-2.06 (2.11-2.06)
Total observations*	640,871 (46,434)	1,014,236 (65,828)
Unique observations*	113,519 (8,266)	136,738 (9,805)
Completeness (%)*	98.3 (97.6)	97.6 (94.8)
Multiplicity*	5.6 (5.6)	7.4 (6.7)
R_{pim} *	0.079 (0.403)	0.042 (0.330)
Mean (I/σ) *	7.4 (2.4)	15.0 (3.6)
Refinement Statistics		
Resolution (Å)	41.14-2.21	43.40-2.06
No. of reflections	107,772	129,508
R/Rfree (%)	22.6/28.2	20.9/25.6
Rmsd bond lengths (Å)	0.021	0.023
Rmsd bond angles (˚)	1.876	1.86
Number of atoms/ Average B-factor	15,327/41.65	15,342/32.74
Protein	15,030/41.61	14,870/32.64
Heme	172/31.53	172/24.48
Ligand	56/85.69	30/86.70
Water	59/50.27	141/35.56

* Parentheses indicate highest-resolution shell

Overall comparison of CYP2A13, CYP2A6, CYP2A6 quad mutant, and CYP2A6 pent mutant structures

To detect any changes that the mutations might have had on the global enzyme structure, the Cα backbones from the CYP2A13 (PDB 2P85), CYP2A6 (PDB 2FDV), CYP2A6 quad mutant, and CYP2A6 pent mutant structures were overlaid. Only minor global differences were observed. The root mean square deviations from the CYP2A13 wild type structure ranged from 0.336 – 0.374 Å for all Cα carbons, confirming the similarity of the structures (Figure 4.10).

Figure 4.10. Structural overlay of CYP2A13 (maroon), CYP2A6 (green), CYP2A6 quad mutant (blue), and CYP2A6 pent mutant (yellow) enzymes.

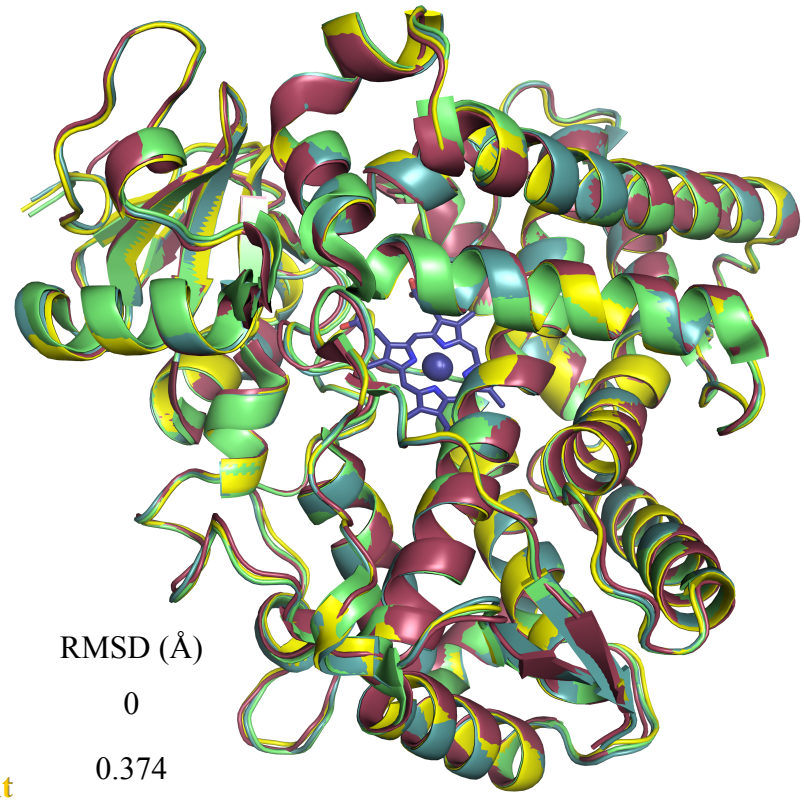

Active Site Volumes

To begin to compare the active sites of the CYP2A wild type enzymes versus the CYP2A6 quad and pent mutants, the probe-occupied volumes were calculated using Voidoo[20] with a probe radius of 1.4 Å. As a point of reference, previous structures revealed that the CYP2A6 wild type active site volume was ~250 $Å^3$, which is 15-20% smaller than the CYP2A13 active site of ~300 $Å^3$.[4,9] The CYP2A6 quad mutant crystallized with **3** had an active site volume of 305 $Å^3$. The CYP2A6 pent mutant structure had a volume of 285 $Å^3$. Both CYP2A6 mutants have cavity volumes greater than the CYP2A6 wild type enzyme, with the total volume of the CYP2A6 quad mutant being closer to the wild type CYP2A13 enzyme than CYP2A6.

Distribution of the active site volumes were similar between the enzymes with small differences (Figure 4.11), such as both the CYP2A6 quad and pent mutants penetrate slightly lower into the active site near I366. Additionally, the CYP2A6 quad and pent mutant deviate from one another near residue 117. The CYP2A6 quad mutant retains the CYP2A6 wild type valine residue, which extends further into the active site than the CYP2A13 alanine residue (Figure 4.11A). The deeper penetration into the active site is reflected in the reduced void volumes surrounding V117 in both CYP2A6 and the CYP2A6 quad mutant. However, the CYP2A6 pent mutant has the CYP2A13 wild type alanine residue at the 117 position, which allows for CYP2A13 and the CYP2A6 pent mutant to occupy a slightly larger volume in this area (Figure 4.11B).

Figure 4.11. Comparison of active site cavities for CYP2A13 (maroon) and CYP2A6 (green) overlaid with the A) CYP2A6 quad mutant (blue) and B) CYP2A6 pent mutant (yellow) demonstrated that the CYP2A6 mutants were more similar to CYP2A13 than CYP2A6. Cavities are probe occupied voids detected with a 1.4 Å probe. The heme is represented by black sticks with the iron atom as a rust colored sphere. The amino acid residues that are highlighted indicate mutated residues or those that are important for substrate binding.

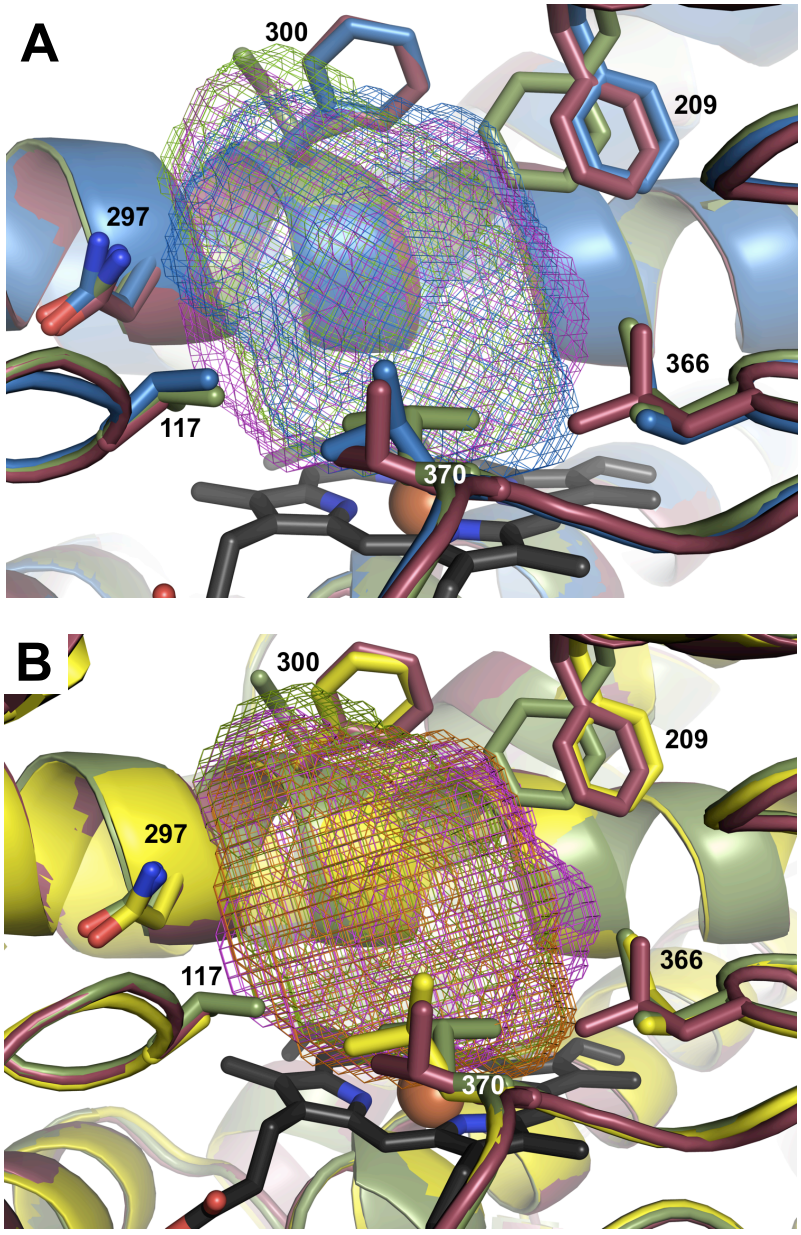

*CYP2A6 I208S/I300F/G301A/S369G (quad) mutant and 4-(2-chlorobenzyl)morpholine (**3**)*

Crystallization and structure determination with the CYP2A6 quad and pent mutants was successful as multiple data sets were collected and solved with four different benzylmorpholine inhibitors. The best data set collected with **3** and the CYP2A6 quad mutant yielded a 2.1 Å structure. Of the 4 molecules in the asymmetric unit, molecules A, B, and D displayed moderate density for a ligand, while molecule C only had a small amount of electron density at 1 σ. The density provided a rough outline as to the overall placement of the ligand, but the lack of well-defined density made the precise ligand orientation less definitive. The ligand was modeled into the $2|F_o| - |F_c|$ electron density map by placing the planar substituted benzene ring in the largest and most planar density with the electronegative chlorine substituent in the bulge of the density (Figure 4.12). The morpholine ring was then rotated into the remaining electron density. The data indicated that in each molecule the ligand was oriented with the morpholine ring toward N297 with a distance of 3.6-4.0 Å. The plane of the substituted benzene ring was almost perpendicular to the heme, and the chlorine atom was angled between F209 and F300. Despite this overall similar orientation in the three molecules, the ligands did appear to deviate from one another with respect to rotations of the morpholine ring. In molecule B, the plane of the morpholine ring through the carbon atoms was perpendicular to the plane of the benzene ring. Molecule D displayed the ring planes as parallel, but the electron density coverage was poor.

Figure 4.12. A 2.1 Å structure with the CYP2A6 quad mutant with compound **3** oriented within the active site of molecule B. The mesh represents the $2|F_o| - |F_c|$ electron density map contoured at 1 σ, while the red sticks represent the heme with the iron atom as a rust colored sphere. The amino acid residues that are highlighted indicate mutated residues or those that are important for substrate binding.

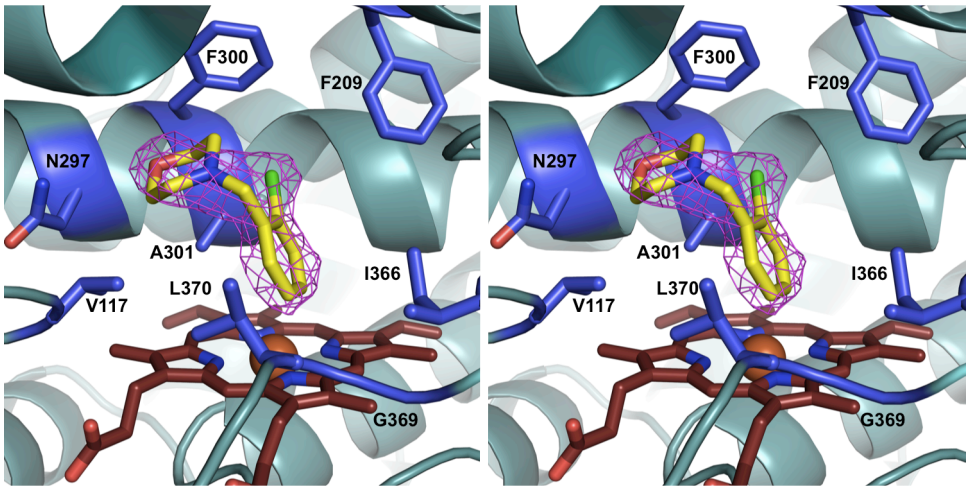

*CYP2A6 I208S/I300F/G301A/S369G (quad) mutant and 4-(2-ethylbenzyl)morpholine (**6**)*

The 2.25 Å data set with the CYP2A6 quad mutant and the ethyl substituted benzylmorpholine ligand (**6**) revealed **6** to bind in three different orientations in molecules A, B, and C (Figure 4.13). Molecule D had density for a water molecule located above the heme. Modeling of the ligands into the electron density began with the placement of the planar substituted benzene ring into the clearly planar portion of the electron density with the ethyl group in the bulge. The morpholine ring was positioned in the remaining electron density, which widened to encompass the width of the morpholine ring. This oriented the morpholine ring either near N297 with a distance of 3.6 - 3.9 Å (molecules A and C) or near the heme (molecule B). Molecules A and B had the best coverage of electron density for ligand placement, and the two orientations that were observed were vertically rotated 180˚ relative to one another. Molecule C did not have as extensive electron density for the ligand, but it was sufficient to demonstrate that while the morpholine ring was near N297 as in molecule A, it was rotated 90˚ (Figure 4.13 A versus C). One residue that clearly differs between molecules A and B versus C in this structure was the position of L370. The leucine side chain was angled in towards the active site ligand in molecule C but deflected toward N297 in molecules A and B. A similarity between the orientations observed in the CYP2A6 quad mutant with **6** and **3** was that the best fit of the ligand within the electron density placed the respective ethyl and chlorine substituents on the benzene ring between F209 and F300 and away from V117.

Figure 4.13. A 2.25 Å structure of **6** bound in the active site of A) molecule A, B) molecule B, and C) molecule C of the CYP2A6 quad mutant. The mesh represents the $2|F_o| - |F_c|$ electron density map contoured at 1 σ, while the red sticks represent the heme with the iron atom as a rust colored sphere. The amino acid residues that are highlighted indicate mutated residues or those that are important for substrate binding.

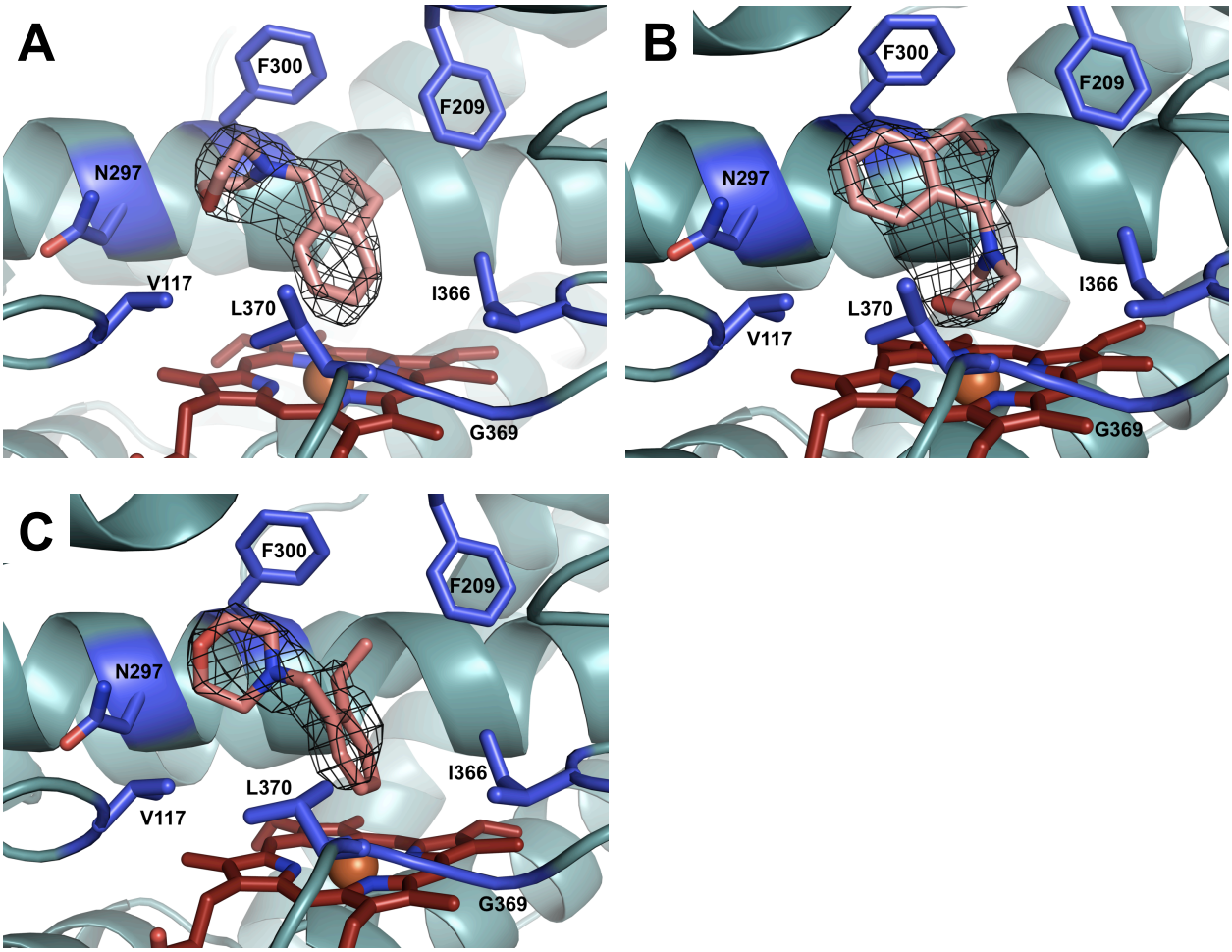

CYP2A6 I208S/I300F/G301A/S369G (quad) mutant and 4-(2-chloro-6-fluorobenzyl)morpholine (7)

A structure with the chlorine and fluorine disubstituted benzylmorpholine analog proved to be more challenging to orient the ligand within the active site due to the poorer definition of the ligand density. Despite data to 1.9 Å with compound **7**, only 3 of the 4 molecules had moderate ligand density. Compound **7** was modeled into the active site by positioning the planar benzene ring in the largest area of density with the chlorine and fluorine atoms in the adjacent bulges. Molecule A had the most defined electron density for the ligand and placed the morpholine ring 3.49 Å from N297 (Figure 4.14). The data suggested that the chlorine atom was positioned towards F300. Similar ligand placements were observed with the remaining two molecules with ligand density.

Figure 4.14. A 1.9 Å structure of the CYP2A6 quad mutant with compound **7** bound within the active site of molecule A. The mesh represents the $2|F_o| - |F_c|$ electron density map contoured at 1 σ, while the red sticks represent the heme with the iron atom as a rust colored sphere. The amino acid residues that are highlighted indicate mutated residues or those that are important for substrate binding.

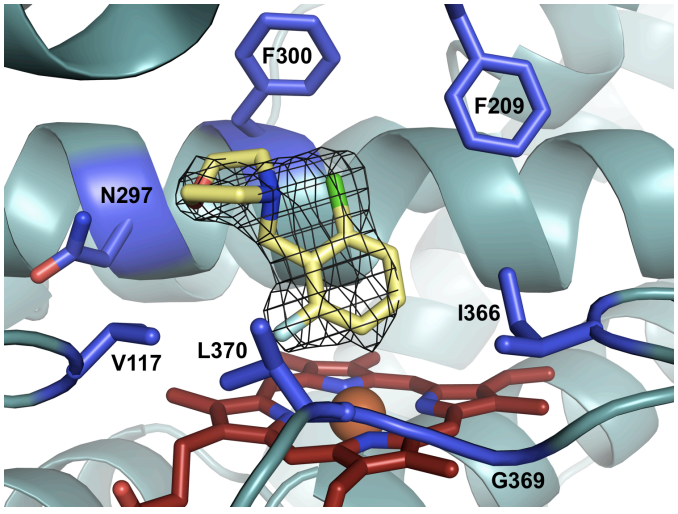

*CYP2A6 I208S/I300F/G301A/S369G (quad) mutant and 4-(2-chloro-6-methylbenzyl)morpholine (**9**)*

The second disubstituted benzylmorpholine analog that was crystallized with the CYP2A6 quad mutant had chlorine and methyl substituents (**9**) and proved to be more problematic to place the ligand than with the previous structure with **7**. A 2.02 Å data set had electron density in only two of the four molecules in the asymmetric unit, but only that in molecule A provided an outline for ligand orientation (Figure 4.15). The ligand was oriented in the active site by first placing the benzene ring and chlorine substituent in the most well-defined planar density. This position placed the morpholine near the heme rather than N297, and the chlorine atom was in a similar position within the active site but angled towards F209 rather than toward F300 as in the previous structure. While the electron density was not as defined for the ligand in molecule B, the data suggested that the ligand was oriented with the morpholine ring pointing towards N297, and the chlorine atom was pointing towards F300 similar to the CYP2A6 quad mutant with **7**.

Figure 4.15. A 2.02 Å structure of the CYP2A6 quad mutant with **9** bound in the active site of molecule A. The mesh represents the $2|F_o| - |F_c|$ electron density map contoured at 1 σ, while the red sticks represent the heme with the iron atom as a rust colored sphere. The amino acid residues that are highlighted indicate mutated residues or those that are important for substrate binding.

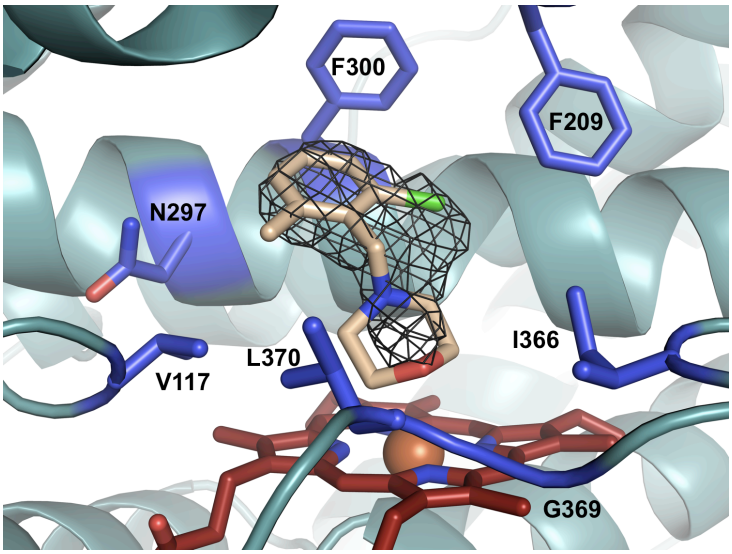

*CYP2A6 V117A/I208S/I300F/G301A/S369G (pent) mutant and 4-(2-chlorobenzyl)morpholine (**3**)*

The CYP2A6 pent mutant with the benzylmorpholine analogs yielded similar results to the CYP2A6 quad mutant. The 2.21 Å data set for the CYP2A6 pent mutant with the chlorine substituted benzylmorpholine (**3**) displayed ligand density for all four molecules within the asymmetric unit. The density supported two orientations previously observed in the CYP2A6 quad structure with **6** (Molecules A and C) in that the morpholine ring was near N297 or parallel to the heme (Figure 4.16 A and B). The substituted benzene ring was positioned in the dominant planar density with the chlorine atom pushing into the bulge of the density. Placement of the morpholine followed into density that widened out to match the width of the morpholine ring in all of the molecules except C (Figure 4.16C). As observed in the previous structures, the chlorine atom was best fit angled towards F209 or F300. Three of the four molecules oriented the ligand with the morpholine towards the heme (Figure 4.16A), with molecule C containing the most well-defined electron density for a ligand in any structure herein. The orientation of the ligand in molecule B (Figure 4.16B) has interesting and distinct differences from the other three molecules. While it could be argued that the ligand could be flipped, it appears that the planes of the morpholine and benzene rings were parallel to one another and the morpholine ring was oriented towards N297. In addition, L370 clearly adopted two alternate confirmations, which is not uncommon for this residue in CYP2A structures and may have affected the orientation of the ligand.

Figure 4.16. A 2.21 Å structure with the CYP2A6 pent mutant with compound **3** oriented within the active sites of A) and C) molecule C and B) molecule B with various orientations and degrees of ligand density. The mesh represents the $2|F_o| - |F_c|$ electron density map contoured at 1 σ, while the red sticks represent the heme with the iron atom as a rust colored sphere. The amino acid residues that are highlighted indicate mutated residues or those that are important for substrate binding.

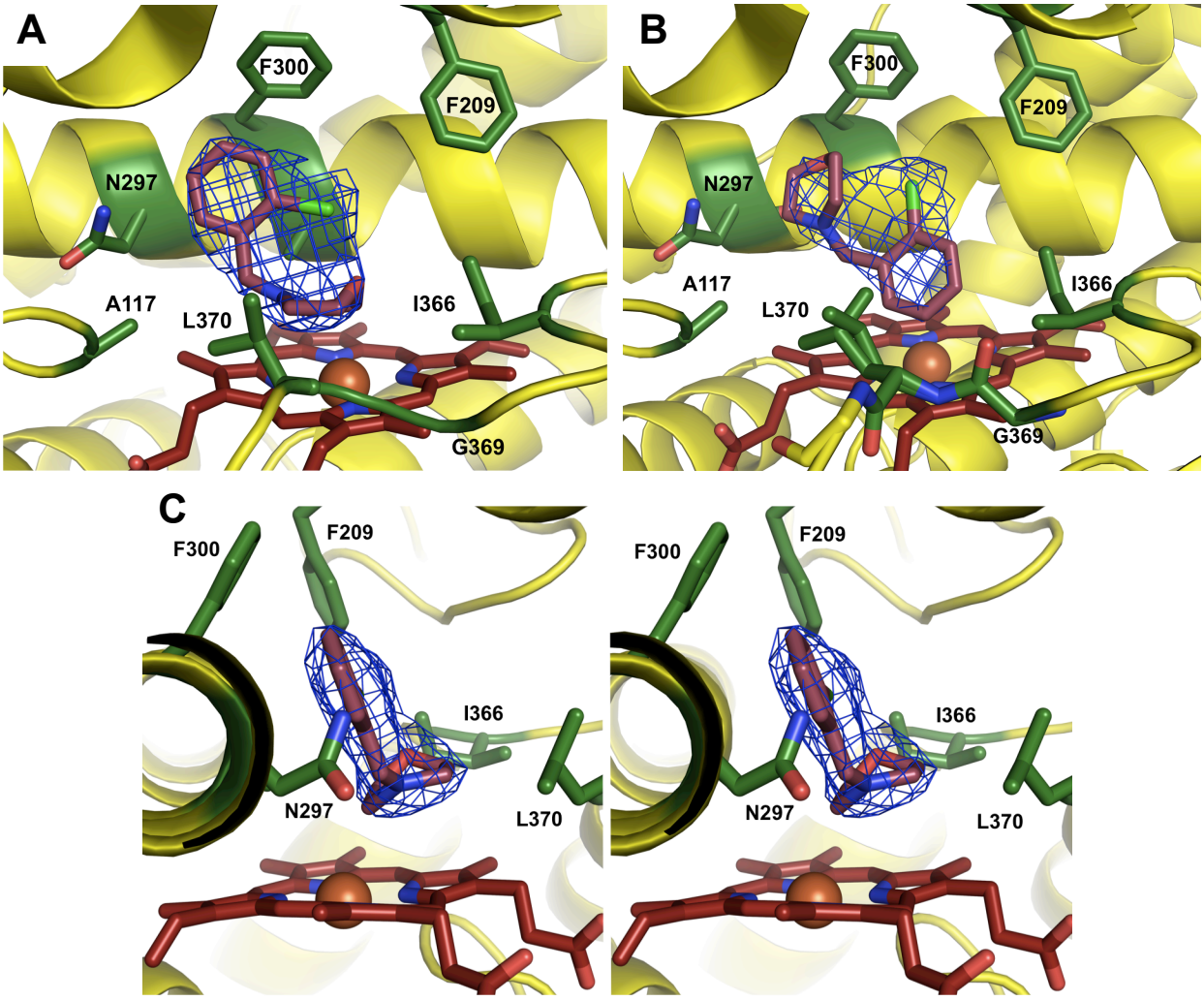

CYP2A6 V117A/I208S/I300F/G301A/S369G (Pent) mutant and 4-(2-chloro-6-fluorobenzyl)morpholine (7)

Analysis of a 2.06 Å data set with the CYP2A6 pent mutant and **7** revealed the same problems as with the other disubstituted ligands with the CYP2A6 quad mutant structures. Only two of the molecules had moderate ligand density while the remaining two molecules had only sparse density. The poor ligand density made it challenging to place the ligands within the active site. The electron density that was present suggested that the morpholine ring was angled towards N297 (3.32 Å), where it could form a weak hydrogen bond (Figure 4.17). The best fit of the ligand density positioned the chlorine atom towards F300.

Figure 4.17. A 2.06 Å crystal structure of CYP2A6 pent mutant with **7** bound in the active site. The mesh represents the $2|F_o| - |F_c|$ electron density map contoured at 1 σ, while the red sticks represent the heme with the iron atom as a rust colored sphere. The amino acid residues that are highlighted indicate mutated residues or those that are important for substrate binding.

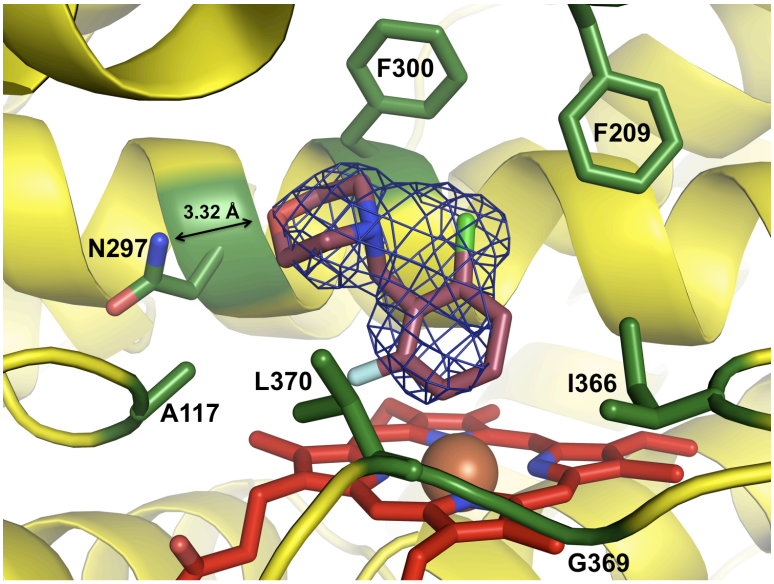

In conclusion, based upon the observation that N297 hydrogen bonds to multiple substrates in both CYP2A13 and CYP2A6,[4,5,9,10] it was hypothesized that a hydrogen bond would form between N297 and the oxygen of the morpholine ring, but either this was not observed or weak in some cases. Without a hydrogen bond to N297, there were no bonding interactions within the active site to lock the ligand into a single orientation, which may allow the ligands to bind in multiple orientations.

Discussion

Prior to X-ray crystallography, docking studies were performed to gain insight into ligand binding orientations within the CYP2A active sites. While the docking studies accurately predicted multiple binding orientations, overall the docking results were not definitive. The docking results were rarely able to accurately predict the selectivity of the ligands or whether the benzylmorpholine compounds were able to bind the CYP2A enzymes in a manner that would coincide with experimental data. However, the results may have been affected by the lack of a positive charge on the ligand during these studies. Regardless, the inaccuracy between the docking studies and functional experimental data illustrated the need for a co-crystal structure to evaluate the interactions between a benzylmorpholine analog and CYP2A13 or CYP2A6 mutated to function like CYP2A13.

The purpose of obtaining a co-crystal structure was to evaluate the atomic level interactions between a benzylmorpholine ligand and CYP2A13 for rational drug design. However, crystallographic attempts with CYP2A13 proved unsuccessful in that electron density for the placement of a ligand within the active site was either not observed or insufficient for ligand orientation. The CYP2A13-like enzymes CYP2A6 I208S/I300F/G301A/S369G (quad) mutant and CYP2A6 V117A/I208S/I300F/G301A/S369G (pent) mutant proved more

advantageous in solving six crystal structures: **3** (CYP2A6 quad 2.1 Å, CYP2A6 pent 2.21 Å), **6** (CYP2A6 quad 2.25 Å), **7** (CYP2A6 quad 1.9 Å, CYP2A6 pent 2.06 Å), and **9** (CYP2A6 quad 2.02 Å). These ligands bound in the active site with varying electron density quality.

Overall, two orientations were observed for the ligands bound to the CYP2A6 quad and pent mutant enzymes. The predominant disubstituted ligand orientation placed the morpholine ring towards the polar residue N297 with a distance of ≥ 3.32 Å, which is in a position to form a weak hydrogen bond. With the singly substituted benzylmorpholine ligands, the most well-defined ligand density placed the morpholine ring parallel to the heme with the benzene ring located near N297. However, the orientation with the morpholine ring near N297 was also observed, but the distance between the ligand and N297 was too great to form a hydrogen bond. Additionally, in two of the instances when the morpholine ring was near N297, the plane of the morpholine ring through the carbon atoms was rotated to be more parallel with the plane of the benzene ring (Figure 4.13C and Figure 4.16B), and L370 was pointing into the active site rather than away. These results indicate that L370 may be important for ligand orientation.

While the ligand density was not definitive, the best fit of the ligands revealed a common feature between the two orientations. The data suggested that there was a consistent placement of the chlorine substituent near the center of the active site and directed towards F209 or F300, which line the roof of the active site. This placement may be indicative of favorable hydrophobic interactions between the chlorine atom and the numerous phenylalanine residues within the active site. In addition to F209 and F300, F107 and F480 also line the roof of the active site near the chlorine atom (Figure 4.18). In the CYP2A6 pent mutant with **3**, F107, F209, and F480 were 4.17 Å – 4.69 Å from the phenyl ring to the chlorine atom. F300 lies further away with distances between 4.64 Å – 5.95 Å. In addition, this consistent placement of the

chlorine atom was not observed in the docking studies, further validating the necessity of X-ray crystallography.

Figure 4.18. Compound **3** bound within the active site of the CYP2A6 pent mutant illustrates potential hydrophobic interactions between the chlorine substituent and the F209 and F300, F107 and F480. The heme is represented by red sticks with a rust colored sphere indicating the the iron atom.

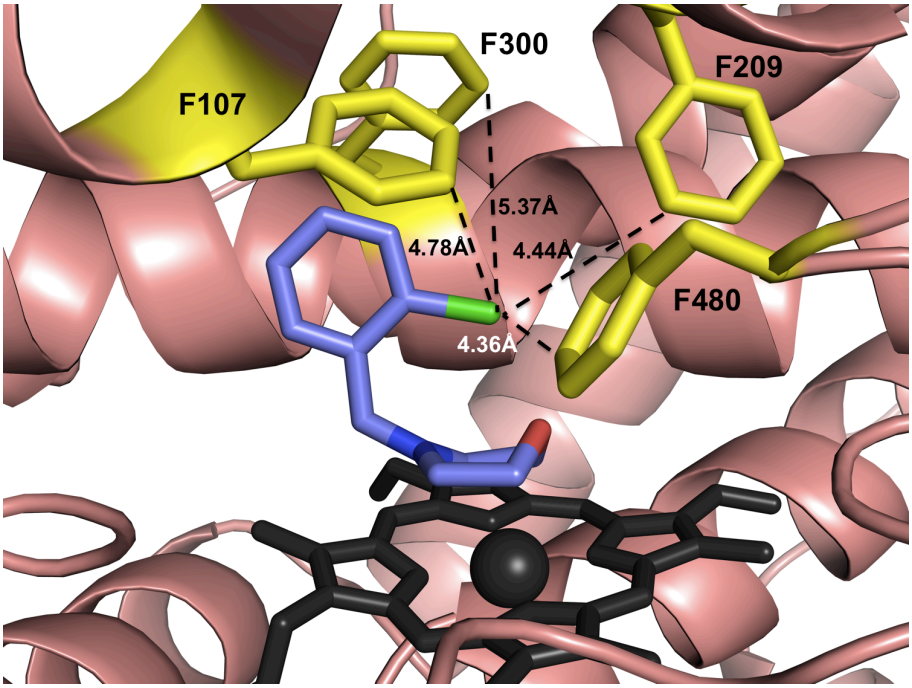

Based upon previous CYP2A13 and CYP2A6 crystal structures, it was anticipated that the oxygen of the morpholine ring would hydrogen bond with N297 and orient the benzylmorpholine ligands. However, in most instances the benzylmorpholine ligands were too far away for a hydrogen bond. Thus, it appears that there were no direct bonding interactions within the CYP2A quad and pent mutant active sites which allowed for multiple ligand orientations resulting in moderate ligand density.

Conclusions

Binding and inhibition analysis of the benzylmorpholine library with CYP2A13 and CYP2A6 provided information as to the behavior of the ligands with these enzymes. However, those results could not provide information pertaining to specific interactions between active site residues and the benzylmorpholine analogs. Thus docking and X-ray crystallography studies were performed to obtain a better understanding of the atomic-level interactions controlling the binding and orientation of the ligands within the CYP2A13 active site. While the docking results displayed multiple binding orientations, which agreed with the X-ray crystallography results, overall, the docking studies proved inconclusive and did not always correlate with experimental data.

X-ray crystallography was able to provide some insight into the ligand binding orientations within a CYP2A13-like active site. Since CYP2A13 crystals could not provide the desired co-crystal structure, the focus turned to CYP2A6 mutants that were engineered to function like CYP2A13. For unknown reasons, the ease with which CYP2A6 crystallizes versus the 94% identical CYP2A13 indicated that the packing interactions between the CYP2A6 molecules were more optimal and could be exploited with the CYP2A6 quad and pent mutant enzymes. The best fit of the electron density indicated that these CYP2A13-like enzymes oriented the morpholine ring towards N297 or parallel to the heme and placed the chlorine substituent in the middle of the active site where it could participate in hydrophobic interactions. This consistent placement of the chlorine atom was not observed during the docking studies, further indicating that the docking results may not be reliable. Combination of the structural information with the structure-activity relationships provides a more complete understanding of the interactions between benzylmorpholine ligands and CYP2A13.

Future directions would include additional attempts in crystallizing the wild type CYP2A13 enzyme to alleviate any concerns regarding the differences between the CYP2A6 mutants and CYP2A13. Recent work in the Scott lab has indicated that the presence of cytochrome b_5 during CYP2A13 crystallization in 0.5 M sucrose and 0.25 M potassium phosphate buffer resulted in consistent crystals with higher symmetry, fewer molecules in the asymmetric unit, and low 2 Å data with ligand present. The inclusion of cytochrome b_5 could yield the desired structural data of a benzylmorpholine analog bound to CYP2A13. An alternative strategy would be to mutate the CYP2A13 hydrophobic surface residues to hydrophilic residues to improve protein packing interactions, which has worked for other P450 enzymes.[23] However, should these techniques prove unsuccessful, binding and inhibition studies with CYP2A13 mutants could identify the amino acid residues controlling benzylmorpholine binding and inhibition. Correlation of these results with the current crystallographic data could provide more insight into the structure/function relationships between CYP2A13 and benzylmorpholine analogs.

Acknowledgements

I would like to thank Michael Urban, Kyle Baily, and Aggie Walsh for their work in the construction of the CYP2A6 quad mutant. In addition, I am grateful to Natasha DeVore for purifying the CYP2A6 quad mutant used for spectral ligand binding assays and inhibition studies.

References

1. Su, T. et al. Human cytochrome P450 CYP2A13: predominant expression in the respiratory tract and its high efficiency metabolic activation of a tobacco-specific carcinogen, 4-(methylnitrosamino)-1-(3-pyridyl)-1-butanone. *Cancer Res* **60**, 5074-5079 (2000).
2. He, X.Y. et al. Efficient activation of aflatoxin B1 by cytochrome P450 2A13, an enzyme predominantly expressed in human respiratory tract. *Int J Cancer* **118**, 2665-71 (2006).
3. DeVore, N.M., Smith, B.D., Wang, J.L., Lushington, G.H. & Scott, E.E. Key residues controlling binding of diverse ligands to human cytochrome P 450 2A enzymes. *Drug Metab Dispos* **37**, 1319-1327 (2009).
4. Smith, B.D. et al. Structure of the human lung cytochrome P450 2A13. *J Biol Chem* **282**, 17306-13 (2007).
5. DeVore, N.M., Smith, B.D., Urban, M.J. & Scott, E.E. Key residues controlling phenacetin metabolism by human cytochrome P450 2A enzymes. *Drug Metab Dispos* **36**, 2582-90 (2008).
6. He, X.Y. et al. Identification of Val117 and Arg372 as critical amino acid residues for the activity difference between human CYP2A6 and CYP2A13 in coumarin 7-hydroxylation. *Arch Biochem Biophys* **427**, 143-53 (2004).
7. He, X.Y., Shen, J., Ding, X., Lu, A.Y. & Hong, J.Y. Identification of critical amino acid residues of human CYP2A13 for the metabolic activation of 4-(methylnitrosamino)-1-(3-pyridyl)-1-butanone, a tobacco-specific carcinogen. *Drug Metab Dispos* **32**, 1516-21 (2004).
8. Schlicht, K.E., Michno, N., Smith, B.D., Scott, E.E. & Murphy, S.E. Functional characterization of CYP2A13 polymorphisms. *Xenobiotica* **37**, 1439-49 (2007).
9. Yano, J.K., Hsu, M.H., Griffin, K.J., Stout, C.D. & Johnson, E.F. Structures of human microsomal cytochrome P450 2A6 complexed with coumarin and methoxsalen. *Nat Struct Mol Biol* **12**, 822-3 (2005).
10. Devore, N.M. et al. Structural comparison of cytochromes P450 2A6, 2A13, and 2E1 with pilocarpine. *FEBS J* (2011).
11. Jain, A.N. Surflex: fully automatic flexible molecular docking using a molecular similarity-based search engine. *J Med Chem* **46**, 499-511 (2003).
12. Jain, A.N. Scoring noncovalent protein-ligand interactions: a continuous differentiable function tuned to compute binding affinities. *J Comput Aided Mol Des* **10**, 427-40 (1996).
13. The PyMOL Molecular Graphics System. Version 1.2r3pre edn (Schrödinger, LLC).
14. McCoy, A.J. et al. Phaser crystallographic software. *J Appl Crystallogr* **40**, 658-674 (2007).
15. Emsley, P. & Cowtan, K. Coot: model-building tools for molecular graphics. *Acta Crystallogr D Biol Crystallogr* **60**, 2126-32 (2004).
16. Murshudov, G.N., Vagin, A.A. & Dodson, E.J. Refinement of macromolecular structures by the maximum-likelihood method. *Acta Crystallogr D Biol Crystallogr* **53**, 240-55 (1997).
17. The CCP4 suite: programs for protein crystallography. *Acta Crystallogr D Biol Crystallogr* **50**, 760-3 (1994).
18. Vriend, G. WHAT IF: a molecular modeling and drug design program. *J Mol Graph* **8**, 52-6, 29 (1990).

19. Laskowski, R.A., MacArthur, M.W., Moss, D.S. & Thornton, J.M. PROCHECK: a program to check the stereochemical quality of protein structures. *J Appl Crystallogr* **26**, 283-91 (1993).
20. Kleywegt, G.J. & Jones, T.A. Detection, delineation, measurement and display of cavities in macromolecular structures. *Acta Crystallogr D Biol Crystallogr* **50**, 178-85 (1994).
21. Porubsky, P.R., Meneely, K.M. & Scott, E.E. Structures of human cytochrome P-450 2E1. Insights into the binding of inhibitors and both small molecular weight and fatty acid substrates. *J Biol Chem* **283**, 33698-707 (2008).
22. Porubsky, P.R., Battaile, K.P. & Scott, E.E. Human cytochrome P450 2E1 structures with fatty acid analogs reveal a previously unobserved binding mode. *J Biol Chem* **285**, 22282-90 (2010).
23. Zhao, B. et al. A Three-dimensional Structure of Steroid 21-Hydroxylase (Cytochrome P450 21A2) with Two Substrates Reveals Locations of Disease-associated Variants. *J Biol Chem* (2012).

Chapter 5

Expression, Purification, and Crystallization of CYP21A2

Introduction

In the pursuit of selective CYP17A1 inhibitors for the treatment of prostate cancer, it is imperative to screen potential drug candidates against protein targets that may also bind compounds of interest. In the case of CYP17A1, potentially selective inhibitors should be evaluated with CYP21A2, as a CYP17A1 substrate and product are substrates for CYP21A2 (Scheme 5.1). CYP17A1 metabolizes progesterone to 17α-hydroxyprogesterone[1] while CYP21A2 metabolizes progesterone to 11-deoxycorticosterone and 17α-hydroxyprogesterone to 11-deoxycortisol. Thus CYP21A2 is an important counter-target.[1] However, in order to evaluate the selectivity of drug candidates and conduct biochemical studies of CYP21A2, large quantities of purified P450 enzyme are necessary. *Escherichia coli* is the desired expression system for the production of large quantities of enzyme as *E. coli* does not contain cytochromes P450 and has proven successful for expression of other P450 enzymes.[2,3] However, human CYP21A2 has only been purified from *E. coli* in low yield of 40-50 nmol/L.[4] Thus until now information pertaining to the biochemical properties of CYP21A2 has primarily relied upon genetic studies,[5-7] homology models,[8-10] studies in microsomes,[3,8] or comparison to the 79% identical bovine CYP21A2 enzyme.[11,12]

Scheme 5.1. Substrate overlap between CYP17A1 and CYP21A2 in the steroid biosynthetic pathway.[1]

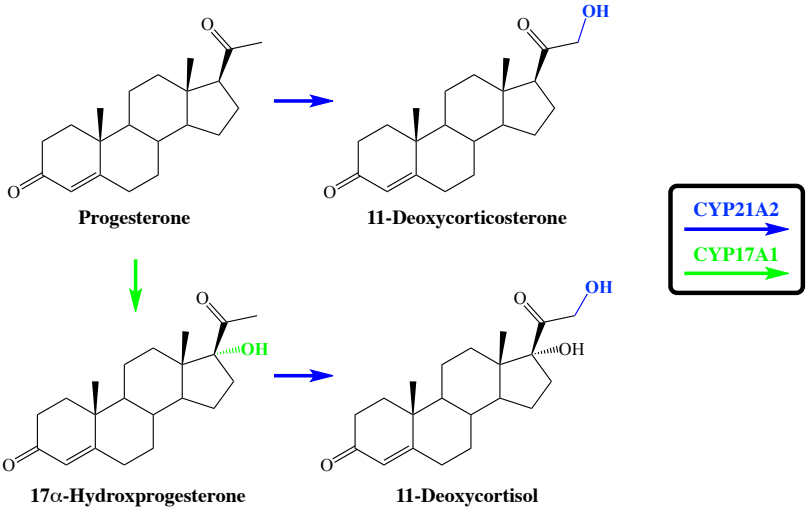

CYP21A2 is expressed in the adrenal cortex and is bound to the membrane of the endoplasmic reticulum. Expression of CYP21A2 is regulated by adrenocorticotropic hormone (ACTH) via a G-protein coupled receptor and the cAMP-dependent signaling pathway.[1] The human enzyme catalyzes the 21-hydroxylation of progesterone to 11-deoxycorticosterone with a V_{max} of 0.12 pmol/min/mg of protein and a K_m value of 1.1 μM in yeast microsomes.[8] Additionally, CYP21A2 converts 17α-hydroxyprogesterone to 11-deoxycortisol with a a V_{max} of 3.3 pmol/min/mg of protein and a K_m value of 1.6 μM with the same expression system.[8] A deficiency in 21-hydroxylase activity is responsible for 90-95% of cases of congenital adrenal hyperplasia (CAH) resulting from excessive ACTH stimulation and the overproduction of androgens.[7,13] Classic CAH involves genital ambiguity in the simple virilizing form of the disease or an aldosterone biosynthetic defect resulting in a more severe form called salt-wasting.[6] An asymptomatic individual with excess androgen synthesis is described as a non-classical form.[6] Recombination of CYP21A2 on chromosome 6 with the pseudogene CYP21A1 leads to

insertions and deletions resulting in missense and nonsense mutations.[1] There are over 150 mutations reported for CYP21A2.[14] These mutations can affect the solubility and stability of the enzyme through interruptions of reductase, heme, or substrate binding depending upon the location of the mutation.[1,10,15]

While significant research has been performed on the clinical role of CYP21A2 deficiencies and corresponding mutations, biochemical studies have been limited due to the lack of large-scale expressions and purifications.[8,11] *E. coli* expression of human CYP21A2 has been reported in low yields (40-50 nmol/L),[4] but the k_{cat} and K_m values were higher than recently reported values.[8] Progesterone and 17α-hydroxyprogesterone were metabolized with a k_{cat} of 192.9 and 198 min^{-1}, respectively, with K_m values of 14.7 μM for progesterone and 13.1 μM for 17α-hydroxyprogesterone. Additionally the K_d value was significantly higher for both progesterone (>100-fold) and 17α-hydroxyprogesterone (45-fold)[4] than experimentally determined herein, illustrating the need for a more thorough biochemical evaluation of CYP21A2.

Recent work has focused on the bovine CYP21A2 enzyme as sufficient quantities have been successfully expressed and purified from *E. coli*.[11,15] Bovine CYP21A2 is 79% identical to human CYP21A2 and was able to catalyze the conversion of progesterone to 11-deoxycorticosterone with a k_{cat} of 12.9 ± 5.8 min^{-1} and a K_m value of 1.88 ± 0.85 μM.[11] Additionally this enzyme catalyzed the conversion of 17α-hydroxyprogesterone to 11-deoxycortisol with a k_{cat} of 10.8 ± 5.3 min^{-1} and a K_m value of 1.04 ± 0.53 μM.[11] 17α-Hydroxyprogesterone was reported to be the preferred substrate for bovine CYP21A2 due to the slightly lower K_m value,[8,11] but the difference in K_m values between the substrates is less than 2-fold. [8,11] [8,11] Comparison of the human and bovine kinetic values for progesterone and 17α-

hydroxyprogesterone (Table 5.1) reveal that the V_{max} and k_{cat} values for human CYP21A2 are >10-fold higher than the bovine enzyme, an important difference which is not yet understood, supporting the need for direct studies of the human CYP21A2 enzyme.

Table 5.1. Summary of the progesterone and 17α-hydroxyprogesterone kinetic values for human and bovine CYP21A2.[4,8,15]

Species	Expression System	Progesterone		17α-hydroxyprogesterone	
		V_{max} or k_{cat}	K_m	V_{max}	K_m
Human	Yeast Microsomes	0.12 pmol/min/mg	1.1 μM	3.3 pmol/min/mg	1.6 μM
Human	*E. coli*	192.9 min^{-1}	14.7 μM	198 min^{-1}	13.1 μM
Bovine	*E. coli*	12.9 ± 5.8 min^{-1}	1.88 ± 0.85 μM	10.8 ± 5.3 min^{-1}	1.04 ± 0.53 μM

The large scale *E. coli* expression of bovine CYP21A2 was also instrumental in solving the first CYP21A2 structure, a 3 Å crystal structure reported recently.[11,15] The structure was consistent with the overall P450 fold with 12 α-helices and reported to contain two rather than four beta sheets.[15] However, a unique feature of the CYP21A2 structure was the observation that two substrates were bound with the proximal substrate located above the heme and the distal substrate located in the entrance of the substrate access channel. Even with the relatively high sequence similarity, it is unknown whether human CYP21A2 will share this feature.

The goal of this project is the expression, purification, and characterization of human CYP21A2 in order to 1) evaluate the structure/function relationships of CYP21A2 and 2) evaluate CYP21A2 as a counter-target for developing selective CYP17A1 inhibitors. The characterization of CYP21A2 can provide an in depth understanding of the biochemical interactions governing CYP21A2 activity. This chapter describes the first large-scale expression

of human CYP21A2 in *E. coli*. Additionally, purifications were successfully completed with multiple detergents and buffers leading to the first crystals of human CYP21A2.

Materials and Methods

Protein Modifications: Codon-optimized CYP21A2 cDNA was synthesized (Blue Heron Biotechnology, Bothel, WA) with NdeI and HindIII restriction sites at the 5′ and 3′ sites, respectively, a Δ2-28 amino acid N-terminal transmembrane deletion, addition of an N-terminal MAKKTSSKGK solubility tag, and a C-terminal 6-histidine tag in a Blue Heron pUCminusMCS vector. Figure 5.1 illustrates the modifications from the full length enzyme.

Figure 5.1. Amino acid sequence alignment of CYP21A2 modified and full length enzyme. Deleted residues are highlighted in red with added residues in blue.

```
                    10          20          30          40          50
Full Length   MLLLGLLLLP LLAGARLLWN WWKLRSLHLP PLAPGFLHLL QPDLPIYLLG
Truncated     MAKKTSSKGK ..................LP PLAPGFLHLL QPDLPIYLLG

                   490         500
Full Length   QPRGMGAHSP GQNQ
Truncated     QPRGMGAHSP GQNQHHHHHH
```

Cloning: A one-hour restriction digest of the pUC21A2 vector with NdeI and HindIII (New England Biolabs, Ipswich, MA) resulted in the desired CYP21A2 DNA fragment. An 0.8% agarose gel was used to separate the DNA fragments before the 1458 base pair CYP21A2 gene insert was extracted from the gel and subsequently purified with a QIAquick Gel Extraction Kit (Qiagen, Germantown, MD). Similar restriction digest and gel extraction were used to obtain the empty pCW vector (5038 base pairs). The purified CYP21A2 insert and pCW vector were ligated together using a quick ligation kit (New England Biolabs, Ipswich, MA). Ligation products were transformed into DH5α competent cells and plated on LB agar media with 50

μg/mL ampicillin. Isolated colonies were grown overnight at 37 ˚C with shaking at 250 rpm in separate 5 mL LB cultures containing 50 μg/mL ampicillin. The plasmid DNA was purified using QIAprep spin miniprep kit (Qiagen, Valencia, CA) and screened by restriction digest with MfeI, since the CYP21A2 gene would incorporate this unique restriction site into plasmid DNA. If a single cut was observed following restriction digest and gel electrophoresis, the complete cDNA in the pCW vector was sequenced by ACGT (ACGT, Wheeling, IL) with the forward (5′ GGAAACAGGATCAGCTTACTCCC-3′) and reverse (5′ GGCGTATCACGAGGCCCTTTCG-3′) pCW primers.

Expression:[11] The resulting pCW21A2 vector was transformed into DH5α *Escherichia coli* competent cells containing the pGro7 plasmid for expression of the GroEL chaperone protein. Cells were plated on LB agar plates containing 50 μg/mL ampicillin and 20 μg/mL chloramphenicol for selection of colonies containing both the pCW21A2 and pGro7 plasmids, respectively, using the methods described in chapter 2. Initially, 250 mL TB media in 1 L flasks containing 50 μg/mL ampicillin, 20 μg/mL chloramphenicol, and 500 μg/mL arabinose (for induction of the GroEL chaperone) were inoculated with 5 mL from a 200 mL LB overnight culture. However, later expressions were performed in 1L TB cultures in 2.5 L flasks and inoculated with 15 mL from an overnight culture as the size of the flask and culture did not impact the quality of the expression. Following incubation at 37 ˚C and shaking at 250 rpm for 2-3 hours an OD_{600} of 1.0-1.5 was reached and CYP21A2 expression was induced with 1 mM isopropyl β-D-1-thiogalactopyranoside (IPTG). In addition, heme synthesis was facilitated by the addition of delta aminolevulinic acid (ALA) to a final concentration of 1 mM. Following induction and ALA addition, the temperature and shaking were reduced to 27 ˚C and 190 rpm,

respectively, and cultures were incubated for 48 hours. Cells were pelleted at 6400 x g for 10 minutes at 4 ˚C, and the cell pellets were stored at -80 ˚C.

Purification: Purification of CYP21A2 for assays was based on the protocol outlined in chapter 2 for CYP2A enzymes with major changes including omission of the flash freeze step and utilization of Tris-based buffers. Harvested pellets were thawed and resuspended with 180-200 mL of resuspension buffer #1 (50 mM Tris-HCl and 20% glycerol). Lysozyme was added to a final concentration of 3 mg/mL and stirred at 4 ˚C for 30 minutes followed by the addition of 200 mL of distilled water and centrifugation at 10,000 x g and 4 ˚C for 15 minutes. The supernatant was discarded, and the pellet was resuspended with resuspension buffer #2 (50 mM Tris-HCl, 20% glycerol, and 300 mM NaCl) with a tissue homogenizer. This mixture was sonicated 3 times for 30 seconds before centrifugation at 10,000 x g for 15 minutes at 4 ˚C. The membrane-associated CYP21A2 enzyme was extracted from the membrane using 1% Emulgen 913 (Desert Biologicals, Phoenix, AZ) with stirring at 4 ˚C for a minimum of one hour. Ultracentrifugation at 4 ˚C and an average speed of 70,400 x g for 1 hour pelleted membranes, and the CYP21A2 containing supernatant was applied to a Ni-NTA affinity column with Ni-NTA loading buffer (50 mM Tris-HCl, 20% glycerol, 300 mM NaCl, and 0.2% Emulgen 913), washed with Ni-NTA wash buffer (50 mM Tris-HCl, 20% glycerol, 300 mM NaCl, 100 mM glycine, and 0.2% Emulgen 913), and eluted with Ni-NTA elution buffer (50 mM Tris-HCl, 20% glycerol, 300 mM NaCl, 100 mM glycine, 80 mM histidine and 0.2% Emulgen 913). Eluted heme protein from Ni-NTA chromatography was diluted 5-fold with CM wash buffer (50 mM Tris-HCl, 20% glycerol, and 100 mM glycine) containing 0.2% Emulgen 913 to decrease the salt concentration. Affinity chromatography was followed by cation exchange with a carboxymethyl (CM) cellulose resin. Protein that bound to the CM column was washed 10 times with CM wash buffer followed by

elution with CM elution buffer (50 mM Tris-HCl, 20% glycerol, 100 mM glycine, and 500 mM NaCl). Protein prepared for X-ray crystallography included a third chromatographic step consisting of size exclusion chromatography with CM elution buffer. A variation from the protocol used for the CYP2A enzymes was the increase in sample loading volume from 1 mL to 4 mL to reduce the risk of protein precipitation, which was observed in initial purification. In addition to purification with Tris buffers, twice the purification was performed with the potassium phosphate buffers described in chapter 2 but using the protocol described above. The only alteration to the potassium phosphate buffers was the reduction to 4 mM histidine in the Ni-NTA wash buffer and the substitution of 0.2% Emulgen 913 for 4.8 mM Cymal-5.

Polyacrylamide Gel Electrophoresis: The purity of the protein samples during the various purification stages was evaluated through sodium dodecyl sulfate polyacrylamide gel electrophoresis (SDS-PAGE). In addition, this technique was used to separate proteins in expression samples for further use in western blot analysis. Protein samples were denatured by diluting 1:1 with reducing sample-loading buffer (100 mM Tris-HCl, pH 6.8, 4% SDS, 200 mM dithiothreitol, and 20% glycerol) and heating for 3-5 minutes at 95 ˚C. The denatured protein was centrifuged up to 10 minutes at 18,000 x g at room temperature before loading 20 µL onto a 10% pre-cast Mini-protein TGX Gel (Bio-Rad, Hercules, CA). In addition 10 µL of a Page-Ruler Plus Pre-stained Protein Ladder (Thermo scientific, Dubuque, IA) was loaded onto the gel. If the SDS-PAGE gel was to be used for western blot analysis, 2.5 µL of 6xHis Protein ladder (Qiagen, Germantown, MD) was also loaded. Two hundred millivolts was applied to the gel submerged in SDS-PAGE running buffer (25 mM Tris, base, 192 mM glycine, and 0.1% SDS) for ~ 30 min. Following electrophoresis separation, the gel was developed or transferred to the western blot using the procedure described below. Development of the gel involved staining

with Coomassie stain (45% methanol, 10% acetic acid, and 0.1% w/v Coomassie) for 30 minutes followed by soaking in a strong destaining solution (45% methanol and 10% acetic acid) for 30 minutes and a weak destaining solution (10% methanol and 5% acetic acid) overnight.

Western Blot: Western blot analysis was used to determine the presence of a histidine tagged protein in expression samples. Samples run on an SDS-PAGE gel were transferred to a polyvinylidine difluoride (PVDF) membrane (Bio-Rad, Hercules, CA) by placing the gel against an activated PVDF membrane between filter paper (Bio-Rad, Hercules, CA), foam pads, and a holder cassette for use in a Mini Trans-Blot Electrophoretic Transfer Cell (Bio-Rad, Hercules, CA). The hydrophobic PDVF membrane was activated by soaking in 100% methanol for 1 minute followed by immersion in water for 3 minutes. The holder cassette was submerged in western transfer buffer (20% v/v methanol, 150 mM glycine, and 20 mM Tris base) and oriented with the gel towards the cathode and PVDF membrane to the anode. A current of 100 mA overnight at 4 ˚C or at 200 mV for 1 hour at room temperature with an ice pack in the apparatus was applied to complete the protein transfer to the PDVF membrane.

Following electrophoretic transfer, the membrane was washed with TBS buffer (10 mM Tris-HCl, pH 7.5, 150 mM sodium chloride) twice for 10 minutes before blocking with 10 mL of 0.3% bovine serum albumin (BSA) in TBS buffer for 1 hour with gentle rocking to prevent non-specific binding of the antibody to the membrane. After blocking, the membrane was washed with TBS-TX buffer (20 mM Tris-HCl, 500 mM sodium chloride, 0.05% Tween 20, and 0.2% Triton X-100) twice and TBS buffer once for 10 minutes each. The washing procedure was repeated following incubation of the membrane with a 1:2,000 ratio of the penta-His primary mouse antibody (Qiagen, Germantown, MD) in 0.3% BSA TBS solution for 1 hour. A secondary anti-mouse IgG-alkaline phosphatase antibody was applied to the blot with a 1:4,000

ratio in a 0.3% BSA TBS solution and reacted for 1 hour before washing for 10 minutes with TBS-TX buffer four times. The bands on the western blot were visualized through incubation with the 5-bromo-4-chloro-3-indolyl phosphate/Nitro blue tetrazolium (BCIP/NBT) color development solution (Sigma Aldrich, St. Louis, MO) for 20-30 minutes without rocking before the reaction was quenched with 1% acetic acid for 15 minutes followed by rinsing with water.

Absolute Absorption Assay and Carbon Monoxide Difference Assay: The absolute absorption and carbon monoxide difference assays for the determination of P450 concentration followed the protocol described in chapter 2 with one modification. Additionally, when Tris buffers were used, 50 μM progesterone was required in the assay buffer as no absorbance maxima was observed without a ligand present.

Spectral Ligand Binding Assays: Determination of the spectral dissociation constant for CYP21A2 with progesterone (Acros Organics via Fisher Scientific, Pittsburgh,VA) and 17α-hydroxyprogesterone (MP Biomedials, Solon, OH) used five centimeter path length cuvettes and the tight binding equation to determine K_d values as described in chapter 2.

Kinetic analysis: Metabolism assays utilized progesterone as the substrate with 11-deoxycorticosterone (Sigma Aldrich, St. Louis, MO) as the metabolic product. As with the CYP2A enzymes, CYP21A2 required the presence of P450 oxidoreductase (POR) for metabolism, but the ratio of P450 to POR needed to be established along with the necessity of the presence of cytochrome b_5. P450, POR, and cytochrome b_5 comprise the reconstituted protein system (RPS). Evaluation of the RPS ratio and incubation times and temperatures is described in the results section. Reaction times with substrate, RPS, 1 mM NADPH, and buffer (50 mM Tris, HCl pH 7.4 and 5 mM magnesium chloride) were also varied as described in the results section. The final assay volume was 500 μL, and all reactions were terminated with 300

μL of 20% trichloroacetic acid. The samples were centrifuged at 4 ˚C and 4,500 x g for 8 minutes and 600 μL was transferred into HPLC vials. Fifteen microliters were injected onto a Luna C18 reverse phase column (Phenomenex). The mobile phase consisted of 64% solvent A (0.2% acetic acid) and 36% solvent B (100% acetonitrile). Each sample was analyzed for absorption at 248 nm over the course of 20 minutes at 1.5 mL/min. Under these conditions, 11-Deoxycorticosterone eluted at 4.1 minutes, while progesterone eluted at 14.6 minutes.

Crystallography: De novo screening was performed with purified CYP21A2 protein concentrated to 14-25 mg/mL. The protein solutions were mixed in a 1:1 ratio with the commercial sparse matrix screen in a 1.2 μL drop. Crystal screens 1 and 2 (Hampton Research, Aliso Viejo, CA), Wizard screens 1-4 (Emerald Biosystems, Bainbridge Island, WA), PEG/Ion (Hampton Research, Aliso Viejo, CA), and MembFac 2 (Hampton Research, Aliso Viejo, CA) comprised the panel of screens that were used in Corning 96 well sitting drop plates (Hampton Research, Aliso Viejo, CA). Crystallization conditions were optimized with 24 well plates (Hampton Research, Aliso Viejo, CA) utilizing hanging drop vapor diffusion as detailed in the results section.

Results

Protein Modifications[11]

The CYP21A2 gene was modified from the full-length form by a Δ2-28 amino acid N-terminal transmembrane deletion and additions of a N-terminal MAKKTSSKGK solubility tag, a 6 residue C-terminal histidine tag, 5′ NdeI restriction site, and a 3′ HindIII restriction site. The modified gene was cloned into a pCW vector and transformed in DH5α/pGro7 *E. coli* competent cells.

Expressions and Purifications

CYP21A2 expressed well in DH5α/pGro7 *E. coli* competent cells resulting in ~30 g of dark brown cell pellet from 2.25 L of culture. A western blot with an anti-His antibody confirmed the presence of histidine-tagged protein at ~55 kDa at 24 and 48 hours after induction, which correlates well with the expected molecular weight of 54.5 kDa for CYP21A2. Due to the lack of specificity of the anti-His antibody, multiple dark bands were observed, but it was clear that expression of a ~55 kDa histidine-tagged protein was induced.

The CYP21A2 purifications followed the CYP2A purification protocol with cell lysis mediated through lysozyme, homogenization, and sonication and then followed by detergent extraction and ultracentrifugation. The enzyme was purified through Ni-NTA affinity and cation exchange chromatography, followed by size exclusion chromatography when the protein was to be used for crystallography. Primary changes to the CYP2A protocol included the use of Tris-based buffers in addition to potassium phosphate buffers, 0.2% Emulgen 913, and the presence of progesterone during some purifications. Purity of the protein samples was determined through SDS-PAGE.

The first purification used Tris buffers with 4.8 mM Cymal-5 and resulted in CYP21A2 protein with only trace impurities after cation exchange chromatography according to SDS-PAGE (Figure 5.2 CM). Unfortunately, a significant quantity of the CYP21A2 protein was not stable during the purification and ultimately precipitated, resulting in substantial losses. This can be visualized by comparing the amount of active P450 enzyme and inactive P420 enzyme using the reduced carbon monoxide difference spectra at the various purification stages (Figure 5.3). For example, the supernatant from ultracentrifugation contained 664 nmol of solubilized CYP21A2, but Ni-NTA affinity chromatography elution fractions contained 12 nmol P450 and

80 nmol P420. After cation exchange chromatography, the sample consisted of 20 nmol of P450 and 20 nmol of P420.

Another interesting observation was the elution of several green fractions from the Ni-NTA column followed by the normally observed red fractions. Absolute absorption and carbon monoxide difference assay spectra indicated that the 67 nmol of P420 that was present in this green fraction was bound to a type II ligand, which is attributed to the histidine present in the Ni-NTA wash and elution buffers. In addition, these green fractions contained more impurities according to SDS-PAGE (Figure 5.2 Ni E. (Green)) and were not included in the remainder of the purification. At this stage it was unclear if the purer red fractions (Figure 5.2 Ni (Red)) also had a type II ligand bound (λ_{max} = 420 nm), but after the CM column, CYP21A2 had a Soret peak at 422 nm indicative of a type II ligand bound in the active site.

Figure 5.2. SDS-PAGE results for the purification of CYP21A2 with Tris buffers and 4.8 mM Cymal-5 indicate that the samples contained only trace impurities following cation exchange chromatography. SDS-PAGE gel key is as follows (S): Solubilized CYP21A2 following detergent extraction and ultracentrifugation, (Ni FT): Ni-NTA flow through during sample loading, (Ni W): Ni-NTA wash fractions, (Ni E.): Ni-NTA elution (Green) and (Red) fractions, (CM): cation exchange elution fractions, (X): empty lane or unrelated sample, and (MW): dual color molecular weight ladder.

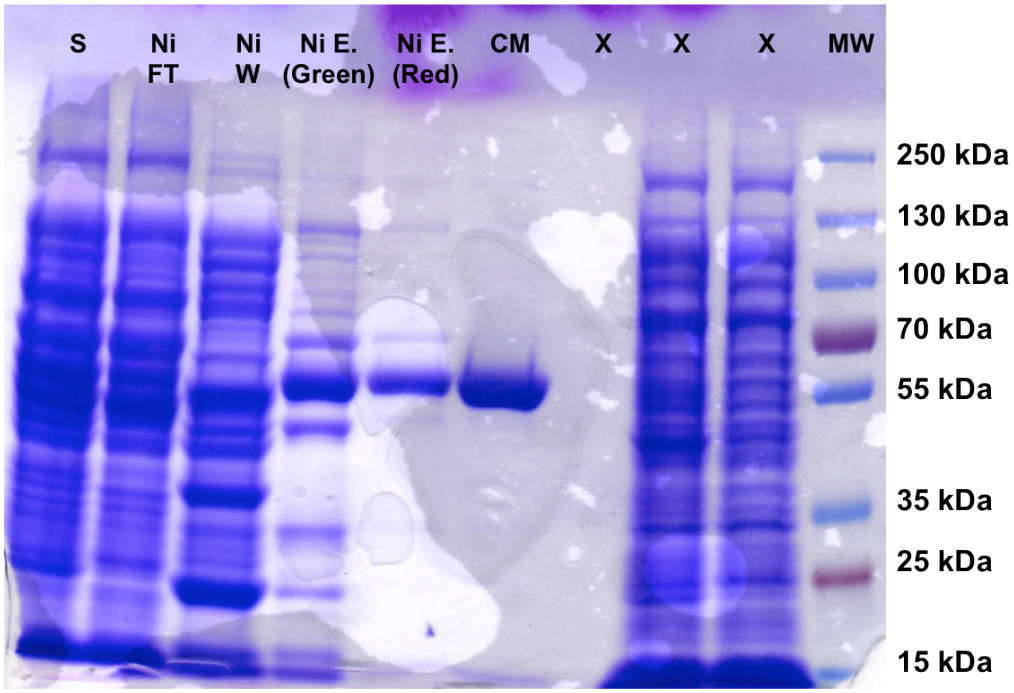

Figure 5.3. Reduced carbon monoxide difference assay spectra from the purification of CYP21A2 with Tris buffers and 4.8 mM Cymal-5 following A) ultracentrifugation, B) Ni-NTA affinity chromatography, and C) cation exchange chromatography.

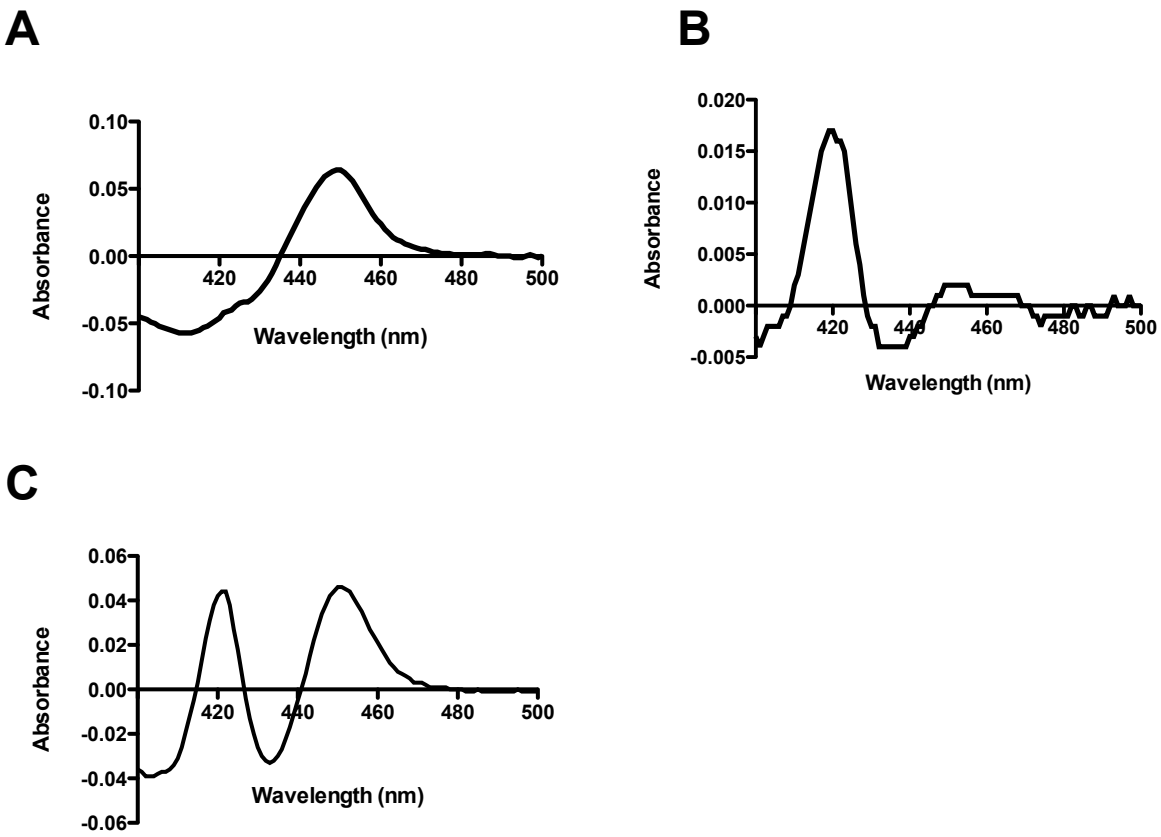

The second purification with CYP21A2 used 0.2% Emulgen 913 rather than 4.8 mM Cymal-5 and resulted in 10-fold more P450 following cation exchange chromatography for a total of 220 nmol. Absolute spectra were consistent with water-bound iron with a Soret peak at 418 nm after Ni-NTA affinity and cation exchange chromatography even though progesterone was present in the cuvette but not purification buffers. Since progesterone is a type I ligand,[11] a Soret peak should have shifted to 393 nm but no shift was observed. Additionally, both red (Figure 5.4 Ni E. (Red)) and green fractions (Figure 5.4 Ni E. (Green)) were again observed

eluting during Ni-NTA affinity chromatography, but only the red fractions were purified further. SDS-PAGE analysis indicated trace impurities following cation exchange but the most prominent band was at 55 kDa (Figure 5.4 CM), and this protein was aliquotted for use with initial binding and kinetic analysis. These results indicated that 0.2% Emulgen 913 was a better detergent for purification of CYP21A2 even though 4.8 mM Cymal-5 resulted in slightly purer protein. Additional purification results for CYP21A2, which included size exclusion chromatography for use in protein crystallography can be found under the crystallography subsection. These results indicate that human CYP21A2 was successfully expressed and purified in sufficient quantities for use in initial biochemical studies.

Figure 5.4. SDS-PAGE results for the purification of CYP21A2 with Tris buffers and 0.2% Emulgen 913 indicate that the final sample contained only trace impurities following cation exchange chromatography. SDS-PAGE gel key is as follows (S): Solubilized CYP21A2, (Ni FT): Ni-NTA flow through, (Ni W): Ni-NTA wash, (Ni E.): Ni-NTA elution (Green) and (Red) fractions, (CM): cation exchange, and (MW): dual color molecular weight ladder.

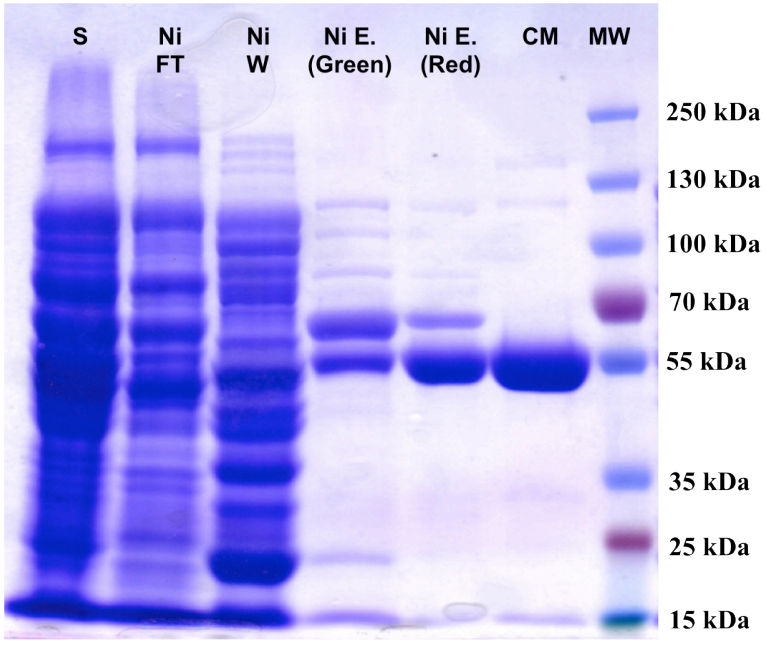

Protein Crystallography

Protein crystallography requires large quantities of monodisperse pure enzyme. The previous purification results demonstrated that large quantities could be obtained. However, size exclusion chromatography was added as an orthogonal purification step to remove any remaining impurities. Size exclusion chromatography has also been known to separate P420 and P450, (Personal communication with Dr. Natasha DeVore) and some P450 enzymes require this chromatographic step for crystal formation. Additionally, in the process of producing protein for crystallography with size exclusion chromatography, we learned some additional information about the earlier steps of CYP21A2 purifications.

Protein crystallization is an iterative process and often requires the evaluation of numerous variations to find the optimal conditions for crystal growth. In the case of CYP21A2, purification trials with various buffers, detergents, and the presence or absence of ligand were evaluated. The purified protein was concentrated to 14-25 mg/mL with either 50 μM progesterone or 50 μM 17α-hydroxyprogesterone and used in *de novo* screening in 96 well plates.

Tris Buffers

The first purification of CYP21A2 for crystallography used Tris buffers with 4.8 mM Cymal-5, and included 50 μM progesterone in every stage of the purification in an effort to stabilize the enzyme. While 4.8 mM Cymal-5 was not optimal for stabilizing CYP21A2, this detergent has been successfully used with other P450 enzymes resulting in crystal structures.[16,17] Unfortunately, the inclusion of ligand did not prevent protein precipitation as precipitate was observed at each purification step, yielding only 37.4 nmol of pure enzyme following size exclusion chromatography (Figure 5.5 cymal-5 SEC (red)). This yield was a significant

reduction from the 1160 nmol of solubilized P450 initially present following ultracentrifugation. However, this was sufficient protein to concentrate CYP21A2 bound to progesterone to 14 mg/mL and survey the panel of available crystallization screens: Crystal screens I and II, Wizard screens I, II, III, IV, PEG Ion, and Memb Fac, but no crystal hits were observed.

The next two purification protocols for crystallography used Tris buffers, 50 μM progesterone, and 0.2% Emulgen 913 as this detergent was more successful in stabilizing CYP21A2. Following size exclusion chromatography, the elution fractions contained ≥78 nmol and 386 nmol of P450 enzyme respectively. The protein from the first purification appeared to contain a smaller quantity of a 70 kDa impurity (Figure 5.5 SEC (black versus green)), but this may have been due to a well loading effect. The purified protein was concentrated to 25 mg/mL and screened against the entire panel of available screens, but only phase separation and precipitate were observed. The screening process did not require the entire quantity of purified CYP21A2, and the unused protein was stored at -80 ˚C for later use as described below.

Figure 5.5. SDS-PAGE gel evaluating protein purity for CYP21A2 purified with either 0.2% Emulgen (black and green) or 4.8 mM Cymal-5 (red) in Tris buffers. Gel key is as follows (S): Solubilized CYP21A2, (Ni): Ni-NTA affinity elution fractions, (CM): cation exchange elution fractions, (SEC): size exclusion elution fractions and (MW): dual color molecular weight ladder.

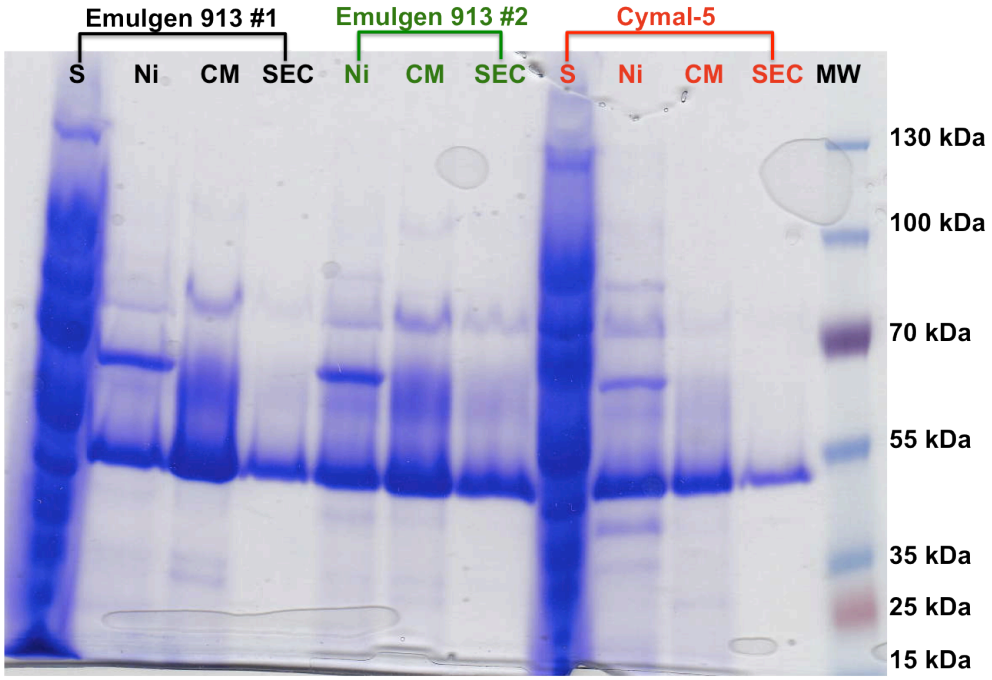

Since the initial purification protocols for crystallography did not yield crystals, an alternative strategy was employed with thawed CYP21A2 protein. In crystallization of the CYP2A enzymes, detergent combinations such as Anapoe-X-405 with either 0.5% Anapoe-35 or 4.8 mM Cymal-5 proved to be successful. This method was attempted prior to screening with the addition of 4.8 mM Cymal-5 to CYP21A2 purified with 0.2% Emulgen 913, but this method was also unsuccessful in producing crystals. Figure 5.6 summarizes the crystallography attempts with Tris-based buffers.

Figure 5.6. Flow chart summary for the crystallography attempts with Tris based buffers.

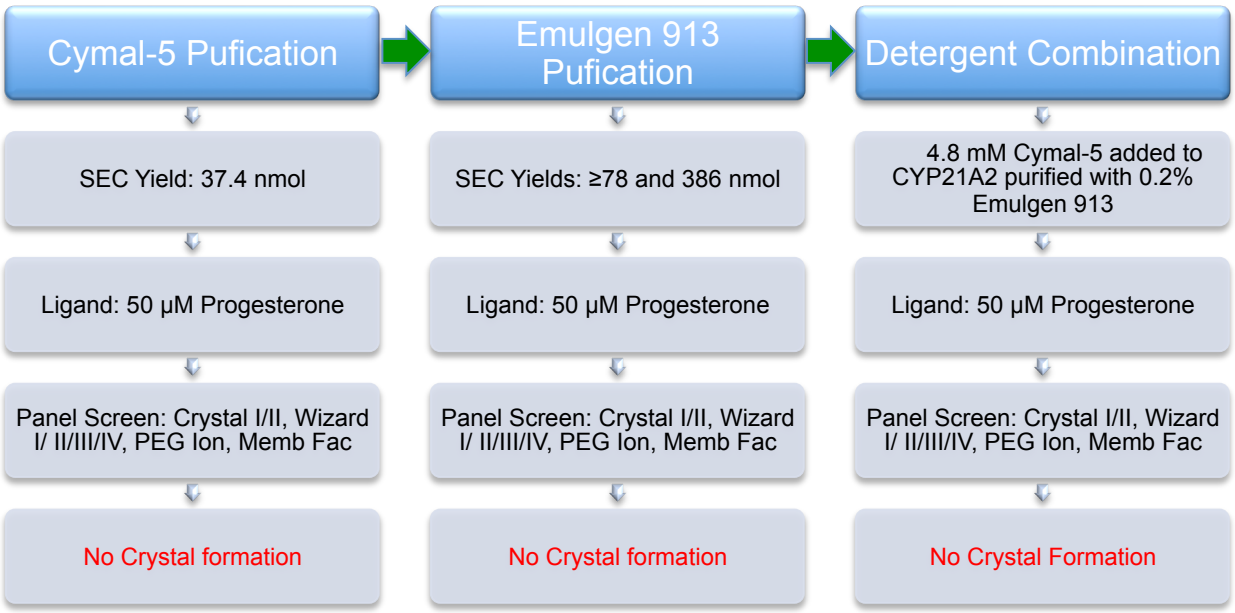

Potassium Phosphate Buffers

The next step in crystallography was to exchange the Tris-based buffers for potassium phosphate buffers as buffers can also effect crystal formation. Twice the purification of CYP21A2 was performed with 0.2% Emulgen 913 in the absence of ligand. Following size exclusion chromatography, the first purification yielded 67 nmol of P450 and 57 nmol of P420. This was the first time a P450 peak was observed with purified CYP21A2 without a ligand present for stabilization, indicating that potassium phosphate buffers may be superior to Tris buffers for stabilization of the CYP21A2 enzyme. The second purification yielded ≥419 nmol of P450 following size exclusion chromtography in the presence of ligand, which was a higher yield than any of the purification trials with Tris buffers. The purified protein was concentrated with either 50 µM progesterone or 50 µM 17α-hydroxyprogesterone to 25 mg/mL. In both cases, however, little or no shift was observed in the Soret peak λ_{max} upon ligand addition.

De novo screening with the panel of crystallization screens resulted in multiple wells with phase separation and the first crystal hit with Wizard screen I #42. Red plates with progesterone or 17α-hydroxyprogesterone formed with 15% ethanol and 0.1 M Tris, pH 7.0 (Figure 5.7). It is unknown as to which ligand is bound because of a labeling error.

Figure 5.7. Red plates formed with Wizard screen I #42 with CYP21A2 purified with 0.2% Emulgen 913 in potassium phosphate buffers. Image contrast and brightness were adjusted for better visualization of the crystals.

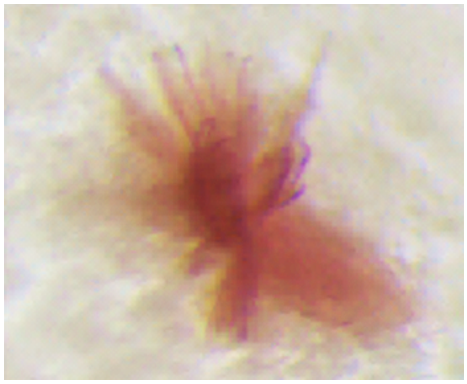

The next step was to duplicate these crystals to demonstrate reproducibility and to optimize crystallization conditions with the goal of generating larger single crystals that were of diffraction quality. Unfortunately, attempts to duplicate the original crystal did not yield the same results, and attempts at optimizing the precipitant solution in either 24 or 96 well plates have been unsuccessful to date. Optimization included varying the ethanol content from 1-15% with 0.05 M – 0.175 M Tris, pH 7.0. However, it should be noted that these duplication and optimization attempts used CYP21A2 protein that had been previously stored at -80 ˚C rather than freshly purified. In addition, a new precipitant solution was used rather than the older original stock solution, and only precipitated protein was observed. Subsequent screening of the

original precipitant solution with a lower protein concentration also did not yield success. The original stock solution and protein concentration will be examined once more with a future purification.

Due to the lack of success with optimization conditions, and the recent publication of the bovine CYP21A2 structure, additional crystallization solutions were examined.[15] The bovine CYP21A2 enzyme was crystallized with 5-15% PEG 3350, 0.5 M ammonium sulfate, and 0.1 M HEPES, pH 7.0 with a protein concentration of 11 mg/mL.[15] This solution was used as a starting point for a 24 well plate optimization screen with 5-15% PEG 3350, 0.5 M ammonium sulfate, and 0.075 M – 0.15 M HEPES, pH 7.0. Protein previously stored at -80 ˚C was thawed and diluted to 11 mg/mL with CM elution buffer containing either 50 μM progesterone or 50 μM 17α-hydroxyprogesterone. The diluted protein solution also contained either 0.2% Emulgen 913 or a combination of 0.2% Emulgen 913 with 4.8 mM Cymal-5. Unfortunately no crystals were observed, but this could have been because the human enzyme was not freshly purified, differences between bovine and human CYP21A2, or differences in the purification detergent. Compared to human CYP21A2 which was purified with 0.2% Emulgen 913, the bovine CYP21A2 was purified with 1% cholate and 1% Tween 20 and later combined with ~ 5 mM Cymal-5 for crystallization.

Finally, the bovine CYP21A2 crystallization solution was similar to the CYP2A and CYP17A1 crystallization solutions (30% PEG 3350, 0.2-0.3 M ammonium sulfate, 0.175 M Tris pH 7.0-8.5, and +/-3% glycerol). Thawed CYP21A2 purified with potassium phosphate buffers was diluted to a final concentration of 11 mg/mL with either 0.2% Emulgen 913 or in combination with 4.8 mM Cymal-5 in buffer containing 50 μM progesterone or 50 μM 17α-hydroxyprogesterone. The protein solution was equilibrated against 30% PEG 3350, 0.175 M

Tris pH 7.0, 0.3 M ammonium sulfate, and +/-3% glycerol with hanging drop vapor diffusion in a 24 well plate. Only the wells containing progesterone and 0% glycerol resulted in phase separation, but no crystals were observed. Figure 5.8 summarizes the crystallization experimentation with CYP21A2.

Figure 5.8. Flow chart summary for the crystallography with potassium phosphate buffers that led to the first protein crystals for human CYP21A2. All screens included 50 µM progesterone or 50 µM 17α–hydroxyprogesterone in the protein drops.

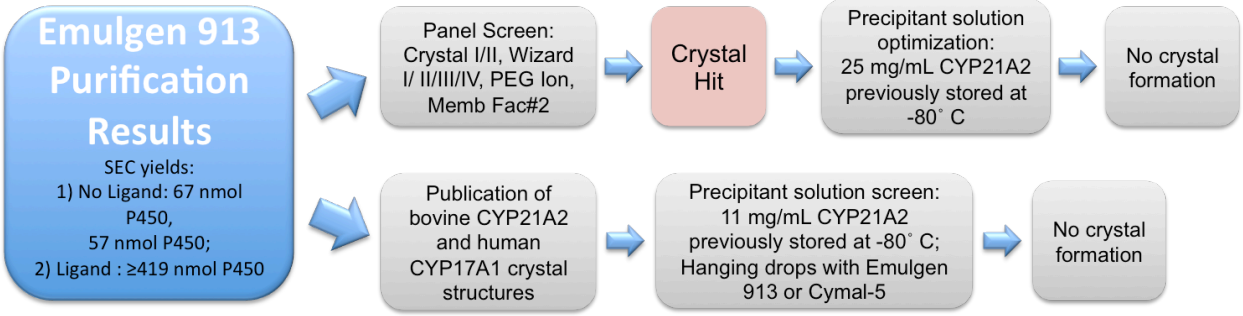

In summary, CYP21A2 was successfully purified and crystallized with potassium phosphate buffers, but these crystals have not been replicated to date (Figure 5.8). Time has been the limiting factor thus far, but future experiments will include purifying CYP21A2 with 1% cholate and 1% Tween-20 for use with the bovine CYP21A2 precipitant solutions or with 0.2% Emulgen 913 for replication of the original precipitant conditions that resulted in the crystal hit. Fresh protein will be used with these conditions to eliminate questions regarding fresh versus frozen protein as crystallography can be sensitive to freeze/thaw cycles.

Substrate Binding

The equilibrium dissociation constants for the substrates progesterone and 17α-hydroxyprogesterone were determined as described in chapter 2 with purified CYP21A2, 5 cm

path length cuvettes, and the tight binding equation. Titration data was not optimal due to the small change in absorbance upon ligand addition, consistent with no observable shift in absolute spectra when ligand was present in purification samples. However in difference mode, it was apparent that addition of progesterone resulted in a blue shift in the Soret peak, causing a small increase at ~390 nm and decrease at ~430 nm indicative of a type I ligand (Figure 5.9A). Fitting the change in absorbance versus progesterone concentration with the tight binding equation yielded a K_d value of 0.11 μM (Figure 5.9B). However, this value may be higher than the true value. The protein concentration was 0.1 μM indicating that the assay detection limits may have been reached. Addition of 17α-hydroxyprogesterone to CYP21A2 also resulted in low absorption changes and an increase and decrease in the Soret peaks at 390 nm and 423 nm, respectively, indicating that 17α-hydroxyprogesterone was also a type I ligand (Figure 5.9C). However plotting the change in absorption versus 17α-hydroxyprogesterone concentration with the tight binding equation was more accurate in determining the K_d value as the curve fit resulted in a dissociation constant of 0.68 μM (Figure 5.9D), which was >6-fold above the protein concentration.

To determine if the CYP17A1 inhibitor and prostate cancer drug abiraterone is selective versus CYP21A2, a preliminary binding assay was performed with CYP21A2 and abiraterone. Addition of abiraterone to 0.1 μM purified CYP21A2 yielded only a small decrease in absorbance at 411 nm and no increase at 385 nm (Figure 5.9E). By comparison, abiraterone bound tightly to CYP17A1 with a strong increase in absorbance at 432 nm and a corresponding decrease in absorbance at 409 nm, resulting in a K_d value <100 nm (Figure 5.9F). This result was promising for abiraterone selectivity for CYP17A1 over CYP21A2.

Figure 5.9. Spectral ligand binding assays and equilibrium dissociation constant determination of CYP21A2 with A) and B) progesterone, C) and D) 17α-hydroxyprogesterone, and E) abiraterone. F) Titration of CYP17A1 with abiraterone for comparison with CYP21A2 (Data courtesy of Dr. Natasha DeVore).

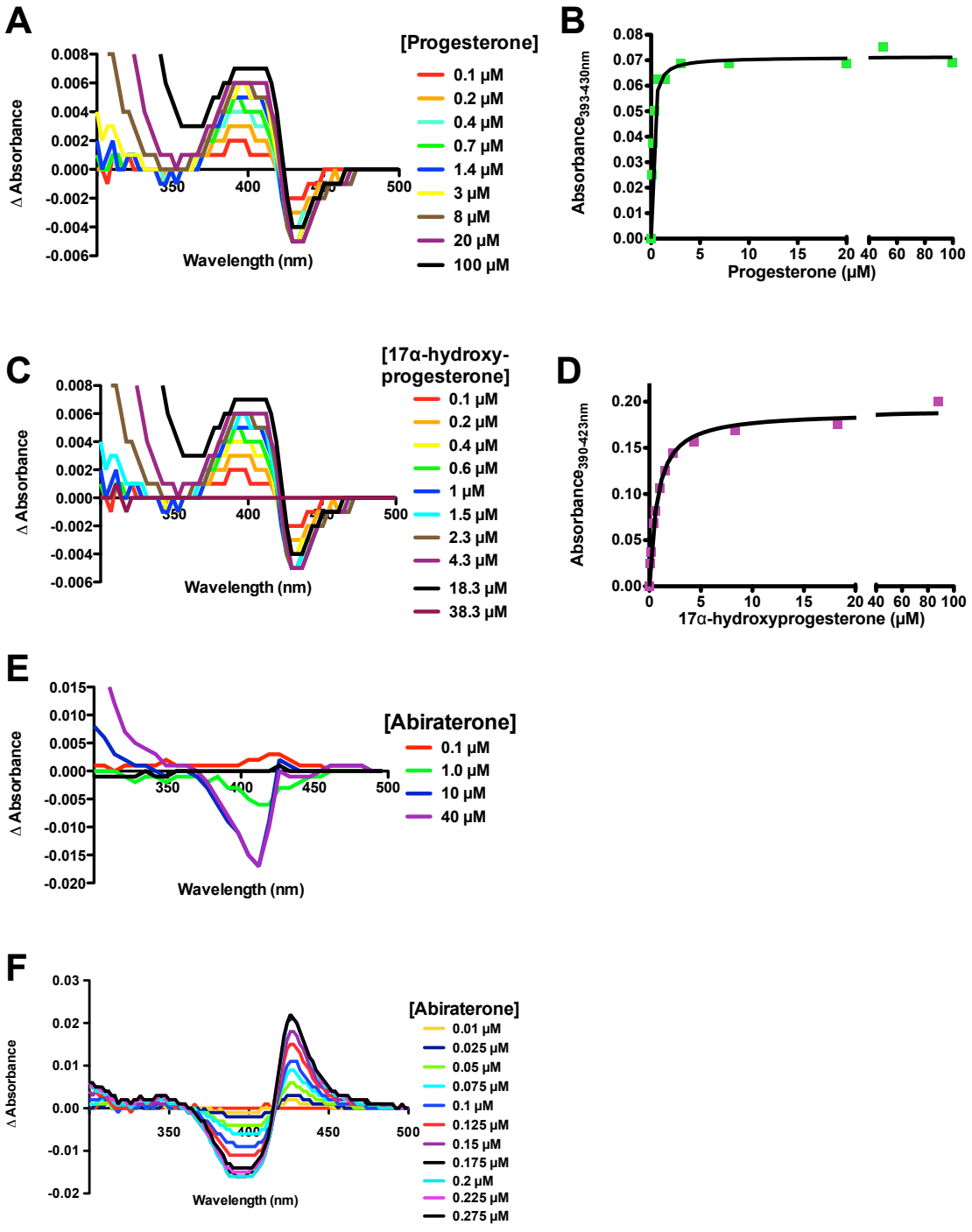

Steady-state Kinetics

Evaluation of steady-state kinetics for purified human CYP21A2 has been an iterative process. Before the k_{cat} and K_m values can be determined for this enzyme, a series of experiments was necessary to establish optimal assay conditions and confirm linearity of product formation over time. Based largely on prior experience with the CYP2A enzyme assays, initial reactions were performed using 50 pmol P450 enzyme, 50 μM progesterone, a 20 minute incubation of reconstituted protein system (RPS) at 4 ˚C, and a reaction time of 10 minutes initiated by 1 mM NADPH at 37 ˚C. The first set of experiments investigated the optimal ratio of P450 enzyme to POR in the RPS and determined the impact of cytochrome b_5. Ratios of P450: POR were varied as follows: 1:1, 1:2, 1:4, 1:6. Additionally, the influence of cytochrome b_5 was evaluated by repeating the assay with P450: POR: cytochrome b_5 ratios of 1:1:2, 1:2:2, 1:4:2, and 1:6:2. These results demonstrated that the P450:POR ratio of 1:4 ratio was optimal as determined by maximal product formation (Figure 5.10). Since the inclusion of cytochrome b_5 did not increase product formation, it was subsequently excluded from metabolism assays.

Figure 5.10. Results from the evaluation of RPS ratios with CYP21A2 with duplicate samples. Sample #1 is in blue and sample #2 is in red.

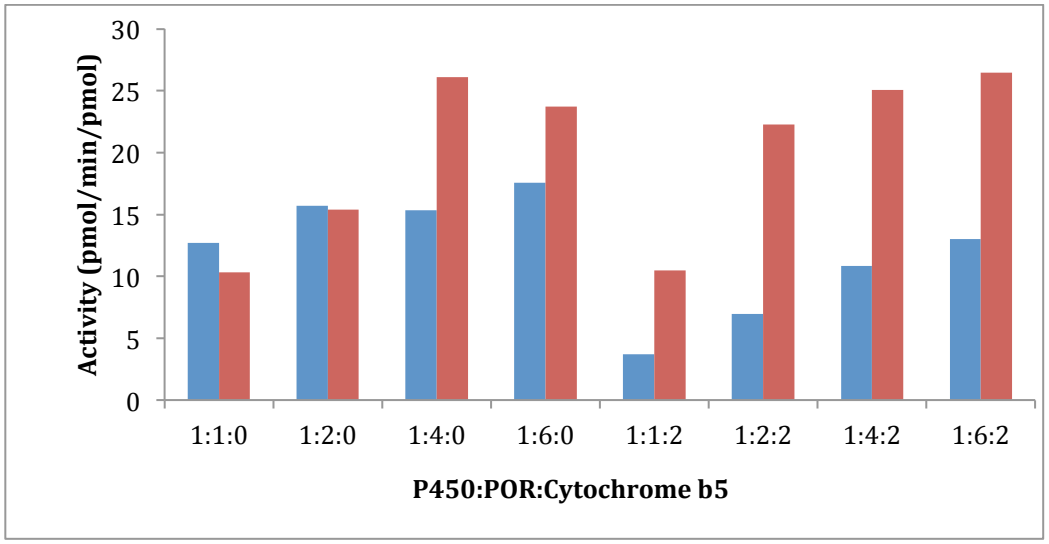

An observation made during the RPS ratio test above was that although the trends were relatively the same, duplicate samples for almost all ratios were not consistent. The only difference between duplicate samples was the pre-incubation time at 37 ˚C prior to NADPH reaction initiation. Samples were analyzed with pre-incubation times of 1, 2, 3, 4, 5, 6, 7, 8, 9, and 10 minutes, but the results did not yield any significant difference between the time points, indicating that the pre-incubation times was not the source for the variation between samples.

The next step in assay optimization was to evaluate the time and temperature of the RPS incubation. Samples were incubated at room temperature and at 4 ˚C for 20, 30, 40, 50, or 60 minutes. RPS samples incubated at 4 ˚C yielded inconsistent product formation (Figure 5.11A), while room temperature incubations were much more consistent (Figure 5.11B). Additionally, product formation did not significantly increase between 30-60 minutes, and 30 minute incubations were used in subsequent assays. This analysis revealed the source of the inconsistencies observed above.

Figure 5.11. Results from the evaluation of the RPS incubation conditions at A) 4˚C and at B)room temperature with varying time points.

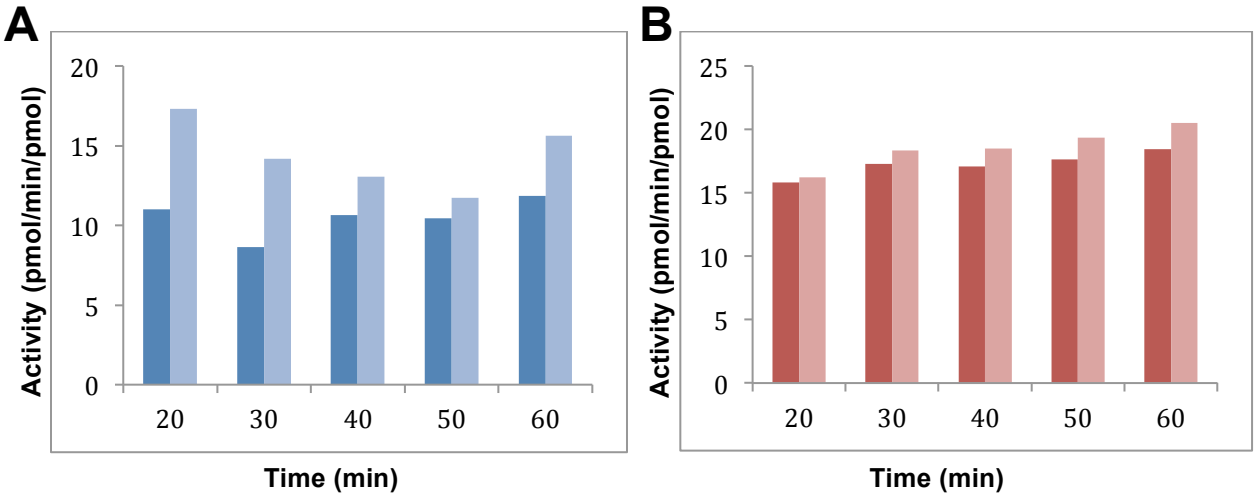

Once the protein ratios and incubation conditions were established, the next step towards determining the k_{cat} and K_m values was the determination of steady state conditions with linear product formation and less than 10% substrate depletion. This has proven to be more challenging due to rapid substrate turnover resulting in significant substrate depletion. When 50 pmol of CYP21A2 in a 1:4 ratio with POR was incubated with 5 µM progesterone, the substrate was completely depleted within 5 minutes. The progesterone concentration was increased to 100 µM and indicated the reaction was linear through 10 minutes, but linearity began to deteriorate between 10 and 20 minutes (Figure 5.12A). In addition the substrate concentration was significantly reduced to 63%, 52%, 32%, 19%, and 12% of the initial concentration over the course of 5, 10, 20, 30, and 40 minutes, respectively (Figure 5.12B).

Figure 5.12. A) Analysis of product formation with 100 µM progesterone and 50 pmol of CYP21A2 indicated the reaction was linear through perhaps 10 minutes. B) However, the HPLC chromatogram revealed significant substrate decrease in the reactions from 0-40 minutes, with only 63% remaining after 5 minutes.

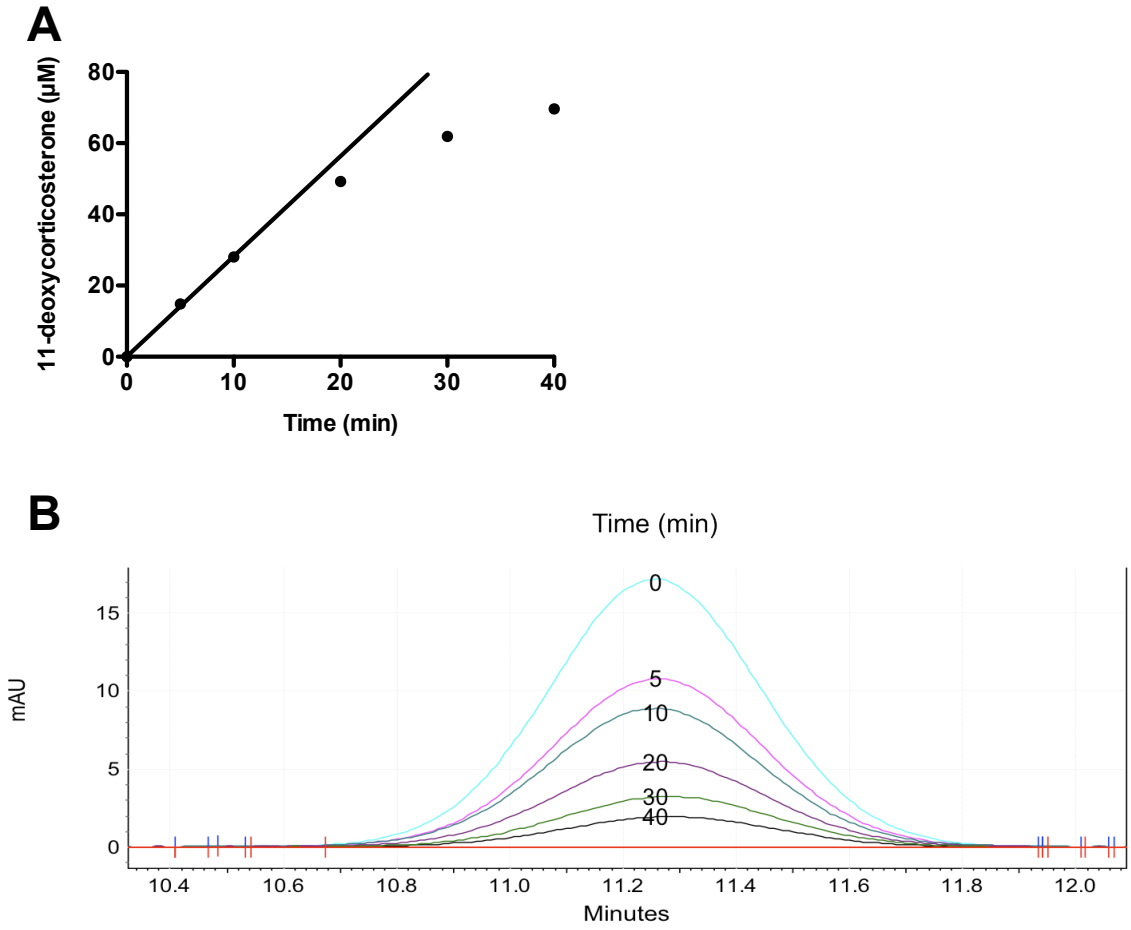

In an attempt to maintain sufficient progesterone levels for steady state analysis, the protein concentration was reduced to 20 pmol and reaction times of 0, 2, 4, 6, 8, and 10 minutes with 10, 20, 40, 60, 80 and 100 µM progesterone were evaluated. Reactions were linear through 6 minutes at all concentrations (Figure 5.13), but the progesterone concentration was reduced >50% at 10 µM progesterone and 6 minutes.

Figure 5.13. Representative results for progesterone metabolism with linear product formation from 0-6 minutes with A) 10 μM, B) 40 μM, and C) 80 μM initial substrate concentrations.

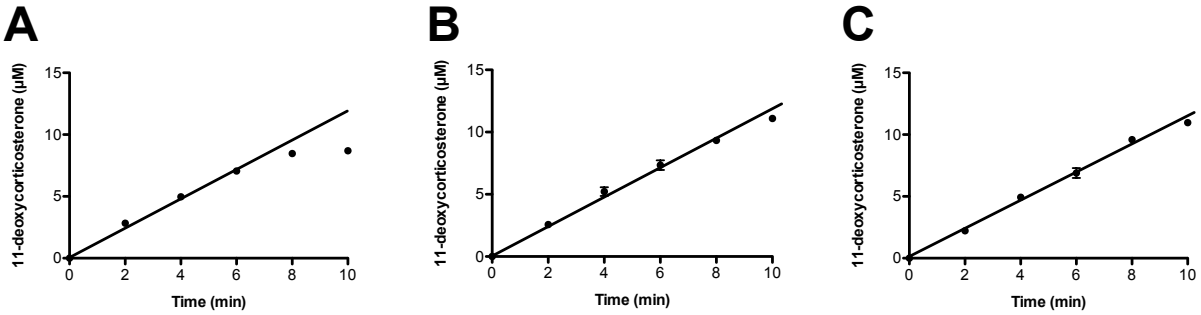

The CYP21A2 concentration was further reduced to 2 pmol, but with a reaction volume of 500 μL, the product formation was inconsistent. The next step is to reduce the reaction volume to 250 μL and will be completed in the near future.

Discussion

Protein Modifications

The human CYP21A2 gene was modified to generate a CYP21A2 protein with a Δ2-28 amino acid N-terminal transmembrane truncation, a MAKKTSSKGK N-terminal solubility tag, and a 6-residue C-terminal histidine tag and was cloned into the pCW vector. These modifications were consistent with the bovine CYP21A2 construct[11] and similar to other P450 constructs that resulted in large quantities of purified enzyme.[18,19] This construct was transformed into DH5α/pGro7 competent cells as this cell line proved advantageous for bovine CYP21A2 expression.[11]

Expressions, Purifications, and Crystallography

The modified construct expressed at 27 ˚C for 48 hours in DH5α/pGro7 competent *E. coli* cells appeared to result in significant production of CYP21A2 protein. Western blots confirmed the presence of a histidine tagged enzyme at the expected molecular weight of 55 kDa after

induction. CYP21A2 was purified with various combinations of detergents and buffers, and each variation proved advantageous in a specific area. Initially Tris buffers were used with either 4.8 mM Cymal-5 or 0.2% Emulgen 913. Emulgen 913 (0.2%) was more successful in stabilizing CYP21A2 as measured by reduced carbon monoxide difference spectra (P450 versus P420) compared to Cymal-5. However, the use of 4.8 mM Cymal-5 resulted in purer protein following cation exchange, but protein was lost to precipitation at each purification step. Trace impurities were present in CYP21A2 purified with 0.2% Emulgen 913 following cation exchange chromatography. However, with Emulgen 913 the 55 kDa band for CYP21A2 was very prominent, and this protein was then used for initial functional characterization of the enzyme.

Of particular note is that CYP21A2 required the presence of a substrate in the assay buffer to generate the expected P450 (or even P420) maxima. It appears that CYP21A2 requires a ligand for stabilization, at least to form the traditional carbon monoxide complex.

Purification of CYP21A2 through size exclusion chromatography with Tris buffers and 4.8 mM Cymal-5 or 0.2% Emulgen 913 for protein crystallography mimicked the results described above. The purification with 4.8 mM Cymal-5 resulted in purer protein, but with a loss of 1120 nmol of P450 between solubilization and size exclusion due to precipitation. CYP21A2 purified with 0.2% Emulgen 913 resulted in larger quantities of protein, but the protein samples had trace impurities ≥70 kDa. However, protein purified with Tris buffers did not yield crystals following *de novo* screening with or without detergent combinations.

The next substantial modification of the purification protocol exchanged Tris buffers for potassium phosphate buffers. This exchange proved advantageous. Potassium phosphate buffers were more successful in stabilizing CYP21A2 as P420 and P450 peaks were observed in reduced

carbon monoxide difference spectra at each stage of the purification without a ligand present. In addition, the use of potassium phosphate buffers was able to increase the yield when comparing the best purification results from each buffer system. In the presence of either 50 μM progesterone or 50 μM 17α-hydroxyprogesterone, the Tris buffer purification sample contained 536 nmol of protein by absolute absorption assay and 386 nmol of P450 by reduced carbon monoxide difference spectra, while the potassium phosphate buffers had 1018 nmol of protein by absolute absorption assay and ≥419 nmol by reduced carbon monoxide difference spectra. The yield of ≥419 nmol is likely lower than the actual value as the assay did not go to completion in that only a single scan was completed for this sample rather than several scans over the course of 40 minutes until the P450 peak no longer increased. The purpose of the reduced carbon monoxide assay at this point in the purification was to confirm the presence of active enzyme before crystallography rather than to determine the final P450 concentration since the absolute absorption spectra is more consistent between purification runs in determining the final protein concentration for crystallography.

Finally, the primary advantage of the potassium phosphate buffers was the formation of CYP21A2 crystals in the form of red plates with Wizard screen I solution #42 (15% ethanol and 0.1 M Tris, pH 7.0). Unfortunately, attempts to optimize or reproduce the crystals in both 96 and 24 well plates have been unsuccessful to date. However, reproducibility attempts were performed with previously frozen CYP21A2 rather than freshly purified, and it is unknown whether a freeze/thaw cycle influences crystal growth. Frozen protein was used due to time constraints, as three days were required to complete a single purification, and to not waste the large quantities of CYP21A2 obtained during the purification. Other crystallization efforts included optimization of this precipitant solution by varying the individual components with both

of the known CYP21A2 substrates, and use of the precipitant solutions that led to the bovine CYP21A2 and human CYP17A1 crystal structures, as these solutions were similar.

In summary, CYP21A2 was successfully expressed, purified, and crystallized. The DH5α/pGro7 cell line with the pCW plasmid was conducive for the expression of large quantities of CYP21A2. The 21-hydroxylase enzyme tolerated purification with 4.8 mM Cymal-5 or 0.2% Emulgen 913 with either Tris and potassium phosphate buffers, but 0.2% Emulgen 913 with potassium phosphate buffers proved more advantageous in stabilizing CYP21A2 and resulted in crystal formation. However, protein crystals have been difficult to reproduce and future crystallization attempts should include freshly purified CYP21A2 with the original protein concentration and the stock solution from the Wizard screening kit. In addition, a purification with 1% cholate and 1% Tween-20 would be interesting as this was successfully used in purifying bovine CYP21A2 for structure determination.

Dissociation Constant Determination:

Initial characterization of the purified CYP21A2 enzyme included the spectral determination of equilibrium dissociation constants for the CYP21A2 substrates progesterone and 17α–hydroxyprogesterone. The results indicated that 17α–hydroxyprogesterone did not bind CYP21A2 (K_d = 0.68 μM) as tightly as progesterone (K_d = ≤0.11 μM). It is also worth noting that the dissociation constant for progesterone is likely to be lower than the value indicated due to the limitations of the binding assay. Regardless, these values are significantly lower than the only known dissociation constants for human CYP21A2 reported in the literature.[4] Guzov *et al* reported K_d values for progesterone (K_d = 14.7 μM) and 17α–hydroxyprogesterone (K_d = 31.1 μM) that were >100-fold and 45-fold, respectively, higher than the values that I experimentally determined. However, the reliability of the literature results is questionable. In comparison to

the results that I determined, bovine CYP21A2 and CYP17A1, which does not metabolize progesterone as efficiently, also have submicromolar binding constants with 17α–hydroxyprogesterone ($K_d \approx 50$ nM)[15] and progesterone ($K_d = 229 \pm 14$ nM),[16] respectively.

While the submicromolar K_d values are consistent between the human and bovine CYP21A2 enzymes, a direct comparison may not be entirely accurate. First, Zhao *et al* reported a K_d value of ≈ 50 nM for 17α–hydroxyprogesterone for bovine CYP21A2, but the experimental conditions contained only 2 μM CYP21A2, indicating that the determination of a submicromolar K_d was beyond the detection limits of their assay. Additionally, the experimental values reported in this dissertation were determined with the tight binding equation for saturation binding with ligand depletion, which only accounts for a single substrate bound within the active site. This distinction is important as the CYP21A2 bovine structure had two molecules of 17α–hydroxyprogesterone bound,[15] which would deplete the substrate in solution more quickly, and it is unknown whether substrates bind in the same manner or if the human enzyme differs in this respect. We did not observe the sigmoidal trends for 17α–hydroxyprogesterone binding to human CYP21A2, but the distal 17α–hydroxyprogesterone binds far enough away from the iron that no direct spectral change is expected from this interaction. A crystal structure with human CYP21A2 and progesterone or 17α–hydroxyprogesterone would help to clarify these questions regarding the number and orientation of the substrates.

Steady-state Kinetics

In addition to needing functional enzyme for investigation of CYP21A2 structure and function itself, the evaluation of CYP21A2 as a counter-target for CYP17A1 inhibitors requires the development of a metabolism assay and determination of k_{cat} and K_m values. However, before these values can be determined the assay conditions need to be established. First, the

optimal ratio of P450 to its redox partner POR was determined. A 1:4 ratio of P450 to POR resulted in the highest product formation. The inclusion of cytochrome b_5, which has been known to facilitate catalytic activity for some P450 enzymes,[20] did not enhance the rate of reaction and was not included in subsequent assays. The temperature and time of the RPS incubation did significantly impact the reactions. Incubation at 4 ˚C yielded inconsistent results at every time point, while 30 minutes at room temperature provided consistent results. However, these conditions may need to be revised due to the significant substrate turnover rate described below.

The final step was the establishment of steady state conditions for the progesterone metabolism, which is still ongoing. In order for steady state conditions to be achieved, product formation must remain linear over time and substrate depletion must be ≤ 10%. Achieving a linear reaction rate is proving to be easier than maintaining substrate concentrations in the reactions. Fifty picomoles of protein completely metabolized 5 μM of progesterone within 5 minutes and significantly reduced the substrate concentration of 100 μM progesterone to 12% of the starting concentration over the course of 40 minutes. The protein concentration in the reactions was subsequently reduced to 20 pmol, and the rate of product formation was linear with concentration ranges of 10-100 μM progesterone for 0-6 minutes. However, after 6 minutes the substrate was depleted by ≥50% compared to its original substrate concentration of 10 μM, suggesting a further decrease in protein concentration is necessary. The utility of using 2 pmol of CYP21A2 in each assay remains undetermined, as a reaction volume of 500 μL was too large to obtain consistent product formation. Future assays will reexamine 2 pmol of CYP21A2 with a smaller reaction volume of 250 μL. Reducing the amount of protein present should decrease substrate depletion in metabolism assays with CYP21A2. Reported kinetic values with the

bovine CYP21A2 enzyme utilized 2 pmol of P450 with a radiography assay.[15] Finally, future assay development will include the use of the substrate 17α–hydroxyprogesterone, which is expected to have equal or greater catalytic activity.

Conclusions

In the development of CYP17A1 inhibitors for prostate cancer, it is important to evaluate obvious protein counter-targets that could challenge the selectivity of potential drug candidates. CYP21A2 binds a substrate and product of CYP17A1,[1] and thus could potentially bind CYP17A1 inhibitors. However, biochemical studies and thus screening of potential of CYP17A1 inhibitors with the human CYP21A2 enzyme have been limited due to the lack of available enzyme. Expression of human CYP21A2 in *E. coli* has previously been achieved in low levels,[4] but minimal research has been performed beyond evaluating genetic mutations and the determination of steady-state kinetic parameters and equilibrium dissociation constants for progesterone and 17α-hydroxyprogesterone.

The successful large-scale expression and purification of stable human CYP21A2 described in this chapter has laid the foundation for evaluating the biochemical properties of CYP21A2. This protein can be used to evaluate key amino acid residues impacting metabolic activity or evaluating CYP21A2 as a counter-target for CYP17A1 inhibitors. In addition, the determination of a human CYP21A2 crystal structure is expected to elucidate the atomic level interactions governing substrate binding and provide insight into the differences between the human CYP17A1 and CYP21A2 enzymes that enable selectivity between the two enzymes. In addition it would be interesting to compare the bovine and human CYP21A2 crystal structures and determine if the human enzyme also concurrently binds multiple substrates.

Acknowledgements

I would like to thank Dr. Natasha DeVore for completing the titration of CYP17A1 with abiraterone.

References

1. *Cytochrome P450: Structure, Mechanism, and Biochemistry*, (Kluwer Academic/ Plenum Publishers, New York, 2005).
2. Barnes, H.J. Maximizing expression of eukaryotic cytochrome P450s in Escherichia coli. *Methods Enzymol* **272**, 3-14 (1996).
3. Harnastai, I.N., Gilep, A.A. & Usanov, S.A. The development of an efficient system for heterologous expression of cytochrome P450s in Escherichia coli using hemA gene co-expression. *Protein Expr Purif* **46**, 47-55 (2006).
4. Guzov, V.M. et al. [Expression of functionally active hyman cytochrome P-450c21 (CYPXXIA2) in Escherichia coli and single-stage purification of it using metal-affinity chromatography]. *Biokhimiia* **61**, 1758-71 (1996).
5. Krone, N. et al. Analyzing the functional and structural consequences of two point mutations (P94L and A368D) in the CYP11B1 gene causing congenital adrenal hyperplasia resulting from 11-hydroxylase deficiency. *J Clin Endocrinol Metab* **91**, 2682-8 (2006).
6. Speiser Phyllis, W. & White Perrin, C. Congenital adrenal hyperplasia. *N Engl J Med* **349**, 776-88 (2003).
7. White, P.C. & Speiser, P.W. Congenital adrenal hyperplasia due to 21-hydroxylase deficiency. *Endocr Rev* **21**, 245-291 (2000).
8. Mizrachi, D. et al. Why human cytochrome P450c21 is a progesterone 21-hydroxylase. *Biochemistry* **50**, 3968-74 (2011).
9. Mornet, E. & Gibrat, J.F. A 3D model of human P450c21: study of the putative effects of steroid 21-hydroxylase gene mutations. *Hum Genet* **106**, 330-9 (2000).
10. Robins, T., Carlsson, J., Sunnerhagen, M., Wedell, A. & Persson, B. Molecular model of human CYP21 based on mammalian CYP2C5: structural features correlate with clinical severity of mutations causing congenital adrenal hyperplasia. *Mol Endocrinol* **20**, 2946-64 (2006).
11. Arase, M., Waterman, M.R. & Kagawa, N. Purification and characterization of bovine steroid 21-hydroxylase (P450c21) efficiently expressed in Escherichia coli. *Biochem Biophys Res Commun* **344**, 400-5 (2006).
12. Zhao, B. et al. Three-dimensional Structure of Steroid 21-Hydroxylase (Cytochrome P450 21A2) with Two Substrates Reveals Locations of Disease-associated Variants. *J Biol Chem* **287**, 10613-22 (2012).
13. White, P.C. Genetic diseases of steroid metabolism. *Vitam Horm* **49**, 131-95 (1994).
14. Database of CYP21A2 by the human cytochrome P450 (CYP) allele nomenclature committee. (2011). http://www.cypalleles.ki.se/cyp21.htm
15. Zhao, B. et al. A Three-dimensional Structure of Steroid 21-Hydroxylase (Cytochrome P450 21A2) with Two Substrates Reveals Locations of Disease-associated Variants. *J Biol Chem* (2012).
16. DeVore, N.M. & Scott, E.E. Structures of cytochrome P450 17A1 with prostate cancer drugs abiraterone and TOK-001. *Nature* **482**, 116-9 (2012).
17. Smith, B.D. et al. Structure of the human lung cytochrome P450 2A13. *J Biol Chem* **282**, 17306-13 (2007).

18. von Wachenfeldt, C., Richardson, T.H., Cosme, J. & Johnson, E.F. Microsomal P450 2C3 is expressed as a soluble dimer in Escherichia coli following modification of its N-terminus. *Arch Biochem Biophys* **339**, 107-14 (1997).
19. Porubsky, P.R., Meneely, K.M. & Scott, E.E. Structures of human cytochrome P-450 2E1. Insights into the binding of inhibitors and both small molecular weight and fatty acid substrates. *J Biol Chem* **283**, 33698-707 (2008).
20. Truan, G., Cullin, C., Reisdorf, P., Urban, P. & Pompon, D. Enhanced in vivo monooxygenase activities of mammalian P450s in engineered yeast cells producing high levels of NADPH-P450 reductase and human cytochrome b5. *Gene* **125**, 49-55 (1993).

Chapter 6

Cloning, Expression, and Purification of CYP11B1

Introduction

As introduced in chapter 1, human cytochrome P450 11B1 (CYP11B1) is involved in the biosynthesis of cortisol. Understanding the structure and function of CYP11B1 is important for two reasons. First, CYP11B1 is a potential therapeutic target for the treatment of cortisol-dependent diseases such as Cushing's disease. Second, CYP11B1 is an important counter-target in the development of selective inhibitors of other steroidogenic P450 enzymes that bind and metabolize very similar substrates. Both rational drug design of CYP11B1 inhibitors and the evaluation of CYP11B1 as a counter-target require a biochemical and biophysical understanding of the enzyme. Unfortunately, biochemical interactions governing CYP11B1 activity remain poorly understood. This is due to the lack of protein availability and in part to the instability of the enzyme during *E. coli* expression, purification,[1] and detergent solubilization.[2]

Cytochrome P450 11B1 is a β-hydroxylase enzyme that can act at either the C11 or C18 position of select steroids. Specifically, CYP11B1 primarily catalyzes the conversion of 11-deoxycortisol to cortisol (k_{cat} = 1.67 s^{-1}, K_m = 338.4 ± 30.2 μM) (Scheme 6.1A). Additionally, although CYP11B1 is not the primary enzyme involved in 11-deoxycorticosterone metabolism *in vivo*, it has been shown to convert 11-deoxycorticosterone to either corticosterone (k_{cat} = 0.85 s^{-1}, K_m = 179.5 ± 19.1 μM) or 18-hydroxy-11-deoxycorticosterone to a minor extent (Scheme 6.1B).[1,3] The metabolites, corticosterone and 18-hydroxy-11-deoxycorticosterone, can be further converted to 18-hydroxycorticosterone by CYP11B1.[3] *In vivo*, however, the 11-deoxycorticosterone reactions are primarily catalyzed by a second human P450 enzyme,

CYP11B2, which is 93% identical to CYP11B1 and plays an important role in the formation of mineralocorticoids (Scheme 6.1B).[3-7]

Scheme 6.1. Metabolic conversions of A) 11-deoxycortisol and B) 11-deoxycorticosterone by CYP11B enzymes ultimately resulting in the formation of aldosterone and cortisol.[3,5,6,8] The larger arrow size indicates the enzyme primarily responsible for the catalytic conversion *in vivo*.

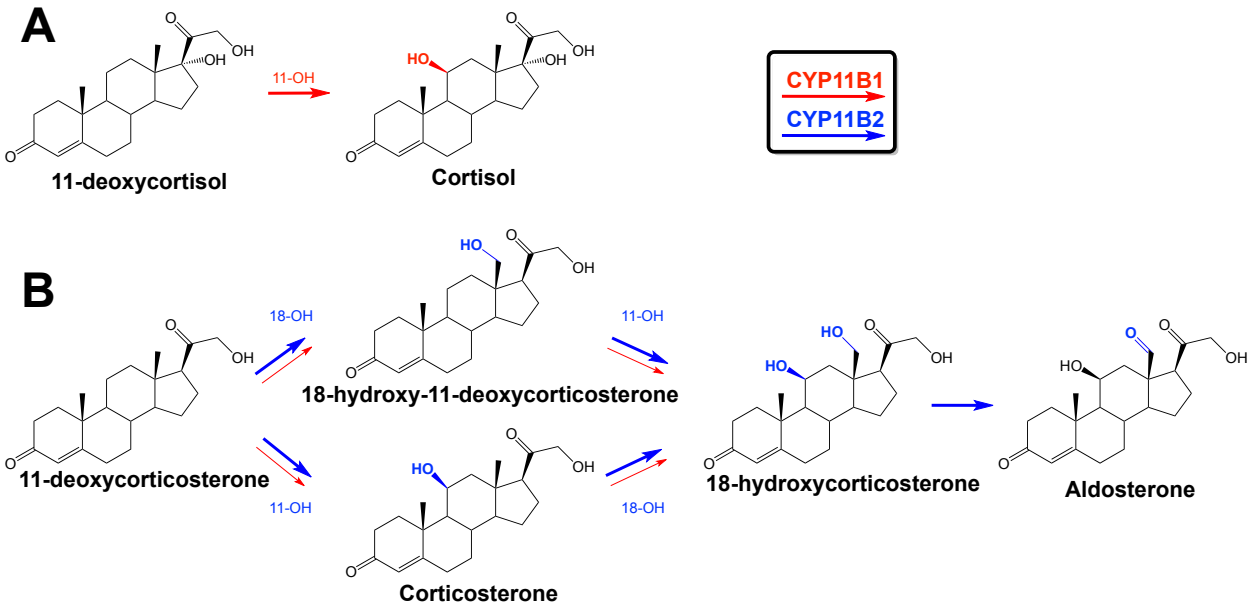

The two human mitochondrial CYP11B enzymes differ in 32 out of 503 amino acids.[4] Previous research has shown that their activities can be interconverted through key amino acid substitutions. For example, the S288G and V320A mutations impart CYP11B1 with the 18 hydroxylation and oxidation steps, respectively, that are typically catalyzed by CYP11B2.[9] Meanwhile the CYP11B2 triple mutant L301P/E302D/A320V/ is able to increase cortisol production from wild type levels of 5% to 85% of CYP11B1 activity.[5,6] Additional differences between CYP11B1 and CYP11B2 arise from gene regulation and location of expression. CYP11B1 is synthesized in the adrenal zona fasciculata and is controlled by

adrenocorticotrophic hormone (ACTH).[4] CYP11B2 is expressed in the adrenal zona glomerulosa and regulated by angiotensin II and potassium as part of the renin angiotensin system.[4]

Due to the critical role of CYP11B1 in cortisol production and maintaining homeostasis, aberrant activity in CYP11B1 can have severe impacts on human health. Significant research has been performed towards the underlying genetic role of CYP11B1 deficiencies, which result in 5-8% of congenital adrenal hyperplasia (CAH) cases and is manifested by genital ambiguity and salt wasting.[10] In addition, CYP11B1 deficiencies decrease cortisol secretion, and both CAH and cortisol reduction result in excess androgen production.[11,12] Several CYP11B1 mutations such as P94L, S217I, T318R, and A368D have been identified as causing clinical CYP11B1 deficiencies.[13-15] Additionally, it has been found that hyperactive CYP11B1 results in an overproduction of cortisol and causes Cushing's disease, presenting CYP11B1 as a therapeutic target.[12] While Cushing's disease is rare (2-3 cases per 1 million individuals),[16] it is commonly caused by exogenous glucocorticoids or adenoma in the pituitary gland (70% of all cases), which secretes the CYP11B1 regulator.[17] Treatments involve removal of the glucocorticoid source, surgical tumor removal, and/or the inhibition of cortisol formation through inhibition of the steroid biosynthetic pathway.[17]

The available steroid-suppressing agents for the treatment of Cushing's disease are limited to four FDA approved drugs and one in clinical trials (Figure 6.1). The most commonly used inhibitor is the antifungal drug ketoconazole, which is a non-selective P450 inhibitor.[17] Secondly, metyrapone has been used in the diagnosis and treatment of Cushing's disease, but is not widely administered due to excess mineralocorticoid formation resulting from CYP11B1 inhibition.[8,18] While this CYP11B1 inhibitor is not optimal, inhibition of CYP11B1 still remains

a promising target. LC1699, which is still in clinical trials, inhibits the 11β-hydroxylase activity of both CYP11B1 and CYP11B2 for the treatment of hypertension and potentially Cushing's Disease.[19] Etomidate is the fourth drug, The typical use of etomidate is as a general anesthetic and as such requires extensive monitoring if used for the treatment of Cushing's disease.[8,17] Finally, mifepristone is a glucocorticoid receptor antagonist and was recently approved by the FDA in February 2012.[17] Wide scale effectiveness is yet to be determined. While these methods have been proven effective for the treatment of Cushing's disease, none are optimal due to efficacy and non-selectivity.

Figure 6.1. Inhibitors of steroid biosynthesis for the treatment of Cushing's Disease.[8,17]

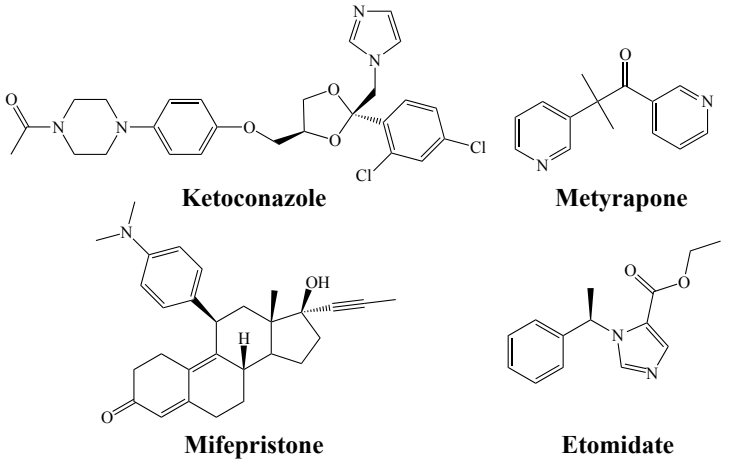

Unfortunately, biochemical studies providing insight into CYP11B1 function leading to the design of novel CYP11B1 inhibitors and the evaluation of CYP11B1 as a counter-target have been limited. Identification of key amino acid residues and subsequent site-directed mutagenesis studies have relied upon homology models based upon bacterial mitochondrial cytochromes P450.[5,8,20] Biochemical studies have also been limited by the lack of reproducible large-scale expression of stable human CYP11B1. Most studies have been conducted in mammalian cell

lines such as V79,[3,8] COS-1,[5] and COS-7.[9] Mammalian cell studies can result in valuable knowledge, but they cannot easily produce the large quantities that are necessary for structural and functional studies. Only one large scale *E. coli* purification was reported to result in 400 nmol/L.[1] However, the reproducibility of the procedure may be questionable. There has been no additional work citing this protocol, and experimentation described herein was unable to match the reported quantities. Additional knowledge about the CYP11B1 enzyme has been inferred from homologous enzymes, which vary in activity from the human isozyme. For example, there is only a single bovine β hydroxylase enzyme that is 73% identical to CYP11B1 and catalyzes the formation of corticosterone with a catalytic efficiency 1/10 of the human enzyme.[1,21] Rats have 4 isoforms (CYP11B1, CYP11B2, CYP11B3, and CYP11B4). While rat CYP11B1 and CYP11B2 have the same function as the human counterparts, CYP11B3 has the same function as CYP11B2 in neonatal rats, and CYP11B4 is a pseudogene.[8,22] Rat CYP11B1 is 64% identical to the human CYP11B1 enzyme[8] and possesses the additional ability to hydroxylate 11-deoxycorticosterone at the C19 position.[22] However, the rate of corticosterone formation for rat CYP11B1 is ~2.5 fold greater than the human recombinant enzyme.[1]

The lack of information pertaining to the structure/function relationships of CYP11B1 and the lack of availability of the enzyme has hindered the development of CYP11B1 inhibitors and evaluation of CYP11B1 as a counter-target. The aim of my project was to further the biochemical understanding of the human CYP11B1 β hydroxylase. This knowledge can be used towards the design of novel CYP11B1 inhibitors for the treatment of cortisol dependent diseases such as Cushing's disease or to evaluate the selectivity of potential CYP17A1 inhibitors. The work herein describes the necessary groundwork in evaluating expression and purification systems to enable functional and structural characterization of CYP11B1.

Materials and Methods

Protein Modifications: Codon-optimized human CYP11B1 cDNA was synthesized by Blue Heron Biotechnology (Bothel, WA) and engineered in the Blue Heron pUCminusMCS vector to contain a Δ3-25 amino acid N-terminal truncation, a C-terminal 4-residue histidine tag, and NdeI (CATATG) and HindIII (AAGCTT) restriction sites at the 5′ and 3′ flanking sites, respectively, to yield pUC11B1. These modifications from the full-length gene were identical to previous work that reported the generation of large quantities of purified enzymes. [1,4] Figure 6.2 displays an alignment of the full length and truncated human CYP11B1 enzymes.

Figure 6.2. Amino acid sequence alignment of the full length and modified CYP11B1 gene.[4] Deleted residues from the N-terminal transmembrane region are colored red, while mutated or added residues in the N- and C-terminal regions are shown in blue.

```
                    10         20         30         40         50
Full Length   MALRAKAEVC MAVPWLSLQR AQALGTRAAR VPRTVLPFEA MPRRPGNRWL
Truncated     MA........ .......... .....TKAAR VPRTVLPFEA MPRRPGNRWL

                   490        500
Full Length   IKMVYSFILR PSMFPLLTFR AIN
Truncated     IKMVYSFILR PSMFPLLTFR AINHHHH
```

Cloning: The pET17b and pUC11B1 plasmids were digested with NdeI and HindIII for one hour at 37 ˚C. The DNA fragments were separated on a 0.8% agarose gel. The desired 3,256 base pair pET17b and the 1,464 base pair CYP11B1 fragments were excised and purified using the QIAquick Gel Extraction Kit (Qiagen, Germantown, MD). The CYP11B1 insert and digested pET17b plasmid were ligated together using a quick ligation kit (New England Biolabs, Ipswich, MA), and the mixture was transformed into DH5α competent cells. The cells were plated on LB plates containing 50 μg/mL ampicillin. Individual colonies were grown in 5 mL LB cultures

containing 50 μg/mL ampicillin, and the plasmid DNA was isolated using QIAprep spin miniprep kit (Qiagen, Valencia, CA) and screened with restriction digest as the CYP11B1 gene introduces a unique MfeI restriction site. Following restriction digest and gel electrophoresis, the entire CYP11B1 gene was sequenced by ACGT (ACGT, Wheeling, IL) using ACGT primers for the pET17b vector with the plasmid DNA that illustrated a single cut site. This same protocol was also used to clone the truncated, histidine tagged CYP11B1 gene into a pCW plasmid, which was then sequenced with the forward pCW (5′ GGAAACAGGATCAGCTTACTCCC-3′) and reverse pCW (5′ GGCGTATCACGAGGCCCTTTCG-3′) primers.

Site-Directed Mutagenesis: Site-directed mutagenesis was later used to insert the codons for two additional histidine residues at the C-terminus in order to extend the histidine tag from four to six amino acid residues. QuikChange Site Directed Mutagenesis Kit (Agilent Technologies, Santa Clara, CA) was used with the forward primer 5′ CCACTCCTCACATTTCGCGCGATTAAC**CACCAC**CATCATCATCATTAAAAGCTTATG, reverse primer 5′ CGATAAGCTTTTAATGATGATGATG**GTGGTG**GTTAATCGCGCGAAATGTGAGGAGT GG (where bold indicates the inserted nucleotides), and the pCW11B1 DNA template. The mutation was confirmed by sequencing through ACGT.

Expression: The pCW11B1 and pET17b11B1 plasmids were individually transformed into BL21(DE3)pLysS, JM109, DH5α, and Topp3 *E. coli* competent cells that already contained the pGro7 expression plasmid for GroEL, a chaperone protein. Cells were plated on LB agar plates containing 50 μg/mL ampicillin and 20 μg/mL chloramphenicol to select for the CYP11B1 and pGro7 plasmids, respectively, following the transformation protocol in chapter 2. Individual

colonies were used to start 5 mL LB cultures containing 50 µg/mL ampicillin and 20 µg/mL chloramphenicol incubated at 37 ˚C with shaking at 250 rpm. These 5 mL cultures were used to inoculate 250 mL TB media containing 50 µg/mL ampicillin and 20 µg/mL chloramphenicol. Arabanose (500 µg/mL) was also included to induce expression of GroEL. Later expression trials utilized larger 1 L cultures in either 2.5 L baffled or non-baffled flasks, as the size of the flask did not appear to effect the expression yield. Baffled flasks were used for expression of the BL21(DE3)pLysS/pGro7 cell line as a slight increase in expression yield was observed over the non-baffled flasks. Expression in the remaining cell lines did not appear to depend on whether the flasks were baffled or not and the non-baffled flasks were used. In addition, the 1 L cultures were inoculated with a minimum of 15 mL from the overnight LB culture.

Large-scale cultures were incubated at 37˚C with shaking at 250 rpm and P450 expression was induced with 1 mM IPTG when an OD_{600} of 1.0-1.8 was reached, typically after 2-3 hours. Following induction and the addition of 1 mM of the heme precursor delta aminolevulinic acid, the temperature was reduced to 27 ˚C or 30 ˚C with shaking at 190 rpm. The cultures were allowed to grow for 48 hours before harvesting by centrifugation at 6,400 x g and storage of the cell pellets at -80 ˚C. The cell pellets from two liters of the BL21pLysS/pGro7 expression were combined and resuspended with Tris resuspension buffer #2 (50 mM Tris-HCl, 20% glycerol, and 300 mM NaCl) prior to storage at -80 ˚C since in this cell line natural production of lysozyme promotes cell lysis upon thawing.

SDS-PAGE: SDS-PAGE gels followed the protocol detailed in chapter 5 for determining purity of purification samples or in preparation for western blot analysis.

Western Blot: Western blot analysis determined the presence of histidine tagged protein in expression samples used the procedure described in chapter 5.

Purification: Initial CYP11B1 purification protocols followed a published procedure[1] with only minor changes. Changes included cell lysis following -80 ˚C storage rather than prior to storage in addition to the exchange of adenosine monophosphate for adenosine triphosphate in wash buffer B due to compound availability. The purification trials began with resuspension of the BL21(DE3)pLysS/pGro7/pET17b11B1 cells either before or after -80 ˚C storage in resuspension buffer (50 mM Tris-HCl, pH 7.4, 250 mM sucrose, 0.5 mM EDTA, and 1 mg/mL lysozyme) with homogenization to lyse the cells and create a homogeneous solution. Centrifugation at 8,700 x g for 10 minutes was used to remove the cytosolic contents. The pellet was resuspended in resuspension buffer 2 (50 mM potassium phosphate pH 7.4, 20% glycerol, 0.1 mM EDTA, 0.1 mM dithiothreitol, 500 mM sodium acetate, 1.5% w/v sodium cholate, 1% v/v Tween 20, and 0.1 mM phenylmethanesulfonyl fluoride) and sonicated 3 times for 30 seconds to further lyse the cells and extract the P450 enzyme with the detergent in the resuspension buffer. Ultracentrifugation at an average speed of 70,400 x g and 4 ˚C for one hour was used to separate the extracted P450 enzyme from the membranes. The P450-containing supernatant was applied to a Ni-NTA resin (Qiagen, Valencia, CA) equilibrated with 3 column volumes of buffer A (50 mM potassium phosphate, pH 7.4, 500 mM sodium acetate, 20% glycerol, 0.1 mM EDTA, 0.1 mM dithiothreitol, 1% sodium cholate, 1% Tween 20, and 0.1 mM phenylmethanesulfonyl fluoride). The column was washed with 2 column volumes of buffer A, washed with 6 column volumes of buffer A with 40 mM imidazole and 2 column volumes of buffer B (50 mM potassium phosphate, pH 7.4, 500 mM sodium acetate, 20% glycerol, 0.1 mM EDTA, 0.1 mM dithiothreitol, 1% sodium cholate, 1% Tween 20, 0.1 mM phenylmethanesulfonyl fluoride, 40 mM imidazole, and 0.1 mM adenosine monophosphate), and eluted with 5 column volumes of

buffer C (200 mM imidazole acetate, pH 7.4, 20% glycerol, 0.1 mM EDTA, 0.1 mM dithiothreitol, 1% sodium cholate, and 1% Tween 20).

Subsequent purification protocols followed the general procedure outlined in chapter 2 with the exclusion of the flash freeze step unless otherwise indicated. In addition, the Tris buffers described in chapter 5 were also used in the purifications when indicated. Finally, additional variations to the purification trials such as detergents and inclusion of a substrate or inhibitor are reported in the results section.

Results

CYP11B1 modifications

The human 11β-hydroxylase enzyme CYP11B1 was initially designed with a Δ3-25 amino acid N-terminal transmembrane truncation and 4-residue histidine tag on the C-terminus to aid in expression and purification of the enzyme. The N-terminal modifications emulated previous CYP11B1 work that resulted in 400 nmol/L of purified protein.[1] Cloning of the synthesized and modified CYP11B1 gene into the pET17b and pCW plasmids with NdeI and HindIII restriction sites was accomplished without difficulties.

BL21(DE3)pLysS/pGro7/pET17b11B1 Expressions and Purifications

The expression and purification of the CYP11B1 enzyme was an iterative process as alterations were made to the protocols in an attempt to obtain large quantities of purified enzyme for structure/function studies. Initial emphasis was placed on the pET17b vector and the BL21(DE3)pLysS/pGro7 cell line because literature had reported this to be the optimal combination for obtaining large quantities (400 nmol/L) of purified human CYP11B1 protein.[1] In order to establish that protein was expressed and induced, samples of cell culture were collected before and after CYP11B1 induction with IPTG. A western blot using a histidine tag

antibody confirmed the presence of strong new band at 50-55 kDa corresponding to a histidine tagged protein at 24 and 48 hours following induction and incubation at 27 ˚C with shaking at 250 rpm (Figure 6.3). This band is slightly lower than the expected 55.6 kDa molecular weight for CYP11B1, but hydrophobic enzymes such as CYP11B1 can run lower than the expected molecular weight due to excessive SDS binding.[1,23] Also, the high background illustrated by multiple bands is due to the lack of specific binding by the anti-His antibody.

Figure 6.3. Western blot of BL21(DE3)pLysS/pGro7 pET17b11B1 expressions at pre and post inductions. The Anti-His ladder is labeled in white (Lane 9) while the dual color ladder is labeled in black (Lane 10).

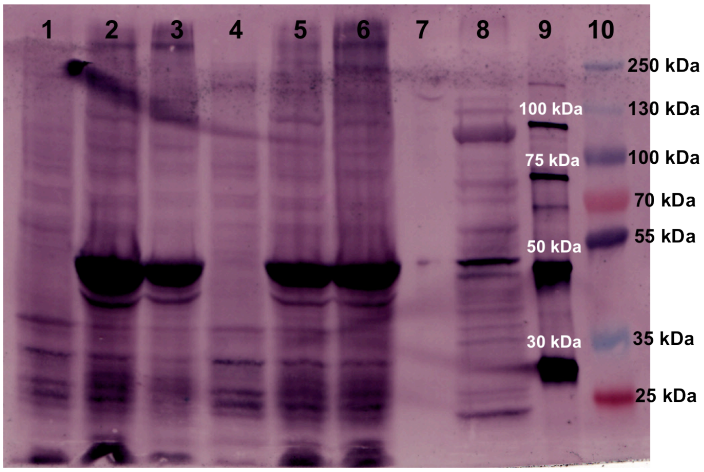

Lane	Sample	Time (hour)
1	Expression #1	0
2	Expression #1	24
3	Expression #1	48
4	Expression #2	0
5	Expression #2	24
6	Expression #2	48
7	Blank	
8	11B1dH Control: Ni-NTA purified sample	
9	Anti-His Ladder	
10	Dual Color molecular weight Ladder	

This western blot indicated strong expression, and cells harvested from 2.25 L culture resulted in a 16.2 g cell pellet (wet weight) following a 24 hour incubation and 19.6 g cell pellet from a 48 hour incubation. The first purification followed the published protocol which utilized endogenous lysozyme from the BL21(DE3)pLysS/pGro7 cell line, homogenization, sonication, and ultracentrifugation with 1% sodium cholate and 1% Tween 20. The second purification had only minor changes from the original protocol in an effort to enhance solubility and extraction.

These minor changes included increasing the centrifugation speed from 8,700 x g to 10,000 x g to increase the cohesiveness of the pellet. Additionally, the incubation time with resuspension buffer #2, which already contained detergent, was increased prior to ultracentrifugation to enhance enzyme extraction. Regardless, following enzyme solubilization and membrane removal by ultracentrifugation, the supernatant contained only 44 nmol and 23 nmol of inactive P420 enzyme determined by reduced carbon monoxide difference spectra from the first and second purification trials, respectively. After the Ni-NTA affinity column, only 3.2 nmol of P420 enzyme were obtained from the first purification (Figure 6.4A). The second purification contained small amounts overall, and similar amounts of inactive P420 with a small amount of active P450 (0.31 nmol) (Figure 6.4B).

Figure 6.4. Reduced carbon monoxide difference spectra of the Ni-NTA elution fractions from the A) first purification and B) second purification of the CYP11B1 enzyme demonstrate only minimal quantities of inactive P420 and active P450 following published procedures.[1]

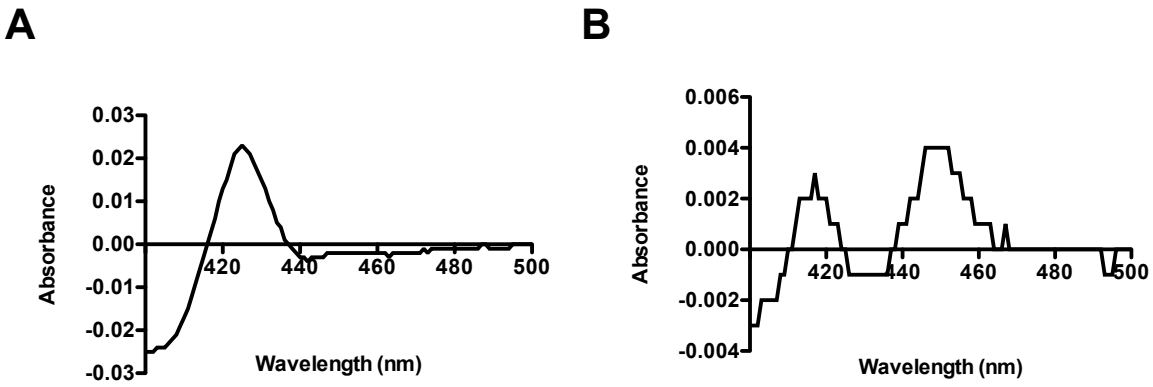

In an attempt to troubleshoot the purification, samples from various stages of Ni-NTA affinity chromatography were analyzed by SDS-PAGE gel electrophoresis (Figure 6.5). All

samples had bands between 50-55 kDa. The Ni-NTA elution fraction #1 (Figure 6.5 Ni. E #1) had two bands between 50-55 kDa. The Ni-NTA elution fraction #2 (Figure 6.5 Ni. E #2) also had two bands near 55 kDa. This same sample was used in the western blot as a control (Figure 6.3 Lane 8) as this sample contained active P450 enzyme. The lower band of the two bands between 50-55 kDa in lane Ni. E #2 of the SDS-PAGE gel appears to correspond to the darker band in the western blot, which also aligned with the dark expression bands resulted from P450 induction. These results indicate that CYP11B1 may run lower than 55 kDa during gel electrophoresis, but the results were not conclusive as the western blot also contained a light band at 55 kDa.

Figure 6.5. SDS-PAGE gel from the second purification of BL21(DE3)pLysS/pGro7/pET17b11B1. Gel key is as follows: (S): solubilized enzyme contained in ultracentrifugation supernatant, (Ni. FT): Ni-NTA flow through from sample loading, (Ni. W): Ni-NTA wash fractions, (Ni E): Ni-NTA elution fractions, (MW): dual color molecular weight ladder.

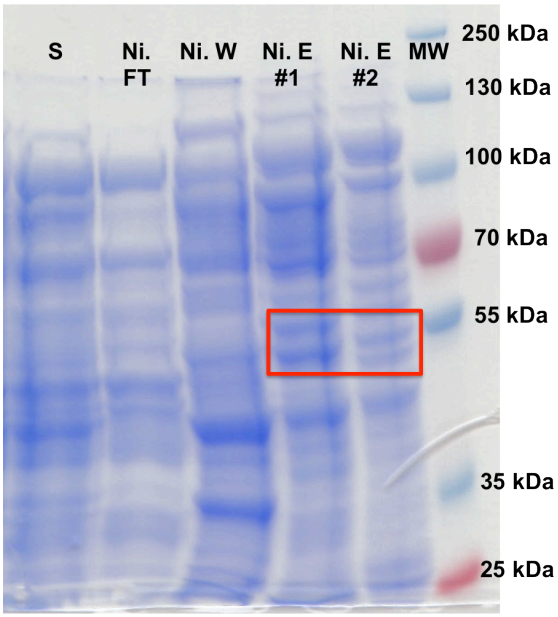

Unfortunately, while the western blot indicated that large amounts of protein were being expressed, this purification protocol did not result in the desired quantities of purified protein, and the yields of 1.4 nmol/L and 0.14 nmol/L did not compare well to the 400 nmol/L of culture that was reported.[1] The comparatively light bands at 50-55 kDa from SDS-PAGE analysis may indicate while the protein is being expressed, the enzyme is not being efficiently extracted from the bacterial membranes in the steps prior to Ni-NTA affinity chromatography.

Therefore, additional detergents, buffers, and the addition of ligand were investigated for increased solubilization and stabilization of the CYP11B1 enzyme during purification. The success of the CYP21A2 purification led to purification trials with Tris based buffers described in chapter 5 with 4.8 mM Cymal-5 or 0.2% Emulgen 913. Additionally, the substrate 11-deoxycortisol was added to some purification attempts because ligands can often aid in stabilization of P450 enzymes. To help prevent any protein degradation, the protease inhibitor phenylmethanesulfonyl fluoride (0.1 mM) was present during all stages of cell lysis and enzyme extraction. Unfortunately, none of these changes resulted in significant quantities of enzyme. The use of 4.8 mM Cymal-5 during the purification did increase the yield to 7.4 nmol P420 following Ni-NTA affinity chromatography, but this quantity was insufficient to continue the purification with cation exchange chromatography. In contrast, 0.2% Emulgen 913 was not an optimal detergent with a lower yield of 1.65 nmol of the P420 form. The presence of 11-deoxycortisol may aid in stabilizing CYP11B1, as the yield increased from 2.2 nmol to 24 nmol of P420 following ultracentrifugation. However, the final yield determined from the Ni-NTA elution fractions was only ~1 nmol of P420 in the presence of substrate.

SDS-PAGE was inconclusive in identifying whether CYP11B1 was being efficiently extracted but suggested that what CYP11B1 was solubilized might not be binding very tightly to

Ni-NTA resin (Figure 6.6). When using Cymal-5 for extraction and stabilization there was a band in the Ni-NTA wash step at the expected 55 kDa (Figure 6.6A Ni. W vs. Ni. FT). This band was very light in the elution fractions (Figure 6.6A Ni. E #1 and #2). Instead, the elution fractions have a more prominent band at ~50 kDa, which might also be CYP11B1. Previous SDS-PAGE and western blot results indicate that CYP11B1 may run lower at ~50 kDa indicating CYP11B1 was present in the elution fractions. When instead 0.2% Emulgen was used to extract and stabilize CYP11B1, several bands were observed in the wash step between 50-55 kDa (Figure 6.6B Ni. W) and no bands near 50-55 kDa in the elution fraction. These results demonstrated the poor yield and purity of CYP11B1 after Ni-NTA column chromatography with both 4.8 mM cymal-5 and 0.2% Emulgen 913 detergents.

Figure 6.6. SDS-PAGE gels from the CYP11B1 purifications with A) 4.8 mM Cymal-5 and B) 0.2% Emulgen 913 indicates the 55 kDA protein may be eluting in the wash step or running at ~50 kDA. Gel key is as follows: (S): solubilized enzyme, (Ni. FT): Ni-NTA flow through, (Ni. W): Ni-NTA wash, (Ni E): Ni-NTA elution, (MW): dual color molecular weight ladder.

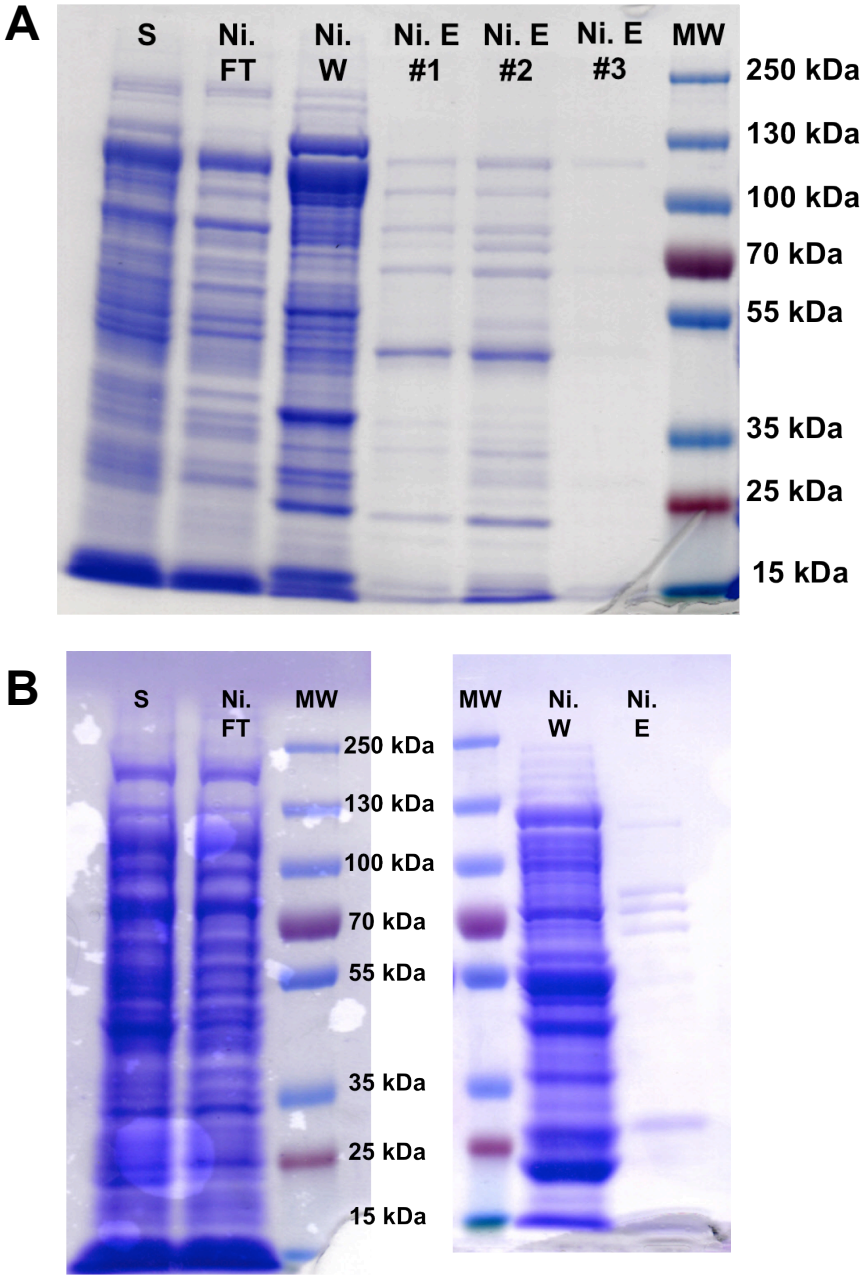

Finally, one purification was performed with Tris buffers, 1% cholate, 1% Tween 20, and 10 μM of the CYP11B1 inhibitor etomidate. While the supernatant from ultracentrifugation contained ≥89 nmol of P420 (Figure 6.7A), only 4.4 nmol of P420 and 1.4 nmol P450 remained following Ni-NTA affinity chromatography (Figure 6.7B). This yield was the highest yield following ultracentrifugation at that time and twice that of the other purifications, but only a small amount of protein was collected following Ni-NTA chromatography. In retrospect, this may have been the first indication that CYP11B1 bound poorly to the Ni-NTA resin, but the primary problem of expression masked this indicator.

Figure 6.7. Reduced carbon monoxide assay spectra of CYP11B1 following A) ultracentrifugation and B) Ni-NTA elution purified with Tris buffers, 1% cholate, 1% Tween 20, and 10 μM etomidate.

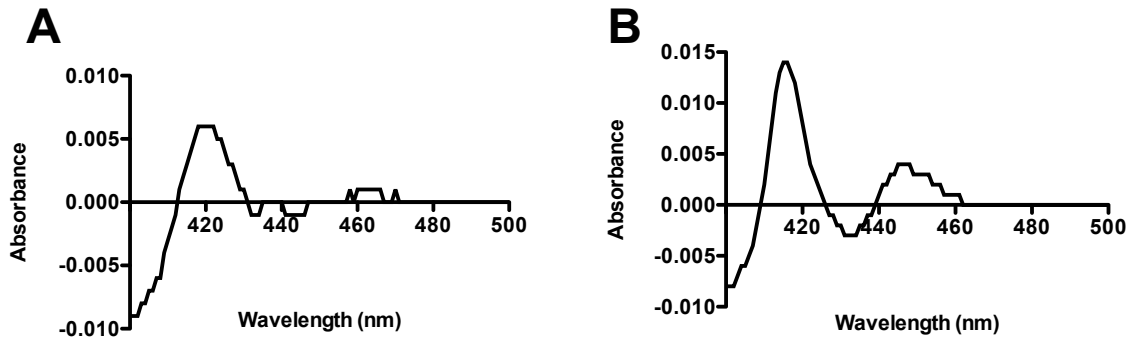

The foregoing attempts at purifying CYP11B1 from BL21(DE3)pLysS/pGro7 were not successful. Initially, it was hypothesized that extraction of the protein with detergent was the primary problem because the western blot indicated the presence of a histidine-tagged protein of approximately the correct molecular weight in whole cell lysate.

CYP11B1 Expression Test

To determine if other cell lines or expression plasmids would yield good quantities of protein that could be readily purified, additional expression systems were investigated. The cell lines of JM109, Topp3, and DH5α were selected for test expressions of CYP11B1 with the pCW plasmid. All cell lines contained the pGro7 plasmid encoding the GroES/GroEL chaperone. These cell lines were chosen based upon their success in expressing CYP17A1, CYP2A13, and CYP21A2, respectively.[24-26] TB cultures (250 mL), grown as described for BL21(DE3)pLysS/pGro7/pET17b11B1 with expression at 27 ˚C for 48 hours, resulted in a range of cell pellet weights (Table 6.1). The cell pellets varied in coloration from a light to dark tan pellets. Typical cell pellets with significant amounts of P450 expression are tan in color with dark tops or a dark tan throughout and often correlate to larger cell pellet weights. A light pellet color as in the case of BL21(DE3)pLysS/pGro7 cell line is usually an indicator of poor expression.

Table 6.1. Cell pellet mass from the CYP11B1 expression tests with the pET17b11B1 and pCW11B1 plasmids transformed into BL21(DE3)pLysS, JM109, Topp3, and DH5α, all with pGro7, and expressed in 250 mL TB cultures for 48 hours.

Cell Line	Co-chaperone	P450 Expression Plasmid	Cell Mass (g)/ 0.25 L
BL21(DE3)pLysS	pGro7	pET17b11B1	1.93
BL21(DE3)pLysS	pGro7	pCW11B1	2.34
JM109	pGro7	pET17b11B1	3.66
JM109	pGro7	pCW11B1	2.60
Topp3	pGro7	pET17b11B1	4.02
Topp3	pGro7	pCW11B1	3.20
DH5α	pGro7	pET17b11B1	3.92
DH5α	pGro7	pCW11B1	3.16

Samples of each growth were collected prior to P450 induction and at 24 and 48 hours after P450 induction and normalized to an OD_{600} of 1. The 48-hour samples were compared by western blot analysis. Aside from the BL21(DE3)pLysS attempt previously described, comparison of the eight samples indicated that the pCW11B1 plasmid resulted in the highest expression of a 50-55 kDa protein in each cell line (data not shown). Thus, the 48-hour sample with the darkest band at 50-55 kDa from each cell line was compared to its respective pre-induction sample on a separate western blot (Figure 6.8). In each case a dark band existed at 50-55 kDa. Of these, the darkest band on the western blot arguably continues to be the BL21(DE3)pLysS/pGro7/pET17b11B1 expression system described previously (Figure 6.8 Lane 2). However, since this expression system has not afforded much success, the JM109/pGro7 and DH5α/pGro7 cell lines with the pCW plasmid were chosen for further experimentation.

Figure 6.8. Western blot of samples before and after P450 induction for the CYP11B1 expression test with BL21(DE3)pLysS/pET17b11B1, JM109/pCW11B1, Topp3/pCW11B1, and DH5α/pCW11B1 all with the pGro7 plasmid and probed with an anti-His antibody. Image transparency was altered for clarity upon printing.

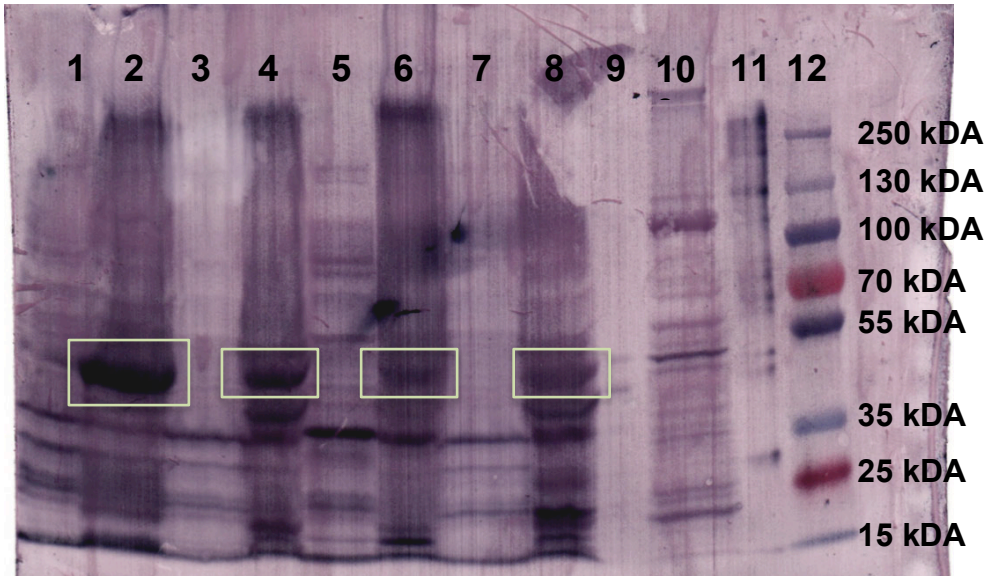

Lane	Cell Line	Chaperone	P450 Expression Plasmid	Time (hour)
1	BL21(DE3)pLysS	pGro7	pET17b11B1	0
2	BL21(DE3)pLysS	pGro7	pET17b11B1	48
3	JM109	pGro7	pCW11B1	0
4	JM109	pGro7	pCW11B1	48
5	Topp3	pGro7	pCW11B1	0
6	Topp3	pGro7	pCW11B1	48
7	DH5α	pGro7	pCW11B1	0
8	DH5α	pGro7	pCW11B1	48
9	X	X	X	X
10	Ni Elution Control	-	-	-
11	Anti-His Ladder	-	-	-
12	Dual Color Ladder	-	-	-

JM109/pGro7/pCW11B1 and DH5α/pGro7/pCW11B1 Expressions and Purifications

CYP11B1 was expressed in JM109/pGro7 or DH5α/pGro7 *E. coli* competent cells for 48 hours at 27 ˚C or 30 ˚C. While the size and color of a cell pellet does not always correlate to good expression levels, it was apparent that these expression systems were more effective in expressing CYP11B1 than BL21(DE3)pLysS/pGro7 as larger, darker cell pellets were obtained.

Generally, purification of 2 L of cell culture using Tris buffers with either 4.8 mM Cymal-5 or 0.2% Emulgen 913 resulted in larger quantities of P450 enzyme in the early purification stages than with BL21(DE3)pLysS/pGro7/pET17b11B1 and could be carried through Ni-NTA affinity and cation exchange chromatography. In addition, all purification stages included 50 μM 11-deoxycortisol to stabilize CYP11B1, and the protease inhibitor phenylmethanesulfonyl fluoride was added to a final concentration of 0.1 mM to decrease degradation of the enzyme during cell lysis and protein extraction.

CYP11B1 expressed in DH5α/pGro7 at 27 ˚C and purified with 4.8 mM Cymal-5 resulted in 30 nmol of active P450 enzyme following Ni-NTA chromatography. This was a significant improvement over the BL21(DE3)pLysS/pGro7 expressions which yielded less than 1 nmol of P450 at this stage. This was sufficient protein that CYP11B1 could be further purified with cation exchange chromatography, resulting in a final yield of 2.2 nmol of P450. Expression at 30˚C with JM109/pGro7 competent cells slightly improved the yield to 3.5 nmol following cation exchange chromatography with 4.8 mM Cymal-5. However, the ultracentrifuge supernatant from the 30 ˚C expression that was applied to the Ni-NTA resin was a significantly darker red color indicative of a higher protein concentration in comparison to the 27 ˚C expression. Unfortunately, the majority of the protein did not bind to the Ni-NTA column. Additionally, the Ni-NTA flow through fractions were collected and diluted 5-fold with CM

wash buffer, 4.8 mM Cymal-5, and 50 µM 11-deoxycortisol. The diluted sample was applied to the carboxymethyl resin for cation exchange, but the protein did not bind to the CM column either.

Since detergents can affect column chromatography the DH5α/pGro7 30 ˚C expression was purified with 0.2% Emulgen 913 in an attempt to enhance binding to the Ni-NTA resin. In addition the glycine content in the Ni-NTA wash buffer was reduced from 100 mM to 20 mM to reduce premature elution of the enzyme during the wash step. However, the dark red cell lysate with >365 nmol of P450 still bound poorly to the Ni-NTA resin resulting in only 5 nmol of P450 enzyme in the elution fractions. The yields at the various purification stages are summarized in table 6.2. It should be noted that the JM109/pGro7/pCW11B1 expression at 27 ˚C was not purified due to time constraints.

Table 6.2. Purification summaries for pCW11B1 expressed in DH5α/pGro7 *E. coli* competent cells.

Cell Line	DH5α/pGro7	DH5α/pGro7	JM109/pGro7
Expression Temperature (˚C)	27	30	30
Detergent	4.8 mM Cymal-5	0.2 % Emulgen 913	4.8 mM Cymal-5
Post Ultracentrifugation (nmol)	-	> 365 (P450)	64.3 (P450) 77.1 (P420)
Ni-NTA (nmol)	30 (P450)	5 (P450)	25.3 (P450) 12.7 (P420)
CM (nmol)	2.2 (P450)	-	3.5 (P450)

These results indicate that CYP11B1 expresses well in both DH5α/pGro7 and JM109/pGro7 *E. coli* competent cells with 30 ˚C being the optimal expression temperature. However, purified enzyme could not be attained due to the poor affinity to the Ni-NTA resin.

Six Residue Histidine Tag

Site-directed mutagenesis was used to incorporate two additional histidine residues at the C-terminus in order to extend the histidine tag and facilitate binding of CYP11B1 to the Ni-NTA resin. The 6X histidine tagged enzyme was expressed in JM109/pGro7 competent *E. coli* cells at 30 ˚C for 48 hours and purified with potassium phosphate buffers described in chapter 2, with 4.8 mM Cymal-5 and 50 μM 11-deoxycortisol. Tris buffers were exchanged for potassium phosphate buffers as this variable had yet to be attempted with the pCW expression systems. It also aided in the stabilization of CYP21A2 and may improve the yield following column chromatography. Unfortunately, the supernatant from ultracentrifugation following cell lysis with lysozyme, flash freeze, homogenization, and sonication was lighter in color than the previous 30 ˚C expressions and resulted in only 15.4 nmol of P450 and 13.5 nmol of P420 following Ni-NTA chromatography (Figure 6.9). While the potassium phosphate buffers could have affected the yield, it is more likely that the expression was the primary problem. The only difference between the expression with the 6X histidine tagged enzyme and the previous expressions was the induction of the 6X histidine tag at an OD_{600} of ~1.1 versus 1.8. A second expression was performed with induction of the CYP11B1 enzyme at 1.8, but the cell pellet was also lighter in color, which leads me to believe that the expression levels were not very high. As a result the impact of the 6X histidine tag on affinity for the Ni-NTA resin has yet to be determined. Future efforts will need to focus on both increasing the consistency of expression and the yield during purification.

Figure 6.9. Reduced carbon monoxide spectra of Ni-NTA purified CYP11B1 with a 6X histidine tag demonstrated both P450 and P420 peaks.

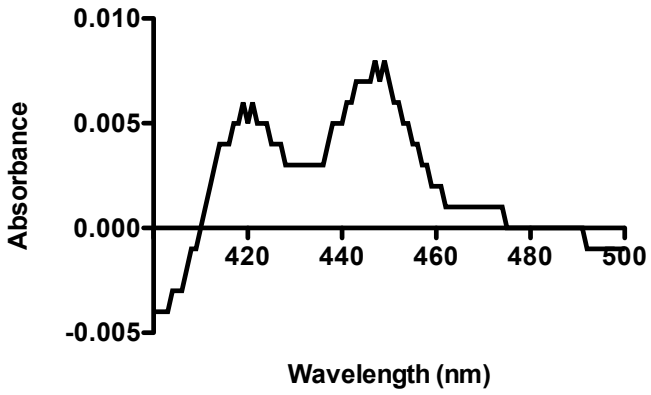

Discussion

CYP11B1 Modifications

Modifications to the CYP11B1 gene included a Δ3-25 deletion, R27K mutation, and a 4 amino acid residue histidine tag.[1] The truncation of the N-terminal transmembrane helix was based upon previous work and secondary structure predictions as CYP11B1 lacks the proline-rich region that often follows the transmembrane helix.[7] The modified enzyme was easily cloned into both pCW and pET17b vectors through NdeI and HindIII restriction sites and transformed into BL21(DE3)pLysS, JM109, DH5α, and Topp3 *E. coli* competent cells along with the pGro7 chaperone for protein expression trials.

BL21(DE3)pLysS/pGro7 pET17b11B1

Initial expression and purification of CYP11B1 followed a published protocol that reported 400 nmol/L of purified enzyme. Western blots indicated that a histidine tagged protein of the expected molecular weight was expressed following induction. However, several purification trials with varying detergents, buffers, and ligand present failed to produce a single

nmol of active P450 following NiTNA chromatography. Table 6.3 summarizes the purification yields with CYP11B1 expressed in BL21(DE3)pLysS/pGro7 competent *E. coli* cells. It remains unclear as to how the authors were able to produce their reported yield. In my experiments, the lack of expression appeared to be the primary problem. One possibility is that the induction of the enzyme at the incorrect OD_{600} value is critical, but the authors did not publish this information. If the BL21(DE3)pLysS/pGro7/pET17b expression is to be considered in the future, an expression test with varying induction times could provide insight as to the optimal OD_{600} value.

Table 6.3. Purification summary for BL21(DE3)pLysS/pGro7 expressed CYP11B1. The purification trials with cholate and Tween 20 followed a published protocol.[1] The remaining purification trials utilized Tris based buffers with 4.8 mM Cymal-5 or 0.2% Emulgen 913 in the presence or absence of ligand.

Detergent	1% Cholate/ 1% Tween 20 Trial 1 (nmol)	1% Cholate/ 1% Tween 20 Trial 2 (nmol)	4.8 mM Cymal-5 (nmol)	0.2% Emulgen 913 (nmol)	0.2% Emulgen 913 (nmol)
Ligand	-	-	-	-	50 µM 11-deoxycortisol
Ultracentrifugaiton Supernatant	44 (P420)	23 (P420)	17.3 (P420)	2.2 (P420)	24 (P420)
Ni-NTA Elution	3.2 (P420)	0.31 (P450)	7.4 (P420)	1.65 (P420)	~1 (P420)

Expression Evaluations

Due to the poor expression and purification of CYP11B1 from the BL21(DE3)pLys/pGro7 cell line, several expression systems were evaluated. Individually, pET17b11B1 and pCW11B1 were transformed into BL21(DE3)pLysS, JM109, DH5α, and

Topp3 *E. coli* competent cells containing pGro7. Western blot comparisons revealed that the BL21(DE3)pLysS/pGro7/pET17b11B1 expression system arguably had the darkest band correlating to a 50-55 kDa histidine tagged enzyme. However, CYP11B1 also appeared to express in both JM109/pGro7 and DH5α/pGro7 cell lines with the pCW expression plasmid, and large-scale expression confirmed this. A 48-hour expression in DH5 pGro7 at 27 ˚C resulted in 30 nmol of P450 following Ni-NTA chromatography, which was enough protein for the purification to be continued through cation exchange chromatography. Additional expression temperatures were evaluated, and while the purification yields are not indicative of the quality of expression, the deep red color of the ultracentrifugation supernatant indicated that a 30 ˚C incubation was optimal. However, the yield was significantly reduced due to the lack of interactions between the four histidine C-terminal tag and the Ni-NTA resin.

Six Residue Histidine Tag

Site-directed mutagenesis was used to extend the 4 residue histidine tag to 6 residues to enhance purification through affinity chromatography. Only one purification has been completed thus far with CYP11B1 expressed in JM109/pGro7 at 30˚, but no improvements to the yield were observed following Ni-NTA affinity chromatography with 15.4 nmol of P450 and 13.5 nmol of P420. However, the effect of the 6X histidine tag cannot be determined, as it appeared that the overall expression was poor. While the size and color of a cell pellet does not necessarily correlate to the quality of expressions, qualitative observations through empirical experimentation can be valuable. The cell pellet from the previous 30 ˚C expression with the 4X histidine tag were darker in color following harvesting resulting in a deep red supernatant after ultracentrifugation. One explanation for subsequent decreased expression levels might be that a poor colony was selected for expression. Inconsistent expression levels between colonies have

been observed for other P450 expressions. Future expression of CYP11B1 should begin from a fresh transformation rather than glycerol stocks to evaluate this variable. In addition, expression in DH5α/pGro7 competent *E. coli* cells should be performed. Should the 6X His tag ultimately prove unsuccessful, additional chromatographic steps will be pursued. P450 enzymes have previously been purified with DEAE-cellulose, hydoxyapetite, and octyl sepharose column chromatography.[27,28] Additionally, affinity chromatography with CYP11B1's redox partner, adrenodoxin, could be used as this approach was successful in purifying the mitochondrial P450 CYP11A1.[29]

Conclusions

Biochemical studies of human CYP11B1 have been hampered by protein availability and the instability of the enzyme during expression, detergent solubilization, and purification in previous work[1,2] and the results described herein. However, the results described in this chapter also illustrate progress towards obtaining purified CYP11B1. This is necessary to provide sufficient quality and quantity of protein to support biochemical studies to elucidate structure/function relationships and evaluate CYP11B1 as a counter-target for CYP17A1 inhibitors. Expression tests completed thus far reveal that the JM109/pGro7 and DH5α/pGro7 cell lines with pCW11B1 prefer incubations at 30 ˚C rather than 27 ˚C for 48 hours, but the expression is inconsistent at present. Purification of CYP11B1 has also proven to be problematic due to poor column affinity, but ongoing experimentation will focus on resolving this obstacle. Advancing knowledge on CYP11B1 could provide a more thorough understanding of the underlying structural interactions of CYP11B1 contributing to normal or impaired CYP11B1 activity and lead to advanced therapeutic treatments for cortisol dependent diseases such as Cushing's disease. In addition, the structural and functional knowledge could aid in the

development of CYP17A1 inhibitors for the treatment of prostate cancer by testing the selectivity of the potential drug candidates against CYP11B1 as a counter-target.

References

1. Zollner, A. et al. Purification and functional characterization of human 11beta hydroxylase expressed in Escherichia coli. *FEBS J* **275**, 799-810 (2008).
2. Ikushiro, S., Kominami, S. & Takemori, S. Adrenal cytochrome P-45011 beta-proteoliposomes catalyzing aldosterone synthesis: preparation and characterization. *Biochim Biophys Acta* **984**, 50-6 (1989).
3. Fisher, A. et al. Effects of 18-hydroxylated steroids on corticosteroid production by human aldosterone synthase and 11beta-hydroxylase. *J Clin Endocrinol Metab* **86**, 4326-9 (2001).
4. Mornet, E., Dupont, J., Vitek, A. & White, P.C. Characterization of two genes encoding human steroid 11 beta-hydroxylase (P-450(11) beta). *J Biol Chem* **264**, 20961-7 (1989).
5. Bottner, B. & Bernhardt, R. Changed ratios of glucocorticoids/mineralocorticoids caused by point mutations in the putative I-helix regions of CYP11B1 and CYP11B2. *Endocr Res* **22**, 455-61 (1996).
6. Mulatero, P. et al. Recombinant CYP11B genes encode enzymes that can catalyze conversion of 11-deoxycortisol to cortisol, 18-hydroxycortisol, and 18-oxocortisol. *J Clin Endocrinol Metab* **83**, 3996-4001 (1998).
7. *Cytochrome P450: Structure, Mechanism, and Biochemistry*, (Kluwer Academic/ Plenum Publishers, New York, 2005).
8. Roumen, L. et al. Construction of 3D models of the CYP11B family as a tool to predict ligand binding characteristics. *J Comput Aided Mol Des* **21**, 455-71 (2007).
9. Curnow, K.M. et al. The amino acid substitutions Ser288Gly and Val320Ala convert the cortisol producing enzyme, CYP11B1, into an aldosterone producing enzyme. *Nat Struct Biol* **4**, 32-5 (1997).
10. Speiser Phyllis, W. & White Perrin, C. Congenital adrenal hyperplasia. *N Engl J Med* **349**, 776-88 (2003).
11. White, P.C., Curnow, K.M. & Pascoe, L. Disorders of steroid 11 beta-hydroxylase isozymes. *Endocr Rev* **15**, 421-38 (1994).
12. Zachmann, M., Tassinari, D. & Prader, A. Clinical and biochemical variability of congenital adrenal hyperplasia due to 11 beta-hydroxylase deficiency. A study of 25 patients. *J Clin Endocrinol Metab* **56**, 222-9 (1983).
13. Ben Charfeddine, I. et al. Two novel CYP11B1 mutations in congenital adrenal hyperplasia due to steroid 11beta hydroxylase deficiency in a Tunisian family. *Gen Comp Endocrinol* **175**, 514-8 (2012).
14. Krone, N. et al. Analyzing the functional and structural consequences of two point mutations (P94L and A368D) in the CYP11B1 gene causing congenital adrenal hyperplasia resulting from 11-hydroxylase deficiency. *J Clin Endocrinol Metab* **91**, 2682-8 (2006).
15. Merke, D.P. et al. Novel CYP11B1 mutations in congenital adrenal hyperplasia due to steroid 11 beta-hydroxylase deficiency. *J Clin Endocrinol Metab* **83**, 270-3 (1998).
16. Lahera Vargas, M. & da Costa, C.V. [Prevalence, etiology and clinical findings of Cushing's syndrome]. *Endocrinol Nutr* **56**, 32-9 (2009).
17. Tritos, N.A. & Biller, B.M. Advances in medical therapies for Cushing's syndrome. *Discov Med* **13**, 171-9 (2012).

18. Schoneshofer, M., Schefzig, B. & Oelkers, W. Evidence of adrenal 18-hydroxylase inhibition by metyrapone in man. *Horm Metab Res* **11**, 306-8 (1979).
19. Calhoun, D.A. et al. Effects of a novel aldosterone synthase inhibitor for treatment of primary hypertension: results of a randomized, double-blind, placebo- and active-controlled phase 2 trial. *Circulation* **124**, 1945-55 (2011).
20. Belkina, N.V., Lisurek, M., Ivanov, A.S. & Bernhardt, R. Modelling of three-dimensional structures of cytochromes P450 11B1 and 11B2. *J Inorg Biochem* **87**, 197-207 (2001).
21. Wada, A., Ohnishi, T., Nonaka, Y., Okamoto, M. & Yamano, T. Synthesis of aldosterone by a reconstituted system of cytochrome P-45011 beta from bovine adrenocortical mitochondria. *J Biochem* **98**, 245-56 (1985).
22. Nonaka, Y. et al. Structure/function relationship of CYP11B1 associated with Dahl's salt-resistant rats--expression of rat CYP11B1 and CYP11B2 in Escherichia coli. *Eur J Biochem* **258**, 869-78 (1998).
23. Gomes, A.V. Protein gel electrophoresis tips and troubleshooting guide. http://aldrin.tripod.com/index-3.html
24. Arase, M., Waterman, M.R. & Kagawa, N. Purification and characterization of bovine steroid 21-hydroxylase (P450c21) efficiently expressed in Escherichia coli. *Biochem Biophys Res Commun* **344**, 400-5 (2006).
25. DeVore, N.M. & Scott, E.E. Structures of cytochrome P450 17A1 with prostate cancer drugs abiraterone and TOK-001. *Nature* **482**, 116-9 (2012).
26. Smith, B.D. et al. Structure of the human lung cytochrome P450 2A13. *J Biol Chem* **282**, 17306-13 (2007).
27. Pikuleva, I.A., Bjorkhem, I. & Waterman, M.R. Expression, purification, and enzymatic properties of recombinant human cytochrome P450c27 (CYP27). *Arch Biochem Biophys* **343**, 123-30 (1997).
28. Saribas, A.S., Gruenke, L. & Waskell, L. Overexpression and purification of the membrane-bound cytochrome P450 2B4. *Protein Expr Purif* **21**, 303-9 (2001).
29. Mast, N. et al. Structural basis for three-step sequential catalysis by the cholesterol side chain cleavage enzyme CYP11A1. *J Biol Chem* **286**, 5607-13 (2011).

Chapter 7

Conclusions

Cytochrome P450 enzymes are involved in both endogenous and exogenous metabolism in maintaining homeostasis and clearance of foreign chemicals from the body. There are 57 human cytochrome P450 enzymes that participate in the metabolism of steroids, xenobiotics, fatty acids, eicosanoids, vitamins, or unknown substrates.[1] While these oxidations are usually advantageous, aberrant activity or activation of procarcinogens can be detrimental to human health. However, these problems can often be addressed through therapeutic intervention. The rational design of inhibitors for modification of disease states requires a biochemical understanding of the enzyme, and the evaluation of potential drug candidates against both targets and counter-targets. The work described thus far has involved the evaluation of selective inhibitors for the therapeutic target CYP2A13, and the biochemical evaluation of cytochromes P450 involved in the steroid biosynthetic pathway as both therapeutic targets and counter-targets.

Lung Cancer Chemoprevention

Lung cancer is the leading cause of all cancer related deaths.[2] With only a 15% 5-year survival rate,[3] current research has been focused on preventative methods. Since tobacco use is responsible for >80% of all lung cancer incidence,[2] the role of specific tobacco carcinogens warrants investigation. NNK is one of the most prevalent procarcinogens in tobacco products and is selectively activated by CYP2A13 metabolism.[4] Therefore, the selective inhibition of CYP2A13 offers a novel therapeutic target. Evaluation of a benzylmorpholine library revealed selective binders and inhibitors of CYP2A13 versus the 94% identical CYP2A6, with K_d and K_i values for CYP2A13 in the low micromolar range. Substitution at the ortho position on the benzene ring proved to be vital for selectivity, affinity, and potency. X-ray crystallography with

select benzylmorpholine analogs suggested that the ligands may bind in multiple orientations with a consistent placement of the chlorine substituent in the center of the active site of CYP2A13-like enzymes. Combination of the binding and enzymatic analysis with the structural data could facilitate the design of more potent inhibitors with an emphasis placed at the ortho substitution. However, further characterization of benzylmorpholine analogs is necessary to determine the utility of this scaffold.

The next step in the development of benzylmorpholine analogs as drug candidates was the determination of an initial safety profile for cytotoxicity, mutagenicity, and hERG interaction in addition to evaluation against a panel of xenobiotic-metabolizing P450 enzymes to determine the metabolic stability in mammalian microsomes. This work was performed for our study by Cerep, Xenotech, or Pfizer as they had the necessary expertise to complete these studies. 4-(2-Chlorobenzyl)morpholine (**3**) and/or 4-(2-chloro-6-fluorobenzyl)morpholine (**7**) were used as test compounds as they were both potent and selective inhibitors of CYP2A13 and represented both the single and disubstituted analogs. First, aqueous solubility was determined since precipitation during subsequent dilutions and incubations can lead to erroneous or irreproducible results. Consistent with our own experience with these compounds, the aqueous solubility was relatively high. Both **3** and **7** were soluble up to 180 μM in phosphate buffered saline, pH 7.4.

Both **3** and **7** were tested for bacterial cytotoxicity and genetic and cardiac toxicity. These compounds were not cytotoxic with *Salmonella typhimurium* strains TA98, TA100, and TA1535 at concentrations ranging from 0.63 – 100 μM with survival rates of ≥86% of control samples at all concentrations. A compound is considered toxic if the bacterial cell growth is less than 60% of control samples at the respective concentrations.

For genetic toxicity, the Ames test was also employed with *Salmonella typhimurium* strains TA98, TA100, and TA1535, which detect frame shifts and base substitutions. Assays were completed +/- S9 fraction to detect toxicity requiring metabolic activation. Growth on selective agar plates revealed that in compound concentrations ranging from 5-100 μM few to no revertants were detected. These negative results suggest that the genetic toxicity of these compounds is very low.

The potential of **3** and **7** to cause cardiac toxicity via inhibition of the hERG channel was evaluated because this can be a major reason for drug withdrawal or limitation. The potential for prolongation of the QT interval associated with sudden cardiac death was determined by exposing mammalian CHO-K1 cells expressing the hERG channel gene to 0.1-10 μM of either **3** or **7** and using an automated patch clamp assay. The percent of inhibition is obtained by measuring the tail current amplitude before and after addition of compound. Using this approach, compounds **3** and **7** inhibited the tail current by 13.9% and 24.8%, respectively, at the highest concentration tested, 10 μM. These results suggest the hERG IC_{50} is >10 μM, placing the potency in the low category and suggesting that cardiac toxicity is unlikely to be relevant for these compounds. Of course, the effective therapeutic plasma concentrations should be considered. The target would be for a drug's hERG IC_{50} to be ≥30-fold higher than the plasma concentration to maximize safety.

The metabolic stability of compounds **3**, **7**, and **8** were evaluated with a panel of recombinant hepatic cytochromes P450 at Pfizer. Compound (1 μM) was incubated with recombinant human CYP1A2, CYP2B6, CYP2C8, CYP2C9, CYP2C19, CYP3A4, CYP2D6, and human liver microsomes over the course of 45 minutes. The percent compound remaining was detected at 0, 5, 10, 20, 30, and 45 minutes. The average half life for the compounds ranged

from <5 minutes with CYP2B6 (**3** and **7**) to 2,317 minutes with CYP1A2 (**3**) (Table 7.1). CYP2B6 was the fastest metabolizer of the benzylmorpholine compounds with 0% compound remaining after only 5 minutes while 100% remained in the control samples, which were not initiated with NADPH (Figure 7.2). These results suggest that the benzylmorpholine compounds herein will be cleared very rapidly from circulation if delivered systematically. All of these enzymes are predominantly hepatic enzymes while CYP2A13 is expressed in the respiratory tract. If a benzylmorpholine inhibitor could be directly administered to the lungs through the use of an inhaler, it would be able to reach its target before the first pass effect would decrease compound concentrations in circulation.

Table 7.1. Results for the average half life of compounds **6**, **7**, and **8** with a panel of human recombinant hepatic cytochromes P450.

Compound	Average $T_{1/2}$ (min)							
	CYP1A2	CYP2C8	CYP2C9	CYP2D6	CYP3A4	CYP2C19	CYP2B6	HLM
3	2317	62	476	61	33	13	<5	23
7	1214	51	230	78	25	18	<5	13
8	244	42	150	55	10	14	12	16

Figure 7.1. Representative data of the metabolic studies with a benzylmorpholine compound (**3**) and CYP2B6.

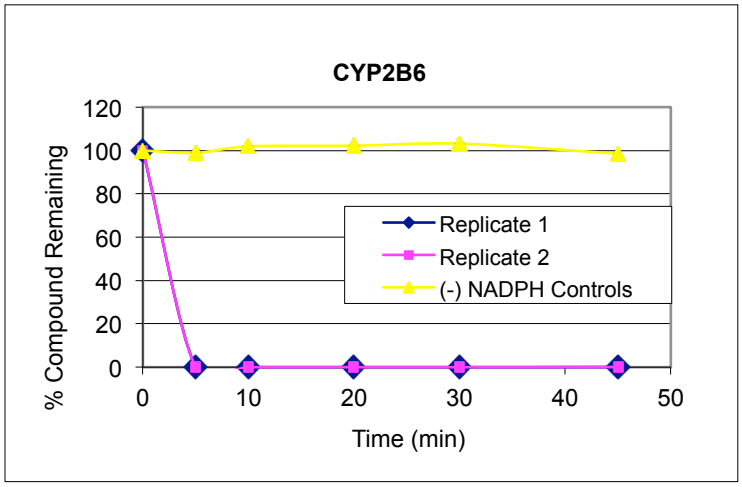

Therefore it was important next to determine the metabolic stability of these compounds in lung microsomes compared to liver microsomes with not only the target organism (human), but also for our potential pre-clinical models, rats and mice. Xenotech performed the metabolic studies with mouse, rat, and human lung and liver microsomes with **3** and **7**. The first concern was that the compounds might not be stable in human lung tissue long enough to have a sustained desired effect of CYP2A13 inhibition. To evaluate this, an assay was performed to detect benzylmorpholine compounds after 5, 10, and 20 minutes with +/- NADPH controls with the microsomes listed above. Since CYP2A13 is located in the respiratory tract, it was reassuring to observe that the benzylmorpholine analogs were very stable in human lung microsomes as minimal or no loss of substrate was observed after 20 minutes (Table 7.2). Following the 20-minute incubations with the mouse and rat lung and liver microsomes, no substrate was detected, indicating that the mouse and rat isozymes metabolize the benzylmorpholine analogs very quickly while the human enzymes result in much slower

clearance. However, there may be some variability in the assay as >100% of compound was detected in human lung microsomes after the allotted time. Regardless, the data was sufficient to illustrate the differences in metabolic stability of the samples between species and different tissues, and the results suggested that dosing in human lung is not problematic and that the compounds will then be quickly cleared from systemic circulation to reduce side effects and toxicity. However, the rat and mouse data raises a concern about the validity of testing these compounds in animal models. The rat and mouse P450 enzymes do not reflect the human case we are targeting. This would make it very difficult to collect *in vivo* data for an investigational new drug (IND) application, which is required before clinical trials.

Table 7.2. Metabolic stability following a 20 minute incubation of **3** (black) and **7** (red) with mouse, rat, and human lung and liver microsomes.

Species	Test System	Percent Loss of Substrate (%)	Percent Remaining (%)	Estimated *in vitro* intrinsic clearance (µL/min/mg protein)
Human	Liver	47.0/85.5	53.1/14.5	152/91.4
	Lung	No Loss/No Loss	111/137	NA/NA
Mouse	Liver	100/100	0/0	3430/916
	Lung	99.9/100	0.1/0	2160/551
Rat	Liver	96.7/97.3	3.3/2.7	744/173
	Lung	99.8/100	0.2/0	1420/478

However, this hurdle of variation between species may be overcome by the use of a humanized mouse model in which the mouse CYP2A enzymes are knocked out and the human CYP2A enzymes are knocked in. Dr. Xinxin Ding from the Wadsworth Center is pioneering this work. In the process of creating the humanized mouse model, Dr. Ding created a CYP2A and CYP2B knockout mouse and generously provided lung and liver microsomes for evaluation. Metabolic studies similar to those described above were conducted by Xenotech to determine the stability of our compounds with lung and liver microsomes. In comparison to wild type microsomes, the compounds were more stable in the knockout mice in both the lung and liver samples and had a similar metabolic profile to the human lung and liver samples with minimal compound disappearance in lung microsomes and a higher rate of metabolism in the liver microsomes (Figure 7.2). The next step would be to analyze benzylmorpholine compounds with a humanized mouse model, which has the human CYP2A13, CYP2B6, and CYP2F1 genes knocked in.[5] This model demonstrated that CYP2A13 and CYP2F1 were expressed in the respiratory tract, while CYP2B6 expression was localized to the liver as is reflective of human enzymes.[5] Noteably, these transgenic mice had a higher rate of NNK metabolism over wild type mice which is consistent with CYP2A13 having a higher catalytic efficiency over the mouse CYP2A5 ortholog.[6] Analysis of benzylmorpholine drug candidates with this humanized mouse model could provide insight into the *in vivo* efficacy of these compounds.

Figure 7.2. Disappearance of **7** during incubation with A) liver and B) lung microsomes from CYP2A/CYP2B knockout (transgenic) mice versus wild type mice (control).

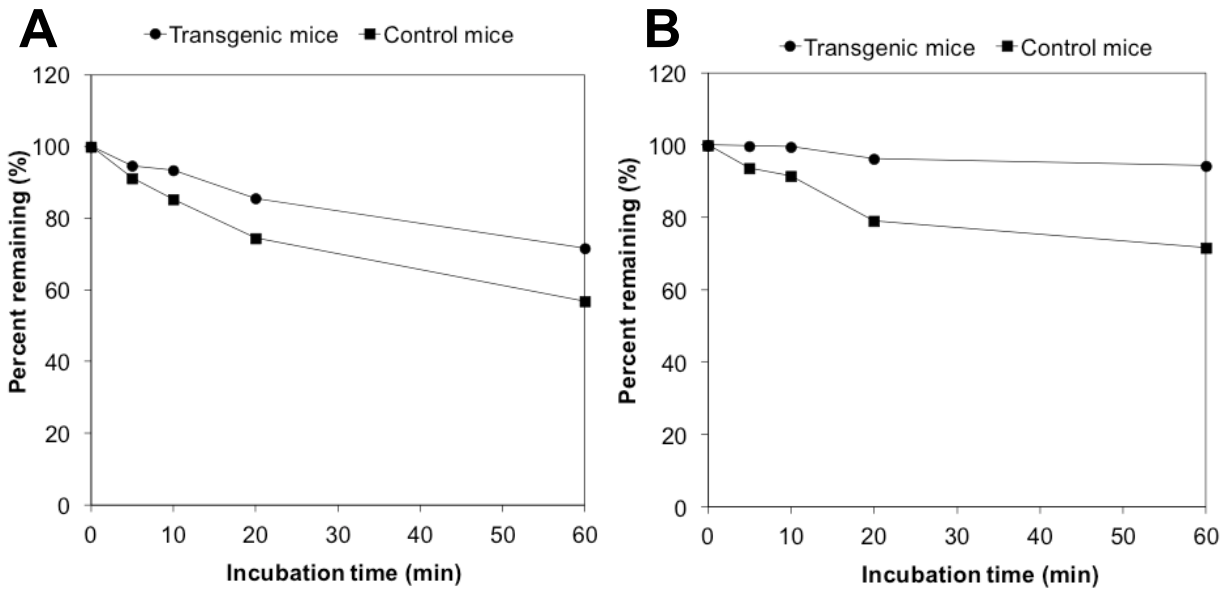

The results above summarize the development of benzylmorpholine analogs for the chemoprevention of lung cancer. Benzylmorpholine analogs **3** and **7** were soluble, did not show toxicity in Ames and hERG, and although rapidly metabolized by human liver microsomes, predominately by CYP2B6, persist in human lung microsomes. Drug delivery through inhalation and decreased systemic exposure is promising for minimal side effects and toxicity. Concerns with rapid clearance in pre-clinical rat and mouse models is seemingly obviated by the development of humanized mouse models that better reflect human CYP activity. *In vivo* studies in humanized mouse models is the next stage in development and can be used to evaluate the protective effects of a benzylmorpholine drug candidate against NNK-induced lung tumors. If successful, our compound could be used individually or in concert with the suppressing agent myo-inosotol to reduce the risk of lung cancer in tobacco users.[3]

Development of CYP21A2 and CYP11B1 for the Counter-target Evaluation of Selective CYP17A1 Inhibitors

CYP2A13 is not the only therapeutic target that has been of interest to the Scott lab. Recent work has resulted in the crystal structure of CYP17A1. Combination of this structural knowledge with biochemical studies is being used to develop selective inhibitors for the treatment of prostate cancer. In order to determine the selectivity for potential drug candidates, these compounds will need to be evaluated against obvious counter-targets. In addition to CYP17A1, CYP21A2 and CYP11B1 are involved in the steroid biosynthetic pathway, and substrate overlap exists between CYP21A2 and CYP17A1. However, biochemical studies for both CYP21A2 and CYP11B1 have been limited in the current literature. The work described in this dissertation lays the groundwork for the structure/function evaluation of these enzymes. Human CYP21A2 was successfully cloned, expressed, purified, and crystallized for the first time. Crystal optimization and development of metabolism assays are still ongoing, and the finalization of the metabolism protocol is vital for determining if new CYP17A1 inhibitors are selective for CYP17A1 over CYP21A2. The structural knowledge that could be gained through X-ray crystallography would provide insight into the active site residues governing substrate selectivity, and comparison to the bovine CYP21A2 structure could inform final differences between species and either validate or invalidate inferences made from the 79%-identical bovine CYP21A2 enzyme.

Biochemical evaluation of CYP11B1 is not only necessary for counter-target evaluation, but the knowledge could be additionally useful in designing selective inhibitors of CYP11B1 for the treatment of Cushing's disease resulting from overproduction of cortisol. Large-scale expression and purification of this enzyme are necessary to complete the desired biochemical

studies. Only one *E. coli* expression and purification resulting in 400 nmol/L of purified enzyme has been reported in the literature.[7] However, we were unable to reproduce these results, and no additional work with this protocol has been published. Therefore, I evaluated different expression systems and purification modifications such as detergents, buffers, and inclusion of ligand. While CYP11B1 has been successfully cloned, expressed, and extracted, expression has been inconsistent, and the purification of this enzyme has proven to be difficult due to the lack of affinity during metal-affinity and cation exchange column chromatography. Future work will include evaluation of expressions at 30˚ C and the ability of a new CYP11B1 construct with a lengthened histidine tag to bind to Ni-NTA resin. Additional chromatographic steps such as DEAE-cellulose, octyl sepharose, hydroxyapatite, and adrenodoxin affinity will be pursued if the extended histidine tag proves unsuccessful.

These results with CYP21A2 and CYP11B1 describe the foundational work that is necessary for the biochemical evaluation of these enzymes in addition to determining their utility as counter-targets. Advancing the knowledge of these enzymes would help provide a more complete picture of the enzymes involved in the steroid biosynthetic pathway.

Acknowledgements

I would like to thank Cerep, Xenotech, and Dave Neul and Mike Wester at Pfizer for completion of the additional characterization of the behavior of the benzylmorpholine drug candidates. In addition, I am grateful for the generosity of Xinxin Ding in providing the lung and liver microsomes from CYP2A/CYP2B knockout mice.

References

1. *Cytochrome P450: Structure, Mechanism, and Biochemistry*, (Kluwer Academic/ Plenum Publishers, New York, 2005).
2. American Cancer Society. Cancer Facts and Figures 2012. (2012). http://www.cancer.org/Research/CancerFactsFigures/index
3. Hecht, S.S., Kassie, F. & Hatsukami, D.K. Chemoprevention of lung carcinogenesis in addicted smokers and ex-smokers. *Nat Rev Cancer* **9**, 476-88 (2009).
4. He, X.Y., Shen, J., Ding, X., Lu, A.Y. & Hong, J.Y. Identification of critical amino acid residues of human CYP2A13 for the metabolic activation of 4-(methylnitrosamino)-1-(3-pyridyl)-1-butanone, a tobacco-specific carcinogen. *Drug Metab Dispos* **32**, 1516-21 (2004).
5. Wei, Y. et al. Generation and Characterization of a CYP2A13/2B6/2F1-transgenic Mouse Model. *Drug Metab Dispos* (2012). In press.
6. Jalas, J.R., Hecht, S.S. & Murphy, S.E. Cytochrome P450 Enzymes as Catalysts of Metabolism of 4-(Methylnitrosamino)-1-(3-pyridyl)-1-butanone, a Tobacco Specific Carcinogen. *Chem. Res. Toxicol.* **18**, 95-110 (2005).
7. Zollner, A. et al. Purification and functional characterization of human 11beta hydroxylase expressed in Escherichia coli. *Febs J* **275**, 799-810 (2008).

Appendix: ^{1}H NMR Spectra

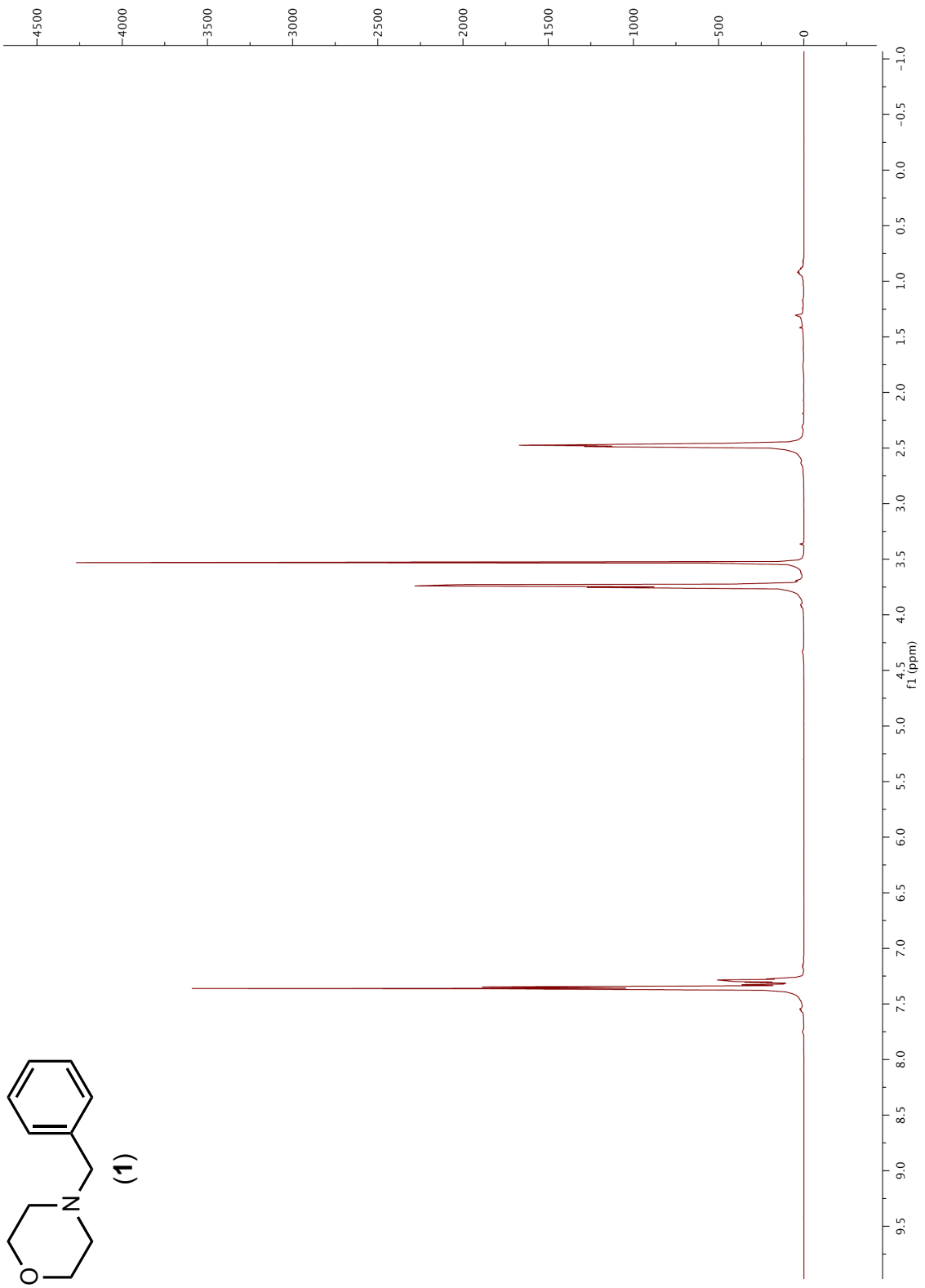

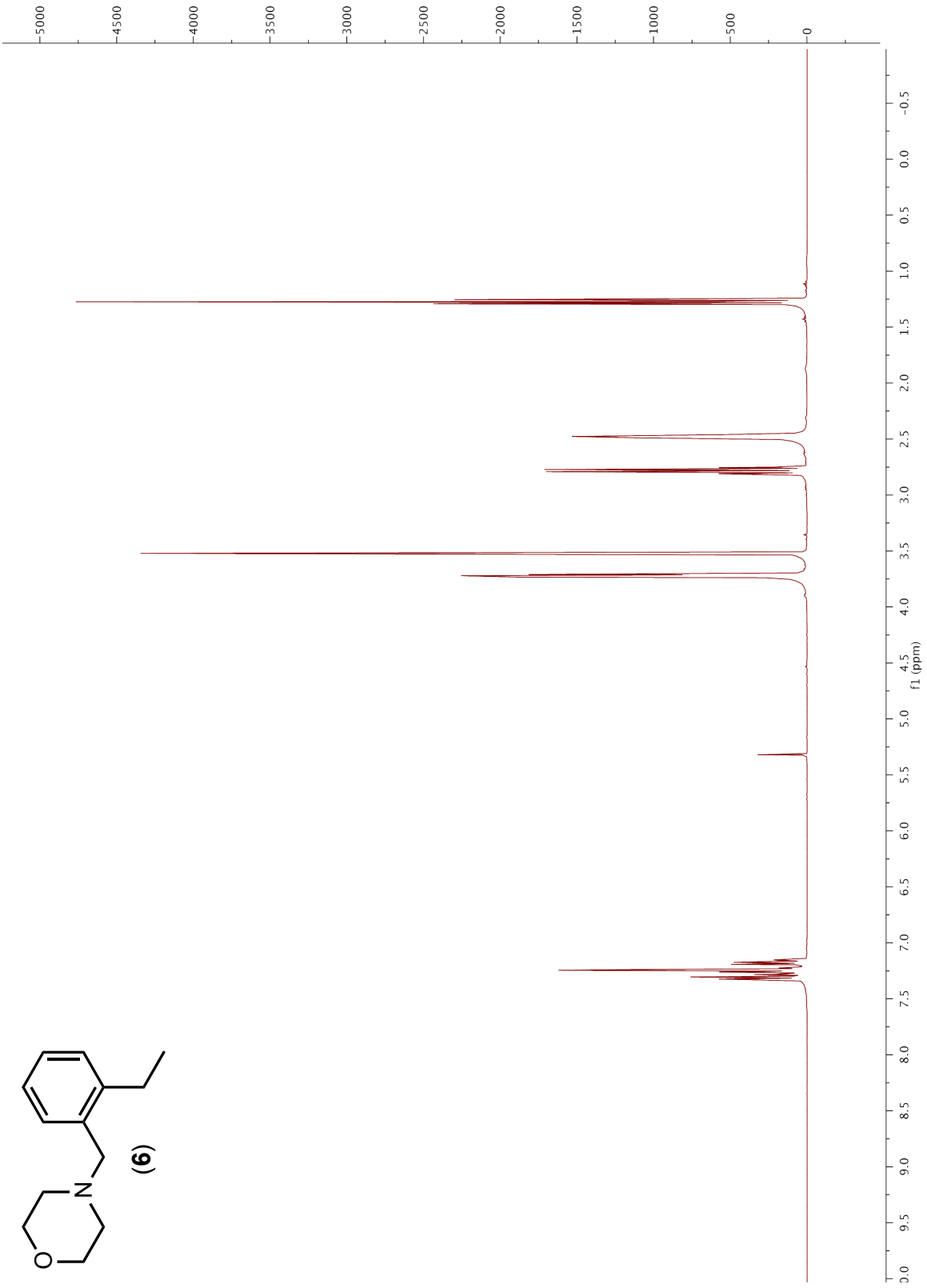
5000
4500
4000
3500
3000
2500
2000
1500
1000
500
0
-0.5
0.0
0.5
1.0
1.5
2.0
2.5
3.0
3.5
4.0
4.5
5.0
5.5
6.0
6.5
7.0
7.5
8.0
8.5
9.0
9.5
10.0
f1 (ppm)
N
O

(6)

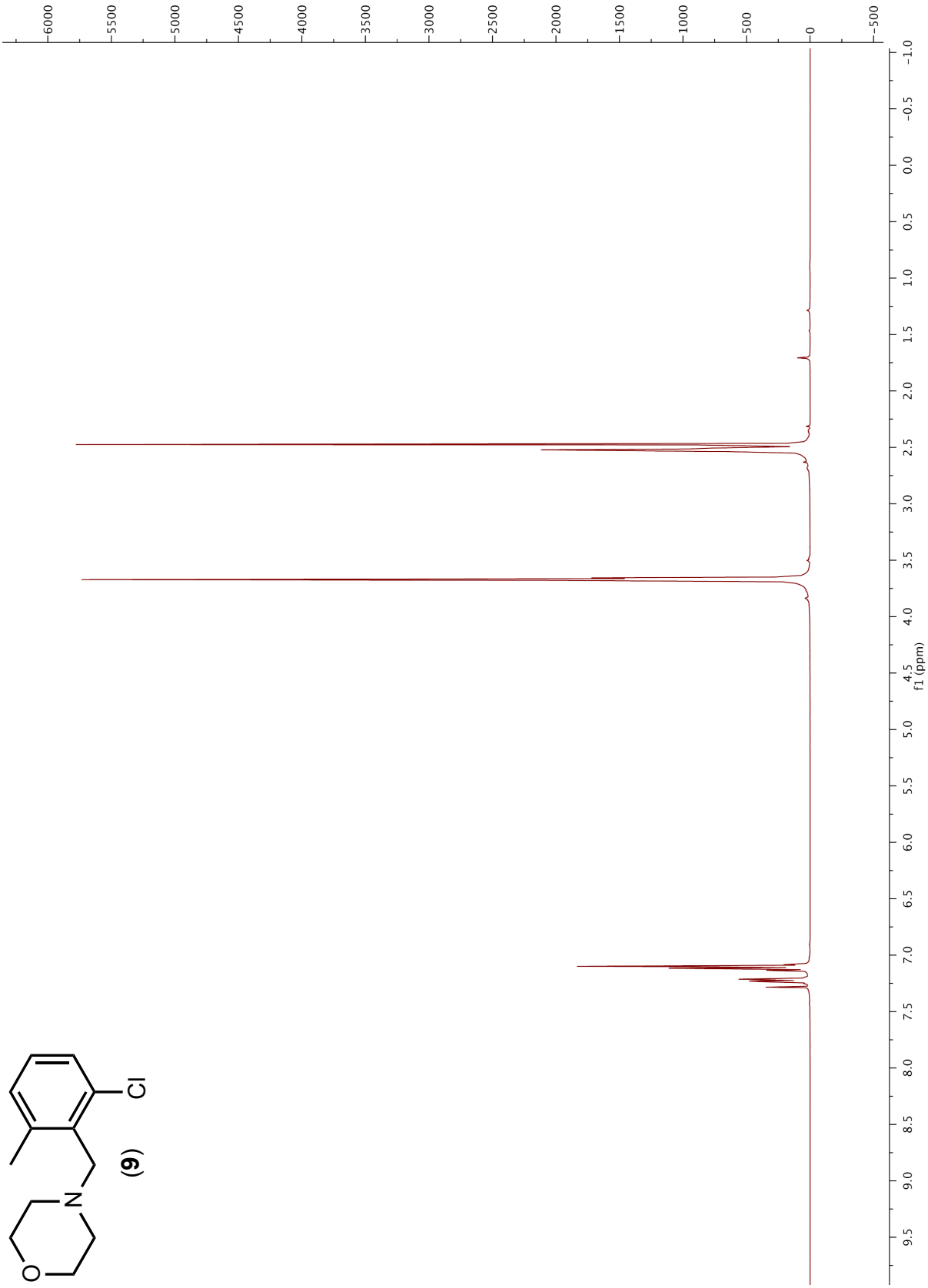
Cl
N
O
(9)
f1 (ppm)

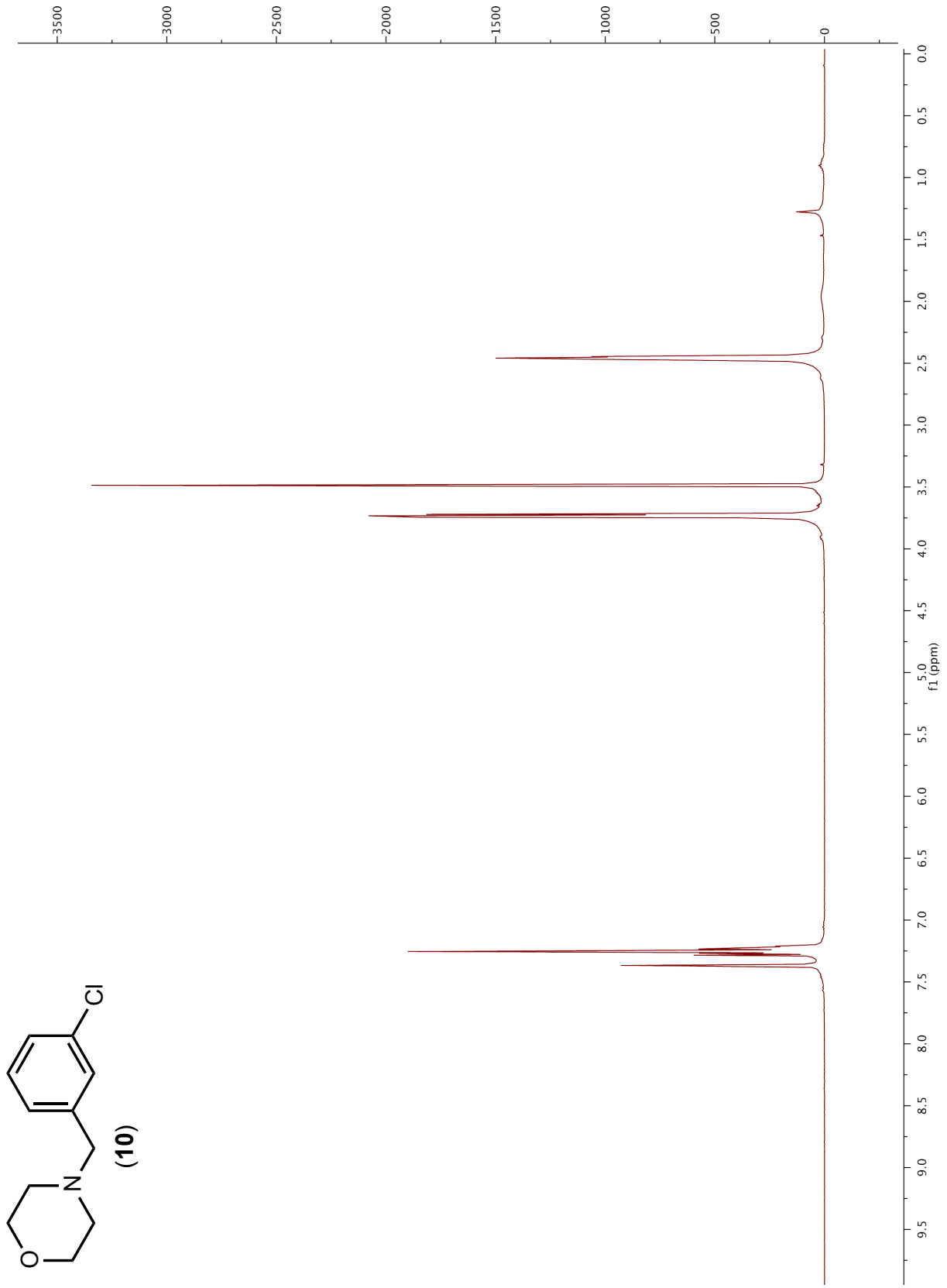
Cl
N
O
(10)
3500
3000
2500
2000
1500
1000
500
0
0.0
0.5
1.0
1.5
2.0
2.5
3.0
3.5
4.0
4.5
5.0
5.5
6.0
6.5
7.0
7.5
8.0
8.5
9.0
9.5
f1 (ppm)

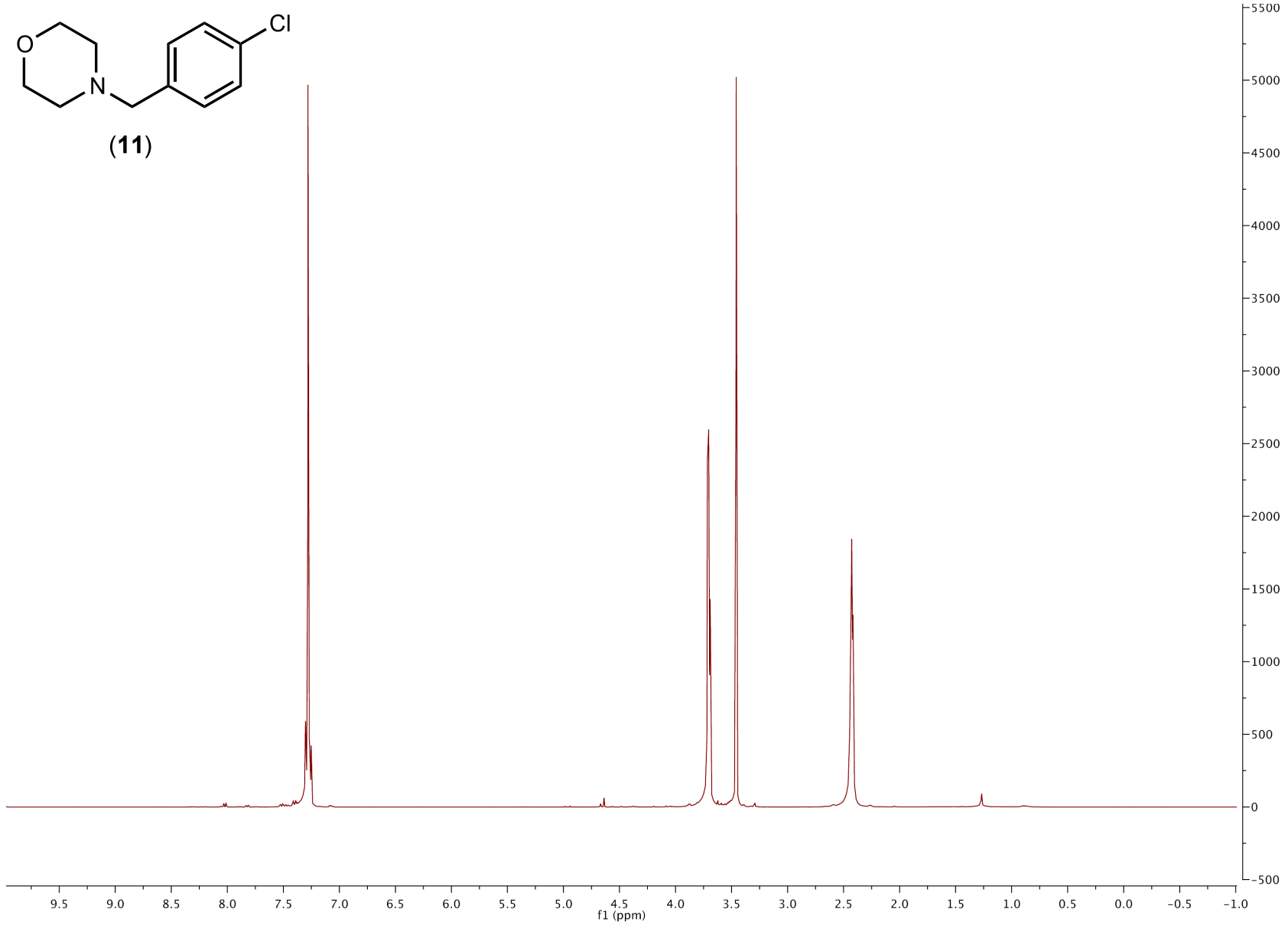
O
N
Cl
(11)
5500
5000
4500
4000
3500
3000
2500
2000
1500
1000
500
0
-500
9.5
9.0
8.5
8.0
7.5
7.0
6.5
6.0
5.5
5.0
4.5
4.0
3.5
3.0
2.5
2.0
1.5
1.0
0.5
0.0
-0.5
-1.0
f1 (ppm)

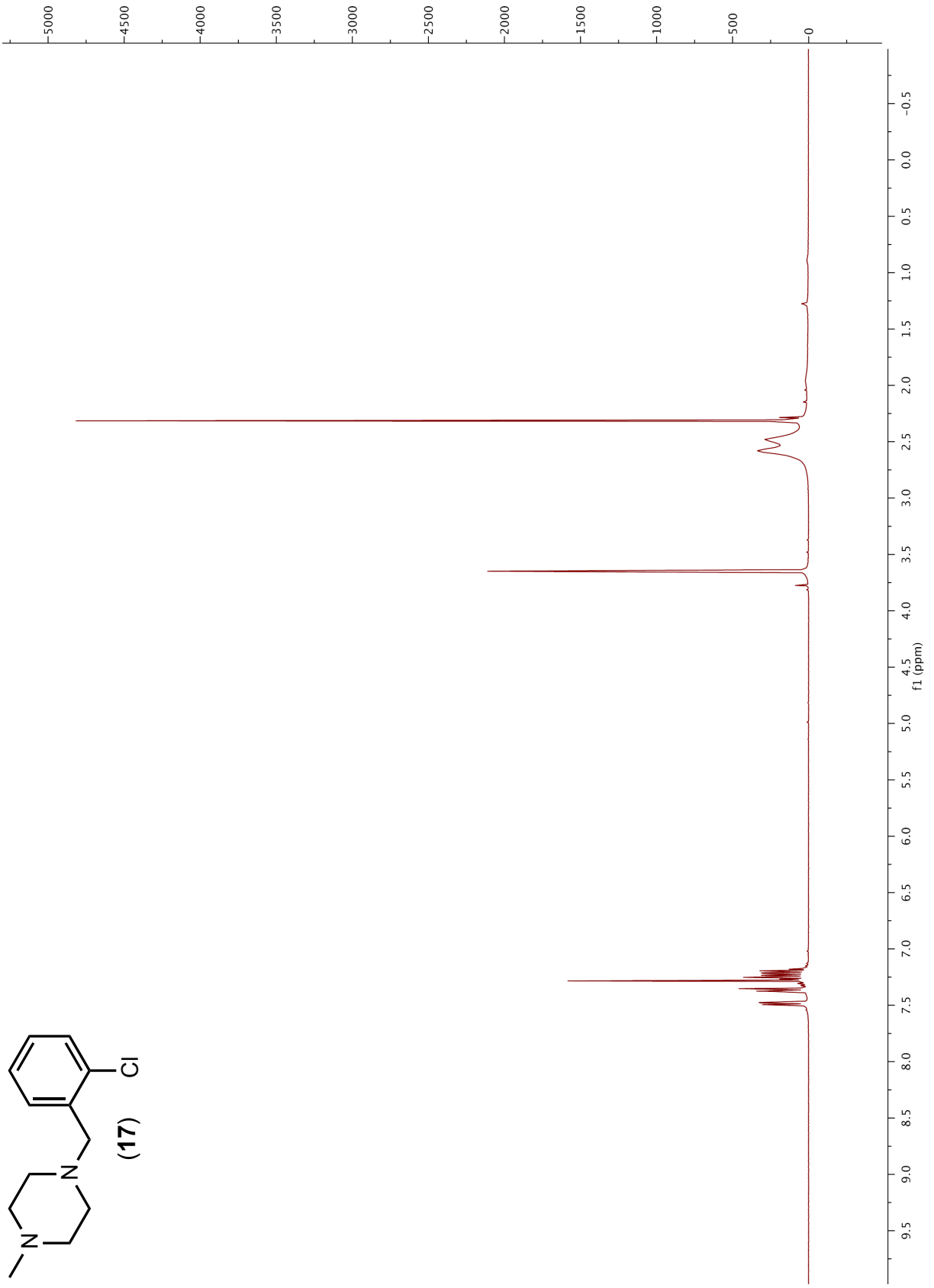
5000
4500
4000
3500
3000
2500
2000
1500
1000
500
0
-0.5
0.0
0.5
1.0
1.5
2.0
2.5
3.0
3.5
4.0
4.5
5.0
5.5
6.0
6.5
7.0
7.5
8.0
8.5
9.0
9.5
f1 (ppm)
Cl
N
N

(17)

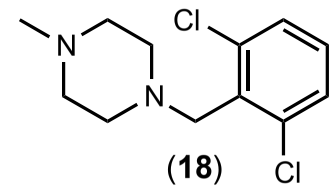
N
N
Cl
Cl

(**18**)

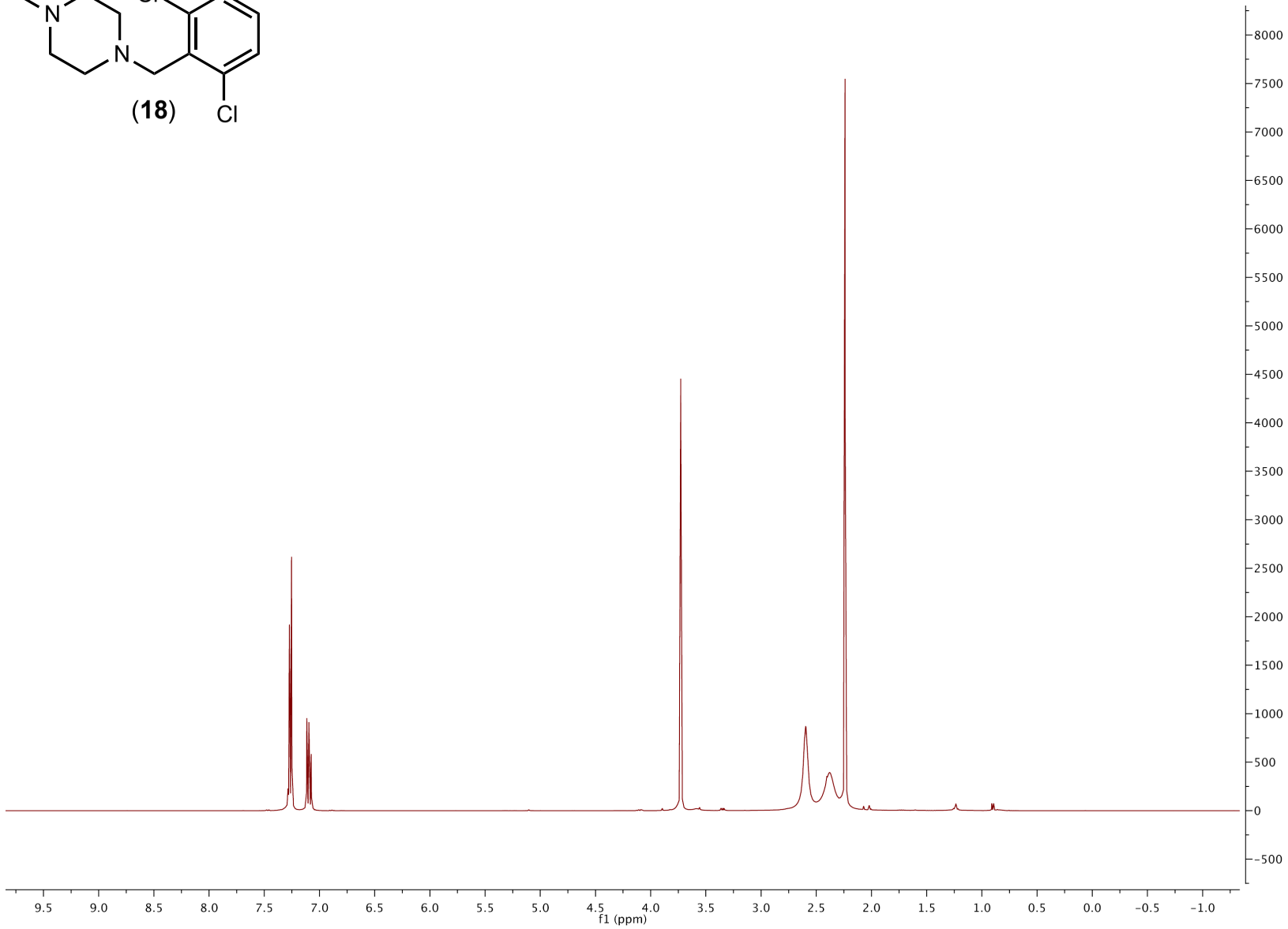
8000
7500
7000
6500
6000
5500
5000
4500
4000
3500
3000
2500
2000
1500
1000
500
0
-500
9.5
9.0
8.5
8.0
7.5
7.0
6.5
6.0
5.5
5.0
4.5
4.0
3.5
3.0
2.5
2.0
1.5
1.0
0.5
0.0
-0.5
-1.0
f1 (ppm)

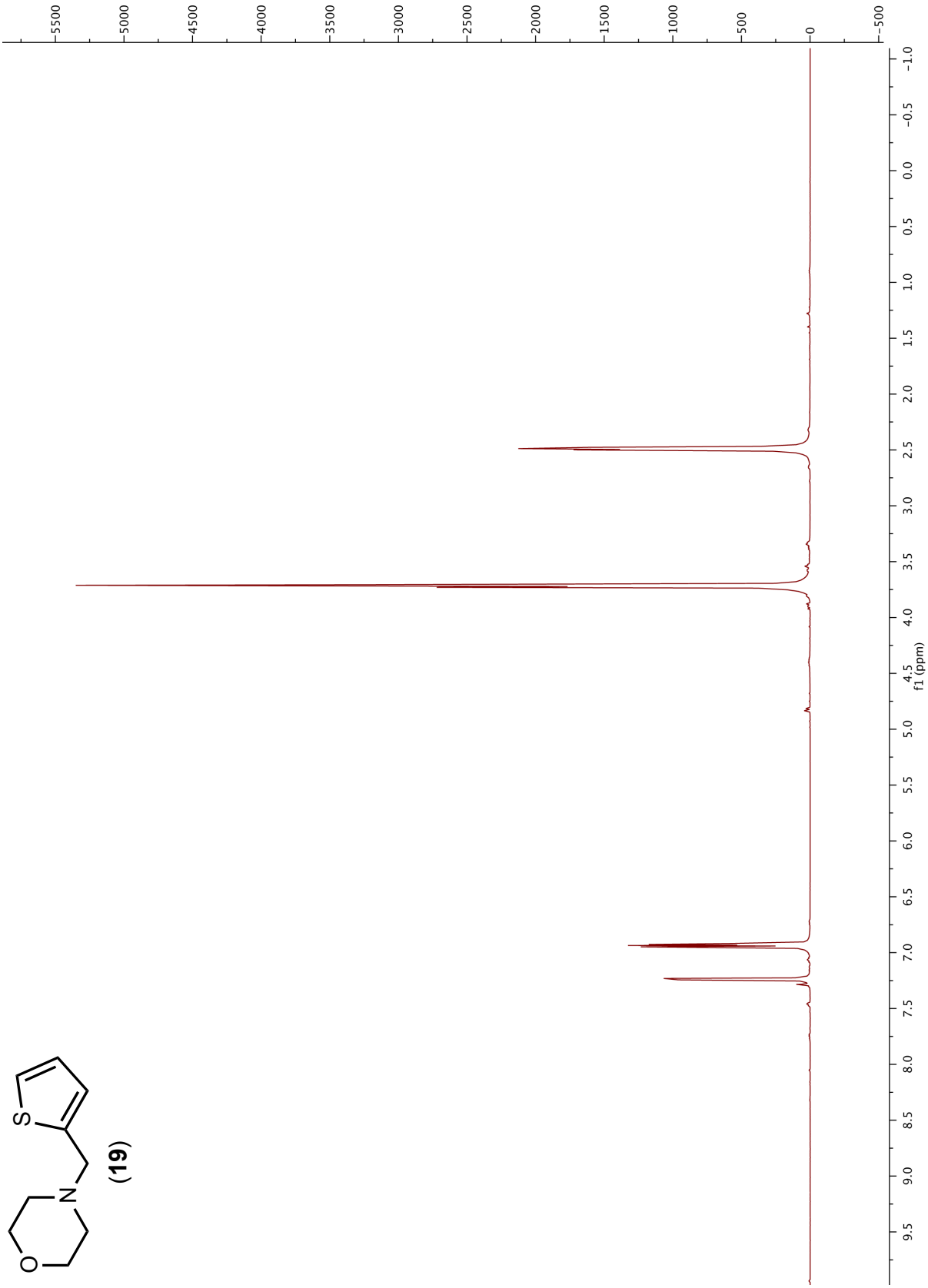
5500
5000
4500
4000
3500
3000
2500
2000
1500
1000
500
0
−500
−1.0
−0.5
0.0
0.5
1.0
1.5
2.0
2.5
3.0
3.5
4.0
4.5
5.0
5.5
6.0
6.5
7.0
7.5
8.0
8.5
9.0
9.5
f1 (ppm)
S
N
O

(**19**)

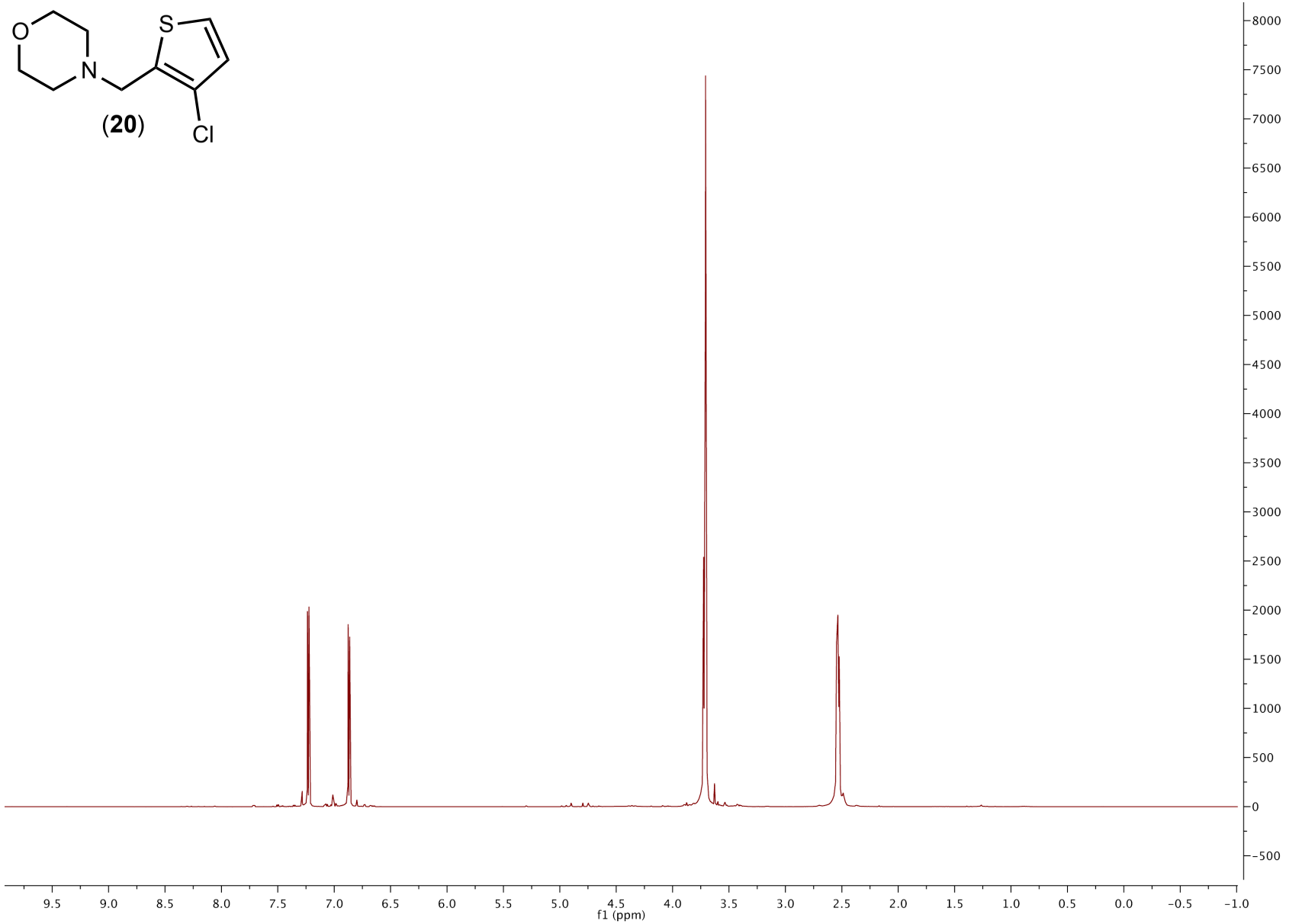
O
N
S
Cl
(20)
8000
7500
7000
6500
6000
5500
5000
4500
4000
3500
3000
2500
2000
1500
1000
500
0
-500
9.5
9.0
8.5
8.0
7.5
7.0
6.5
6.0
5.5
5.0
4.5
4.0
3.5
3.0
2.5
2.0
1.5
1.0
0.5
0.0
-0.5
-1.0
f1 (ppm)

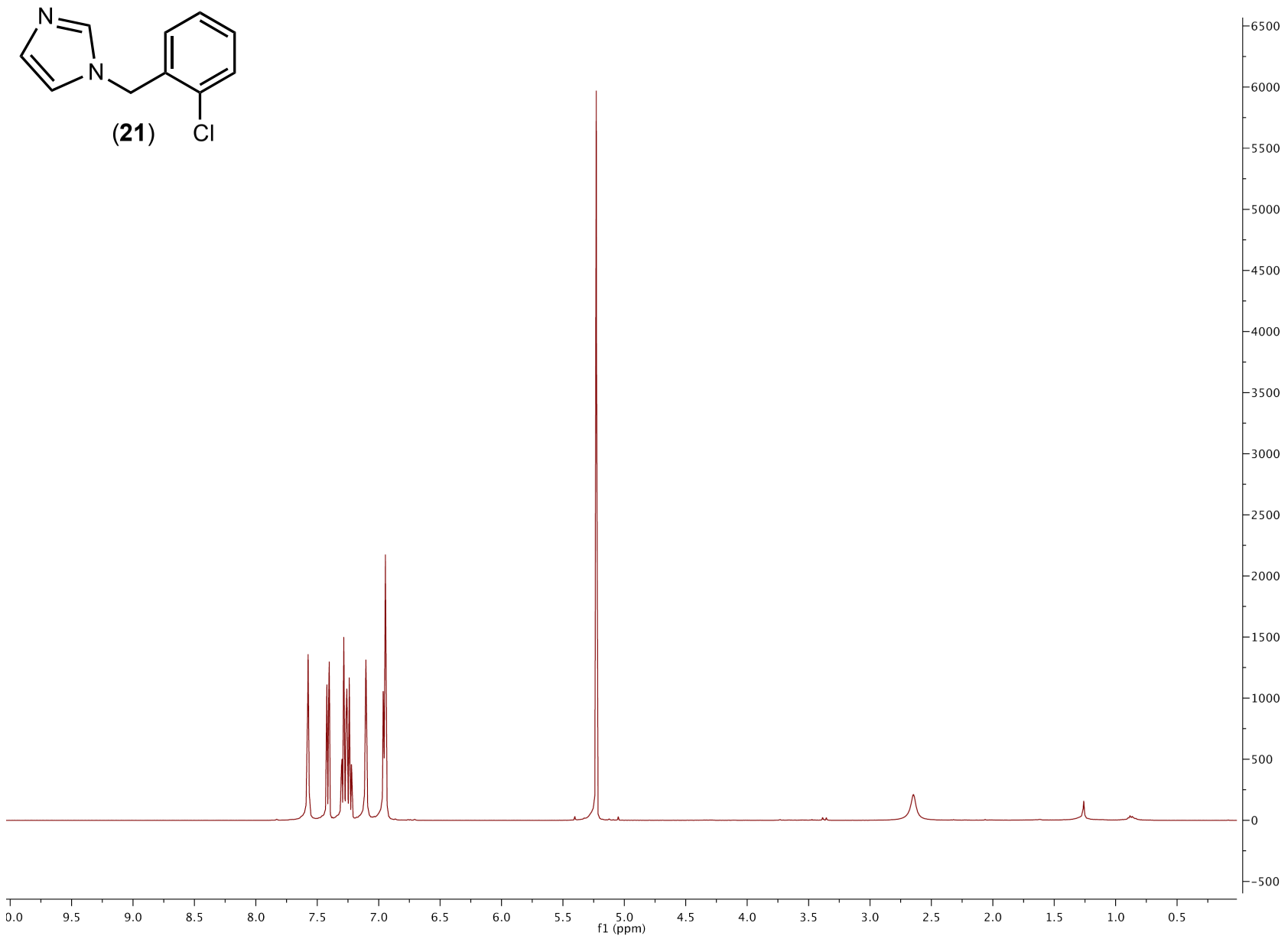
N
N
Cl
(21)
6500
6000
5500
5000
4500
4000
3500
3000
2500
2000
1500
1000
500
0
-500
0.0
9.5
9.0
8.5
8.0
7.5
7.0
6.5
6.0
5.5
5.0
4.5
4.0
3.5
3.0
2.5
2.0
1.5
1.0
0.5
f1 (ppm)

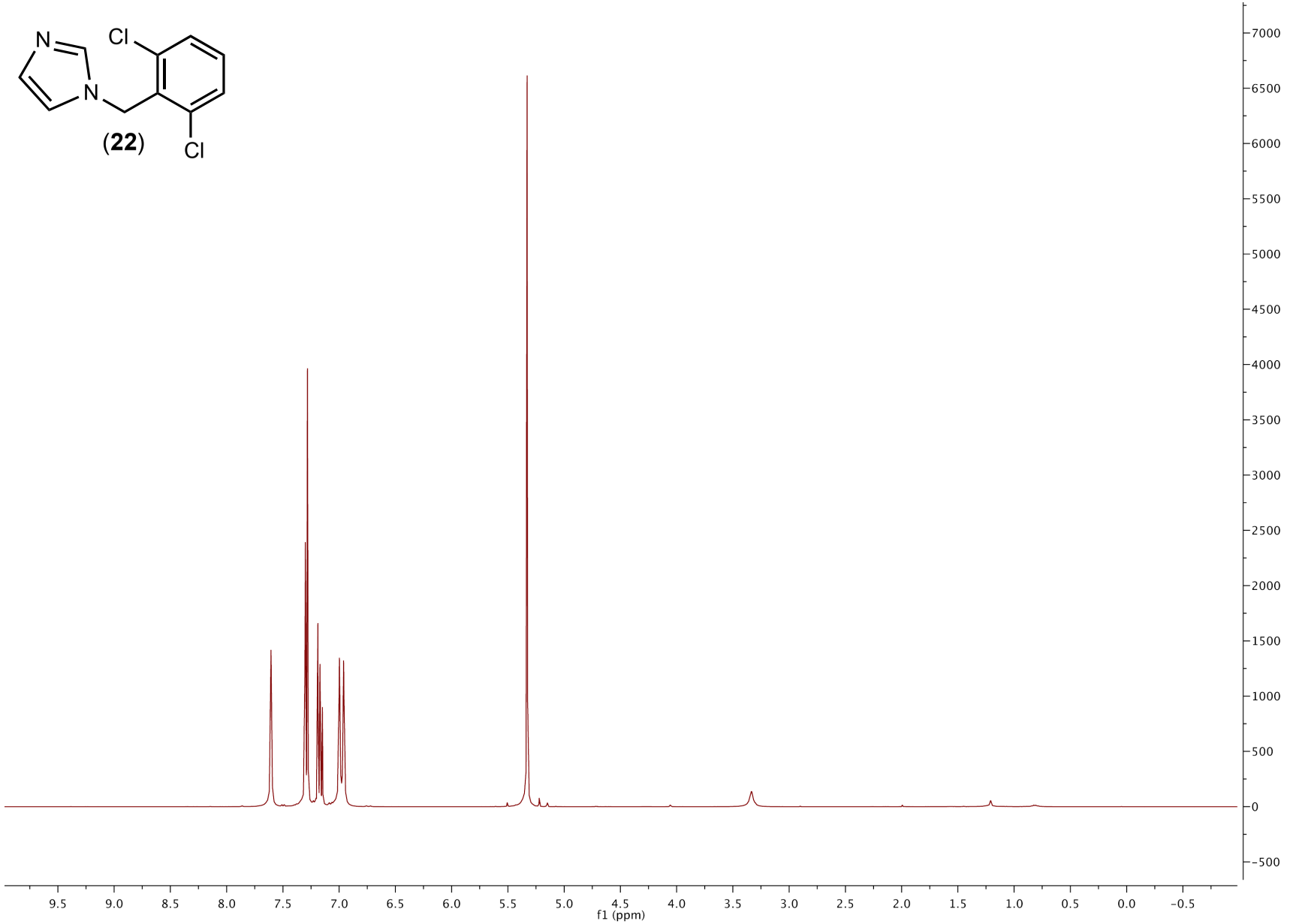
N
N
Cl
Cl
(22)
7000
6500
6000
5500
5000
4500
4000
3500
3000
2500
2000
1500
1000
500
0
-500
9.5
9.0
8.5
8.0
7.5
7.0
6.5
6.0
5.5
5.0
4.5
4.0
3.5
3.0
2.5
2.0
1.5
1.0
0.5
0.0
-0.5
f1 (ppm)

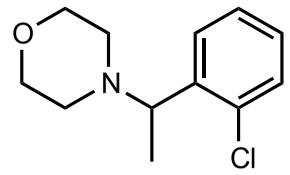
O
N
Cl

(**23**)

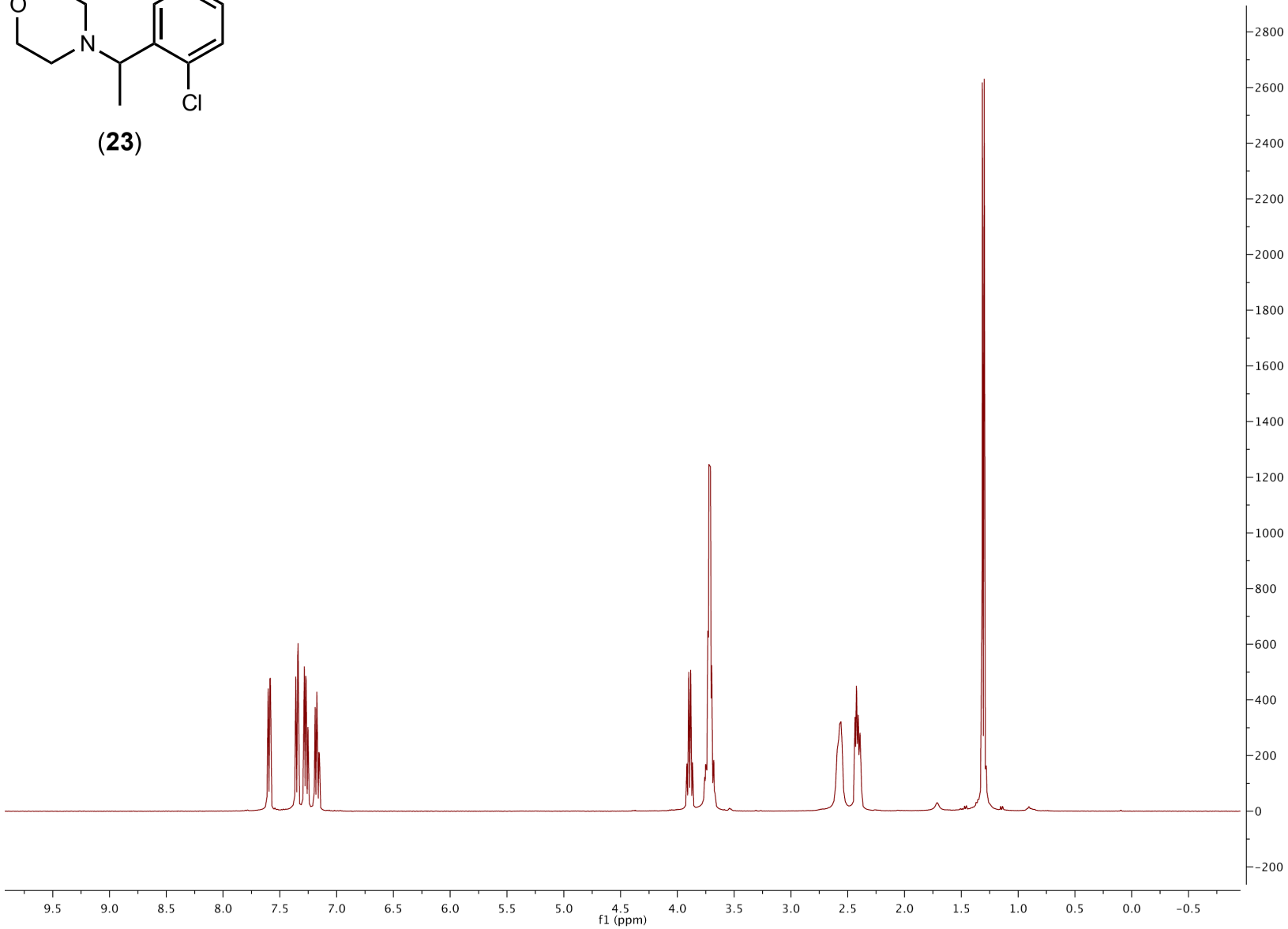
2800
2600
2400
2200
2000
1800
1600
1400
1200
1000
800
600
400
200
0
-200
9.5
9.0
8.5
8.0
7.5
7.0
6.5
6.0
5.5
5.0
4.5
4.0
3.5
3.0
2.5
2.0
1.5
1.0
0.5
0.0
-0.5
f1 (ppm)

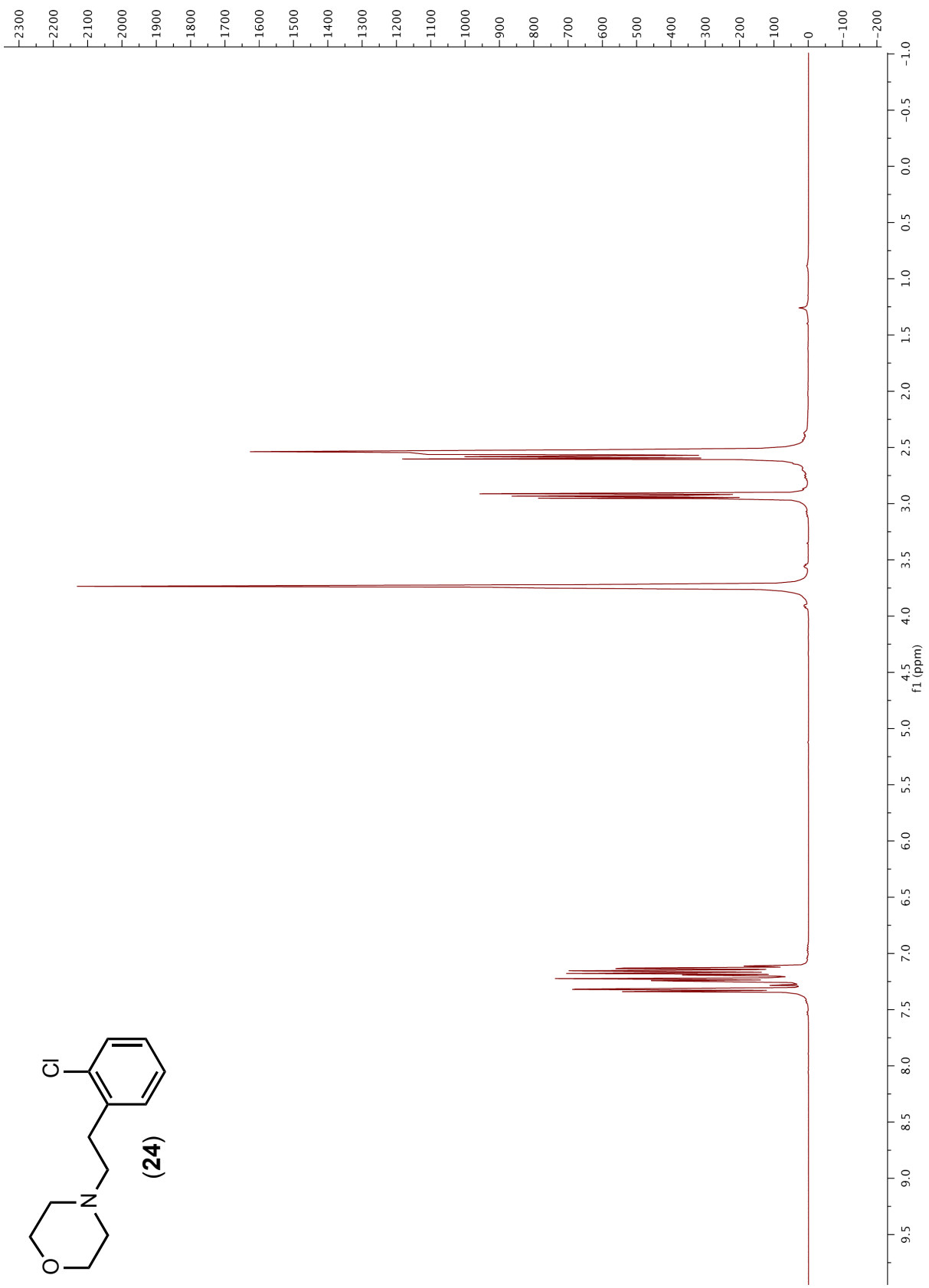
Cl
N
O
(24)
f1 (ppm)